A CO-AXIALLY CONFIGURED SUBMILLIMETER SPECTROMETER AND INVESTIGATIONS OF HYDROGEN BOUND MOLECULAR COMPLEXES

A Dissertation

by

BLAKE ANTHONY MCELMURRY

Submitted to the Office of Graduate Studies of
Texas A&M University
in partial fulfillment of the requirements for the degree of

DOCTOR OF PHILOSOPHY

December 2008

Major Subject: Chemistry

A CO-AXIALLY CONFIGURED SUBMILLIMETER SPECTROMETER AND INVESTIGATIONS OF HYDROGEN BOUND MOLECULAR COMPLEXES

A Dissertation

by

BLAKE ANTHONY MCELMURRY

Submitted to the Office of Graduate Studies of
Texas A&M University
in partial fulfillment of the requirements for the degree of

DOCTOR OF PHILOSOPHY

Approved by:

Chair of Committee,	John W. Bevan
Committee Members,	Lewis A. Ford
	Robert R. Lucchese
	Simon W. North
Head of Department,	David H. Russell

December 2008

Major Subject: Chemistry

ABSTRACT

A Co-axially Configured Submillimeter Spectrometer and Investigations of Hydrogen Bound Molecular Complexes. (December 2008)

Blake Anthony McElmurry, B.S., Texas A&M University

Chair of Advisory Committee: Dr. John W. Bevan

The development of a co-axially configured submillimeter spectrometer is reported. The spectrometer has been constructed to observe molecular complexes that exhibit non-covalent interactions with energies much less than that of a traditional covalent bond. The structure of molecular complexes such as those formed between a rare gas and a hydrogen halide, Rg:HX where Rg is a rare gas (Rg=Ne, Ar and Kr) and HX (X=F, Cl, Br and I) can be determined directly and accurately. The center of mass interaction distance, R_{CM}, as well as the angle of the hydrogen halide is determined, along with direct evaluation of the intermolecular vibrations as well as accurate isomerization energies between the hydrogen bound and van der Waals forms. The accuracy of the frequency determination of rovibrational transitions using the submillimeter spectrometer is also evaluated by direct comparison with the state-of-the-art pulsed nozzle Fourier transform microwave spectrometer, and this accuracy is estimated to be less than 1 kHz at 300 GHz.

The tunneling or geared bending vibration of a dimer of hydrogen bromide or hydrogen iodide has been investigated. The selection rules, nuclear statistics and

intensity alternation for transitions observed in these dimmers, which is a consequence of interchanging two identical nuclei in the low frequency geared bending vibration of the molecular complex, are reported. Furthermore, the rotation and quadrupole coupling constants are used to determine a vibrationally averaged structure of the complex. The energy of the low frequency bending vibration can then be compared with ab initio based potential energy surfaces.

A study of the multiple isomeric forms of the molecular complex OC:HI is also presented. Multiple isotopic substitutions are used to determine the relevant ground state structures and data reported evidence for an anomalous isotope effect supporting a ground state isotopic isomerization effect.

All spectroscopic data that has been reported here has been additionally used to subsequently model and generate vibrationally complete morphed potential energy surfaces that are capable or reproducing the experimentally observed data. The utility of this procedure is evaluated on a predicative basis and comparisons made with newly observed data.

DEDICATION

To my parents

and

Melissa

ACKNOWLEDGEMENTS

I would like thank a number of people who supported me along the way in my journey and study of the fundamental philosophy of science and chemistry. First of all my mentor, Professor John W. Bevan who initially made the push for me to attend graduate school at Texas A&M and his interest in my work in the spectroscopic science.

I also express my appreciation to Walter and Steven Reid who through their support with the resources of Mobile Analytical Labs, Inc. in Odessa, TX made it possible for me not to only attend Texas A&M University as an undergraduate, but also granted me the opportunity to obtain experience with the workings of an analytical laboratory in the oil field of west Texas.

I would also like to thank members of the group, in particular Sergey Belov who taught me the use of submillimeter technology, which sparked the drive to find fundamental truths of science. Further thanks are extended to Fabrice Willaert for his contributions to the operation of the instrumentation in the laboratory, development of ideas that have extended the available instrumentation, and his friendship.

I would like to personally thank Michelle Frantzen who acted as both friend and associate in and out of the lab. Further to those who have both supported me with friendship and scientific discussions, in particular Bill Merka, Guido Verbeck, Jody May, Bill Russell and Stacy Sherrod. To these I owe much gratitude.

My family has been especially supportive of my endeavors. My father Larry, and my mother Dixie have offered their support in all aspects of my life which has been

very important to me. My grandparents, Marlin and Yvonne Collins and Doris McElmurry, who I know are proud of me for what I have done. And I know that my grandfather, Jack McElmurry, would be equally as proud.

Melissa Haas, the woman who has supported me and has been a part of my life throughout my graduate career and her family have been equally supportive, and to them I owe special appreciation and thanks.

Finally, I would like to thank the Robert A. Welch Foundation for support in the form of a pre-doctoral fellowship (Grant No. A747) and the National Science Foundation for funding the research.

TABLE OF CONTENTS

Page

Page

LIST OF FIGURES

Page

Page

Page

Page

LIST OF TABLES

Page

Page

Page

CHAPTER I

INTRODUCTION: NON-COVALENT INTERACTIONS

A non-covalent bond is a type of chemical bonding that does not involve the sharing of pairs of electrons but rather more dispersed variations of electromagnetic interactions that are generally significantly weaker than conventional covalent bonds. In general, non-covalent bonding refers to a variety of interactions that provide forces which hold molecules or parts of molecules together in specific orientations or conformations. The combined strength of intermolecular interactions are greater than the sum of the individual component bonds because the free energy of the multiple types of bonds between two molecules is greater than the sum of the enthalpies of each bond due to entropic effects. Intermolecular forces thus play a fundamental role in the nature of non-covalent interactions between molecules. In particular, they involve primarily four types of bonding that include hydrogen bonding, ionic, van der Waals and hydrophobic interactions. Frequently such forces act in concert, though they are generally significantly weaker than a covalent bond[1]. As a consequence of the fact that non-covalent interactions are ubiquitous throughout nature, such types of bonding are consequently significant in determining a wide range of properties of matter in all states whether in gas or condensed phases. Examples of the effects of non-covalent bonding include binding interactions that are considered of fundamental importance in holding

---

This dissertation follows the style of *Physical Chemistry Chemical Physics*.

the two strands of DNA in the double helix together[2], those that determine the folding of proteins and polypeptides[3] as well as those that enable enzymes to bind to their substrates[4]. All these considered examples are of immense significance in biology. However, a plethora of other non-covalent interactions exist that vary from the immensely complicated and intricate kind of interactions such as those just discussed, to interactions that involve relatively small numbers of atoms and are comparatively simple (i.e. rare gas-hydrogen halide dimeric complexes). However, whatever the nature of the non-covalent interaction involved, they all have the capability of fundamentally impacting phenomena in a wide range of fields including chemistry, nanotechnology, genetics and others to varying extents. Indeed, as an example, it can be stated without exaggeration that "…one simple consequence of the existence of the hydrogen bond: water would be a gas at room temperature were it not for this type of interaction and life on earth would not be possible in its present form."[5] Physicists and chemists alike have thus recognized the importance of characterizing the properties of such non-covalent bonding and have been studying these weak interactions for the past century. Such investigations have involved a combination of the use of theory and experiment including a wide range of physical approaches and methodologies often applied in a synergistic manner to enhance understanding and prediction of the influence of interactions on a wide variety of phenomena[6, 7]. Certainly, one of the ultimate goals of these studies has been the generation of models which describe the fundamental properties of these interactions in a wide variety of chemical environments. The objective is that these models will not only be to characterize non-covalent interactions,

but also to have the capability of accurately predicting their properties in the widest range of circumstances. This is especially so in larger systems and more complex environments, such as the bulk properties of water or the influence of non-covalent interactions in the case of proteins and DNA. The characteristics of the interactions vary considerably in the aqueous environment of cells, especially human cells, where they impact pharmaceutical applications in the treatment of disease and development of medicines. An approach to understanding the nature of the intermolecular forces in such complex situations and environments is to develop effective methodologies that stress fundamental and detailed understanding of relatively simple and prototypical interactions. Generalization of such methodologies to a description of the more complex phenomena such as those described above would represent a major achievement. The development of effective methodologies and experimental approaches has been adopted for the studies that have been carried out in this dissertation. Relatively simple prototypical interactions will be investigated using newly developed instrumentation with the explicit objective of enhancing the detailed characterization and modeling of such relatively simple intermolecular interactions at the microscopic/molecular level free from the complications of matrix and other environmental effects. The prototypical systems selected for investigation will be chosen carefully to generate new intrinsic data that can support the modeling methodologies intended ultimately to be generalized to more complex interactions not amenable to such detailed study.

As discussed previously, weakly bound complexes can be defined as an assembly of two or more well defined chemical species held together by interactions weaker than a

conventional covalent bond[1]. A covalent bond typically has a bond strength of about 200-500 kJ/mol, while a single intermolecular van der Waals bond can be as low as just 1 kJ/mol, while neutral hydrogen bonded interactions generally have larger binding interactions in the range 20 to 50 kJ/mol. However, the characterization and fundamental properties of even single non-covalent interactions are currently not generally as well understood as covalently bound molecular species. This is a consequence of many factors but especially due to large amplitude and highly anharmonic intermolecular vibrations that are associated with these types of weakly bound interactions. Furthermore, as the number of the atoms involved in such interactions increase, their vibrational dimensionality also increases rapidly, significantly enhancing the complexity of models that are required to describe the interaction. These factors contribute immensely to the complexities of their intrinsic properties and are frequently found in the subtleties of the characteristics that determine the properties of these types of interactions.

In this dissertation, analyses will be reported for some of the simplest manifestations of van der Waals and hydrogen bonding in closed shell atom-molecule or molecule-molecule interactions such as Rg-HX and $(HX)_2$. Here, Rg is a rare gas atom (Ne, Ar, Kr) and HX is a hydrogen halide (X=F, Cl, Br and I). While these specific systems are not the only complexes that can be formed between the component monomers, they do represent a subset of prototypical molecular complexes that are referred to as molecular dimers. These are most suitable for the detailed investigation and analysis of the fundamental nature of the forces involved. An example of the

magnitude and variety of the current state of this field is demonstrated in the contents of the "Bibliography of Rotational Spectra of Weakly Bound Spectra [8]." In addition, it is now routine to model a molecule with the advancements of computational power and programs to describe molecules from a quantum mechanical perspective. However, the generation of accurate vibrationally complete potential energy surfaces (PES), is another issue. For example, those that include all intra- and intermolecular vibrational motions capable of accurately predicting the properties of non-covalent interactions with quantifiable uncertainties have proven significantly more elusive. Indeed, this is not possible with present day quantum chemistry calculations alone despite frequent statements to the contrary. The absolute energy accuracy required is too high and approximate methods for the cancellation of errors cannot be relied upon. Here, theory is still dependent on benchmark experimental data. Thus, experimental research in this area has focused primarily on the spectroscopic analysis of prototypical interactions in the gas phase or supersonic jets to definitively characterize selected isolated complexes. As mentioned previously, such studies are free from complications such as those found in matrix effects, thereby yielding information of direct relevance to these interactions themselves. However, the experimental studies necessary for modeling these weakly bound species are still frequently challenging. The structure and dynamics of the inherently weak nature of intermolecular interactions and bonding has been the subject of a wide array of experimental and theoretical investigations over the past four decades. It is recognized that even now concerted generalized methods for investigating such interactions are still not available. Characterization of the large amplitude highly

anharmonic vibrations and additional difficulties that arise from providing a sufficiently diverse range of experimental spectroscopic data complicate generation of accurate vibrationally complete PES.

It is from the perspective above that experimental studies included in this dissertation will be directed. The Introduction will, in the first place, give a more detailed perspective of the field, particularly those aspects more directly relevant to the subject of this thesis. This will be followed by presentation of investigations on the rare gas and hydrogen halide molecules (Rg:HX) and hydrogen halide dimers $(HX)_2$ emphasized as prototypical systems for current study. These types of molecular complexes will be studied using relatively high resolution spectroscopic techniques including microwave, infrared, and most recently submillimeter techniques. The design, development and construction of the submillimeter spectrometer and its application to the observation of molecular complexes will be the focus of much of the reported work. The results on dimer systems that have been studied will be the major components of the initial part of this thesis. Specifically, an example of the qualitative information that has been determined for the Rg-HX series is demonstrated in Table 1. This table depicts the ground state and equilibrium structures of the complexes as a function of Rg and HX substituents. Here, the impact of our investigations, shown in bold face, Rg - HX(X= Br, I) have given fundamentally new perspectives on this important prototypical homologous series including unequivocal evidence for differentiation of ground and equilibrium structures in Ar-HBr. Publications associated with this work have already appeared in peer reviewed journals[9-11]. Also, reports associated with more complex

diatomic-diatomic interactions have been published[12] or presented at international conferences[13-15]. This work will also be included and the significance of these contributions further addressed. The analysis of HI dimer in particular and its unexpected structural and dynamical characteristics will be the subject of considerable discussion. Some of this latter work and the results of hitherto unpublished investigations will then bring the thesis to its conclusion.

Table 1. Ground state and equilibrium structures of Rg-HX.

Rg:HX		HF	HCl	HBr	HI
Ne	GS	Ne-HF	Ne(HCl)	Ne(HBr)	Ne(HI)
	EQ	Ne-HF	Ne-HCl	Ne-BrH	Ne-IH
Ar	GS	Ar-HF	Ar-HCl	**Ar-HBr**	**Ar-IH**
	EQ	Ar-HF	Ar-HCl	**Ar-BrH**	**Ar-IH**
Kr	GS	Kr-HF	Kr-HCl	Kr-HBr	Kr-IH
	EQ	Kr-HF	Kr-HCl	Kr-BrH	Kr-IH

Intermolecular Forces: Non-covalent Bonding

The simple interaction of two atoms or molecules may be described through the use of an equation which takes into account the magnitude of the attractive and repulsive forces that each particle exerts on the other. From a theoretical point of view, each type of interaction can be separated from another and described by an analytical function which relates the magnitude of the interaction to the distance between the subunits. One type of this equation is a Leonard-Jones potential[6] which has the form:

$$V^{LJ}(R) = \frac{a}{R^{12}} - \frac{b}{R^{6}} \qquad (1)$$

From this equation, the specific distance at which the attractive and repulsive forces

cancel each other out is given by the interaction energy, $V^{LJ}(R)=0$. The minimum in the energy is a condition defined as $R_0^6=a/b$ and $dV^{LJ}(R)/dR = 0$. The minimum energy, denoted ε, satisfies the relationship ($\varepsilon= b^2/4a$). The Leonard-Jones potential can then be put into the form of:

$$V^{LJ}(R) = 4\varepsilon\left[\left(\frac{R_0}{R}\right)^{12} - \left(\frac{R_0}{R}\right)^{6}\right] \qquad (2)$$

The interaction energy of two particles can be described by taking two extreme cases. First when the atoms are very far apart there is no interaction and the energy of attraction is 0. Second, if the particles are very close together the repulsive energy rises to a very large value because the electron clouds of the two particles cannot occupy the same space. However, when the interacting particles are at a distance where the contribution from the attractive and repulsive forces is equivalent the atoms are at the equilibrium distance, and the total energy of the interaction is at a minimum. The Leonard-Jones equation is a simple expression which describes the interaction of two particles which only have an attractive and repulsive energy. However, this simple equation does not describe the interaction of chemical species such as rare gas atoms and diatomic molecules where other more subtle forces come into play.

Interactions of systems with greater complexity are of more importance to the more general study of chemical processes. However, without a working model of these interactions, it is impossible to make quantitative predictions of how a given system will behave. It is the goal of the theory of intermolecular interactions to be able to accurately evaluate the potential energy surface using computational models, in the hope of

building a basis for the study of larger and larger molecules which may not be amenable to detailed study with an experimental technique which is currently available.

The fundamental processes which determine the dynamics and structure of weakly bound molecular complexes are frequently dominated by the interaction of two or more atoms or molecules through the van der Waals forces or hydrogen bonding. These forces are much weaker than those found in covalent bonding, as discussed previously. An example of the molecular complex formed from a rare gas atom and a hydrogen halide is given in Figure 1. This simple representation is typical of the homologous series of Rg-HX and depicts the orientation of the molecule with an angle θ of the HX component to the major molecular axis, or the axis on which the two heavy atoms fall. Also shown is the distance between the centers of mass, R_{CM}, of the rare gas atom and the diatomic molecule. The Rg:HX molecular complex is a prototype for the study of non-covalent bonding as it demonstrates the interactions of an atoms and molecules in a system with a restricted number of intramolecular modes.

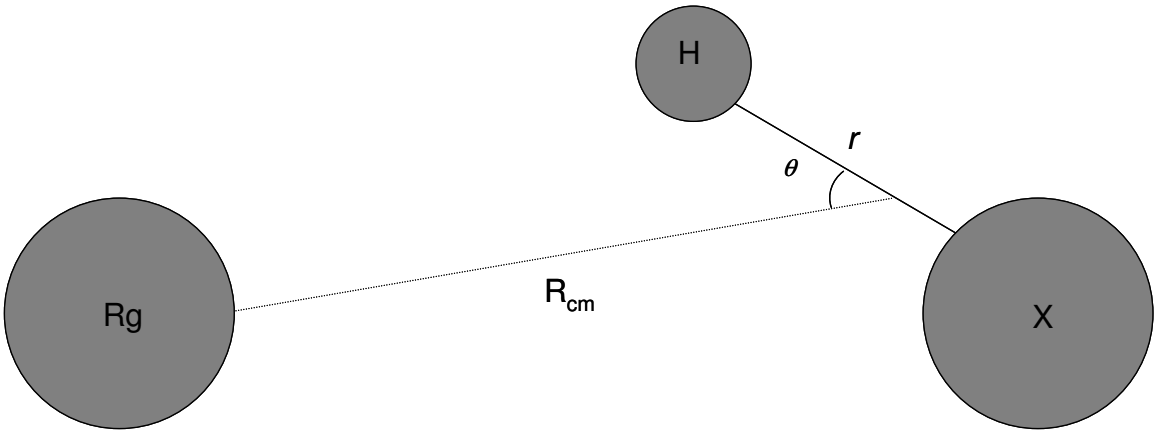

Figure 1. Jacobian coordinate system for a Rg-HX molecular dimer.

Figure 1 is an example of a molecular dimer formed from a rare gas atom and a hydrogen halide. This complex, described through the Jacobian co-ordinate system, has specific parameters, the R_{CM}, which is the distance between the centers of mass of the components of the complex, θ, the angle of the diatomic to the center of mass and finally, r, which is the bond length of the diatomic. The Jacobian co-ordinate system is used to describe polyatomic systems as it relates the structure of the system to the center of mass in the inertial axis frame. This treatment also simplifies the computational requirements due to the reduced number of variables. In the Cartesian coordinate system, the location of each atom is related to the distance from a common point in X, Y and Z space and the origin is the center of mass of the complex. The Jacobian system allows the change of the location of atoms in XYZ space due to rotation to be removed from the expression of the inertia of the complex and by association the contribution to the energy of the complex.

Major interactions present in molecular complexes such as Rg:HX are dependent on the orientation and distances of the two components in the complex. Repulsive forces that are the most prevalent at close range are different than those that contribute to the attractive interaction at long range. The Leonard-Jones potential treats two interactions, the attractive and repulsive, individually and the relationship is dependent on distance. Equation 2 demonstrates this as the attractive force is subtracted from the repulsive force to give the energy of interaction. However, the types of interactions which can be accounted for in a system such as Rg:HX are indeed more complex than the simple

attractive and repulsive forces as in the van der Waals equation, and each force has a slightly different dependence on the distance in which they act.

There are three basic classes of interactions which can be grouped together based on the ranges of distances in which they act. These are the short range, intermediate and long range interactive forces. In each range, there are special characteristics of interactions. The short range interactions are dominated by the repulsive nature of the two components where electronic exchange takes place due to the close proximity of the electron clouds of each subunit. This is contrasted with the interactions which are important at long range where the electronic exchange and repulsion, or the interaction of electron clouds through covalent bonding, is almost non-existent but where the attractive nature of the intermolecular forces dominates. The intermediate range, around the minimum of the potential energy surface, is where a combination of the previously mentioned forces contributes to the interaction. These forces can be treated with theoretical functions and are dependent on the distance between them. Each force has a specific functional form which can predict the magnitude of the interaction reasonably well. The treatment of each of the forces and their contributions to the energy of the complex has been reviewed by Buckingham et al.[16].

Contributions to the Energy of a Complex

Each interaction contributes to the total energy of the molecular complex. The partitioning of each type of interaction energy follows the form of:

$$V_{\text{int}} = V^{short} + V^{elec} + V^{ind} + V^{disp} \qquad (3)$$

Where V_{int} is the energy of the intermolecular potential and the remaining terms V^{short}, V^{elec}, V^{ind} and V^{disp} are the contributions from the short-range, electrostatic, induction and dispersion energies.

Table 2. Interaction energy terms and effects.

Partition	Effect
Short-range	Repulsive interaction
Electrostatic	Multipole-multipole interaction
Induction	Polarization
Dispersion	Induced Dipole (Instantaneous Dipole)

Table 2 describes the types of interactions that are separable from the total interaction of the complex.

Short-Range Interactions

Short range interactions are dominated by the valence repulsion term, or the intermolecular Coulomb and exchange terms, of the different monomers. This term is proportional to the square of an overlap integral between the orbitals of the two molecules and can be represented by the following equation

$$V^{short}(R,\theta) = A'\exp\left[-\beta(\theta)(R - R_{ref}(\theta))\right] \quad (4)$$

where

$$R_{ref}(\theta) = \sum_{\lambda} R_{ref,\lambda} P_{\lambda}(\cos\theta) \quad (5)$$

$$\beta(\theta) = \sum_{\lambda} \beta_{\lambda} P_{\lambda}(\cos\theta) \tag{6}$$

R_{ref} or reference distance is expanded along with the exponent in order to rectify the problem associated with the treatment of the equation where the use of angular functions become prohibitive[16]. These equations can be fitted to a potential, which is generated from experimental data, of the short-range interaction energy of a rare gas and hydrogen halide molecule or other linear triatomic molecules. In Equations 5 and 6, λ refers to a Legendre polynomial and to the dependence of the angle for the interaction and β refers to the exponential dependence of the interaction.

Electrostatic Interactions

The contribution to the total energy of a complex from electrostatic interactions is fundamentally dependent on the charge of each subunit and the distance between them. A molecule such as a hydrogen halide has a permanent charge distribution and this creates a dipole moment and the electron density of a molecule is greater at the halide than at the hydrogen atom. When a molecule of this type interacts with another molecule or atom, the orientation of the diatomic will significantly affect the energy of the interaction. This can be taken into account via an equation that describes the charge dependent orientation of the molecule with another when integrated over the space of each molecule. The equation of the electrostatic energy

$$V^{elec} = \frac{1}{4\pi\varepsilon_0} \int \Psi_a^{(0)} * \Psi_b^{(0)} * \sum_{ij} \frac{e_i^{(a)} e_j^{(b)}}{R_{ij}} \Psi_a^{(0)} \Psi_b^{(0)} \mathrm{d}\tau_a \mathrm{d}\tau_b \tag{7}$$

where $\Psi_a^{(0)}$ and $\Psi_b^{(0)}$ are the ground state wave functions of each molecule and e_i and e_j

are the charges of molecules or atoms a and b with the distance R_{ij} between them. The electrostatic interaction is dependent on the distance between the atoms as $\frac{1}{R}$.

Induction Energy

The induction energy of a molecular complex arises due to the simple fact that when two molecules interact, each molecule changes one another because of the interaction of the electrons around each atom. As two molecules approach one another, the shape and distribution of their respective electron clouds is modified so that they can come closer together. The changing of the electron clouds can be described as the induced electric moments of the molecule with respect to the permanent charge distribution of the other molecule. This force is rather weak when compared with the electrostatic and dispersion forces for a molecular complex. The energy for induction can be described by the following equation which is the second order of the perturbation theory for the interaction

$$V^{ind} = (4\pi\varepsilon_0)^{-1}\left[\begin{array}{l}\int \Psi_a^{(0)} * \Psi_b^{(0)} * \sum_{ij} \frac{e_i^{(a)} e_j^{(b)}}{R_{ij}} \Psi_a^{(0)} \Psi_b^{(1)} \mathrm{d}\tau_a \mathrm{d}\tau_b + \\ \int \Psi_a^{(0)} * \Psi_b^{(0)} * \sum_{ij} \frac{e_i^{(a)} e_j^{(b)}}{R_{ij}} \Psi_a^{(1)} \Psi_b^{(0)} \mathrm{d}\tau_a \mathrm{d}\tau_b \end{array}\right] \quad (8)$$

where $\Psi_a^{(0)}$ and $\Psi_b^{(0)}$ are the ground state wave functions of each molecule, and e_i and e_j are the charges of molecules or atoms a and b with the distance R_{ij} between them. $\Psi_a^{(1)}$ is the first-order change from the electrostatic field (non-uniform) of a or b. The induction energy is the result of the presence of neighboring molecules whose charge distributions distort the electric field gradient of the molecule. Indeed, the opposite case

is true when the other molecule is distorted and this is taken into account by the second part of the above equation.

Dispersion Interactions

The dispersion interaction is one of the most important attractive forces for molecules that do not have a dipole moment. The energy is determined by the quantum-mechanical fluctuations of the electron density. As the electron density around a molecule or atom is changed, an instantaneous dipole moment is induced in the atom or molecule, which then creates a dipole in a neighboring molecule or atom. This interaction defines the magnitude of the dispersion force. The dispersion is always attractive for molecules in the ground state.

$$E_{disp} = -\sum_{n=6}^{\infty} \frac{C_n}{R_n} \tag{9}$$

Equation 9 defines the series expansion of the dispersion coefficients with even powers of *n*. The first term in the series is proportional to $1/R^6$ and describes the dipole-dipole interaction, the second term which is proportional to $1/R^8$ is the quadrupole-dipole interaction and higher order terms such as the quadrupole-quadrupole and dipole-octopole are taken into account with the third term and scale with $1/R^{10}$.

While these interactions describe the most important aspects of the forces involved in intermolecular non-covalent bonding they are applied in a rather arbitrary manner to fit experimental data.

Structure of van der Waals Complexes

The molecule and the bonds that bind its constituent atoms together is a fundamental concept in the physical and chemical sciences. The study of the relative interaction distances and the energetics involved between nuclei is one manner in which the forces between molecules can be characterized. Pauling discussed a theory in which the radii of nuclei in different bonding environments can be used to predict the internuclear distances in a molecule in his book "The Nature of the Chemical Bond."[17] However, as the bonding involved in van der Waals complex is very weak and largely anisotropic the exact structure of the complex cannot be effectively predicted. There have been several review articles in the literature which address the trends in the effective van der Walls radii of atoms in a molecular complex[18-20]. Pauling evaluated the van der Waals radii of nuclei, as well as an equation to predict the distance between 2 atoms. Bondi[21] has also addressed the volume of the van der Waals radius, as well as giving a table of van der Waals radii determined from x-ray crystallography, which is presented in Table 3.

Table 3. Mean van der Waals radii (Bondi 1964) of selected nuclei.

Atom	Radii (Å)	Atom	Radii (Å)
H	1.20	He	1.40
F	1.47	Ne	1.54
Cl	1.75	Ar	1.88
Br	1.85	Kr	2.02
I	1.98	Xe	2.16

The structure of a molecule or molecular complex is directly related to the bond lengths and bond angles as well as the coordinates of each nucleus in the complex. The distance of the hydrogen bond length has been investigated by Arunan and coworkers[20] for a variety of complexes where hydrogen bonding exists.

The properties of the complex containing the intermolecular bond, be it hydrogen bound or van der Waals, are dependent on the forces discussed previously and are directly related to the nature of each component of the complex and has a direct effect on the structure of the complex. Preparation of an isolated sample of the complex is achieved by numerous techniques employing supersonic expansion of small amounts of the target gases in an inert carrier adiabatically into vacuum, or by reducing the temperature of a static gas phase cell, provided that a sufficient concentration of the complex remains in the vapor phase at reduced temperature. Upon formation, the complex usually has characteristic structural properties, such as moment of inertia and bond length, as well as the orientation of the molecule relative to the major molecular axis of the complex as shown in Figure 1. By observing the rotational transitions between the energy levels of a complex, the structure can be derived using an equation which relates the mass of each nucleus and its distance to the center of mass of the complex. The moment of inertia of the complex is given by the following equation.

$$I = \sum_i m_i R_i^2 \qquad (10)$$

where m_i and R_i are the masses and distances respectively, from the center of mass of the complex along an axis of the complex. The axes can be x, y or z and are relative to the

A, B and C molecular axes respectively. The rotation constant is related to the moment of inertia by the following expression:

$$B = \frac{h}{8\pi^2 I} \tag{11}$$

The complex created from an atom and molecule can be represented by a characteristic distance, R_{cm} which is the distance between the nucleus of the atom and center of mass of the diatomic molecule, and is related to the rotational constant of the complex given by

$$R_{cm} = \left(\frac{h}{8\pi^2 \mu_r B_0} \right)^{1/2} \tag{12}$$

where B_0 is the ground state rotational constant and μ_r is the reduced mass which is of the form

$$\mu_r = \frac{m_a m_b}{m_a + m_b} \tag{13}$$

where m_a and m_b are the masses of the respective atom or molecule. The R_{CM} separation is dependent on the forces discussed above and the strength of the bond formed between the components.

The structure of the molecule can also be determined through the use of isotopic substitution, such as the exchange of a hydrogen atom with a deuterium atom.
The value of the rotational constant can be determined by observing the pure rotational spectrum or rotationally resolved vibrational spectra of the complex. A complex which has a significant dipole moment can be observed via techniques such as microwave

spectroscopy, infrared spectroscopy and submillimeter spectroscopy, which is the subject of this dissertation.

The structure of the complex at equilibrium, neglecting mass effects and vibrational motion, may be determined by corrections to the rotational constants of multiple isotopic species for the anharmonic nature of the intermolecular bond. This method is presented in detail [22-24] and relates the determined rotation distortion constants to the stretching frequency of the intramolecular bond and applying a correction to the determined rotational constant, B_0, from the fit to derive a equilibrium rotational constant B_e , which is then used to determine an equilibrium bond distance, r_e. The equation[22] describing the relationship between B_e and B_0 in the harmonic limit is given in Equation 14.

$$B_0 = B_e - 18(B_e^2 / \nu_s) \qquad (14)$$

where B_0 is the rotational constant and ν_s is the stretching frequency of the intermolecular bond.

However, the methods rely heavily on the assumption that the structure of the complex is related to a semi-rigid pseudodiatomic in the harmonic approximation. Improvements to the above methods have been reviewed recently in the literature [25] and the author evaluates the internuclear distance in the Rg:HX (X=F, Cl, Br, I) series by the different methods.

The determined structure of a complex corrected for the mass dependent nature of the rotation constant, can be compared to those determined from ab-initio potentials directly. However, the utility of this exercise is greatly affected by the quality of the ab-

initio potential and the determined equilibrium structure. The development of methods to modify ab-initio potentials to reproduce spectroscopic data is a research direction that is being actively pursued in our research group and will be discussed in later chapters.

CHAPTER II

TAMU SUBMILLIMETER SPECTROMETER

Spectroscopic techniques utilizing microwave radiation and the relevant sources and detectors associated with this frequency range were greatly influenced by the development of microwave radar during World War II. The frequency range accessible was extended into the submillimeter and millimeter wave region through the development of crystal harmonic generators, which have been reported by King and Gordy [26-28]. The development of backward wave oscillators for use in the submillimeter and millimeter wave region has been reported by Krupnov and co-workers[29, 30].

Contributions to the development of submillimeter and millimeter wave spectrometers have been made in Russia[29], Germany[31], France[32], Japan[33], Canada[34] and the USA[35]. Backward wave oscillator based spectrometers have been made possible by ISTOK, a company which produces the BWOs, and technologies associated with frequency stabilization. Spectroscopic investigation of factors such as line position, pressure broadening and absolute line intensity have been undertaken with these spectrometers up to 1.2 THz[36]. The development of such spectrometers for investigations in gas phase and supersonic jets have also been made by the groups discussed above and in a review on "Laboratory Submillimeter-Wave Spectroscopy[37]."

The Texas A&M University submillimeter spectrometer is a frequency and phase stabilized backward wave oscillator (BWO) based instrument. The spectrometer was constructed to take advantage of a fast scanning BWO and a supersonic pulsed jet with a

co-axial configuration of a pulse nozzle expansion with respect to the incident BWO radiation source. Rotational spectra of diatomic molecules or the rovibrational spectra of van der Waals molecules in a supersonic jet expansion have so far been recorded with this instrument.

The backward wave oscillators used as the radiation sources are capable of directly producing radiation from ~ 78-1250 GHz through the use of different versions of the BWO tubes. Each tube covers a specific portion of the submillimeter region of the electromagnetic spectrum. Through the use of specialized high voltage power supplies, where the voltage is stabilized to 1 mV, the frequency of the output radiation of the tube can be changed in a fast frequency scan (2μs per frequency step) by changing the voltage applied to the tube in a suitable manner. A diagram of the spectrometer in the pulsed jet configuration is shown in Figure 2. This spectrometer was designed and constructed to enable measurements in a supersonic jet or alternatively in a static gas cell. As mentioned previously, the supersonic jet configuration of the spectrometer is setup so that the radiation from the BWO tube is overlapped with the supersonic pulse jet in a coaxial manner. The coaxial configuration produces Doppler split components in the observed spectrum which is a consequence of the relative direction and velocity of the molecules with respect to the incident radiation of the BWO tube. This splitting is dependent on the carrier gas, frequency of the radiation and the pressure in the vacuum chamber.

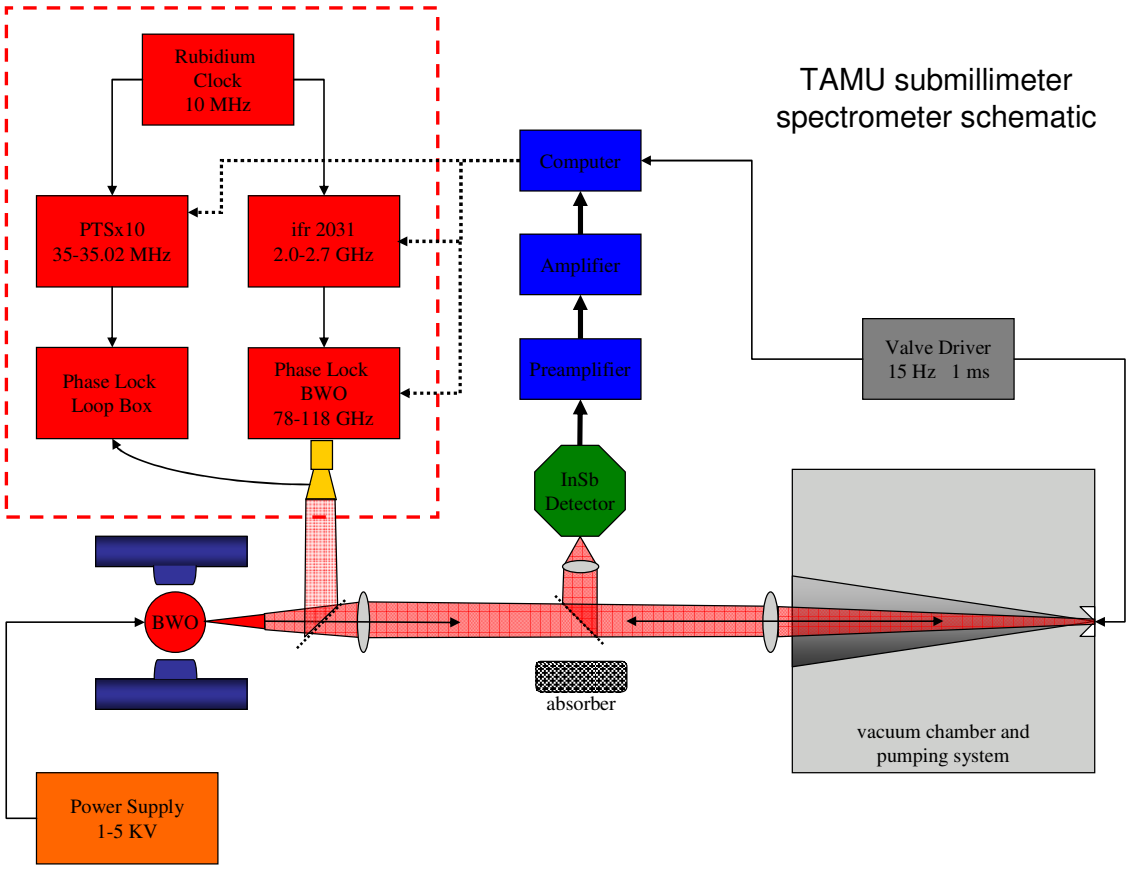

Figure 2. Schematic of the TAMU submillimeter spectrometer.

The BWO source used in the spectrometer can be continuously tuned throughout the operation range of the tube based on the voltage potential applied to the electrons in the tube. The output radiation frequency of the BWO tube is compared to a Rubidium atomic clock (frequency stability 3310^{-11}) through the use of harmonic comparators in the phase lock system[29]. The supersonic jet expansion is used to generate molecular complexes such as those of the homologous series Rg:HX (Rare gas atoms and Hydrogen Halides, HF, HCl, HBr and HI) as well as molecules which have rovibrational transitions or pure rotational spectra of the low rotational transitions in the submillimeter

region. Each major component will be described so that the integrated spectrometer and the operation of the instrument can be discussed.

The Backward Wave Oscillator

The backward-wave oscillator is a source of radiation in the microwave, millimeter or submillimeter regions. A schematic diagram is given in Figure 3 to identify the internal parts of the tube and its operation.

The cathode and filament are placed at a negative potential with a stabilized high voltage power supply which produces a voltage of 1 to 5 KV with a stability of about 1 mV, and operates the filament or heater at a voltage of 6V and current of 1.5A. The filament and cathode are independently biased by the power supply but they have a common reference point, the filament-cathode. The filament heats the cathode creating an electron beam that when placed in a magnetic field propagates over the slow wave structure. An interaction of the electron beam with the electric field of the slow wave structure creates a periodic nature to the electron beam. As the electron beam interacts with the slow wave structure, the electrons initiate a fluctuating electric field which leads to a periodic nature in the electron beam. As the electrons interact they produce photons which make up the output radiation. The frequency of the photons emitted from the BWO tube is dependent on both the velocity of the electrons and the physical size of the slow wave structure period. The velocity of the electron beam is directly dependent on the potential seen by the electron beam. However, as the name implies, the photons are counter propagated to the direction of the electron beam, which emits radiation more

efficiently than the similar transverse wave tube. Each BWO tube has a characteristic period to the slow wave structure which effectively changes the range of frequency of the photons emitted by the tube.

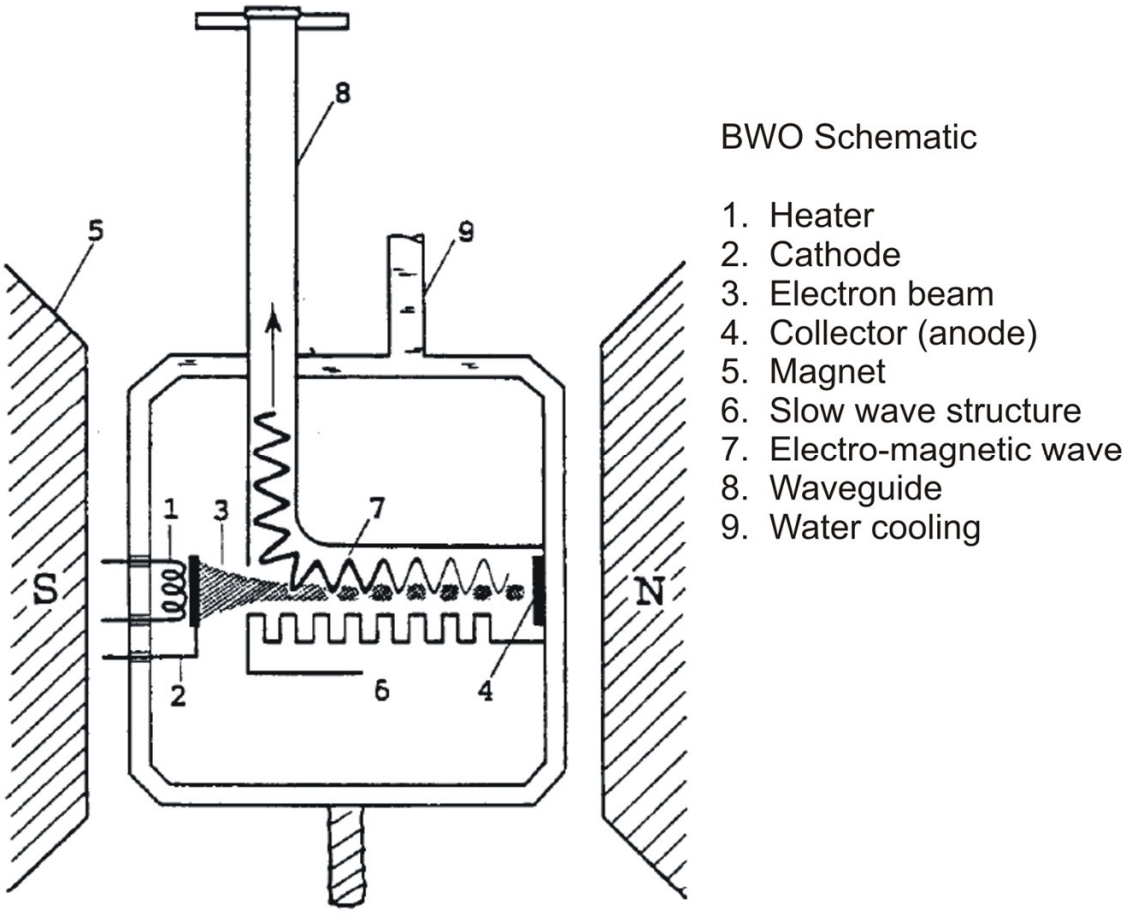

Figure 3. BWO schematic.

Through the use of different tubes, the frequency range of about 70 GHz to 1 THz and higher can be covered. The output power of the BWO ranges from one to tens of milliwatts. Higher frequency tubes produce lower powers (~1 mW) and need a larger

magnetic field (1 Tesla) for their operation as well as greater cooling capacity to keep the tube components at operational temperature without overheating. Each tube is affixed to a positioner, which is needed to orientate the electron beam. This is so that the latter passes along the slow wave structure efficiently to produce the radiation needed. Each positioner has the ability to rotate the BWO on two axes, one in the horizontal plane and one in the vertical plane. The respective tube is also fitted with an oversized waveguide to direct the radiation. The waveguides are corrugated so that they operate over the frequency range of the waveguide and reduce the magnitude of the multimodal characteristics of the output radiation.

Figure 4 depicts the particular BWO tube versions with their identifiers and operational frequency ranges in a log scale.

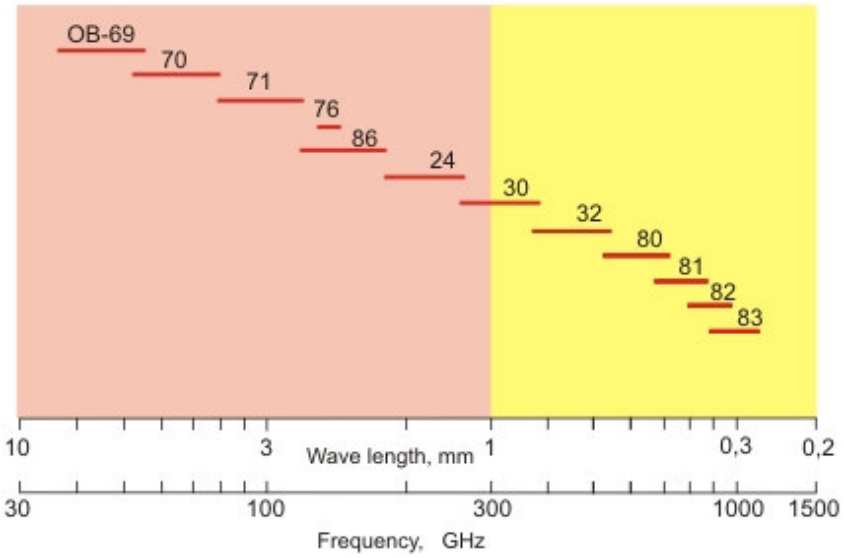

Figure 4. Backward wave oscillator tubes and frequency ranges

Frequency Scanning of the Spectrometer

The BWO frequency can be tuned by application of a variable high voltage from a BWO power supply operating in the range of 1 to 5 KV. This power supply, designed and constructed at the Institute for Physics of Microstructures, Nizhny Novgorod, Russia, has a stability of better than 1 mV at the voltage ranges specified. The output frequency of the BWO is monitored by a phase and frequency stabilization system which is similar to the system described by Winnewisser et al[30]. An intermediate frequency (IF) signal is produced in a quasi-optical broadband harmonic mixer that is driven by the output of the BWO and a millimeter wave synthesizer. The millimeter wave synthesizer (Gas spectrometer (GS)) consists of a phase and frequency locked BWO tube operating between 78-118 GHz. The GS is referenced to an ifr2031 signal generator which has a functional operational frequency range of 2.3 to 2.7 GHz. This signal generator inputs a reference signal into the GS to generate a stabilized frequency that is locked to a harmonic of the reference frequency. This can be calculated by the equation below

$$f_{GS} = N * f_{RF} + 400\text{MHz} \qquad (15)$$

where N is the number of harmonics of the reference signal and f_{RF} is the frequency of the reference signal (between 2.3 and 2.7 GHz). For instance, if the output frequency of the GS is required to be 100.000000 GHz then the harmonic, N, is needed to be 44 and the f_{RF} is then 2263.636364 MHz. 100,000.000 MHz = 44 * 2263.636364 + 400 MHz. The harmonic output of the GS (the radiation which has a frequency harmonic equal to the BWO radiation) is then mixed with the frequency output of the BWO in the harmonic mixer. The harmonic mixer produces the IF signal which is then carried to the

PLL Synchronizer that applies the control signal to the BWO tube changing the output frequency.

The frequency of the IF signal produced in the harmonic mixer, should be 350.2000 MHz. This signal is compared to a 35.0200 MHz signal supplied by a PTSx10 synthesizer (Programmed Test Sources, Inc.) in the PLL circuit. The PLL circuit also uses a 5 MHz signal generated by the Rubidium Atomic clock. If the IF signal from the harmonic mixer matches the input from the PTSx10, then a lock is achieved and the PLL box keeps this state though the control signal. The frequency of the BWO can be described by

$$f_{BWO} = M * f_{GS} - 350.200\text{MHz} \qquad (16)$$

where f_{GS} is the frequency of the Gas Spectrometer (also given by equation 1) and the M is the harmonic needed of the output of the Gas spectrometer. For example, if the frequency of the BWO is needed to be 330.000000 GHz then the M harmonic number should be 3 and the GS frequency should be 110.116733 GHz. The frequency of the GS would be set with f_{RF}=2.4935621 GHz and the 44^{th} harmonic.

Scanning the BWO

The output frequency of the BWO is scanned by changing the reference signal to the PLL system. The PTSx10 synthesizer is capable of a 1 Hz frequency step in 2μs. If the frequency of the PTSx10 is scanned from 35 to 35.1 MHz with a 1 kHz step, it can cover 100 points in 200 μs. This translates to a scan in the BWO of 1 MHz with a 10 kHz step. As the frequency is scanned, the PLL box is able to reference the IF (the

output of the harmonic mixer at 350 MHz) to the reference frequency from the PTSx10 (10^{th} harmonic). If the values are incongruent, then the PLL can apply a control voltage to the BWO tube which changes the output frequency of the BWO radiation. In the small frequency scans that are generally used (1-2 MHz), the BWO control voltage is not generally changed. In the case of initiating broadband scanning, as much as 20 MHz can be covered by using 10 scans with 100 points and a 20 kHz step. This assumes that approximately 75 MHz can be covered with a 1 volt change in the voltage applied to the BWO. To cover 20 MHz, the control voltage is changed by ~250 mV. The phase locked mode ensures that the output frequency of the BWO is directly referenced to the Rubidium atomic clock through the harmonic mixers and comparators in the PLL loop.

The accuracy and stability of the output radiation frequency is dependent on the quality of the atomic clock used as the frequency reference, which is accurate to better than 1 part in 10^{10} for the Rubidium frequency standard used in the frequency and phase stabilization loop.

Supersonic Jet Configuration

Supersonic expansions have been used in spectroscopic applications to effectively prepare molecules with low rotational and vibrational temperatures. There are a variety of supersonic expansions which are in use in the current literature including continuous slit jet, pulsed slit jet and pulsed orifice (pinhole) expansions. A supersonic expansion is produced by the passage of high pressure gas (high density) through a small restriction into high vacuum. The restriction can be either an orifice with diameters from

0.01 to 1 mm or a slit with a distance between two plates of 0.06 to 0.15 mm over a 50 to 100 mm distance. As the gas expands the density decreases as the gas propagates into the vacuum chamber. Collisions that occur in the expansion reduce the temperature by removing rotational energy from molecules through inelastic collisions and increase the translational velocity of the monoatomic carrier gas. The lowest effective temperature of the jet is dependent on the monoatomic gas used as the carrier in the expansion, as well as the pressure differential. The effective translational temperature[38] of the jet can be estimated by using the following equation for an argon carrier

$$T \approx \frac{T_0}{1+5896(P_0 D)^{0.8}}$$

T_0 – temperature of the nozzle (K) (17)

P_0 – stagnation pressure (ATM)

D - diameter of the nozzle (cm)

Given the typical operation parameters of the supersonic jet (P_0=2 ATM, T=298 K and D=0.02 cm) an effective temperature of the jet is about 0.66 K, and the rotational temperature is estimated to be 0.5 to 3K. A slit jet (with continuous operation) has an effective temperature of 8-20 K while an expansion through an orifice with a diameter of 0.5mm produces a temperature of 1-3 K. Miller[39] describes the temperature and pressure of a supersonic expansion of helium through a 0.15 mm orifice to the distance in nozzle diameters from the source. The temperature of the expansion is less than 1K and the pressure is about 3.5 mTorr at a distance of 30 nozzle diameters or about 4.5 mm. The velocity of the molecules in the jet can also be estimated by evaluating the terminal Mach number M_∞ with the nozzle diameter, D (cm), and pressure P_0 (atm).

$$M_{\infty} = 133(P_0 D)^{0.4} \tag{18}$$

For the jet used in the TAMU Spectrometer, the velocity at 1 cm from the face of the nozzle is about 36 Mach number. This estimate of effective velocity also depends on the backing pressure in the chamber and the formation of a Mach disk, or the point at which the supersonic expansion is destroyed. $X_M = 0.67 D \sqrt{\frac{P_0}{P_{Chamber}}}$ gives X_M, the distance of the Mach disk in cm, to the chamber pressure and the stagnation pressure of the expansion (atm), and the nozzle diameter (cm). The Mach disk forms approximately 3 cm from the nozzle. Although the distance at which the supersonic expansion is destroyed seems quite short, the velocity of the jet after the Mach disk is still quite high. We have estimated the velocity to be ~560 m/s from the Doppler components of a molecular transition.

The effective vibrational and rotational temperature of the expansion can be determined by investigation of the processes which take place in the expansion. In the high pressure area of the expansion behind the nozzle orifice, the molecules have the ambient vibrational, rotational and velocity distribution of 300K. The monoatomic carrier gas is in equilibrium with the molecular seed gas. The opening of the valve produces an adiabatic expansion of the molecules through the orifice. The collisions in the expansion produce an energy exchange of the rotational and vibrational energy of the seed molecules to the translational velocity of the monoatomic carrier gas. The rotational and vibrational energy is reduced to an effective temperature of 1K in about 5mm of the nozzle. The expanding gas enters a “zone of silence” or area of the

expansion where the number of collisions between molecules are greatly reduced, and the temperature is minimized[38]. This state is considered a free jet expansion and is an ideal situation in which to study molecules and molecular complexes as the effective temperature is very low and the pressure is only a few mTorr but the density in the free expansion is that of an equivalent pressure of 1-3 Torr.

The spectrometer system can be configured so that a supersonic jet expansion into high vacuum can be used to admit molecules and molecular complexes at low rotational temperature (1.2K) from the collisional cooling achieved in the adiabatic expansion. In order for the expansion to be maintained, a vacuum chamber is used that is pumped by a Varian VHS-400 diffusion pump. The diffusion pump is backed by a WA-251 Roots blower and a Welch 1398 rotary vane pump. The vacuum chamber is a custom-made stainless steel chamber that has been modified to accept polyethylene windows and a pulse valve. The diffusion pump removes the background gases from the vacuum chamber following the actuation of the valve producing the gas pulse. The average pressure when the valve is in operation is about 1.0×10^{-4} Torr.

The pulse valve is a Series 9 solenoid valve (Parker Hannifin, General Valve) with a 500 μm orifice. The valve is affixed to the wall of the vacuum chamber with a turret that allows adjustment of the valve without breaking vacuum. An aluminum rooftop reflector is also positioned to the chamber wall with a spacer so that the valve outlet is directed through the rooftop reflector into the high vacuum region of the vacuum chamber. The valve is typically operated at a pulse rate of 15 Hz with an opening duration of about 1 ms. The gas mixture, which is about 2% of a seed molecule

such as HBr in argon or another noble carrier gas is expanded into the vacuum chamber. This expansion collisionally cools the seed gas from room temperature to an effective rotational temperature of about 1.2 K.

The output radiation of the BWO tube is focused onto the rooftop reflector through the use of polyethylene lenses and wire grid polarizers which act as beam splitters. Due to the sizes of the components, the rooftop reflector and vacuum chamber are on different levels than the output of the BWO tube. A periscope is used so that the radiation beam can be directed along the required optical path into the chamber. The area around the rooftop reflector is blocked by an absorber so that any radiation that does not efficiently interact with the jet, or is not reflected via the rooftop, is removed and is thus not detected.

The BWO radiation is propagated through a wire grid polarizer or beam splitter. A part of the radiation (10-50%) is reflected onto a harmonic mixer for the frequency stabilization, and the remaining polarized portion is transmitted onto the periscope. Following reorientation by the periscope, a lens is used to focus the polarized radiation on the rooftop reflector through a second wire grid polarizer. The second wire grid polarizer allows the radiation to pass into the vacuum chamber and onto the rooftop reflector. The polarization of the radiation reflected by the rooftop undergoes a total rotation of 90° and will not pass through the second wire grid polarizer but is reflected to the detector.

The pulse valve is synchronized so that a gas pulse is admitted into the vacuum chamber, the frequency output of the radiation scanned and a molecular absorption

signal is detected using the liquid helium cooled bolometer. The BWO tube can be scanned at 3.8 μs/step with a step size of 10 Hz to 100 kHz to cover a frequency range of 1 kHz to 10MHz. The signal that is detected by the bolometer is digitized by the computer and stored as a file containing the frequency and amplitude data for later analysis.

Typical operational parameters of the pulse jet are specified by a stagnation pressure of 20-40 psia and pulse duration of about 1 ms. The velocity of the molecules as well as the frequency of the radiation produces a Doppler splitting which is about 1.2 MHz at 340 GHz using argon as the carrier gas. It should be noted here that the base pressure of the vacuum chamber when the valve is not operating is about $2*10^{-6}$ Torr but when the valve is functioning a pressure of $\leq 1.0*10^{-4}$. These parameters are typical for the optimal complex formation with an estimated effective rotational temperature of 1 K.

The observed signal of the molecular transition due to an absorption is recorded with the bolometer and data acquisition system with a computer. In order to remove any frequency shift from the observed Doppler displaced components, the BWO frequency is scanned as a round trip. The round trip consists of a scan from the start frequency down in frequency. The BWO will then be scanned up in frequency from the stopping point. The frequency scan depends on the number of steps and step size used, to give the round trip frequency scan. This effectively makes 2 recordings of the same line in one round trip scan giving a total of 4 measured components, 2 Doppler components for each frequency scan direction, for each specific spectral feature. The frequency of each of the

four signals is then measured and the average taken to determine the frequency of the transition.

Sub-Doppler Saturation Spectroscopy: Lamb-dip Method

Gas phase Doppler-limited spectroscopy is a traditional means of observing molecular transitions at ambient temperatures and reduced pressures. A cell filled with a relatively low pressure (0.1 to 1 Torr) of a gaseous molecular compound is frequently used to record molecular transitions. However, a problem associated with this experiment is attributable to the pressure increasing the observed linewidth, γ, of a transition due to pressure broadening effects. The total line profile is dependent on the natural line width, the Doppler width, and collision or pressure broadening and power broadening. Carbon monoxide has an approximate pressure broadening coefficient of 3.4 MHz/Torr[40]. A spectrum of CO at 1 Torr will have a full width at half maximum of about 3.4 MHz for the J=1←0 self broadened line. The profile of the line is quite broad, making it difficult to determine the exact line center precisely if there are inhomogeneous broadening effects, which produces a non-uniform line profile.

This problem can be overcome by sub-Doppler saturation spectroscopy, or the Lamb-dip method[41]. This method produces a feature in the line profile which reduces the pressure and Doppler broadening effects and has a width that is very close to the natural linewidth of a molecular transition at a frequency corresponding to that of the molecule with zero velocity. Figure 5 shows the Lamb-dip profile which is at the line center for explanation purposes. This effect was initially discovered by Lamb,

Macfarlane and Bennett in 1963. In laser spectroscopy, this technique is a consequence of "the selective saturation of an inhomogeneously broadened molecular transition by optical pumping with a monochromatic tunable laser." In our case, the laser output is replaced with a backward wave oscillator radiation output of sufficient power and with a linewidth less than 1 kHz.

The spectrum of a molecule such as CO can be observed by scanning the frequency of a radiation source through the line where an absorption occurs, such as the J=1←0 rotational transition of CO. The spectrum of this line recorded by traditional means will produce a Lorentzian line profile which has a characteristic line width. The linewidth of the line will be dependent on the major effects that broaden a line, namely pressure, Doppler and saturation broadening. As discussed before, the linewidth of the transitions will be 3.4 MHz at 1 Torr. The Lamb-dip feature is observed by passing a high intensity saturating radiation beam through the cell, one pass will create the Lorentzian profile with characteristic linewidth, but if a part of the radiation is reflected back through the cell as a probe, along nearly the same pathway, utilizing a mirror, the radiation will interact with molecules of the same velocity distribution at the line center.

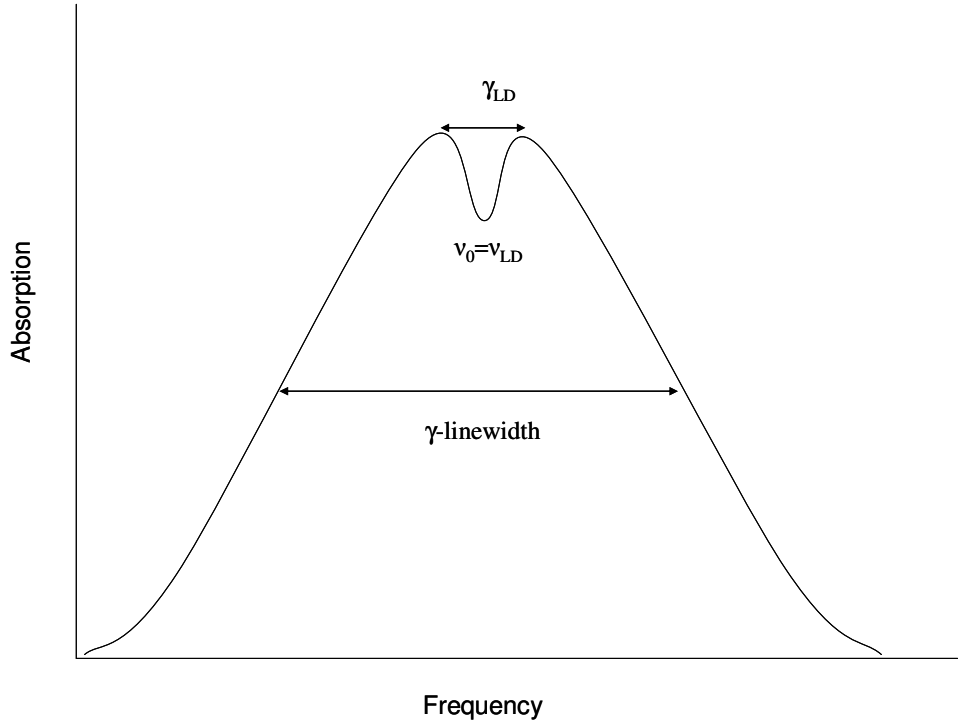

Figure 5. Lamb-dip feature in a Doppler broadened line profile.

The radiation depletes the population of molecules in a given state which have velocity components given by:

$$v_z \pm dv_z = (\omega_0 - \omega \pm \delta\omega)/k$$

ω_0 is the center of the line profile (19)
ω is radiation frequency
v_z is the velocity distribution.

This describes the interaction for the radiation in propagating and counter-propagating directions. The first beam saturates the transitions depleting the equilibrium population of the original transition state that is then probed by the counter propagating weaker beam. If the radiation is resonant with the line center, it effectively doubles the power of radiation that will induce a change in the rotational state of the molecule. The molecules

that are close to zero in the velocity distribution relative to the source will be saturated and will be pumped into the excited state. The population difference due to this absorption is given in the following equation:

$$\Delta N(v_z)dv_z = \Delta N^0(v_z)\times\left[1-\frac{S_0(\gamma/2)^2}{(\omega_0-\omega-kv_s)^2+(\gamma_s/2)^2}-\frac{S_0(\gamma/2)^2}{(\omega_0-\omega+kv_s)^2+(\gamma_s/2)^2}\right]$$

S_0 – saturation parameter
γ,γ_s – linewidth, saturation linewidth
v_z – velocity (20)
kv_s – velocity relative to radiation wave propagation
ω_0 – line center
ω – frequency of radiation

The line profile (see Figure 5) can then be described by:

$$\alpha_s(\omega)=\alpha_0(\omega)\left[1-\frac{S_0}{2}\left(1+\frac{(\gamma_s/2)^2}{(\omega-\omega_0)^2+(\gamma_s/2)^2}\right)\right]$$

$\alpha_0(\omega)$ – Doppler or Lorentzian line profile
S_0 – Saturation parameter (21)
γ_s – Lorentizian width of Lamb dip feature
ω_0 – line center frequency

This is a modification of a Lorentzian or Doppler profile with the small Lamb-dip feature at the line center. The Lamb-dip feature has a line width, γ_S, which is less than the Doppler width of the line profile.

This phenomenon in the submillimeter has been demonstrated to produce very narrow line widths for CO J=4←3 of 40 kHz and 30 kHz for J=6←5 [42]. The Lamb dip feature produced in the line profile is due to the saturation of the absorption of the molecules which are being excited by the radiation.

Spectrometer Frequency Accuracy

The absolute accuracy of frequency measurement for the submillimeter spectrometer can be estimated by direct comparison with literature values of known molecular transition. For this calibration, the molecule $^2H^{79}Br$ was selected as it has a rotational transition at 8.491596446(5) cm^{-1}. This transition is well within the operational range of the OB-30 BWO tube version (200-385 GHz). This molecule has been previously observed in a molecular beam experiment by Dymanus and van Dijk [43]. This work provided very accurate frequencies for the J= 1 ← 0 rotational transition of $^2H^{79}Br$ and $^2H^{81}Br$, with completely resolved deuterium hyperfine structure for most of the transitions. The transitions used were the F=1/2 ← 3/2 bromine quadrupole transition in the J= 1 ← 0 rotational transition of deuterium bromide, $^2H^{79}Br$, with a deuterium hyperfine splitting of the F=1/2 and 3/2 of 4.8 kHz. Using the Lamb-dip method, the TAMU spectrometer was used to determine the frequency of the weighted average of these transitions. The two transitions have an intensity ratio of 2:1 and the weighted average rest frequency is f_D=254571.6577(15) MHz. The radiation was then detected on the bolometer and a lock-in amplifier was used to record the spectrum. Figure 6 shows the recorded spectrum of the J=1 ← 0, F_1',F' ← F_1'',F'' =1/2,3/2;1/2,1/2←3/2;1/2,3/2,5/2 transitions of $^2H^{79}Br$ at 1 mTorr pressure with unresolved deuterium substructure. This spectrum shows the weighted average of the unresolved deuterium hyperfine components which are shown in the simulated spectrum in Figure 7. The observed second derivative line profile has a line width of 19 kHz and the calculated frequency is f_L=254571.6585(5) MHz.

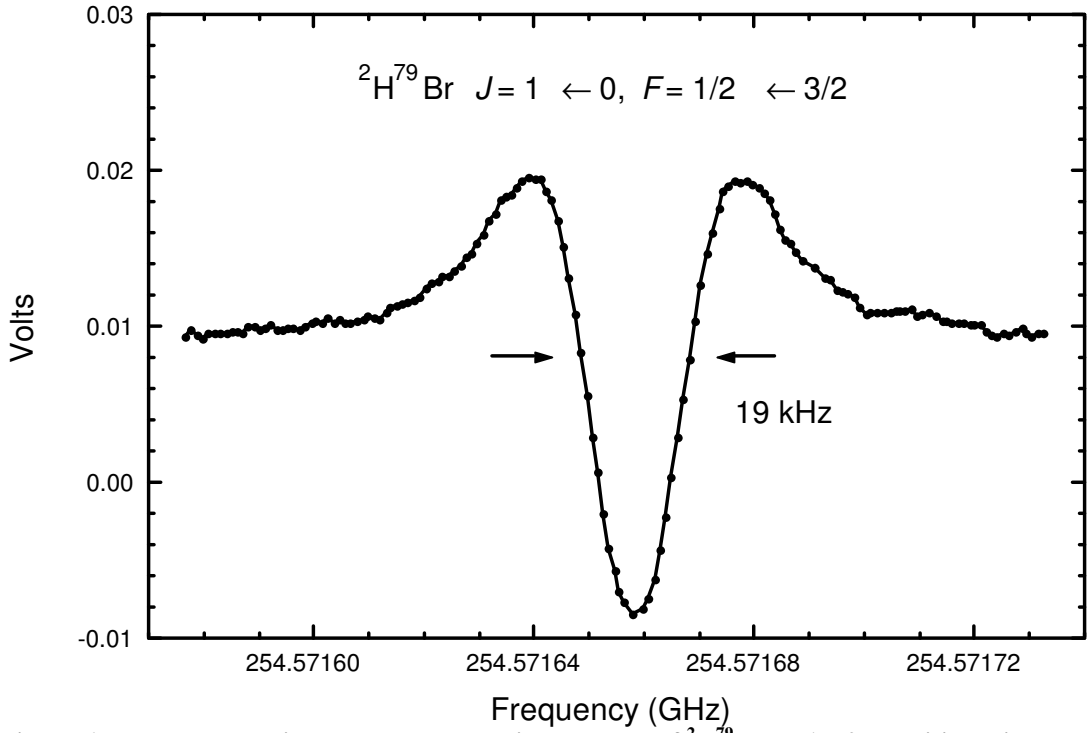

Figure 6. Recorded static gas phase Lamb-dip spectrum of $^2H^{79}Br$ J= 1←0 transition with unresolved deuterium hyperfine F_1',F'←F_1'', F''; 1/2, 3/2;1/2,1/2 ← 3/2; 1/2, 3/2, 5/2 components(254 571.6545(15), 254 571.6593(15) MHz) recorded at 1 mTorr total pressure.

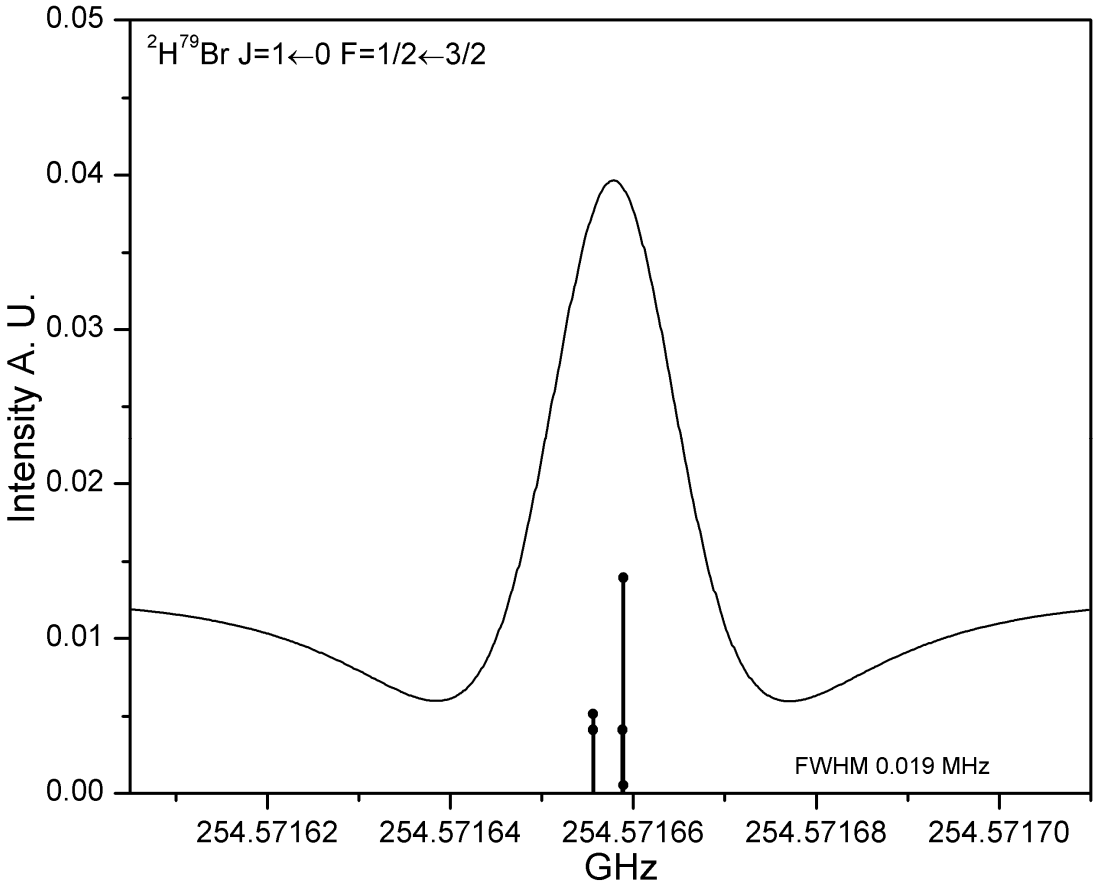

Figure 7. Simulated spectrum second derivative of $^2H^{79}Br$ of the J=1←0 F_1',F'←F_1'', F''; 1/2, 3/2;1/2,1/2 ← 3/2; 1/2, 3/2, 5/2 transitions with deuterium substructure. FWHM 0.019 MHz.

The transition J= 1 ← 0 F=1/2 ← 3/2 of $^2H^{79}Br$ was also recorded in the supersonic jet expansion with the TAMU Spectrometer. The simulated spectrum and the experimentally observed spectrum are shown in Figure 8 and Figure 9 respectively. The comparison of the three methods is given in Table 4. As shown the data recorded in the pulsed jet expansion is shifted from the Lamb-dip method but is within 300 Hz of the molecular beam experiment. The shift in the observed Lamb-dip line frequency is most likely due to residual pressure effects which produce the asymmetric frequency shift of the line position, or other contributions such as optical alignment issues and baseline

aberrations. However these contributions are likely less than 1 kHz in the case of the recorded spectrum of DBr at 1 mTorr pressure. This indicates that the spectrometer should be capable of absolute frequency accuracy better than 1 kHz as determined by the TAMU spectrometer.

Table 4. Comparison of the accuracy of absolute frequency measurement of J=1←0, F=1/2←3/2 transition of $^{2}H^{79}Br$ with the TAMU fast scan submillimeter-wave spectrometer with a coaxial pulsed jet. f_L is the Lamb-dip measured frequency and f_D=254 571.6577(15) MHz is the weighted frequency.

Pulse jet expansion f_0 (MHz)	Static cell f_0-f_L (MHz)	Molecular beam f_0-f_D (MHz)
254 517.6574	-0.0011	-0.0003
254 571.6576	-0.0009	-0.0001
254 571.6581	-0.0004	+0.0004
254 571.6578	-0.0007	+0.0001
254 571.6545(15)[a]		
254 571.6593(15)[a]		

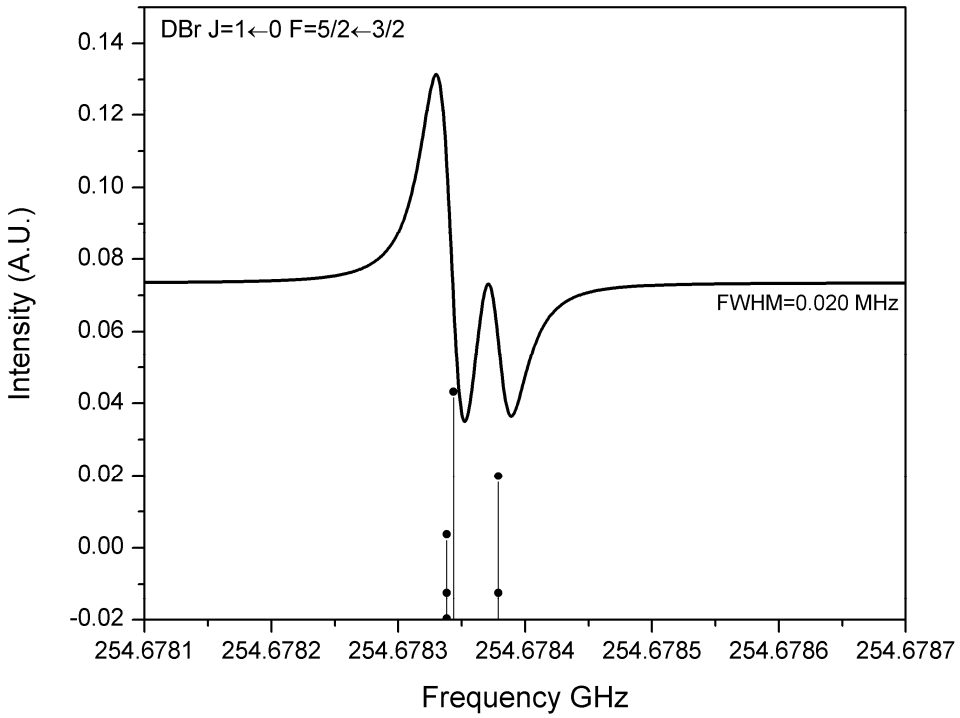

Figure 8. Simulated spectrum of $^{2}H^{79}Br$ J=1←0, F_1',F'← F_1",F"=5/2;3/2,7/2,5/2 ← 3/2;1/2,3/2,5/2 bromine quadrupole transition with deuterium substructure. First derivative spectrum simulated with FWHM 0.020 MHz.

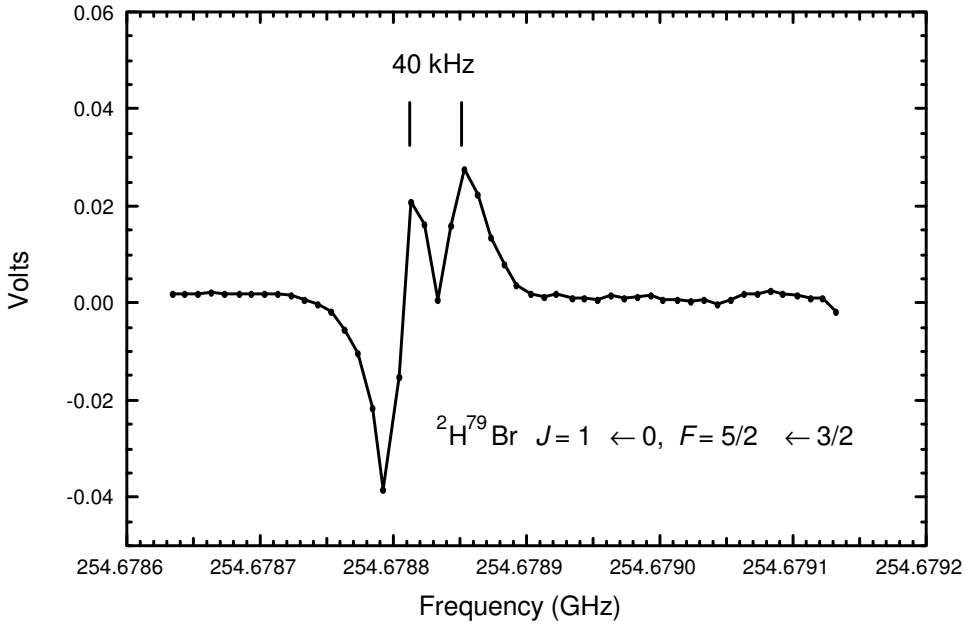

Figure 9. Supersonic jet spectrum of the J=1←0, F_1',F'← F_1",F"=5/2;3/2,7/2,5/2 ← 3/2;1/2,3/2,5/2 quadrupole transition with partially resolved deuterium substructure. Recorded points are separated by 10 kHz.

The estimated accuracy of the TAMU submillimeter spectrometer can be best demonstrated with the direct experimental comparison of combinations of measured frequencies with the state of the art PN-FTMW spectrometer measurements. Ar-HBr is the molecular system that has been recorded with the highest degree of accuracy by both methods. The spectroscopic analysis of Ar-HBr will be the subject of the next chapter.

Ar-HBr was measured with a PN-FTMW spectrometer with an estimated absolute frequency accuracy of 200 Hz. The spectrometer is referenced to a GPS frequency standard with a frequency accuracy of 1 part in 10^{12}. A low frequency vibration of Ar-HBr has also been observed in the submillimeter frequency range. Direct comparison of the measured submillimeter wave and microwave frequencies is made through a series of 24 combinations of frequency transitions with corresponding

sum frequencies. The combinations are determined by the comparison of the sum of two rotational transitions from the microwave and the difference of two rovibrational transitions in the submillimeter spectroscopic investigation.

Table 5 lists the combination differences between the submillimeter data and the PN-FTMW for transitions associated with the combinations such as shown in Figure 10. The observed differences are determined by $\lfloor f_{R(J,F)} - f_{P(J+2,F+2)} \rfloor - \lfloor f_{(J,F)} + f_{(J+1,F+1)} \rfloor$ where the R and P transitions are from the submillimeter data are displayed in the first term and the second term is the combination of two transitions in the microwave. The final column showing the difference between the microwave and submillimeter methods has an RMS deviation of ~370 Hz. The majority of the combination differences have a difference of less than 1 kHz, thus giving strong evidence that the accuracy and precision of the frequency measurement of the submillimeter spectrometer is conservatively estimated to be less than 1 kHz.

Table 5. Combination frequency differences of submillimeter-wave and microwave transitions for Ar:H^{79}Br and Ar:H^{81}Br. All transition frequencies are in units of MHz.

J,F	Microwave Data $f_{(J,F)}$[a]	$f_{(J+1,F+1)}$	$f_{(J,F)} + f_{(J+1,F+1)}$	Submillimeter Data $f_{R(J,F)}$[b]	$f_{P(J+2,F+2)}$[c]	$f_{R(J,F)} - f_{P(J+2,F+2)}$	Difference[d]
Ar:H^{79}Br							
$2,\frac{1}{2}$	6647.38485	8853.86864	15501.25349	337798.3503	322297.0960	15501.2543	0.00081
$2,\frac{3}{2}$	6647.23095	8853.85453	15501.08548	337820.0836	322318.9970	15501.0866	0.00112
$2,\frac{5}{2}$	6636.64188	8848.89459	15485.53647	337819.4418	322333.9053	15485.5365	0.00003
$2,\frac{7}{2}$	6636.63578	8848.87148	15485.50726	337797.6296	322312.1230	15485.5066	-0.00066
$3,\frac{3}{2}$	8853.86864	11062.52265	19916.39129	341044.6861	321128.2946	19916.3915	0.00021
$3,\frac{5}{2}$	8853.85453	11062.54665	19916.40118	341066.4112	321150.0103	19916.4009	-0.00028
$3,\frac{7}{2}$	8848.89459	11059.61550	19908.51009	341068.9003	321160.3902	19908.5101	0.00001
$3,\frac{9}{2}$	8848.87148	11059.57871	19908.45019	341047.1800	321138.7307	19908.4493	-0.00089
$4,\frac{5}{2}$	11062.52265	13270.60769	24333.13034	344551.8020	320218.6725	24333.1295	-0.00084
$4,\frac{7}{2}$	11062.54665	13270.65077	24333.19742	344573.4231	320240.2263	24333.1968	-0.00062
$4,\frac{9}{2}$	11059.61550	13268.69975	24328.31525	344576.4543	320248.1391	24328.3152	-0.00005
$4,\frac{11}{2}$	11059.57871	13268.65213	24328.23084	344554.8511	320226.6206	24328.2305	-0.00034

Table 5. (continued)

J,F	Microwave Data $f_{(J,F)}$[a]	$f_{(J+1,F+1)}$	$f_{(J,F)} + f_{(J+1,F+1)}$	Submillimeter Data $f_{R(J,F)}$[b]	$f_{P(J+2,F+2)}$[c]	$f_{R(J,F)} - f_{P(J+2,F+2)}$	Difference[d]
Ar:H^{81}Br							
2, $\frac{1}{2}$	6591.43430	8780.60063	15372.03493	337352.9207	321980.8838	15372.0369	0.00197
2, $\frac{3}{2}$	6591.32966	8780.59531	15371.92497	337371.0415	321999.1158	15371.9257	0.00073
2, $\frac{5}{2}$	6582.45982	8776.44197	15358.90179	337370.4929	322011.5889	15358.9040	0.00221
2, $\frac{7}{2}$	6582.45370	8776.42108	15358.87478	337352.3195	321993.4448	15358.8747	-0.00008
3, $\frac{3}{2}$	8780.60063	10971.39779	19751.99842	340577.2026	320825.2034	19751.9992	0.00078
3, $\frac{5}{2}$	8780.59531	10971.42045	19752.01576	340595.3066	320843.2911	19752.0155	-0.00026
3, $\frac{7}{2}$	8776.44197	10968.96606	19745.40803	340597.3825	320851.9751	19745.4074	-0.00063
3, $\frac{9}{2}$	8776.42108	10968.93484	19745.35592	340579.2856	320833.9299	19745.3557	-0.00022
4, $\frac{5}{2}$	10971.39779	13161.50034	24132.89813	344060.7539	319927.8561	24132.8978	-0.00033
4, $\frac{7}{2}$	10971.42045	13161.53718	24132.95763	344078.7711	319945.8133	24132.9578	0.00017
4, $\frac{9}{2}$	10968.96606	13159.90410	24128.87016	344081.3036	319952.4333	24128.8703	0.00014
4, $\frac{11}{2}$	10968.93484	13159.86411	24128.79895	344063.3031	319934.5048	24128.7983	-0.00065

[a] Measured frequency of microwave transitions $\Delta J=+1$ $\Delta F=+1$.

[b] Measured frequency of rovibrational transitions with $\Delta J=+1$ $\Delta F=+1$

[c] Measured frequency of rovibrational transitions with $\Delta J=-1$ $\Delta F=-1$

[d] The difference is $[f_{R(J,F)} - f_{P(J+2,F+2)}] - [f_{(J,F)} + f_{(J+1,F+1)}]$

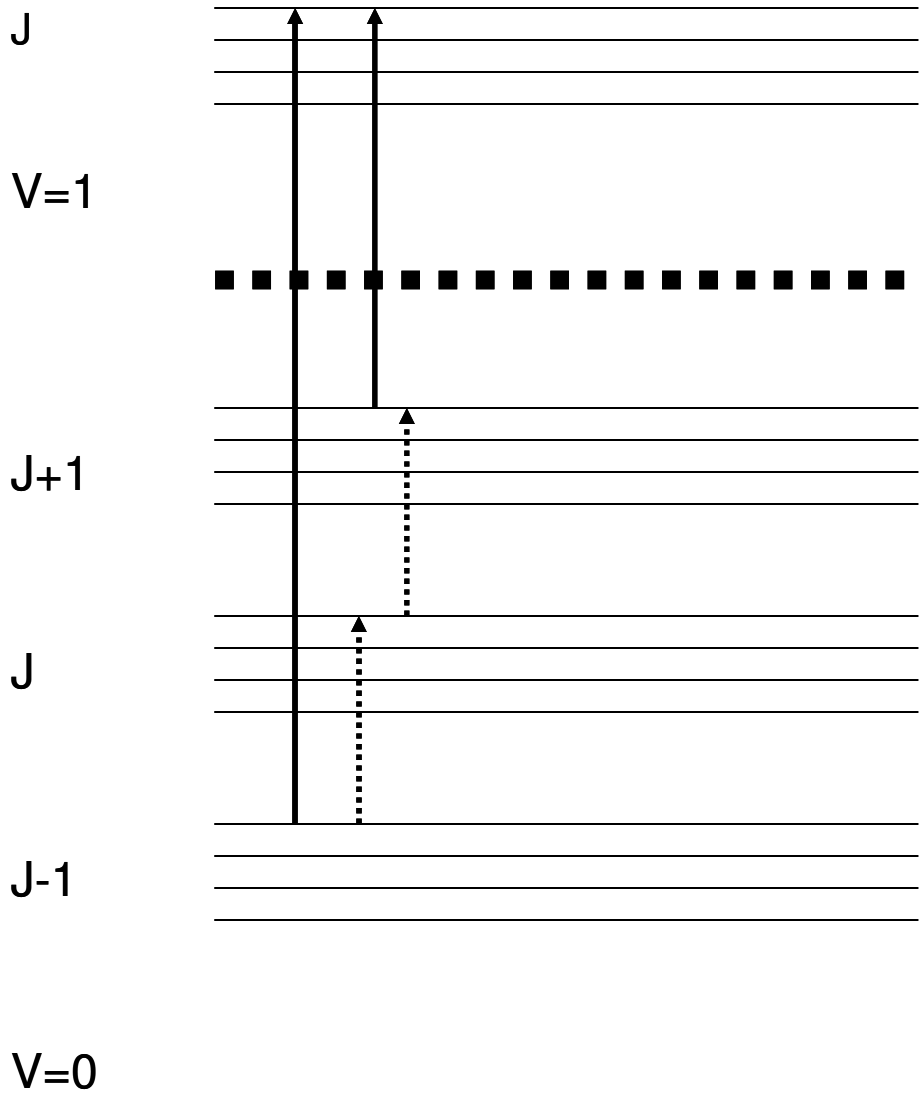

Figure 10. Energy level diagram showing the combinations for submillimeter and PN-FTMW frequencies.

Conclusion

A description of the TAMU submillimeter spectrometer has been given to relate the operation of the spectrometer as well as the experimental capabilities achieved with the co-axial configuration. Characteristic line widths of 40 kHz have also been

demonstrated in the first derivative spectra of DBr, indicating the potential resolution of this technique. The frequency scanning of the backward wave oscillator tube and the manner in which the phase and frequency stabilization electronics work has been presented and discussed in detail. The determination of the frequency accuracy of the spectrometer and its other characteristics has been demonstrated through experimental observations of ^{2}HBr and Ar-HBr. The state-of-the-art PN-FTMW spectrometer has been used to provide energy differences of Ar-HBr which when compared with experimental data using the TAMU submillimeter spectrometer. The absolute frequency accuracy of the TAMU submillimeter spectrometer is determined to be 370 Hz at 330 GHz.

CHAPTER III

RG:HX SPECTROSCOPY AND THEORY

There has been significant interest in the study and characterization of the prototypical molecular complex Rg:HX where Rg is a rare gas (Ne, Ar and Kr) and HX is a hydrogen halide (HF, HCl, HBr, HI). This class of complex is ideal for the study of the properties and dynamics of the intermolecular non-covalent bonding of molecules. This is not only from an experimental point of view but also from the perspective of quantum chemical calculations, as the three atom system provides one of the simplest manifestations of intermolecular interactions.

There is a considerable amount of experimental data determined for certain members of the Rg:HX system which is available in the literature. Some of the major work in this area has been presented in a bibliographic form and is available online[8]. It would therefore be quite difficult to present all of the work on Rg:HX in a meaningful manner here, and this is not the purpose of this work. However, there are a variety of reviews[5, 8, 25, 44-50] available that can be consulted on the matter that relates the experimental and theoretical observations for such complexes.

As shown in Table 1, the complexes that are formed from a hydrogen halide diatomic molecule and a rare gas atom may have different ground state and equilibrium structures. The molecules also have proven to be some of the most fundamental of intermolecular interactions that can be studied directly by experimental techniques such as microwave and infrared spectroscopy. The supersonic jet expansions used in the

experimental techniques allow the study of molecular complexes without the many body effects present in condensed phases or high pressure multi-component mixtures.

Microwave spectroscopy, in particular, has been used to study these complexes in great detail. Techniques such as molecular beam electric resonance and pulsed nozzle Fourier transform microwave spectroscopy have been most widely applied for the determination of very accurate structural parameters in the ground state of such complexes as Ar-HCl[51, 52], Ar-HF[53] and Ar-HBr[24] to name a few associated with the Rg:HX series. Some predictions can be made on the relative energy of intermolecular modes through the analysis of the data generated with these techniques, such as the stretching vibrations of the van der Waals bond.

Infrared spectroscopy has also been used to observe intramolecular vibrations, by the excitation of the diatomic molecule in the complex, as well as the associated combination bands and overtone spectra that give information about the complex not able to be determined in the microwave analysis. Accurate rotational constants can be determined by the observation and fitting of a large range of rotational levels. Additionally, the relative energies of vibrations can be calculated through combination differences. Furthermore, as infrared spectroscopy generally lacks the resolution to observe the quadrupole hyperfine structure of a transition, the exact structure can only be inferred through the rotation constants. However, in special cases, such as low *J* rotational transitions or complexes with an atom having a quadrupole coupling constant of large magnitude (Ar-HCl[54], Ar-HBr[55] and Ar-HI[56]) the quadrupole structure can be somewhat resolved. These points give some of the limitations of the different

techniques and justify the use of different methods to investigate the Rg:HX systems further.

There have been a few applications of submillimeter and terahertz spectroscopy to supersonic jets for the observation of van der Waals complexes. The groups at The Ohio State University used BWO based spectrometers to observe complexes such as Ar-CO and Ar-ND_3[57]. Winnewisser and his group at Cologne have also observed the Ar-CO complex[58, 59]. The complexes Kr-CO and Xe-CO have also been observed in the millimeter region with BWO based spectrometers by McKellar[34]. Some other types of spectroscopy in the submillimeter have been done for Rg:HX van der Waals complexes. Leopold has observed the high frequency bend in Ar-HBr[60] by far infrared difference spectroscopy using MIM diodes while Saykally, using laser sideband generation, has observed fundamental stretching vibration, ν_3, and the low frequency Σ bending vibration, ν_2, of Ar-HCl[61-63].

Ab initio calculations have also been used to study the dynamics of the Rg:HX complex. The development of computers and programs that have the ability to perform very complex calculations in a short period of time with the development of larger basis sets have made modeling of complexes such as these almost routine. However, as the interaction is quite weak these calculations are generally unable to reproduce the spectroscopic parameters to any degree of certainty, due to the approximations used in the quantum calculations. It is the goal of a collaboration with the Lucchese Group at Texas A&M University to overcome such limitations. The development of a new methodology, the combination of ab initio potential energy surfaces with experimental

data, to generate a morphed potential energy surface would be a major scientific achievement. The morphed potential energy surfaces should not only be able to reproduce the experimental data but also predict to almost experimental accuracy other observables, such as bending vibrations or structure in different vibrational states. This methodology has been introduced at almost the same time by two different groups [56, 64].

The interaction between the atom of a rare gas and the diatomic hydrogen halide is dominated by the dispersion forces and the dipole-induced dipole force. It is apparent in the Rg:HX class of complexes that the magnitude of these forces changes as the character of different substituted atoms, such as Ne and Kr for Ar with differing polarizibility. Furthermore, component molecules, HCl, HBr and HI have different dipole moments, providing an informative comparison of their properties in this homologous series. Through the different effects that each atom or molecule contributes in a complex, fundamental information is determined, that can be incorporated into the fundamental models developed for characterizing the intermolecular interaction and bonding.

Ar-HBr

Ar-HBr is a molecular complex that has been studied by several currently available experimental spectroscopic techniques (microwave, infrared and submillimeter methods), and these will be summarized in the following introduction. The information that is available on the ground state hydrogen bound isomer of Ar-HBr is quite large,

and specific data on the hydrogen bound isomer as well information about the van der Waals form will be presented in the following pages.

The ground state is characterized by a hydrogen bound structure with the proton between the Br nucleus of the monomer component and the argon atom. The structural parameters of this isomer have been determined and the R_{CM} distance and the angle of the interaction have been calculated. The determination of the structure of the complex will be a central theme in the following discussion. Infrared spectroscopy has been used to determine accurate band origin frequencies and energy manifolds associated with the intermolecular vibrations of the complex through combination bands with the fundamental HBr stretching vibration. The ground state microwave spectrum of the deuterated complex Ar-DBr has also been observed and the structure determined[23, 24].

Computational methodologies[65] involving intermolecular interactions have been an area of active development in our group and others. Specifically, they have been used to generate potential energy surfaces which can then be used to predict properties that can be experimentally observed. Comparison of the predicted values of the molecular parameters such as quadrupole coupling constants (more directly the angle of interaction), rotation distortion constants (measure of the curvature of the well), and dissociation energy can be made with experimentally determined values. On the theory side issues have included fundamental questions with regard to the validity and accuracy of potential energy surfaces. The morphed potentials are based on ab initio calculation and semi-emperical expansions[56, 64] to fit the experimental data. The observation of

experimental data is needed so that the quality of the morphed potentials can be evaluated and additional information can be incorporated into the morphed potentials.

The deuterated complex Ar-DBr has not previously been the subject of the considerable attention given to the Ar-HBr complex. The high resolution studies of Ar-DBr in the microwave[23, 24] providing very accurate structural parameters but does not address the large amplitude motion associated with the first excited Σ vibrational state. The van der Waals isomer associated with excited bending state, Ar-BrD, samples a different portion of the potential around the second minima of the van der Waals form, a very significant factor in quantitative evaluation of model potentials. Experimental observations of this isomer can be compared with the morphed potential energy surface generated using the previously observed infrared and microwave data of the Ar-HBr complex.

The TAMU submillimeter spectrometer has been used to make observations that will aide in the evaluation of the validity of a morphed potential energy surface generated from previously available data[65]. The TAMU Spectrometer has been used to observe the Σ-bending vibration of Ar:HBr, the associated deuterated complex, Ar:DBr, as well as the excited intramolecular stretching vibration of HBr. The experimental data for each of these complexes will then be included to generate a fully converged 3D potential energy surface capable of predicting experimental observables with near experimental accuracy.

Introduction

Evidence for the existence of the molecular complex of HBr with a rare gas was first observed by Rank, Rao and Wiggins using a grating infrared spectrometer with a high pressure static gas phase sample in a cell. Transitions in the complex were observed in the null gap of HBr monomer and was considered to be associated with the molecular complex Ar-HBr[66]. The evidence for the existence of the complex was the changing position of the observed band with the addition of different gases such as Kr and Ne. Flygare and coworkers also investigated HBr dimer in rare gas matricies but reported no transitions which could be assigned as Ar-HBr[67, 68].

One of the first reports in the literature of a high resolution study of Ar:HBr was the radiofrequency and microwave spectroscopy using Molecular Beam Electric Resonance (MBER) by Jackson and coworkers[24]. This experimental technique which was introduced for spectroscopic studies of molecular complexes by Klemperer and co-workers[51-53, 69]. Using this method, experimental data was observed that allowed the structure of the complex to be estimated. The center of mass interaction distances and the angle of the monomer to the major axis of the complex were determined. On the basis of these studies, it was concluded that the ground state structure of the molecular complex was hydrogen bound with a vibrationally averaged structure of 42.11° with an internuclear distance of 4.1331Å.

Molecular Beam Electric Resonance Spectroscopy

The Molecular Beam Electric Resonance method has been described as "…a technique where a transition or transitions are induced between energy levels of a linear

rotor in an electric field by a superimposed radiofrequency field"[70]. Figure 11 depicts such a spectrometer as was described by Lee and co-workers[71]. In general, this spectrometer is made up of a source of molecules (a molecular beam), a detector (magnet sector mass spectrometer) and electric fields with an interaction region for radiofrequency, microwave radiation or a static electric field. The source of the Ar:HBr molecular complex in this work was an expansion of 2% HBr in and argon carrier through a 500 micron orifice. The backing pressure is typically 600-800 Torr.

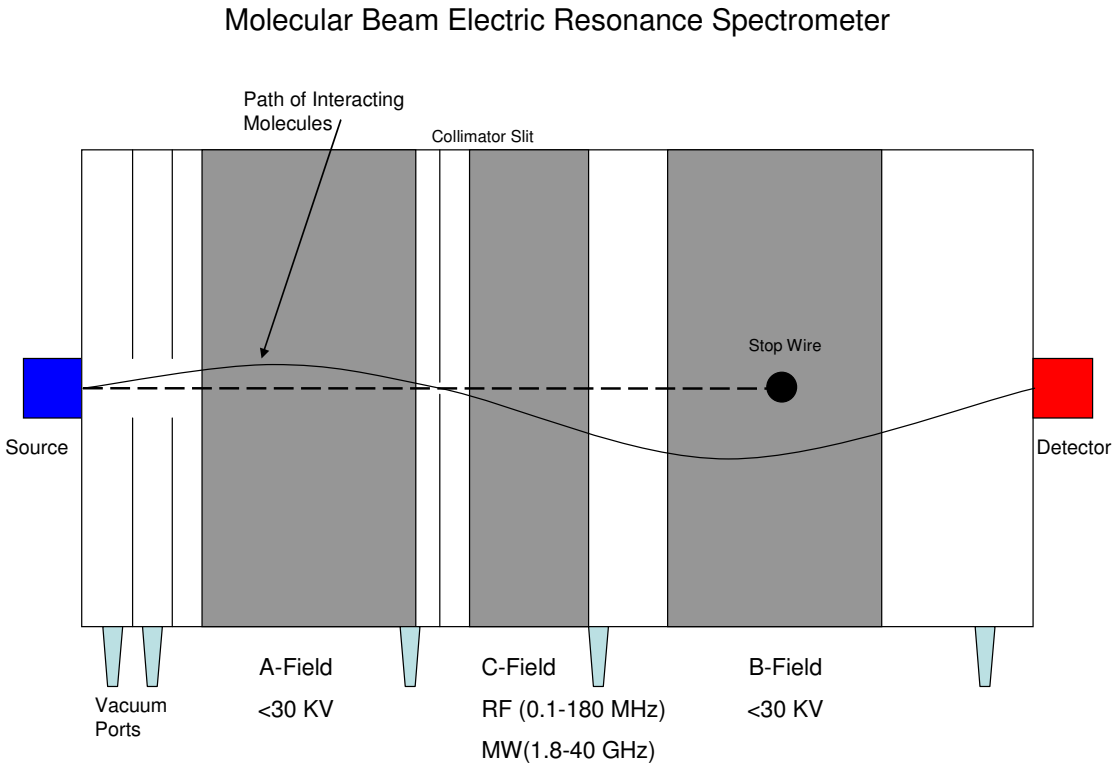

Figure 11. MBER Spectrometer.

As the molecules travel through the electric field regions in the spectrometer, their path is diverted by the Stark effect and travel through collimators on a non-linear path. Application of a microwave, radiofrequency or electric field in the C-Field region induces a change in the energy state of the molecule. This state of the complex is then focused by the following B-Field and the complex is diverted into the mass spectrometer for detection.

The radiofrequency source operated from 0.1 to 180 MHz, while the microwave radiation was supplied by solid state oscillators or klystrons operating from 1.8 to 40 GHz. The frequency of the microwave sources was referenced to a frequency counter (accuracy of 1 part in 10^8). The excited state of the complex was focused to the detector, a Weiss type electron bombardment ionizer with a 60° magnetic mass analyzer and electron multiplier, where the parent peak $(Ar:HBr)^+$ is monitored.

Microwave (ΔJ=1,ΔM_J=0) and radiofrequency Stark transitions (ΔJ=0,ΔM_J=1) were measured for the 4 isotopomers of Ar:DBr. Figure 10 depicts the transitions associated with the measured pure rotational microwave transitions for Ar:HBr which are given in Table 6. The associated quantum numbers, *J* and *F* for the lower and upper states of the complex are given to identify the states used to determine the energy between said states. The error in the frequency measurement was estimated to be 0.4-3kHz.

The transitions of the deuterated species Ar-DBr were also measured using this technique and are given in Table 7. The spectra associated with the isotopomer are more complex as there are two nuclei with quadrupole moments which split the rotational

levels into different states. The transitions of Ar-DBr are given in Table 7, the hypothetical line center is the center frequency of the bromine quadrupole transition with the D quadrupole substructure neglected. The small splitting in the deuterium substructure was averaged so that the bromine quadrupole structure could be fitted with an equation that only has contributions for the bromine splitting.

Table 6. MBER microwave transition frequencies of Ar-HBr.

				$Ar:H^{79}Br$	$Ar:H^{81}Br$
J'	F'	J''	F''	Frequency/MHz	Frequency/MHz
0	3/2	1	3/2	2248.1656(15)	2224.2380(15)
2	1/2	1	3/2	4348.3588(10)	4324.7841(6)
2	3/2	1	3/2	4391.9761(15)	4361.2086(30)
1	3/2	2	5/2	4422.5891(20)	4386.8415(15)
1	5/2	2	5/2	4466.0015(15)	4423.1220(20)
3	5/2	2	5/2	6616.6202(4)	6565.6949(30)
3	7/2	2	5/2	6636.6414(25)	6582.4608(4)

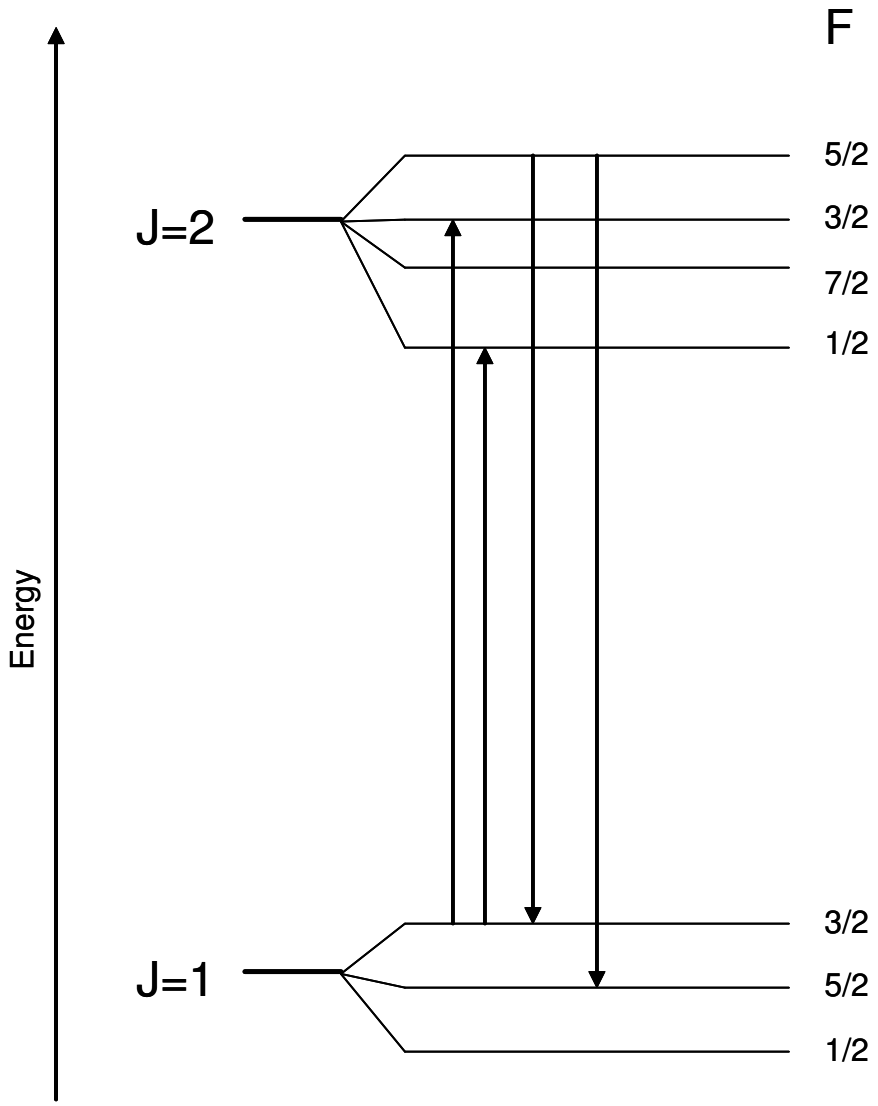

Figure 12. Energy level diagram showing bromine quadrupole transitions in Ar-HBr observed by MBER Spectroscopy.

Table 7. MBER transition frequencies of Ar:DBr

Transition					$ArD^{79}Br$		$ArD^{81}Br$	
Final State		Initial State						
J'	F'	J''	F''	F'-F	Frequency/MHz	Hypothetical Center/MHz	Frequency/MHz	Hypothetical Center/MHz
				5/2-3/2,3/2-3/2				
0	3/2	1	3/2	1/2-3/2	2230.79376	2230.80515(40)	2203.72517	2203.73642(40)
				5/2-5/2,3/2-5/2	2230.80697		2203.73806	
				3/2-1/2,1/2-1/2	2230.82223		2203.75369	
2	1/2	1	3/2	3/2-1/2,1/2-1/2	4225.57448	4225.59095(60)	4210.28112	4210.29750(50)
				3/2-5/2	4225.58791		4210.29444	
				3/2-3/2,1/2-3/2	4225.60295		4210.30927	
2	3/2	1	3/2	3/2-1/2,1/2-1/2	4295.38639	4295.40186(60)		4268.5506(40)
				5/2-5/2,3/2-5/2	4295.39954		4268.54854	
				5/2-3/2,3/2-3/2				
				1/2-3/2	4295.41358		4268.56241	
1	3/2	2	5/2	1/2-3/2				4309.17016(50)
				5/2-3/2,5/2-7/2	4343.85403	4343.85938(40)	4309.16525	
				5/2-5/2,3/2-3/2	4343.86505		4309.1759	
				3/2-5/2	4343.87684		4309.18795	
1	5/2	2	5/2			4413.1855(30)		4367.0809(30)
3	3/2	2	5/2			6419.8182(50)		
3	5/2	2	5/2					6441.3634(50)
3	7/2	2	5/2			6520.38754(50)		6467.9301(50)

Pulsed Nozzle Fourier Transform Microwave Spectroscopy

Pulsed-nozzle Fourier-transform microwave spectroscopy is another microwave technique that has been used to observe rotational transitions in Ar:HBr [23]. Pulsed-nozzle Fourier transform microwave spectroscopy (PN-FTMW) has been widely used and has become recognized as the preferred method to determine the structural parameters of molecules such as van der Waals complexes and other small molecules. There have also been a number of review articles in the literature that involve this technique[5, 72]. Of particular note, has been the continued improvement in resolution, range of frequency operation and sensitivity of this technique since its introduction. The first spectrometer had a resolution of about 10 kHz and frequency accuracy of about 5 kHz. Now the state of the art instruments are capable of frequency accuracy of 200 Hz and a resolution of 1.5 kHz.

The initial observation of the 4 isotopomers in the Ar:HBr complex using PN-FTMW spectrometer by Flygare and co-workers sampled a different range of rotational levels than were observed with the MBER study. Rotational transitions of the J=4←3 and J=5←4 was observed with resolved bromine quadrupole structure for Ar-H^{79}Br, Ar-H^{81}Br, Ar-D^{79}Br and Ar-D^{81}Br.

The PN-FTMW technique as described below was used to observe the pure rotational spectra of 4 isotopomers of Ar:HBr[23]. In a collaboration with Anthony Legon and his group, then at University of Exeter, state-of-the-art measurements of Ar:HBr were made and will be discussed in detail later. The spectrometer and experimental applications had been described previously [22, 73] for experiments with Kr:HCl. The Ar-

HBr complex was remeasured for two reasons. First, the original PN-FTMW data on the complex did not resolve the hydrogen hyperfine structure in the complex due to a lack of resolution. Additionally, the data that was generated lacked diversity in rotational transitions which limited the accuracy of the determined rotation distortion constants. In the previous work, the authors assumed that the global minimum was that of Ar-HBr, which is conflicting with the more recent results from the analysis of the infrared data[55].

In general, the PN-FTMW spectrometer is made up of basic components which include a supersonic pulse valve, microwave oscillators and mixers, and a Fabry-Perot cavity. The Fabry-Perot cavity is housed in a vacuum chamber pumped by a diffusion pump. The mirrors of the cavity are made of highly polished aluminum and are about 30-50 cm in diameter. This gives a large Q factor for the reflection of the microwave radiation ($Q \sim 10^4$). The pulse valve can be positioned orthogonally to the cavity so that the jet is directed into the throat of the diffusion pump. Another configuration may also be used if the valve is attached to the mirror and the supersonic jet is propagated coaxially to the cavity to increase resolution by a factor of 2 as in other designs[74, 75]. The co-axial configuration is used in the studies of Ar-HBr.

The source of the microwave radiation is an oscillator operating at a frequency, ν. The output of this oscillator is mixed with a radiofrequency source typically operating at 30 MHz. The radiation is used to impose a macroscopic polarization to the molecules in the supersonic jet in the center of the cavity. After polarization is achieved the microwave source is switched off and the decay in the emission of the molecules is digitized and collected for application of the Fourier transformation from time domain to

frequency domain. Typically, the bandwidth of the Fabry-Perot cavity is about 1 MHz. This makes it difficult to scan large regions of the range of the spectrometer (4-26 GHz typically) without having automated tuning for the cavity.

Far Infrared Spectroscopy

Π bending transitions in Ar-HBr have also been observed using a MIM diode spectrometer[60]. This study provided experimental data of the bending energy of the Ar-$H^{79}Br$ and Ar-$H^{81}Br$ isotopomers, as well as the Π excited state rotational and quadrupole coupling constants. The Π bending state lies 26.665635(4)cm^{-1} and 26.665284(4)cm^{-1} above the ground state for the $ArH^{79}Br$ and $ArH^{81}Br$ isotopomers respectively. However, only the Q branch of this spectrum was assigned as the authors stated that there was significant perturbation in the R(0) and P(1) branches of the spectrum. They were unable to assign the transitions due to Coriolis interactions between the Σ bending state and Π state. The assignment of the spectra was later determined to be shifted by B_f by the infrared analysis[55].

Infrared Spectroscopy

Infrared intramolecular vibrations and intermolecular combination bands have been observed using a lead salt diode high frequency supersonic slit jet spectrometer[55]. The transitions associated with the infrared HBr stretching vibration include the fundamental ν_1, combinations $\nu_1+2\nu_2^0$, $\nu_1+\nu_2^1$, $\nu_1+\nu_3$, $\nu_1+2\nu_2^0+\nu_3$, hot band $\nu_1+2\nu_2^0-2\nu_2^0$, and difference band $\nu_1-2\nu_2^0$ for both isotopomers of HBr. The bands involving the $2\nu_2^0$ state have direct information about the potential in the area of the local minimum of Ar-

BrH isomer. The $2\nu_2^0$ band is associated directly with the isomerization of the complex from hydrogen bound to van der Waals via the Σ bending vibration. The rotational constants and the energy difference between the 00^00 and 02^00 states are given in Table 8. The constants associated with the other bands are available in the previous reference[55].

Table 8. Selected Ar:HBr infrared spectroscopic constants for Σ bending vibration.

	Ar:H^{79}Br		Ar:H^{81}Br	
	00^00	02^00	00^00	02^00
ν_v cm^{-1}		10.99487(13)		10.98270(13)
$B_v/10^{-2}$ cm^{-1}	3.69145214(57)[a]	4.12391(13)	3.66113643(50)[a]	4.09164(15)
$D_v/10^{-7}$ cm^{-1}	4.1352(13)[a]	4.103(44)	4.0782(10)[a]	4.061(52)
$H_v/10^{-10}$ cm^{-1}	0.461(10)	-0.790(39)	0.4499(99)	-0.782(48)
$L_v/10^{-14}$ cm^{-1}	-1.012(59)		-0.979(57)	

[a] Fixed to Microwave Values [23]

The infrared study provided an accurate estimate of the Σ bending vibration in both the ArH^{79}Br and ArH^{81}Br isotopomers, which could then be compared with the best potential energy surface available at the time[47], the H4 potential. This potential predicts the Σ bending vibration to be 10.8 cm^{-1} which is in reasonable agreement with the combination difference value of 10.98270(13) cm^{-1} for Ar-H^{79}Br subsequently determined from the infrared combination band. As discussed previously, it was necessary that the Q-branch of the Π bending transition observed by Firth[60] be reassigned and shifted by B_f'.

The experimental data which had been determined through the many experiments on the Ar:HBr complex was then used to generate a fully three dimensional morphed

potential energy surface [65]. This particular morphed potential was initially generated by scaling and shifting an *ab initio* potential with parameterized functions and non-linear least squares fitting to the experimental data. The morphed potential demonstrated unequivocally that this was a unique instance where the ground state of a molecular species was the hydrogen bound Ar-HBr was in fact different than the global minimum of the potential energy surface, the van der Waals form Ar-BrH. This global minimum was initially predicted to be about 20.9 cm^{-1} lower in energy than the Ar-HBr hydrogen bound minimum of the potential energy surface. The energy difference between the hydrogen bound and van der Waals isomer states are estimated to be 10.99 cm^{-1} from the infrared data and the morphed potential. The estimated energy of the isomerization needed to be experimentally determined directly as this was different from the previous studies of the complex[44, 47, 48] where the global minimum of the potential energy surface was concluded to be that of the hydrogen bound Ar-HBr structure. A simple representation of the energy of the complex as it depends on the angle of the HBr monomer unit is shown in Figure 13.

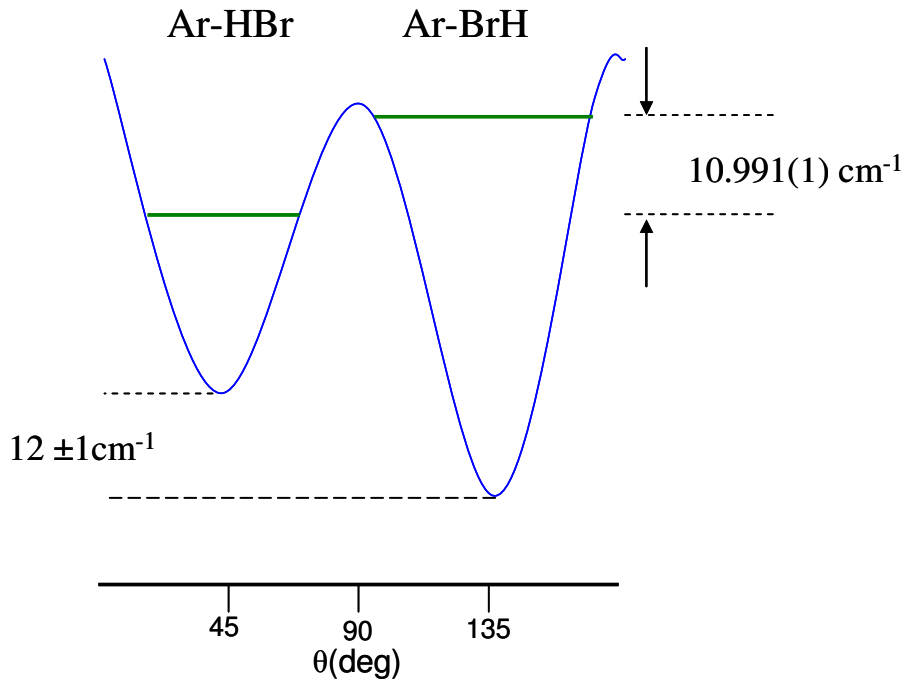

Figure 13. A slice of the potential of Ar-HBr showing the lowest vibrational states associated with the hydrogen bound isomer and the Ar-BrH van der Waals isomer. The angle of the monomer is plotted to demonstrate the change in energy from one isomer to the other.

Recently, Ar:HBr has been studied using the TAMU submillimeter spectrometer and PN-FTMW spectroscopy. The spectra of Ar-H^{79}Br and Ar-H^{81}Br as well as the deuterated form Ar-D^{79}Br and Ar-D^{81}Br have been observed and will be compared with the available information from previous microwave and infrared observations. In addition, the submillimeter spectrum of the Σ bending vibration has also been observed directly for the excited HBr ν=1 vibration state of Ar:HBr through the application of a DC discharge. These data will then be used to critically evaluate the previously morphed potentials by comparing predictions based on this morphed potential with the newly analyzed spectroscopic data.

The direct observation of the energy difference between the two isomeric structures of Ar-HBr is an ideal problem for the TAMU submillimeter spectrometer. The spectrometer performance characteristics including its absolute frequency accuracy, resolution and sensitivity, were tested using newly generated data for this complex. In addition, the spectroscopic constants determined from the data were compared with those generated from infrared and microwave studies. The data determined for the direct Σ bending vibration can then be used as benchmark data for evaluating the accuracy of the morphed potential generated in the work mentioned previously[65]. Furthermore, determination of additional data can be used to further optimize the potential of Ar:HBr. The observed energy difference between the two Σ states of Ar:HBr as mentioned previously is a direct measure of the isomerization energy of the complex and is extremely sensitive to the energy difference between the minima of the potential.

Experimental

The ∑-bending vibration of Ar-HBr was recorded by direct observation of its rovibrational band centered at 10.991 cm^{-1} in a supersonic nozzle expansion with the frequency and phase stabilized TAMU submillimeter spectrometer. The rovibrational transitions of P(8) to R(9) for the two isotopomers, Ar-H^{79}Br and Ar-H^{81}Br, were observed with resolved bromine hyperfine quadrupole structure, in the spectral range of 319 GHz to 366 GHz. The spectrum was recorded with an ISTOK OB-30 BWO tube with a stated operation range of 240-360 GHz. The Ar-HBr molecular complex was formed by expanding a mixture of ~1.6% HBr and 98.4% Argon with a stagnation pressure of 40 psia through a Series 9 valve with a 500μm orifice. The valve operated

at a repetition rate of 15 Hz with an open time of 1.5 ms. The pulse of the supersonic jet is synchronized with the beginning of the fast frequency scan, which makes a frequency step in 10μs, later upgraded to 3.8 μs/step, and can perform frequency step sizes from 1 to 100 kHz as discussed earlier. The output of the BWO source has a demonstrated instrumental resolution of better than 1 kHz, and can be configured to scan 2 MHz segments with a frequency step of 50 kHz. Each individual fast scan frequency segment is stored in the computer and frequency scans of 40 MHz can be made by consecutively collecting 2 MHz sections and storing them for later manipulation and data analysis. The vacuum system used to maintain a base pressure of $2.0*10^{-6}$ Torr in the vacuum chamber was a Varian 400M diffusion pump backed by a Leybold RUVAC WA-251 Roots blower and a 1398 Welch mechanical pump.

The P(J) head, illustrated in the simulated stick spectrum in Figure 14, was readily identified for both isotopomers of Ar:HBr at P(9). The quadrupole substructure of the R(0) transition covered about 100 MHz which decreased in magnitude to 20 MHz for the R(8) transition as the hyperfine substructure collapses. The most intense quadrupole transitions of $\Delta F=1$ for the R branch and $\Delta F=-1$ for the P branch were observed, as well as the weaker $\Delta F=0$ transitions. Figure 15 depicts the 4 Doppler split components associated with the $F=11/2 \leftarrow 9/2$ quadrupole component observed in the R(3) transition of Ar-H^{81}Br. The small peak in the center is one of the Doppler components of the $F=7/2 \leftarrow 7/2$ quadrupole transition. The Doppler splitting in this region is about 1.89 MHz, with a line width slightly less than 40 kHz.

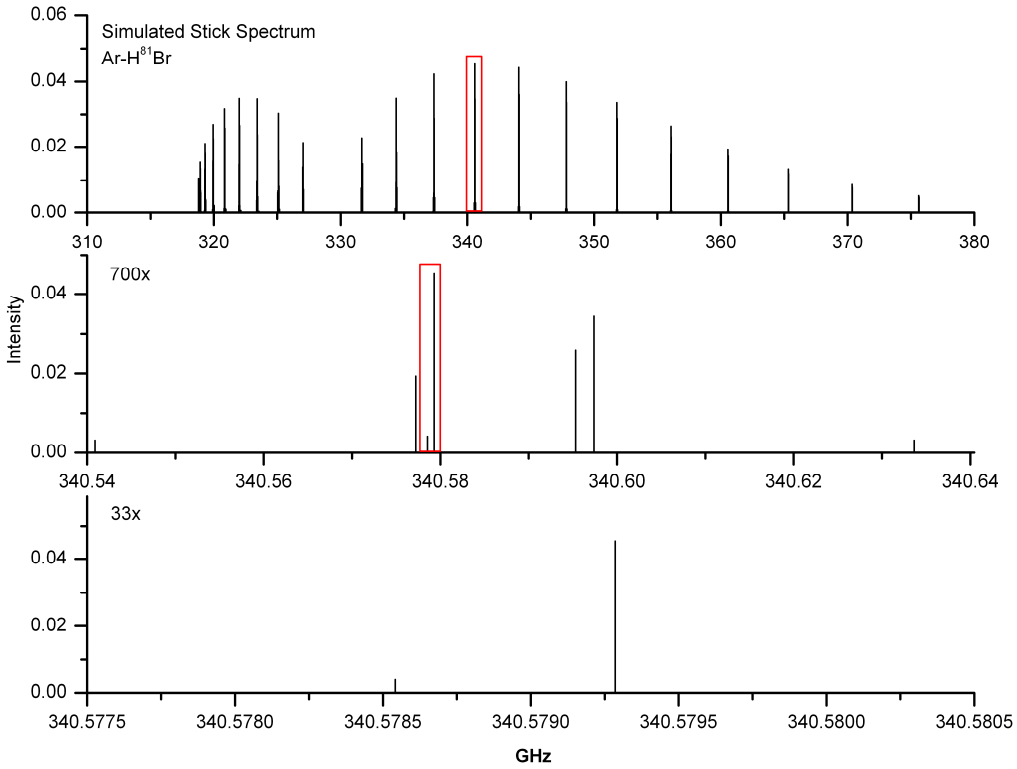

Figure 14. Simulated stick spectrum of Ar-H^{81}Br with zoom factors to show quadrupole substructure observed. The bottom graph is the same frequency scale as is in Figure 15.

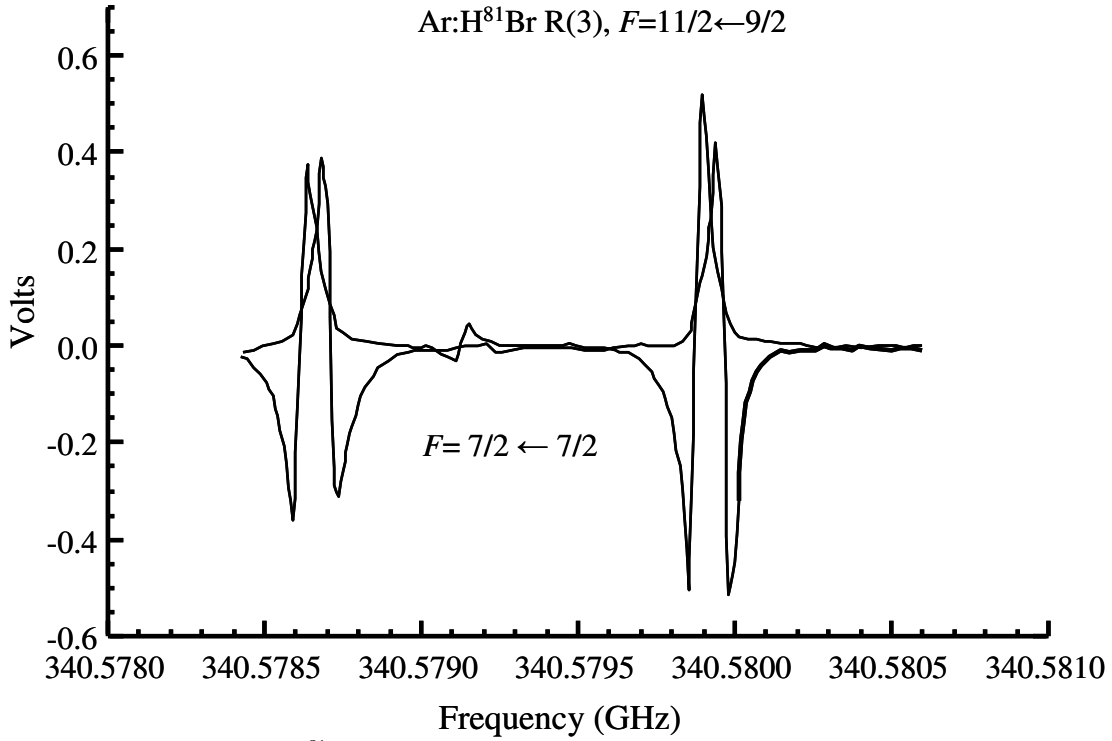

Figure 15. Spectra of Ar:H^{81}Br showing the four Doppler components of the R(3) *F*=11/2← 9/2 quadrupole and one Doppler component of the *F*=7/2← 7/2 transition.

The spectrum of Ar-D^{79}Br and Ar-D^{81}Br was also observed from 205-265 GHz for rovibrational transitions P(10) to R(11), using an OB-24 BWO tube version. A total of 89 transitions for Ar:D^{79}Br and 92 transitions for Ar:D^{81}Br have been observed with resolved bromine quadrupole structure. Figure 16 is an example of a typical line observed for the J=4←3, F=9/2←11/2 transition of Ar-H^{79}Br. The estimated accuracy of the frequency of each transition is about 2 kHz, due to unresolved deuterium hyperfine quadrupole substructure.

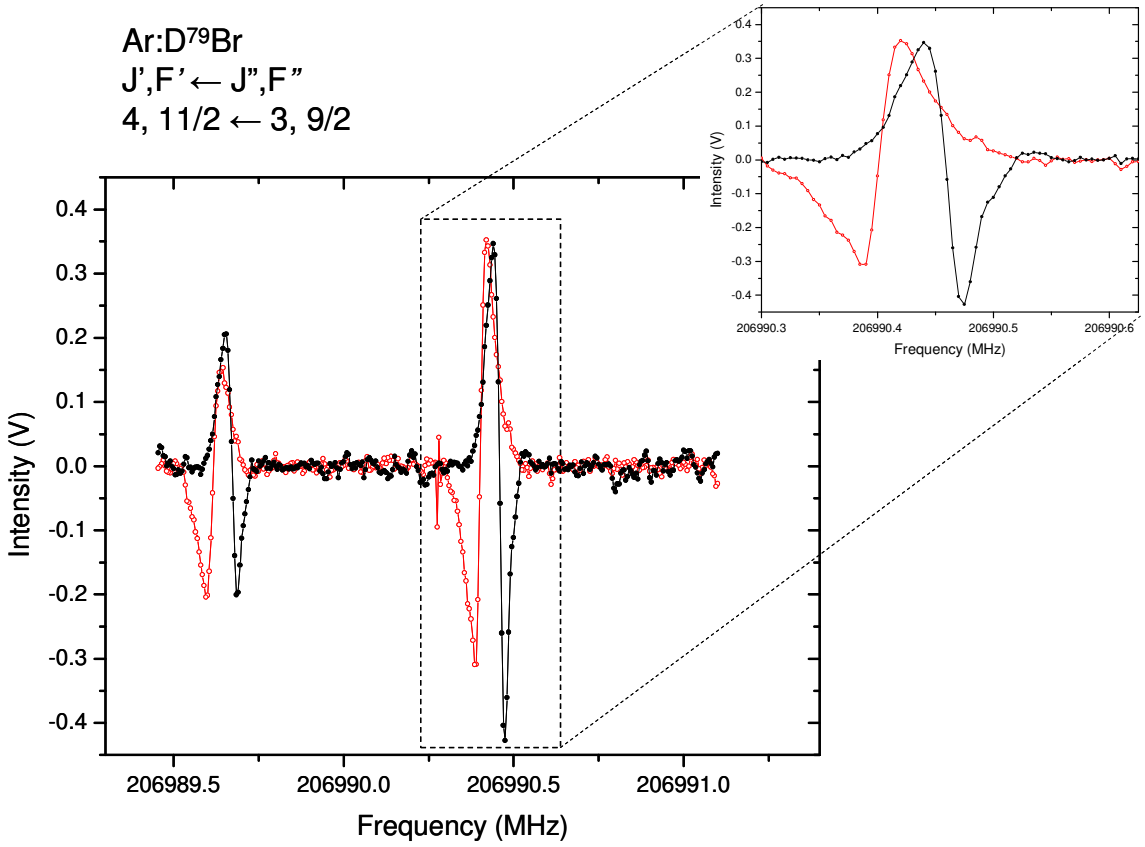

Figure 16. First derivative spectrum of the Doppler displaced components of the P(4) *F'*←*F"* 9/2←11/2 transition of Ar:^{2}H^{79}Br. The average of the four Doppler split components is 206990.037 MHz.

A DC discharge nozzle was constructed and integrated into the spectrometer for the generation of vibrationally excited dimers similar to that previously used for pulsed-nozzle FT microwave spectroscopy in vibrationally excited Ar-HCl, Kr-HCl and other molecules[76-79]. This provides an effective means to generate van der Waals complexes in which the intramolecular vibrations of the component monomer are excited in higher vibrational states. This is particularly attractive as at room temperature the population of the excited vibrational state of HBr is less then 1 part in 10^{6} when compared to the population of the ground state. However, in the discharge assisted expansions the

relative populations can be in the range of several percent making a population sufficient for complexation with Ar and subsequent spectroscopic investigation. Figure 17 shows the configuration of the nozzle and the associated Teflon spacers, electrode and rooftop reflector. A Teflon spacer of 5 mm thickness and 3 mm hole in the center is placed between the nozzle and the anode.

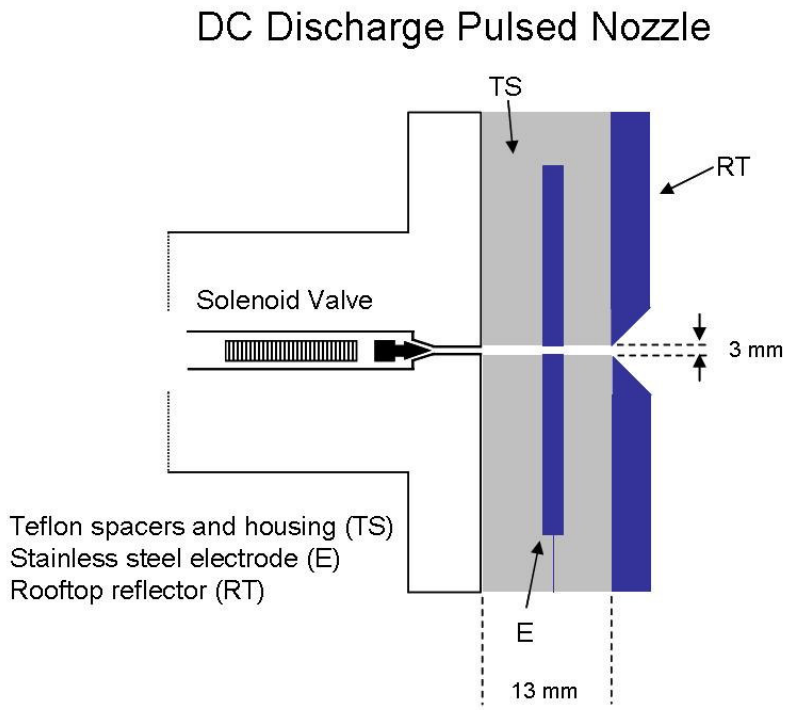

Figure 17. DC discharge nozzle.

The anode is a stainless steel disc with 2 mm thickness and a 3 mm hole in the center. A second Teflon spacer (6 mm thick, 3 mm hole) is placed between the anode and the rooftop reflector. The rooftop reflector is 12.7 mm thick with a 3 mm hole in the

center with a 90° machined channel to make the reflecting surfaces. A high voltage DC power supply, Universal Voltronics BAM 10-80, was used between 600 and 1500 VDC to produce the vibrationally excited complex. The negative voltage was applied to the electrode keeping the rooftop reflector at ground potential. We investigated the characteristics of the DC discharge by modifying the voltage, the repetition rate, the pulse duration as well as the backing pressure on the valve to obtain the maximum signal. The sample used for this experiment was a 2% HBr (Matheson Gas, Parsippany, NJ) concentration of the seed gas in an argon carrier. Optimized conditions were found with a 1ms pulse duration at a 15 Hz repetition rate, the same as the operation conditions used in the aforementioned study of Ar:DBr, but with application of -800VDC to the nozzle with a backing pressure of 15 psig.

An OB-30 tube version was used to observe the rovibrational transitions of the complex for transitions of R(9) to P(8) for the Ar-H^{79}Br isotopomer. 44 transitions were recorded with a line width of 50 kHz, as shown in Figure 18.

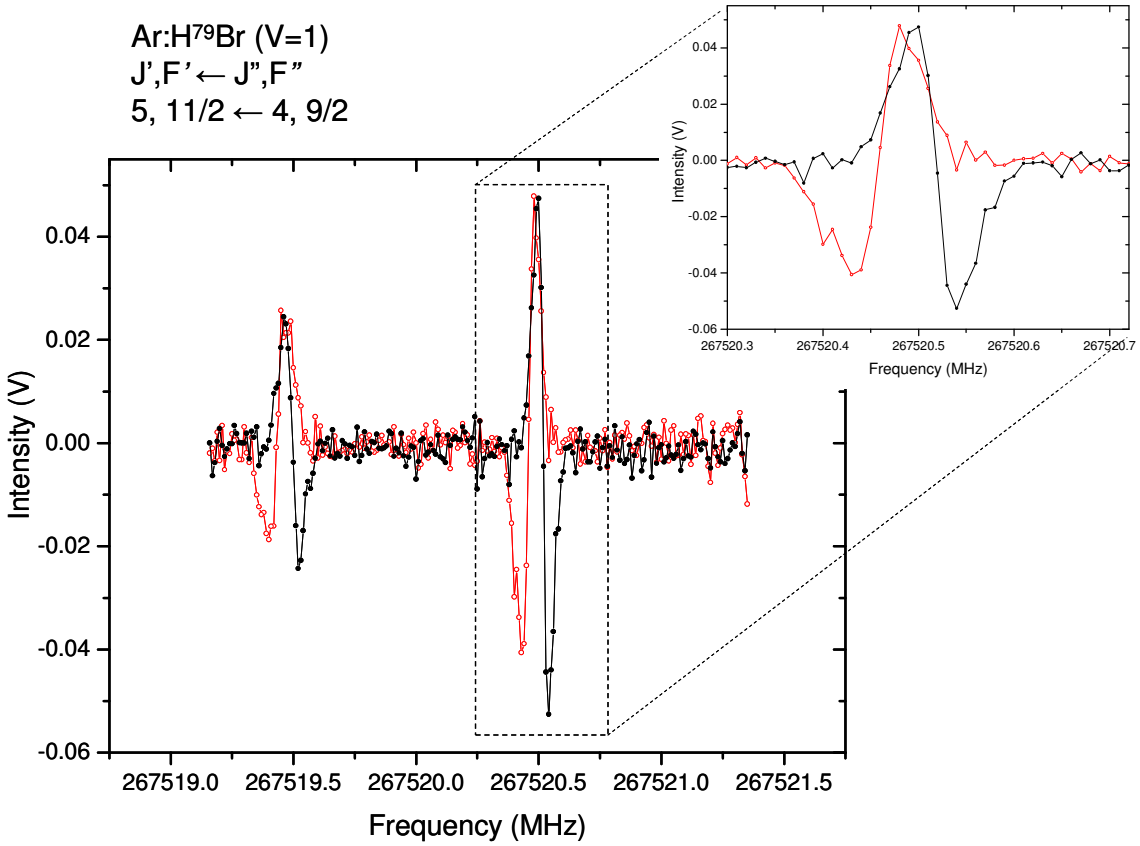

Figure 18. The first derivative Doppler displaced components recorded in the submillimeter spectrum of the P(5) *F'*←*F"*: 9/2←11/2 Σ bending transition in the HBr stretch of Ar-H^{79}Br having a center frequency at 267519.997 MHz.

The microwave spectrum of the *J*=6←5,5←4,4←3 and 3←2 pure rotational transitions of both the ArH^{79}Br and ArH^{81}Br were rerecorded with the upgraded pulsed nozzle microwave FT spectrometer with co-axial configuration at the School of Chemistry, University of Exeter. The spectrometer has been described previously and is based on the design of Grabow et. al.[80] and the operation of the spectrometer in a general sense is given in a review on hydrogen bound dimers[50].

The pulse jet is propagated along the axis of the Fabry-Perot cavity with a mixture of Ar and HBr (98% Ar:2% HBr) and a stagnation pressure of 40 PSI through

an orifice of 500μm. Figure 19 shows a typical spectrum of Ar:HBr recorded with the FTMW spectrometer. The larger splitting is due to the Doppler split components and the smaller splitting is from the H·Br spin-spin coupling. The average of the split components yields 8833.83252 and 8833.83569 MHz which correspond to the $J'F_1'F' \leftarrow J'' F_1'' F''$ transitions assigned to $4,\frac{7}{2} \leftarrow 3, \frac{7}{2}$.

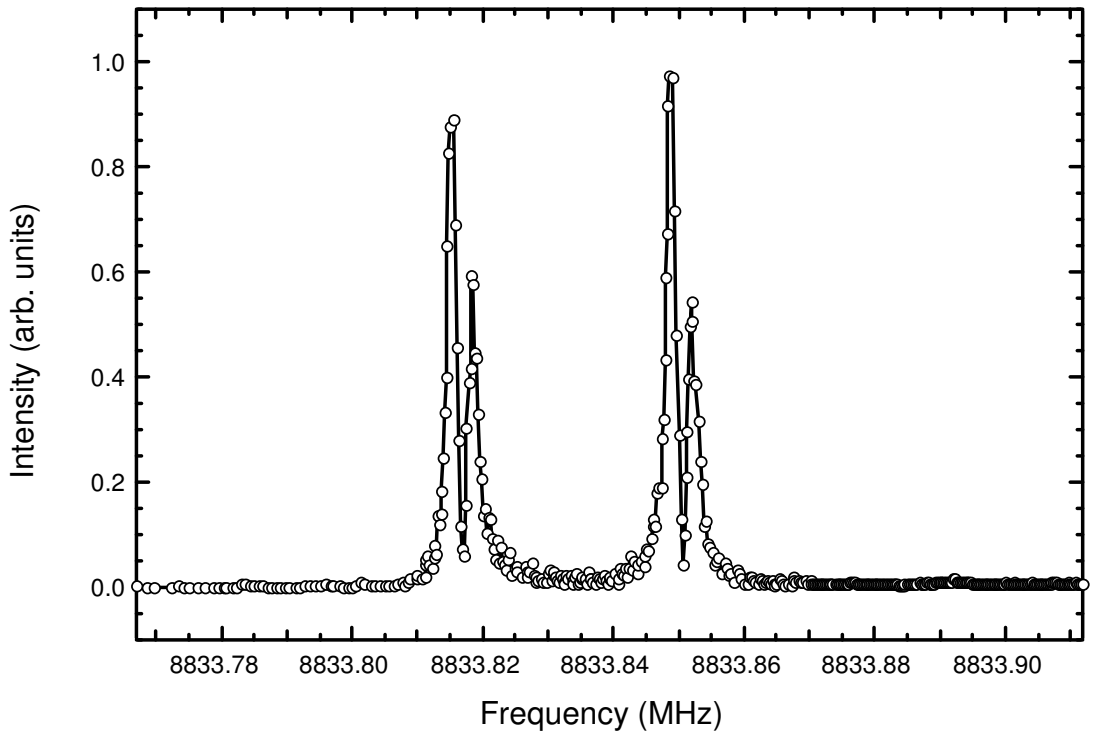

Figure 19. PN-FTMW Spectrum with the hydrogen hyperfine splitting of the *J*=4←3, *F*=7/2←7/2 quadrupole transition of Ar:H^{79}Br.

Analysis

The ∑ bending vibration of Ar-HBr has been recorded with resolved rotational and quadrupole substructure. A Hamiltonian can be written to describe the energy

splitting of the rotational and quadrupole levels as

$$H = H_{vib} + H_{rot} + H_{quad} + H_{SR}(Br) + H_{SR}(H) + H_{SS}(H, Br) \tag{22}$$

Where H_{vib} and H_{rot} describe the operators for the vibrational and rotational energy levels and are of the following well-known form

$$H_{rot} = BJ(J+1) - D_J J^2 (J+1)^2 + H_J J^3 (J+1)^3 \tag{23}$$

where B is the rotational constant, and D_J and H_J are the corresponding rotation distortion constants. This equation is used to define the contribution of the rotational energy to the total Hamiltonian for both the ground and excited states with the requisite values of J. The quadrupole contribution is defined by the following equation

$$\begin{aligned} H_{quad} = &[\chi_{aa} + D_\chi J(J+1)] \times \left\{ \frac{\frac{3}{4}c(c+1) - I(I+1)J(J+1)}{2I(I+1)(2J-1)(2J+3)} \right\} \\ &+ \frac{\left[\chi_{aa} + D_\chi J(J+1)\right]^2}{B} g \times 10^{-3} \\ &+ \frac{c}{2}\left[F(F+1) - I(I+1) - J(J+1)\right] \end{aligned} \tag{24}$$

where χ_{aa} is the quadrupole moment along the major axis of the complex and D_χ is the associated rotation dependent distortion constant. I for Bromine is 3/2 and F is the spin state of the complex for the given transitions and can be determined by

$$F = [J + I] \ldots |[J - I]| \tag{25}$$

for the J rotational level 3 the valid values of F are 9/2,7/2,5/2 and 3/2. The term $H_{SR}(X)$ = $\mathbf{I}_X \cdot \mathbf{M}(X) \cdot \mathbf{J}$ describes the magnetic interaction coupling of the nuclear spin $\mathbf{I}_X$ to the

rotational **J** angular momentum. The remaining term H_{SS}(H,Br)=$\mathbf{I}_H \cdot \mathbf{D} \cdot \mathbf{I}_{Br}$ is the spin-spin interaction of the hydrogen nucleus to the bromine in the HBr diatomic.

In the fit of the submillimeter data, the H_{SR}(H) and H_{SS}(H,Br) terms were excluded as the splitting due to these terms were not resolved in the submillimeter experiments. We used the coupling scheme of **F=I+J** to describe the quantum numbers of the bromine quadrupole transitions. Each observed transition was included in the fit with equal weighting. This treatment produced an RMS deviation of 0.8 and 0.9 kHz for the Ar:H^{79}Br and Ar:H^{81}Br isotopomers respectively. The data included in the fit as well as deviations are given in Table A 2 for the Ar-H^{79}Br and Ar-H^{81}Br isotopomers.

The microwave spectrum was treated in a similar manner by including only ground state rotation and quadrupole constant and including the H_{SR}(H) and H_{SS}(H,Br) terms in the Hamiltonian. Additional quantum numbers associated with the hydrogen hyperfine splitting were also included to give a coupling scheme of $\mathbf{F_1=I_{Br}+J}$ and $\mathbf{F=F_1+I_H}$ where the spin of hydrogen $I_H=\frac{1}{2}$. In the previous microwave work, the hydrogen hyperfine splitting was not resolved so this gives additional information about the molecular complex through the spin rotation term.

The fits of the data were performed through the use of the SPFIT package[81] using the rotational constants and coupling schemes as discussed above. The molecular constants associated with each set of data are presented in Table 9. The transitions associated with the Ar:D^{79}Br and Ar:D^{81}Br isotopes as well as those associated with the Ar:H^{79}Br (ν=1) spectrum have been analyzed in the same manner as discussed above, and are given in Table 10.

Table 9. Ar:H^{79}Br and Ar:H^{81}Br spectroscopic constants.

	ν_0 (MHz)	B (MHz)	D_J (kHz)	H_J (MHz)	χ_R (MHz)	χ_J (kHz)	M_{bb} (kHz)
Ar:H^{79}Br[a]	329611.4298(3)	1236.413360(50)	12.4623(23)	-2.690(40)e-6	260.39770(80)	-31.608(30)	1.955(31)
Ar:H^{79}Br[b]		1106.671230(60)	12.5018(35)	1.709(73)e-6	173.22710(90)	17.450(34)	0.654(32)
Ar:H^{79}Br[c]		1106.671310(27)	12.5022(13)	1.669(19)e-6	173.22878(53)	17.434(26)	0.564(28)
Ar:H^{79}Br[d]		1106.67018(20)	12.41(1)		173.2209(46)	17.63(3)	
Ar:H^{81}Br[a]	329225.6797(3)	1226.773350(60)	12.2947(27)	-2.724(47)e-6	217.8983(10)	-26.260(33)	1.995(35)
Ar:H^{81}Br[b]		1097.581990(70)	12.3016(41)	1.677(87)e-6	144.8074(10)	14.545(37)	0.674(35)
Ar:H^{81}Br[c]		1097.581982(29)	12.2980(13)	1.598(19)e-6	144.81000(53)	14.515(27)	0.620(28)
Ar:H^{81}Br[d]		1097.58119(15)	12.23(3)		144.8067(5)	14.71(23)	

[a] Σ bending vibrational state parameters from submillimeter-wave data.
[b] Ground state parameters from submillimeter-wave data.
[c] Ground state parameters from microwave FT data.
[d] Ground state parameters from fit of Flygare *et al.*[23] and Jackson et. al.[24]

Table 10. Ar:^{2}H^{79}Br, Ar:^{2}H^{81}Br and Ar:H^{79}Br (v=1) spectroscopic constants.

	ν_0/MHz	B_J/MHz	D_J/kHz	H_J/Hz	χ_{aa}/MHz	$D\chi_{aa}$/kHz	M_{bb}/kHz
Ar:^{79}Br^{2}H	213555.04193(52)	1265.627468(74)	12.6807(13)	-1.1451(67)	347.5917(25)	-18.44(15)	2.63(27)
Ar:^{79}Br^{2}H[a]	216450.15	1262.13	12.5		345.44		
Ar:^{2}H^{79}Br		1087.508875(82)	8.5138(16)	0.422(10)	276.2253(25)	14.57(15)	1.97(28)
Ar:^{2}H^{79}Br[b]		1087.50889(27)	8.497(6)		276.223(9)	14.73(41)	0.94(20)
Ar: ^{81}Br^{2}H	213135.62080(51)	1256.309511(74)	12.4991(13)	-1.1212(61)	290.5018(25)	-15.22(13)	2.98(28)
Ar:^{2}H^{81}Br		1078.593360(83)	8.3737(16)	0.4163(93)	230.8771(25)	12.15(14)	2.20(29)
Ar:^{2}H^{81}Br[b]		1078.59315(22)	8.352(5)		230.878(8)	12.26(37)	1.02(16)
Ar:^{79}Br^{1}H	275714.7057(11)	1236.87666(3)	9.4857(27)	-4.465(17)	274.8247(24)	-33.09(23)	
Ar:^{79}Br^{1}H[c]	275727.0(30)	1236.853(42)	9.68(16)	-3.53(16)			
Ar:^{1}H^{79}Br		1098.66014(16)	16.1786(39)	3.626(28)	172.5873(23)	23.39(29)	
Ar:^{1}H^{79}Br[c]		1098.579(19)	15.532(51)	2.479(30)			

[a] Wang, et. al. [82]
[b] Keenan, et. al. [23]
[c] Han, et. al. [55]

Discussion

The determination of the molecular parameters derived from both PN-FTMW and submillimeter experiments allow for a direct comparison for the performance of the submillimeter spectrometer to that of the state of the art PN-FTMW spectrometer. The determined constants for the current submillimeter treatment are given in Table 9 as well as the constants determined from a global fit of the rerecorded data using PN-FTMW and the original FTMW and MBER data of Flygare and Jackson [23, 24]. The determined values from this study are within 2σ (2 standard deviations) between the PN-FTMW and the submillimeter for the majority of the determined constants. However, a limited number of the deviations of the determined errors for the constants are within 3σ, such as the quadrupole rotation distortion term and the spin rotation interaction. The previous data [23, 24] for the Ar:H^{79}Br agree within 10 σ due to the lower number of rotational transitions observed and the restricted accuracy of the transition frequency determinations in the original work. The constants determined from this study demonstrate that the submillimeter constants in both the ground and excited states are determined to microwave accuracy. This also is the first report of the high resolution constants of the Ar-BrH isomeric structural form including the determination of the quadrupole constant that is so important in the detailed structural investigation.

The structure of the complex can be determined from the rotational constant and the quadrupole coupling constant provided that it is assumed that the HBr component is structurally unchanged on complex formation. The rotational constant is related to the moment of inertia about an axis using the following equation

$$I_{complex} = \frac{h}{8\pi^2 B_{complex}} \tag{26}$$

In this equation, h is Planck's constant and $B_{complex}$ is the constant determined from the fitting procedure. The moment of inertia is then used to determine the structure of the complex by the relationship

$$I_{complex} = \mu R_0^2 \tag{27}$$

where $M_{Rg:HX} = \mu = \frac{m_{HX} m_{RG}}{m_{HX} + m_{RG}}$, the reduced mass of the complex, and R_0 is the distance between the two masses. In the case of the van der Waals complex Ar-HBr the argon atom and the HBr diatomic are treated as two masses. There are limitations to the simple treatment as two point masses. A more appropriate expression with corrections due to the moment of inertia of the monomer unit, is given in the following equation

$$R_{cm} = \sqrt{\frac{1}{M_{Rg:HX}}\left(I_{Complex} - \left(\frac{I_{HX}}{2} \right) * \left(\cos^2 \theta + 1 \right) \right)} \tag{28}$$

where the angle of the HX diatomic and the displacement of the center of mass of the HX monomer is related to the complex as a whole. The R_{CM} distance of the complex can then be directly determined if the angle θ is known. The moment of inertia of the complex can be determined using the simple expression

$$I_{Complex}\left(amu\text{Å}^2 \right) = \frac{505379.006(51)}{B_{Complex}(\text{MHz})} \tag{29}$$

where the rotational constant B is determined in MHz and the moment of inertia is of units of amuÅ^2 and they are related by the appropriate conversion factor. In order to determine the exact structure of the complex, the angle of the HX diatomic to the figure

axis of the complex must also be determined. The following equation is used to determine the angle, θ

$$\chi_{aa} = \chi_0\left(3\left\langle\cos^2\theta\right\rangle - 1\right)/2 \tag{30}$$

where the coupling of the bromine nucleus in the free HBr is χ_{aa}(diatomic) and the χ_{aa}(complex) is taken from the fit. This equation is used to determine the angle of the quadrupole moment of the diatomic projection to the figure axis of the complex. As the angle is dependent on $\cos^2\theta$, only the magnitude of the value but not the absolute sign can be determined and the angle may have values of $0\pm\theta$ or $\pi\pm\theta$. Careful consideration of the structure of the complex must be addressed, such as van der Waals radii and plausible hydrogen bond length, to determine if the acute or obtuse angle is appropriate.

Table 11. Structural parameters of Ar:HBr.

	Reference	R_{CM}/ Å	Rg-Br/ Å	θ /deg
Ar-H^{79}Br	MBER[24]	4.1331	4.1464[a]	42.11
Ar-^{2}H^{79}Br	MBER[24]	4.1529	4.1821[a]	34.43
Ar-H^{79}Br	FTMW[23]	4.1331[a]	4.1464	42.08
Ar-^{2}H^{79}Br	FTMW[23]	4.1528[a]	4.1820	34.38
Ar-H^{79}Br	Submm	4.1331	4.1464	42.11
Ar-^{79}BrH	Submm	3.9090	3.8943	144.29
Ar-^{2}H^{79}Br	Submm	4.1528	4.1820	34.43
Ar-^{79}Br^{2}H	Submm	3.8464	3.8154	151.34
Ar-H^{79}Br (ν=1)	Submm	4.1480	4.1614	42.43
Ar-^{79}BrH (ν=1)	Submm	3.9079	3.8930	137.56

[a]Values recalculated from experimental data
H^{79}Br r_0=1.4242662Å
D^{79}Br r_0=1.4214374Å
H^{79}Br (ν=1)r_0=1.444468Å
R_{CM} and Rg-Br errors are less than 0.00001 Å
Error in θ is less than 0.0001

Table 11 shows the variety of calculated R_{CM} and Rg-Br distances as well as θ for Ar:HBr for the hydrogen and deuterium bound complexes and the van der Waals isomers. This information was determined from the current submillimeter data together with the previously evaluated MBER data of Jackson and the PN-FTMW of Flygare[23, 24]. The structure of Ar:HBr as determined by the rotation constants, which were determined to within 2 σ in the ground state by each method is in fair agreement (<0.00001 Å and 0.03°) for the two treatments. There is a very small variance in the R_{CM} distance as the rotational constants are slightly different. The distances, R_{CM}, determined by Jackson[24], Flygare[83] and our submillimeter agree to the number of significant figures quoted by the previous studies 4.1331(1) Å.

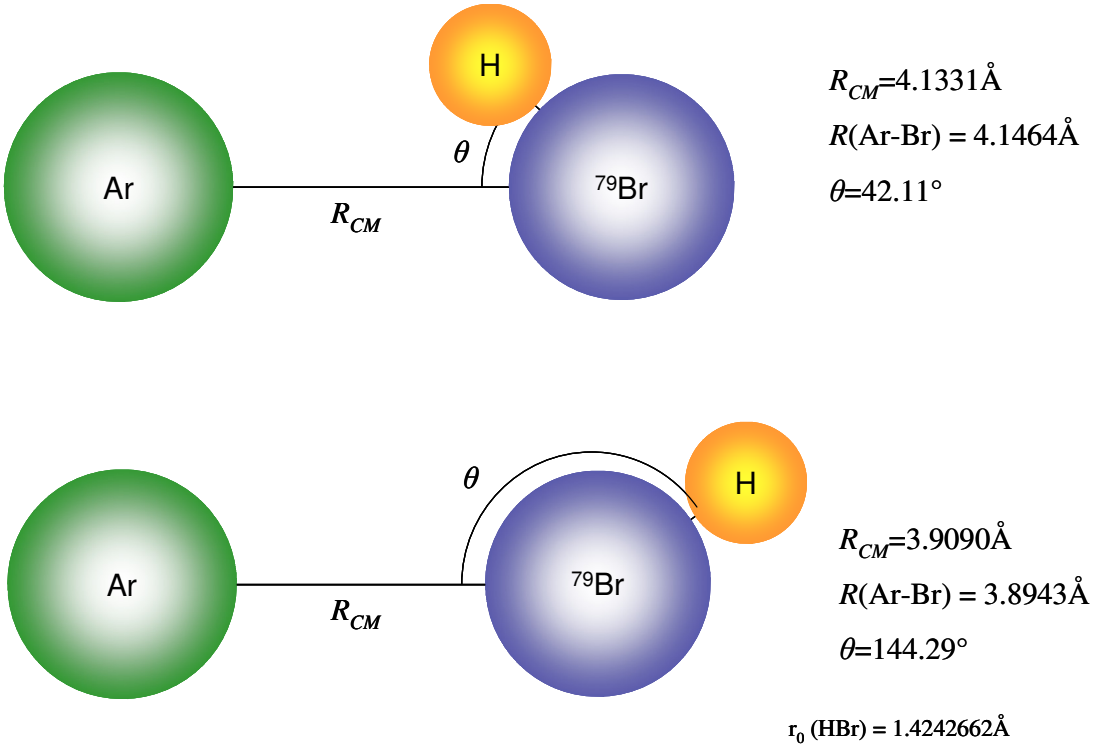

Figure 20. Ar-HBr and Ar-BrH showing the structural parameters determined from the analysis.

The changes in the R_{CM} distance in the complex as the HBr bond is vibrationally excited or is deuterium substituted in DBr can also be evaluated. The ΔR_{CM} (Å) from the ground state Ar-^{1}H^{79}Br to that of the deuterium substituted complex or the excited vibration mode of HBr is 0.0198 Å and 0.0149 Å respectively. This correlates to a lengthening of the weak non-covalent hydrogen bond in the complex due to the effects of the dynamics of the monomer unit in the complex. This is opposite of the trends observed in the Rg:HF and Rg:HCl complexes where the intermolecular bond decreases by 0.05Å and 0.02Å respectively.

In the case of the deuterated complex, the heavier deuterium atom does not undergo as large of an amplitude bending motion that is associated with the HBr component, largely due to the mass increase in the deuterium. This is demonstrated in the observed angle from the quadrupole moment of 34.43° for Ar-D^{79}Br compared to that of Ar-H^{79}Br with 42.11° as shown in Figure 21. If the HBr is in the excited vibrational state, the bond length increases by 0.0202 Å, which indicates a slightly larger repulsive shell around the HBr monomer unit. Although the large amplitude bending angle of 42.43° is larger than that of the Ar-HBr complex in the ground vibrational state of the monomer HBr component, this is still consistent with a hydrogen bound ground state with a van der Waals isomeric equilibrium structure.

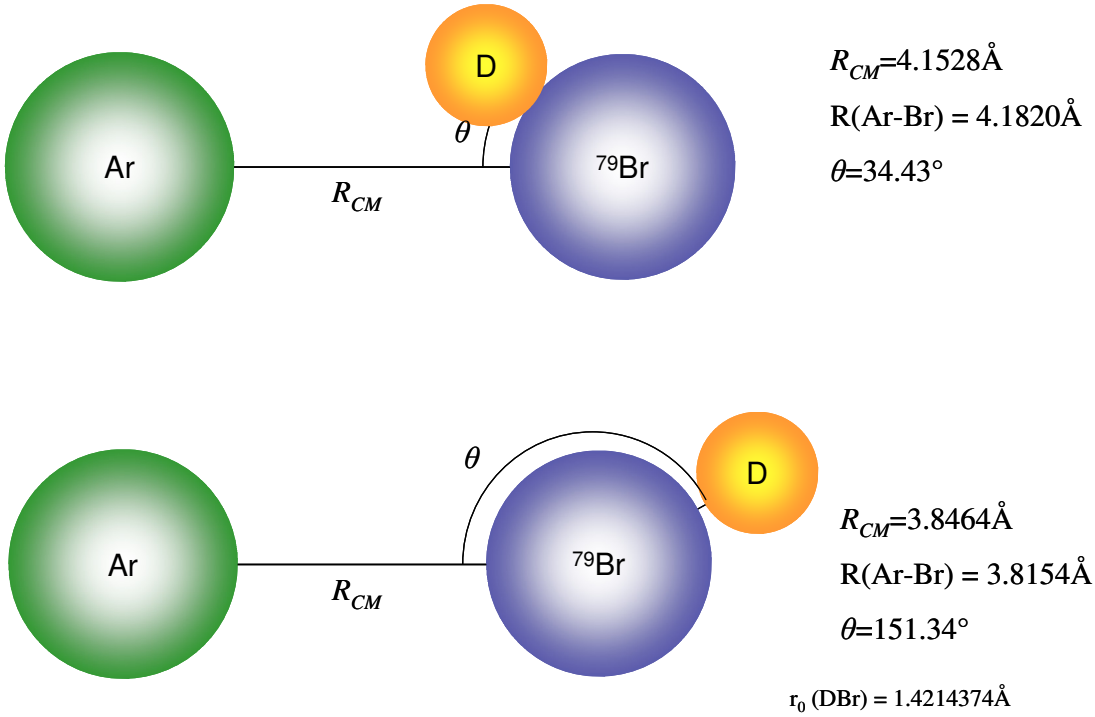

Figure 21. Ar-DBr and Ar-BrD showing the structural parameters determined from the analysis.

Based upon the above treatment, the structure of the complex is known to a high degree of accuracy. In the original treatment of the FTMW and MBER data, the authors used generalized equations in the diatom harmonic approximation[84] to determine information for the force constants of the bond in the bending and stretching modes to estimate an intermolecular potential for the complex. The authors noted in these approximations that the stretching frequency, ν_s, is related to the rotation distortion constant, D_J, by the relationship

$$D_J = \frac{4\bar{B}_0^3}{\nu_s^2} \tag{31}$$

where $\bar{B}_0$ is the rotational constant of the complex. This expression leads to an estimate

of the stretching frequency of 22.1 cm^{-1} and 20.9 cm^{-1} (D_J=12.397 and 12.2223 kHz) for the Ar-$H^{79}Br$ and Ar-$H^{81}Br$ complexes respectively, as reported for the PN-FTMW data, and values of 22.0 and 21.9 cm^{-1} (D_J=12.462 and 12.269 kHz) for the MBER data. These values are consistent due to the fact that the same equation was used to predict the stretching frequency as well as similar rotation distortion constants. The bending frequency can also be estimated by the square of the bending amplitude in the bond as in the following equation

$$\left\langle \theta^2 \right\rangle = \frac{h}{8\pi^2 \mu_b \nu_b} \tag{32}$$

The high frequency Π bending vibration is estimated to be 30.8 cm^{-1} with the constants determined and compares favorably with the value determined previously[55] of 26.67 cm^{-1}.

The calculation of an intermolecular potential for the complex has also been made with a Lennard-Jones 6/12 potential. The equilibrium bond distance in the complexes was computed using the expression $B_0 = B_e - 18\frac{B_e^2}{\nu_s}$, and $B_e = \frac{h}{8\pi^2 \mu r_e^2}$ and the well depth is estimated by $\frac{1}{2}k_s = \frac{36\varepsilon}{R_e}$ where ε is the well depth in cm^{-1}, k_s is the bending force constant (mdyne/Å or Nm^{-1}) and R_e is the equilibrium intermolecular distance.

With these values as determined by the authors, they estimate R_e to be 4.2113Å and ε is 206.0 cm^{-1}. This can be compared with Jackson et. al. who assume an approximation of R_e distance by R_0 (Rg-Br)(corrected) distance of 4.1483 Å and

estimate the well depth, ε, to be 262.0 cm^{-1}. The difference in the two values of the well depth is largely due to the difference in the R_e distance used in the Lennard-Jones Potential form.

Another factor that may lead to some incorrect assumptions in the treatment of the structure and dynamics of the complex is the change in structure via the bending vibration from a hydrogen bound complex to one that is van der Waals, which was not considered in the diatom approximations used previously. The presence of a double minima potential in Ar-HBr that was not considered in the previous work, leads to the conclusion that the parameters such as the well depth and the equilibrium intermolecular distance are not very good approximations of the true dynamics in the complex and a more sophisticated treatment is warranted.

The fully converged morphed potential energy surface[82], generated by fitting the most complete set of experimental data available provides a more sophisticated approach to the dynamics of Ar-HBr. It indicates a linear molecular geometry is preferred with an intermolecular bond length, $R_{min,}$ of 4.20(1) Å and a minimum energy at -176.4(10) cm^{-1}. The van der Waals form of the complex is characterized by R_{min} of 3.67(1) Å and a minimum of -188.3(10) cm^{-1} which are significantly shallower than those found by the harmonic approximations made by Flygare and Jackson as well as shorter equilibrium bond lengths. The discrepancy of the two values of the well depth could possibly be explained by the different interpretations of the structure. In one case, the equilibrium internuclear distance of the complex is calculated on the basis of a harmonic approximation. In the second case, the internuclear distance is calculated and taken to

be the distance between the heavy atoms Ar and Br in the complex. While both of the interpretations are accurate, the well depth of a potential function taken on those parameters obviously will not agree. The morphed potential that is determined from the experimental data and ab initio potentials is used to determined the minimum energy of the hydrogen bound or van der Waals complexes in the Born-Oppenheimer approximation limit. The values computed for the internuclear distance remove the effect of the vibration of the monomer unit. This cannot be done with the experimental data alone. It also introduces an error when comparing experimentally determined values of the structure with those that are determined from the potential. The structure of the complex in the various states in effect has no bearing on the potential as it is fitted to the available experimental data.

Figure 23 depicts the structure of a Rg-HX complex showing the two structural parameters that are commonly used in the previous work of Flygare and Jackson. Specifically, the angles α and θ are shown as the angle between the Rg-center of mass of HX and the hydrogen atom and the Rg-X-H angles respectively. The angle α is determined from the quadrupole moment projection to the major inertial axis which is coincident with the R_{CM} distance. The angle θ is determined by the Rg-X distance and the projection of the hydrogen atom and the HX bond. While these angles are usually within 0.2°, there is a small correction that may be applied but the distance determined after the correction is in agreement to the number of significant digits reported in this and previous work. This correction does not account for the discrepancy in the internuclear separation.

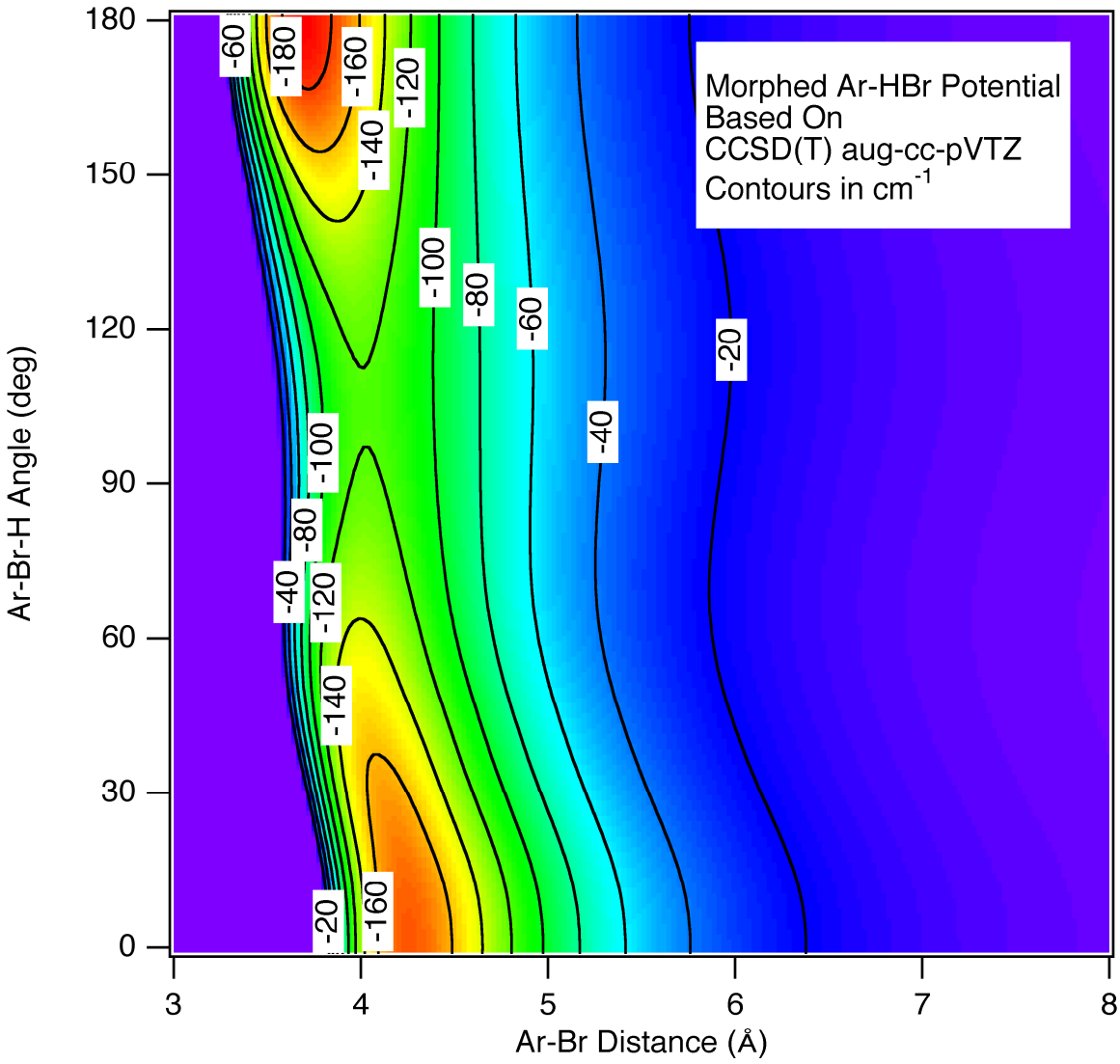

Figure 22. 3D CCSD(T) morphed potential of Ar-HBr.

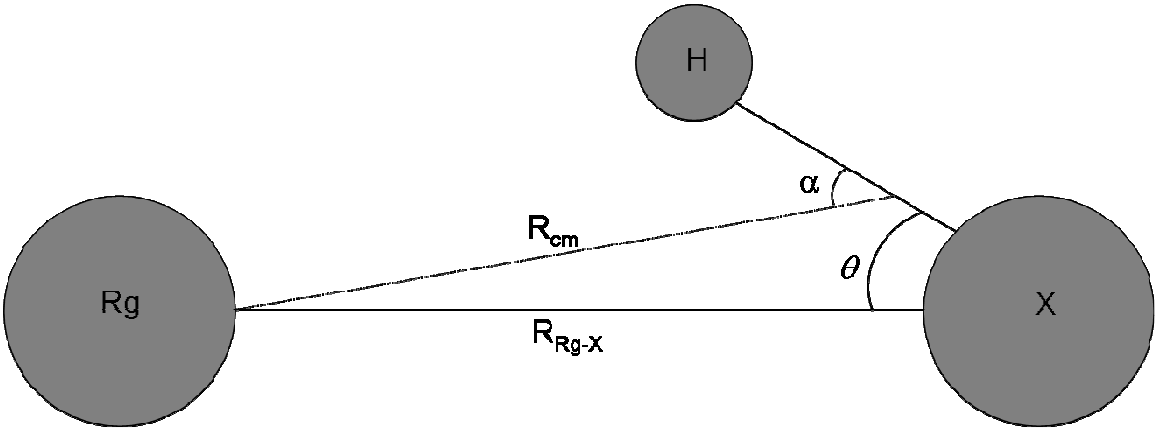

Figure 23. Rg-HX structure with angles α and θ.

Conclusions on Ar-HBr

The study of Ar-HBr reported here has utilized the TAMU submillimeter spectrometer in a co-axial configuration and phase and frequency stabilized backward wave oscillator. It is the first report of a range of new and accurate rotational and quadrupole constants for the Ar-HBr molecular dimer. These constants have been demonstrated to be determined to microwave accuracy in both the ground and first excited Σ bending state of the molecular complex. The observation of this transition provides the unequivocal experimental determination of the isomerization energy between the hydrogen bound and van der Waals forms of Ar:HBr.

The generation of a fully converged CCCC (Coupled Cluster Correlation Consistent) morphed potential energy surface that reproduces experimental observables to near spectroscopic accuracy has also been achieved. This morphed potential demonstrates and confirms that the ground state is hydrogen bound. However, the global minimum is in fact the van der Waals structure with an energy 11.9 cm^{-1} below the hydrogen bound form. An estimate of the dissociation energy is also obtained

through the morphed potential and experimental observations. The vibrational predissociation of Ar-HBr of the fundamental stretching vibration of HBr monomer in the complex was used to estimate the dissociation energy. The noticeable absence of the rotational progression occurring at J=80 indicated that the complex can no longer exist with the internal energy at that state and it predissociates. Based on this information, we estimate the dissociation energy to be 131±1 cm^{-1}. This value is slightly larger than the value previously determined value of 121 cm^{-1}, [47].

Ar-HI

Introduction

Ar-IH, has been one of the least investigated members of the prototypical Rg:HX (Rg=Ne, Ar, Kr and X=F, Cl, Br, I) series referred to in Table 1. A limited number of previous studies have involved several spectroscopic methods, such as infrared matrix isolation spectroscopy[68], as well as molecular orbital calculations[85]. The Ar:HI complex offers the opportunity, as with all of the Rg:HX series, to evaluate the factors that affect the bonding and dynamics of a complex by measuring the properties and the effect of polarizibility and dipole moment on the complex. It also enables a comparison with other complexes providing a basis for interpreting different interaction effects. It is interesting to investigate the influence of the relatively small dipole moment of HI (0.44 D) relative to the HF (1.92 D), HCl (1.02 D) and HBr (0.78 D) and increased polarizibility in progressing from HF, HCl and HBr to HI on the forces that determine non-covalent interactions. Initial unreported attempts to observe the microwave

spectrum of Ar-HI were unsuccessful. However, based on studies of the high-n Rydberg time-of-flight spectrum[86], which correlated the photoinitiated dissociation of the Ar-IH complex via loss of the hydrogen atom, the lack of a low energy tail was interpreted as evidence that the hydrogen atom was exterior to the Ar-I bonding. This is in contrast to what was known about the ground state structures of the other complexes formed from Rg-HF, Rg-HCl and Rg-HBr (Rg=Ar, Kr, Xe) where the hydrogen atom is interior to the Rg and halide atom. A subsequent study which utilized REMPI (2+1) spectroscopy of the REMPI (2+1) spectroscopic investigation of the $g^3\Sigma(0^+) - X^1\Sigma(0^+)$ band of Ar-IH and a fourth order Møller-Plesset (MP4) ab-initio calculation[87] also indicated that the equilibrium structure of the complex was that of the linear Ar-IH isomer. This was subsequently confirmed by the high resolution microwave and infrared spectra of Ar-IH and Ar-ID[56].

The microwave spectrum of Ar-IH and Ar-ID was observed using a PN-FTMW spectrometer at the National Institute of Standards and Technology in Gaithersburg, MD. The "mini-FT" spectrometer, with an operational frequency range of ~8-18 GHz, was used with a 1% HI/DI, in an Ar carrier was used to produce the supersonic jet expansion through a 500μm orifice. Rotational transitions associated with the J=5←4, 6←5, 7←6 with resolved quadrupole substructure due to iodine were observed characteristic of χ_{aa} associated with the large quadrupole coupling of monomeric HI (I=5/2) and χ_0=-1828.286(9) MHz.

The extreme accuracy of the ground state parameters associated with the two isotopomers Ar-IH and Ar-ID allows a detailed evaluation of the ground state structure

of the complex in the van der Waals form. The respective rotational constants were determined to be 1034.0832(4) and 1052.3598(10) MHz for the Ar-IH and Ar-ID isotopomers indicating an anomalous structural deuterium isotope effect in which the rotational constant of Ar-ID is unexpectedly greater than Ar-IH. The angular dependence of the hydrogen or deuterium atom, measured via the quadrupole coupling constant, χ_{aa}, demonstrated that the vibrationally averaged structure is consistent with an angle of 149.33° and 157.11° for the Ar-IH and ID respectively. The R_{CM} distance was calculated using Equations 28-29. The values of 3.9975 and 3.9483 Å for Ar-IH and Ar-ID indicate that the center of mass separation decreases upon deuteration, results consistent with deuterium substitution in Ar-BrH and Ar-BrD van der Waals structures as discussed in the previous chapter. This effect is a product of the zero point energy and the decrease in the large amplitude bending motion of the proton upon deuteration. The structure of Ar-IH and Ar-ID can be evaluated with the Pauling Radii listed in Table 3. The radius of iodine is 1.98 Å and 1.88 Å for Ar. We can compare the sum of the respective radii to test the assumption that the ground state of the complex is the van der Waals isomer. Taking the sum to be 3.86 Å it is seen that the value is very close to the experimentally determined value of 3.9975 Å. This simple observation supports the van der Waals complex in a qualitative manner. The effect of deuteration on the bending amplitude can be explained by the change in mass upon the substitution of HI for DI. In this case, the reduced mass of the monomers increases from 0.999884352 amu to 1.98263537 amu. This affects the monomer by increasing the center of mass to iodine distance from 0.012Å for HI to 0.025 Å in DI. This has an effect on the structure of the

complex in that the R_{CM} distance decreases by 0.0192 Å and reducing the effective angle of the H/D nucleus by 7.78°. The effective Ar-I distance in the complex is reduced upon deuteration, indicating a more localized strongly bound structure than in protonated form. This correlates with a reduced zero point energy effect on deuteration.

The constants determined from these spectra enabled the determination of an accurate morphed potential energy surface that combines experimental and theoretical data. The previously determined microwave data shows that the ground state structure is consistent with an R_{CM} distance of 3.9975(1) Å and an angle of 149.33(1)°. From the previous morphed potential the minimum of the potential energy surface is the linear Ar-IH isomer with an equilibrium internuclear distance, R_e = 3.79 Å. A prediction of the direct $\sum \rightarrow \sum$ vibrational transition, or the isomerization from Ar-IH (ground state) van der Waals form to the hydrogen bound Ar-HI (first excited state) isomer, was made at 7.89 cm^{-1} based on the previous microwave and infrared experimental and theoretical data. This prediction is in contradiction to the calculated energy of 5.737 cm^{-1} which was determined from CCSD(T) level *ab initio* calculation[85].

It is through the direct observation of the Σ bending vibration band that a critical evaluation of the proposed potentials can be made as well as providing more detailed information of the complex which can be used to further improve the MP2 morphed potential energy surface.

The TAMU submillimeter spectrometer was thus employed to observe the energy of the $\sum \rightarrow \sum$ low frequency bending vibration of Ar-IH. The spectroscopic constants determined from this study will allow the determination of the structure of the

complex in both the ground Ar-IH and the first excited Ar-HI isomeric states. The effective rotational temperature in the supersonic jet is also evaluated by a detailed study of the relative intensities in rotation and quadrupole transitions.

Experimental

The spectrum of the $\sum \rightarrow \sum$ vibrational transition of Ar:HI was recorded using the TAMU submillimeter spectrometer with coaxial configuration. The source of the submillimeter radiation was an OB-30 BWO (ISTOK, Russia) which can be tuned from 220 to 385 GHz. The associated electronics and their functions have been described previously for Ar:HBr. The R(J) head of the spectrum of Ar-IH was easily observed based on the predictions made by the original morphed potential energy surface[56] and associated predicted simulated spectra.

A sample of the complex was produced though the expansion of a gas made up of ~2% HI: 98% Ar expanded at 40 psig through a nozzle with diameter of 500μm into the interaction region of the vacuum chamber. The pulse rate of the valve was 15 Hz with a pulse duration of 1 ms. This gave a base pressure in the vacuum chamber of 10^{-6} Torr when the valve was closed. Figure 25 shows the J=3←2 F=11/2←9/2 transition spectra recorded with the noted experimental conditions.

The spectrum was recorded from 237 to 268 GHz with the ranges of transitions from P(8) to R(10). Observed and measured transition frequencies of the spectrum comprised of 104 lines from the completely resolved iodine quadrupole substructure of the complex in much the same manner as that of Ar-HBr. The experimental spectrum

associated with the R(2) F=11/2←9/2 quadrupole transition is shown in Figure 24, the scan in the forward frequency direction has been removed for simplification.

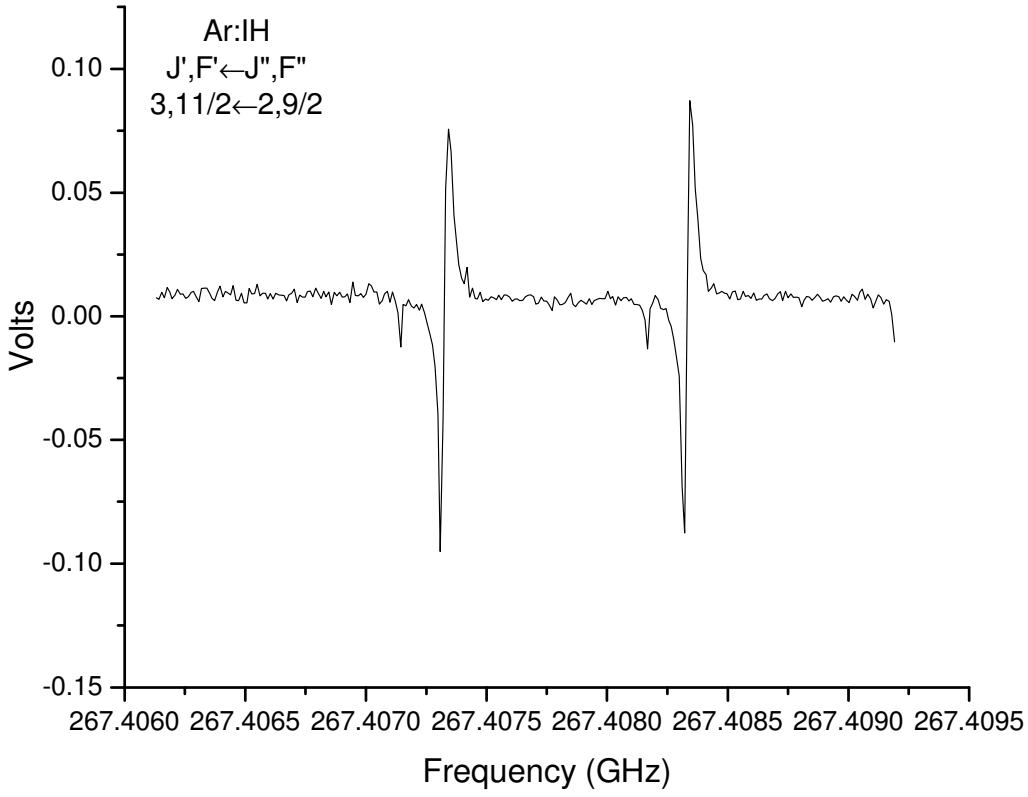

Figure 24. First derivative Doppler displaced components of the R(2) *F'*←*F"* =11/2←9/2 transition of Ar-IH. The center frequency of the transition is 267407.8588(14) MHz. The negative features to the left of each component are due to instrumental marker signals.

Results

The spectrum of Ar:HI is characterized by a prominent R(J) bandhead at J=5 which is indicative of a quasi-linear triatomic complex. This is expected as the rotational constant of the ground state Ar-IH isomer is greater by 157.60463(46) MHz than the Ar-HI excited state structure. The separation between adjacent rotational levels is related to the difference in the ground state and excited state rotational constants. In the case of the isomerization of Ar:HI, the difference of the rotational constants is large thus creating a band head, with a frequency at which the progression of rotational transitions inverts, and successive rotation transitions of higher J in the R-branch appear closer and closer to the band origin. Figure 25 demonstrates this phenomenon in the simulated stick spectrum. The closer spacing at about R(5) produces a dense region in the spectrum where the components of the rotational transitions are almost overlapped completely. The transition at the band origin is not due to a Q-branch as this transition is not allowed in the complex due to the selection rule of $\Delta J=\pm 1$.

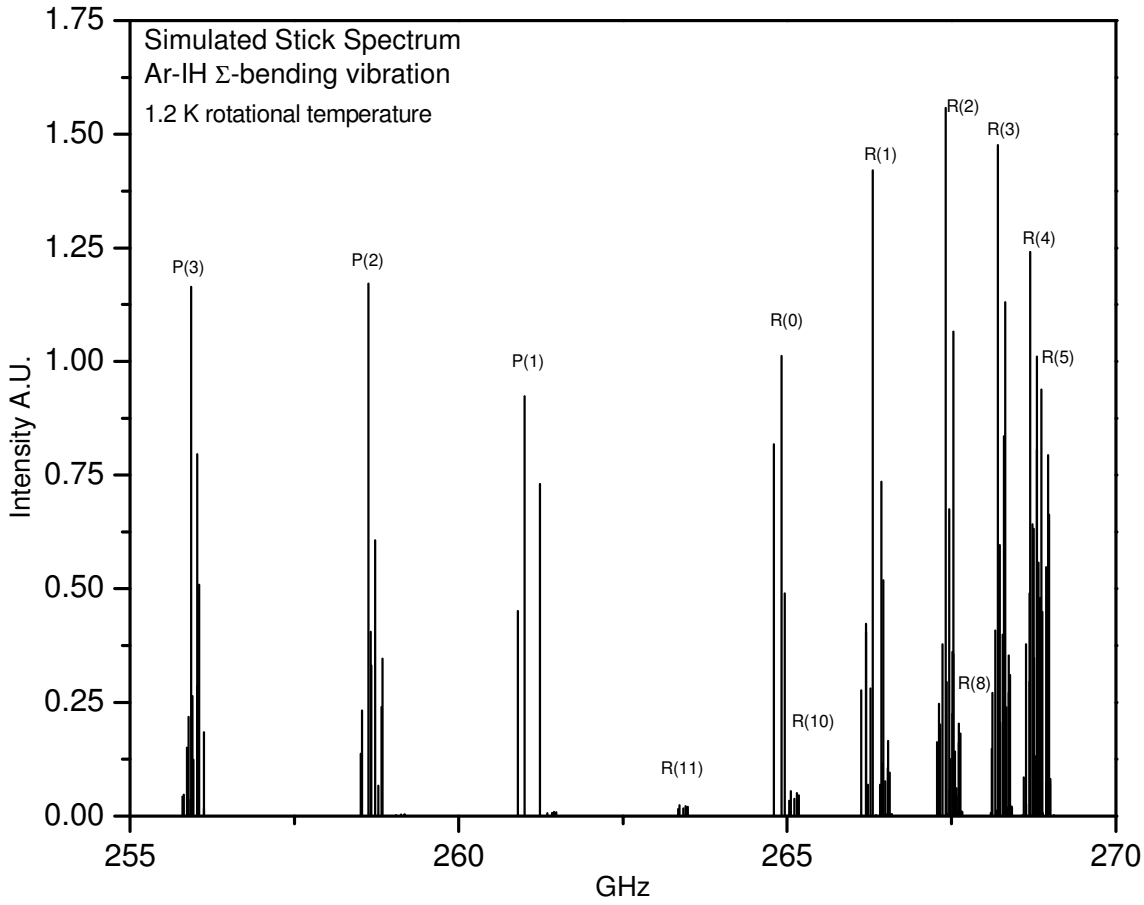

Figure 25. Stick spectrum of Ar-IH Σ-bending vibration centered at 263128.0649(14) MHz. The rotational transitions are labeled with the R(J) band head at R(5).

The 104 quadrupole transitions were fitted using the JPL SPFIT package[81] using the appropriate rotational constants for a linear molecule with one quadrupole nucleus. The standard deviation of the fit was 7.0 kHz and the determined constants are given in Table 12. We have measured the intensity ratios of rotational transitions in Ar-IH to estimate the likely temperature in the supersonic jet expansion. The results of the intensity measurements are given in Table A 7.

Transitions between rotational levels of like quadrupole transitions were compared with predictions using the SPCAT program at 3 temperatures, 1.0 K, 1.2 K, and 2.0K. The measured values of the peak intensities for the observed transitions are compared with the predictions in Figure 26.

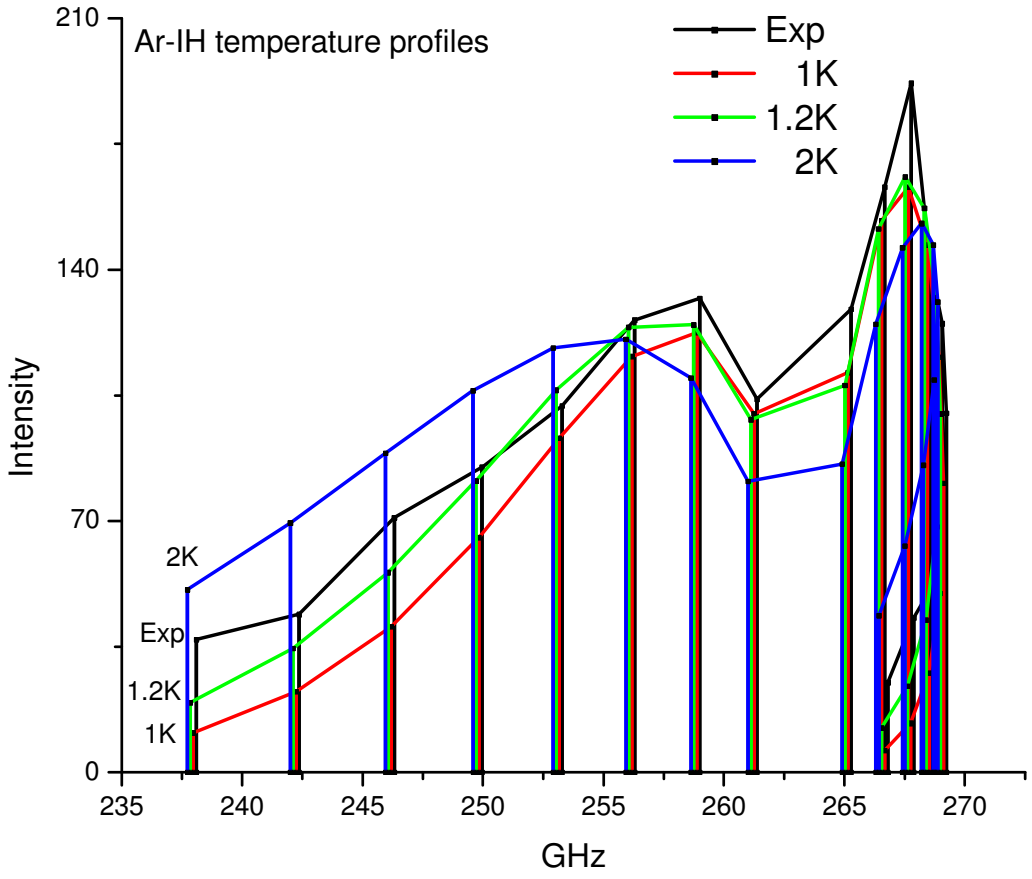

Figure 26. Temperature profiles for Ar-IH prediction and experiment. Three temperatures of 1.0, 1.2, and 2.0 K are plotted with the experimental data.

The temperature in the jet as determined in this analysis is most likely 1 K at low J transitions and between 1.2 and 2K for observed higher J transitions. It is evidence that we can determine the relative intensities of transitions over a large range of rotational transitions to uncertainties of about 10%. The temperature distribution in the supersonic jet is most likely a cause of the inhomogeneitites in the jet expansion affecting the formation of the dimer, and the cooling effects of the number of possible states at higher rotational quanta.

Table 12. The fitted submillimeter constants for Ar:HI.

	Upper State	Lower State	Lower State[a]
ν/MHz	263128.0649(14)		
B_J /MHz	876.47909(21)	1034.08372(25)	1034.0832(2)
D_J /kHz	5.3692(52)	10.5962(77)	10.596(4)
H_J /Hz	1.669(38)	-1.678(69)	-1.68(2)
χ_{aa}/MHz	-535.421(10)	-1114.4014(12)	-1114.40(1)
$D\chi_{aa}$/kHz	-106.2(11)	82.3(12)	80.8(5)
M_{bb}/kHz	1.48(24)	1.69(25)	1.56(9)

[a] McIntosh et. al. [56]

As shown in Table 12, the constants of the ground state determined from the submillimeter study are in excellent agreement with the microwave study to within one standard deviation of the fit. This is in spite of the fact that the submillimeter spectral resolution (40 kHz) is 20 times less than that of the associated microwave resolution of 2 kHz.

Figure 27 shows the experimentally determined structure of Ar:IH. The ground state van der Waals form is characterized by a center of mass distance, R_{CM}, of

3.9975(1)Å and an angle of the monomer unit, θ, of 149.33(1)°. The structure is markedly different in the excited state hydrogen bound form with a R_{CM} distance of 4.3440(1)Å and θ=43.362(10)°.

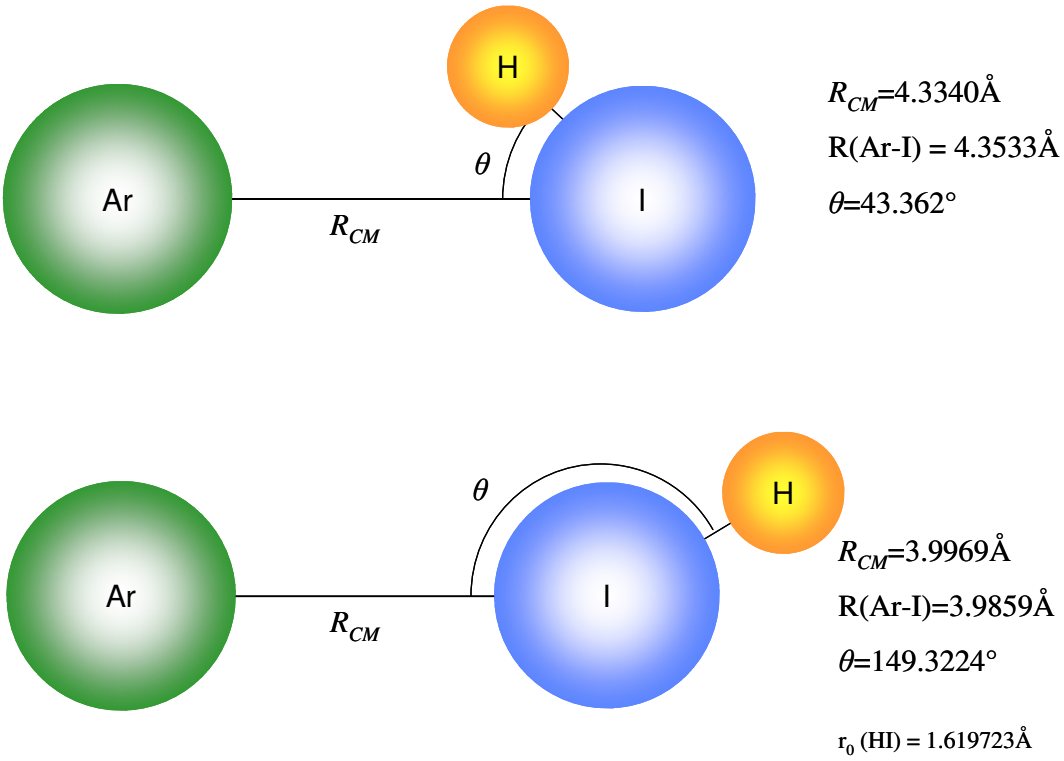

Figure 27. Experimentally determined structures of Ar:IH.

Discussion

The analysis of the 104 observed quadrupole component transitions associated with the P(8) to R(10) of Ar:HI produces spectroscopic constants which give structural information about the ground and isomeric excited states of Ar:HI. The constant associated with the projection of the quadrupole moment onto the figure axis of the complex, χ_{aa}, can only be determined for the magnitude of the value, the sign is not

determined. The angle of the HI subunit to the major axis of the complex is still able to be determined as $\cos^{-1}\left(\left\langle \cos^2\theta \right\rangle^{1/2}\right)$. In the excited state of the complex the R_{CM}=4.3440(1) Å and the angle θ=43.362(10)°. This is consistent with the a structure of having a proton between the heavy atoms of the complex. Contrary to this is the R_{CM}=3.9975(1) Å of the Ar-IH ground state where this value is consistent to the sum of the van der Waals radii of the two nuclei. Table 13 shows the R_{CM} and θ associated with the vibrationally averaged structure of each complex in the hydrogen bound and van der Waals states for the homologous series Ar-HX (X=F, Cl, Br and I). The difference in the ground state structure of Ar-IH can be rationalized by the fact that the decreasing dipole moment of the HX component and the corresponding increase in the polarizibility of the argon atoms changes the interaction in the complex. In particular, the competition between decreasing dipole-induced dipole forces in the hydrogen bond configuration coupled with the increased dispersive interactions in the van der Waals structures produces a complex that is van der Waals in the ground state. The global minima of Ar-BrH and Ar-IH are also interesting as they show that the dominant interaction determines the resulting observed structures. Generally as the size of the halide atom increases the intermolecular distance increases and the angle of the hydrogen atom becomes greater.

Table 13. Rg:HX vibrationally averaged structural information.

	Hydrogen Bound		van der Waals		Energy Difference
	Ar-X/ Å	θ	Ar-X/ Å	θ	cm^{-1}
Ar-HF	3.545	41.13	NA	NA	52.056[a]
Ar-HCl	4.007	41.53	3.858	138.6	23.657[b]
Ar-HBr	4.146	42.11	3.894	144.3	10.995[c]
Ar-HI	4.353	43.36	3.986	149.3	-8.777[c]

[a] Hutson[88]
[b] Busarow[63]
[c] Current Data
Note: The ground state of Ar-IH is van der Waals.

A morphed potential energy surface has been generated using the previously observed infrared, microwave and the current submillimeter data[11]. The morphed potential illustrates the global minima is associated with the van der Waals structure. The isomerization energy which is a value that is contested in the literature is now known to be 8.777007489(47) cm^{-1}. This value is slightly higher than the initially predicted value of 7.89 cm^{-1} based on a previous morphed potential energy surface[11]. The experimentally observed value can be compared with a prediction based on a CCSD(T) ab initio potential[85] of 5.737 cm^{-1}. The conclusion here is that even with a high level ab initio calculation the energy of two isomeric states cannot be calculated reliably without the inclusion of spectroscopic data. Table 14 lists the experimental data used to fit an ab initio potential to generate the morphed potential energy surface shown in Figure 28. The errors indicate that the morphed potential is converged with the data set used and the level of theory employed to calculate the ab initio potential.

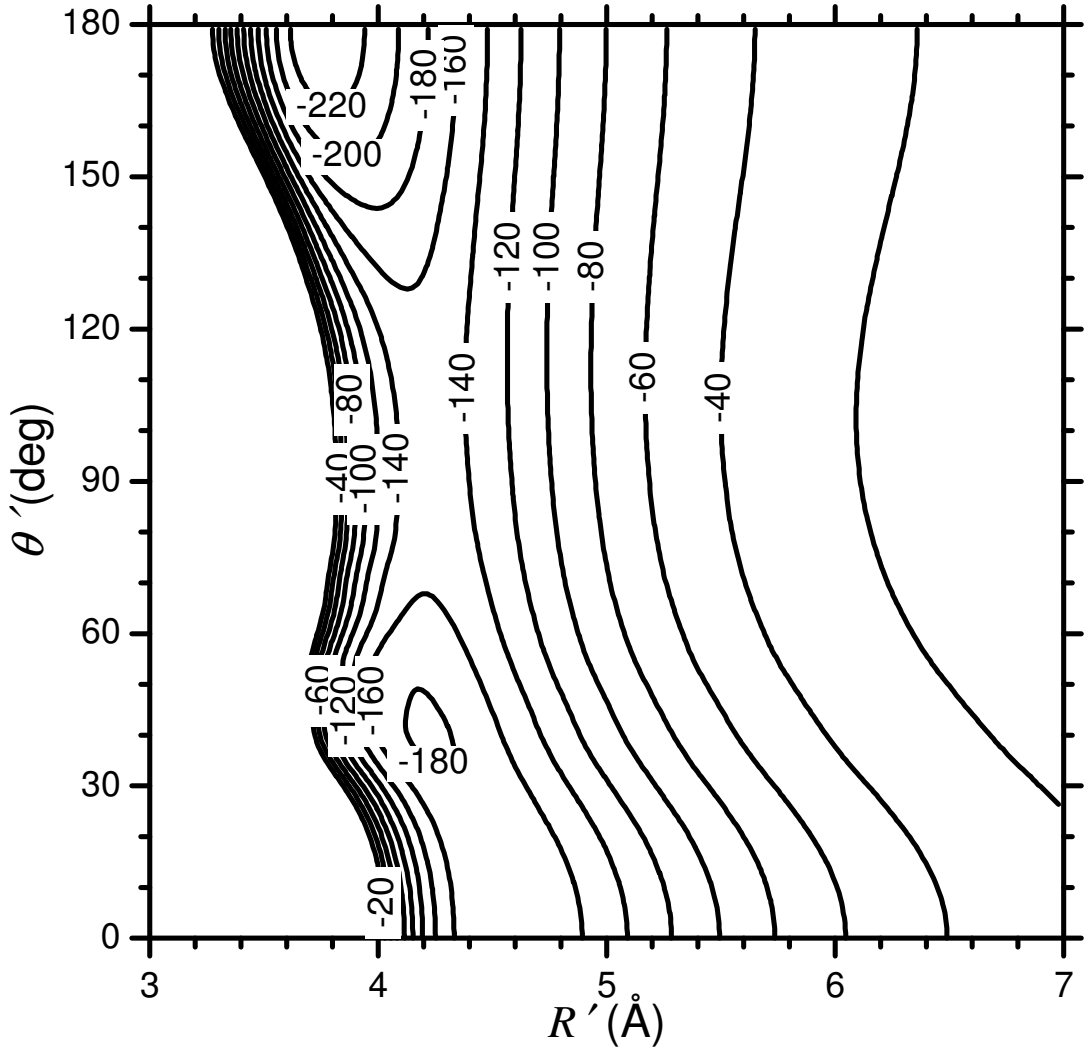

Figure 28. Morphed Ar-IH Potential. All energy contours are given in units of cm^{-1}. The coordinates used to plot this potential *R'* and *θ'* are the Jacobi coordinates for this isotopomer.

Table 14. Experimental data used in the fits and the values obtained in the fit with the uncertainties used. The RMS deviation between the computed and experimental values is 0.83.

	Value for Fit	Experimental Value	Uncertainty Used
Ar-IH B_0 (0,0^0,0)/10^{-2} cm^{-1}	3.45	3.45	0.01
Ar-IH D_J (0,0^0,0)/10^{-7} cm^{-1}	3.54	3.53	0.01
Ar-IH $\langle P_2 \cos(\theta) \rangle$ (0,0^0,0)	0.611	0.610	0.004
Ar-IH D_θ (0,0^0,0) /10^{-6}	-45.3	-44.3	1.5
Ar-ID B_0(0,0^0,0) /10^{-2} cm^{-1}	3.51	3.51	0.01
Ar-ID D_J(0,0^0,0) /10^{-7} cm^{-1}	2.29	2.33	0.03
Ar-ID $\langle P_2 \cos(\theta) \rangle$ (0,0^0,0)	0.767	0.771	0.004
Ar-ID D_θ (0,0^0,0) /10^{-6}	-12.5	-15.5	1.5
Ar-IH (E(0,2^0,0)$_{J=0}$– E(0,0^0,0)$_{J=0}$)/cm^{-1}	8.777	8.777	0.008
Ar-HI B_0(0,2^0,0)/10^{-2} cm^{-1}	2.92	2.92	0.01
Ar-HI D_J(0,2^0,0)/10^{-7} cm^{-1}	1.79	1.79	0.01
Ar-HI $\langle P_2 \cos(\theta) \rangle$ (0,2^0,0)	0.295	0.293	0.004
Ar-HI D_θ (0,2^0,0) /10^{-6}	56.4	58.1	1.5

Conclusions on Ar-IH

The observed Σ bending vibration of Ar-IH has been observed using the TAMU submillimeter spectrometer. The ground state structure is determined to be van der Waals, which is markedly different than the other members of the Rg:HX homologous series. The ground and excited state constants have been determined to near microwave accuracy. The quadrupole coupling constant is used to determine the structure of the complex in both the hydrogen bound and van der Waals states.

The spectroscopic data is combined with previously determined data of Ar-IH from microwave and infrared spectroscopic studies to determine a morphed potential energy surface. As indicated, the previous morphed potential [56] predicted the value of the Σ bending vibration with greater accuracy than the subsequent work [85]. In addition,

from the observed structure of the complex gives support to the assumption that the ground state of the Ar-IH complex is in fact van der Waals as initially proposed from the REMPI photodissociation experiments of Suzuki, Katayanagi and Heaven[87].

Rg:HX Conclusions

The observation and analysis of the low frequency bending vibrations of Ar-HBr, Ar-DBr, Ar-HBr (v=1) and Ar-IH have provided important experimental information of the relative energetics and the structures of the hydrogen bound and van der Waals complexes. As members of the Rg:HX homologous series the experimental data and the associated morphed potential energy surfaces, a qualitative picture of the Rg:HX complex is now becoming clear that can be rationalized in terms of decreasing dipole moment of the hydrogen halides and increasing polarizibility of the corresponding halide atom. This conclusion reflects the result of decreasing dipole-induced dipole interactions with decreasing dipole moment along the series HX (X=F, Cl, Br and I) in competition with increased polarizibility of the corresponding halogen.

The previously held tenet of molecular spectroscopy, that the ground state is always the lowest energy structure, has been challenged and proven to be incorrect. Through the direct observation of experimental data and the generation of morphed potential energy surfaces it is now demonstrated that the structure of a molecular complex can be determined with almost spectroscopic accuracy. The use of the TAMU submillimeter spectrometer in these cases has been shown to be invaluable, as the structure of different isomers in a molecular complex can be determined with a very high

degree of accuracy (R_{CM}=±0.000001Å, θ=±0.0001°). In addition, the absolute energy associated with the low frequency vibrations can also be determined to microwave accuracy.

CHAPTER IV

HYDROGEN HALIDE DIMERS

Introduction

The hydrogen halide dimers $(HX)_2$ (X=F, Cl, Br, I) are a class of complexes which have been the subject of intense investigation. These complexes are indeed the prototype for the weakly bound interaction in which the proton undergoes vibration rotation tunneling. In these cases, the homodimers are more strongly bound than those found in the corresponding member of the Rg:HX homologous series. This behavior can be rationalized in terms of the additional contributions of dipole-dipole and electrostatic interactions. The hydrogen bond in $(HF)_2$ and $(HCl)_2$ has been studied using high resolution spectroscopy and theoretical techniques[69, 89-98] and the equilibrium structures of the hydrogen halide dimers are typically L-Shaped, as shown in Figure 29. The Jacobi coordinate system is again used to model the geometry of the complex in a similar fashion as for Rg-HX. The complex has two angles, θ_1 and θ_2, which define the angular displacement of the respective monomer units from the major molecular axis. The axis which bisects the centers of mass of the monomer units also has a characteristic distance defined as $R_{CM,}$ but an additional angle, ϕ, which relates the relative orientation of the monomers as a rotation about the major molecular axis.

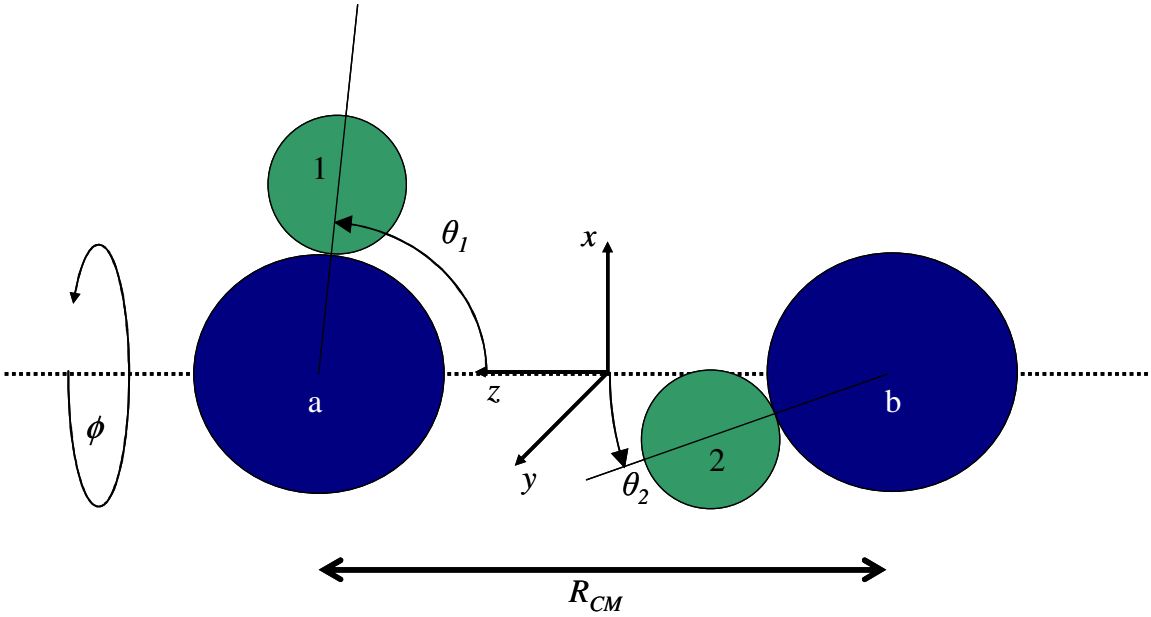

Figure 29. Coordinate system used for the HX dimers.

The location of the hydrogen nuclei, labeled 1 or 2 in Figure 29, is either bound and between the heavy atoms (a or b) or exterior in an L-shaped isomer. The non-rigid structure of the dimer leads to a structural degeneracy where the hydrogen bond exists between two different labeled structures which are can be interconverted by the tunneling inversion motion of the hydrogen nuclei. The large amplitude motion of the hydrogen nuclei interchanges the two equivalent hydrogen bonded structures by hydrogen inversion through the tunneling pathway. The quantum mechanical consequence of this motion is the perturbation of the energy level which induces a splitting of the energy levels separated by the tunneling frequency, ν_5^1, as shown in Figure 30.

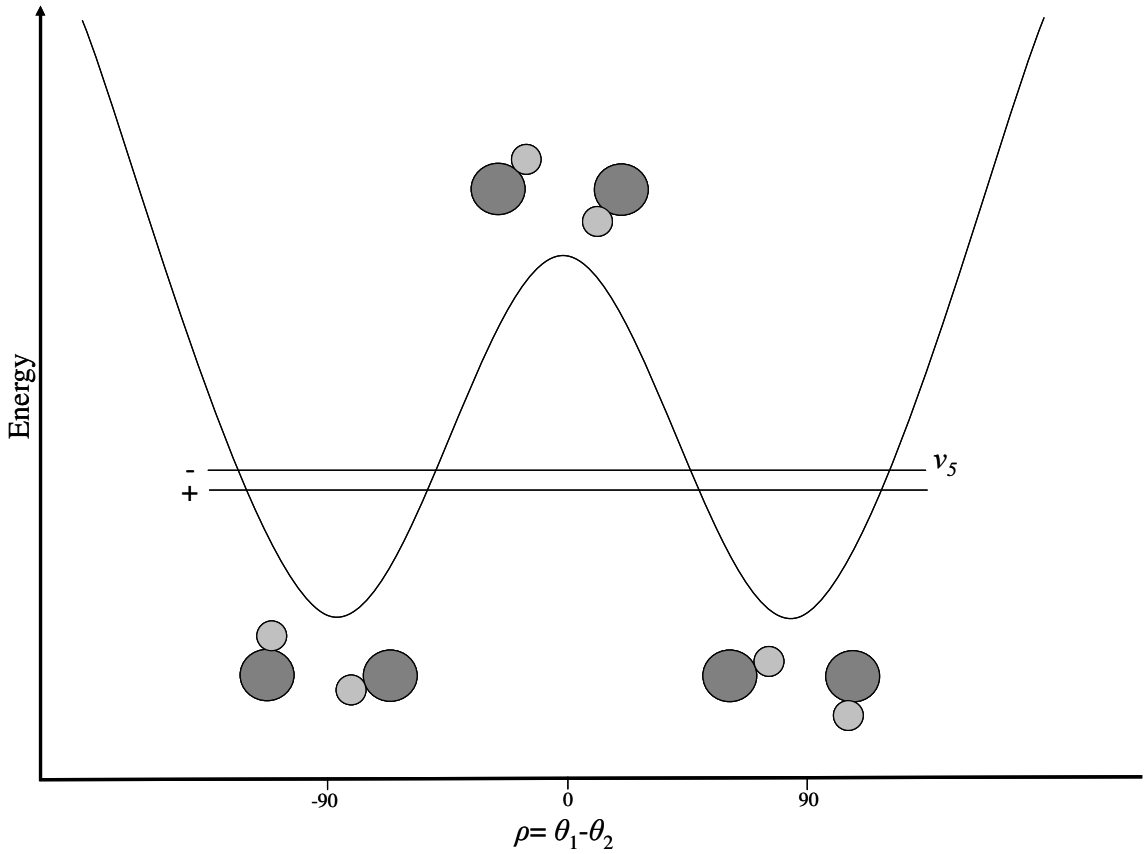

Figure 30. Simple potential diagram which demonstrates the two isoenergetic forms and the barrier for the $(HX)_2$ (X=F and Cl) complex.

Adhering to the labeling convention, the six fundamental vibrations are as follows ν_1, is the frequency of the "free" H-X stretch of the acceptor monomer, ν_2, is the frequency of the "bound" H-X stretch of the donor monomer, ν_3, is the frequency of the "antigeared bend", ν_4^1 is the frequency of the intermolecular stretch, ν_5^1, is the frequency of the "geared" bend that is also the tunneling motion, and ν_6, is the frequency of the out-of-plane torsion. The gross motion of the hydrogen nuclei are shown in Figure 31 for clarity.

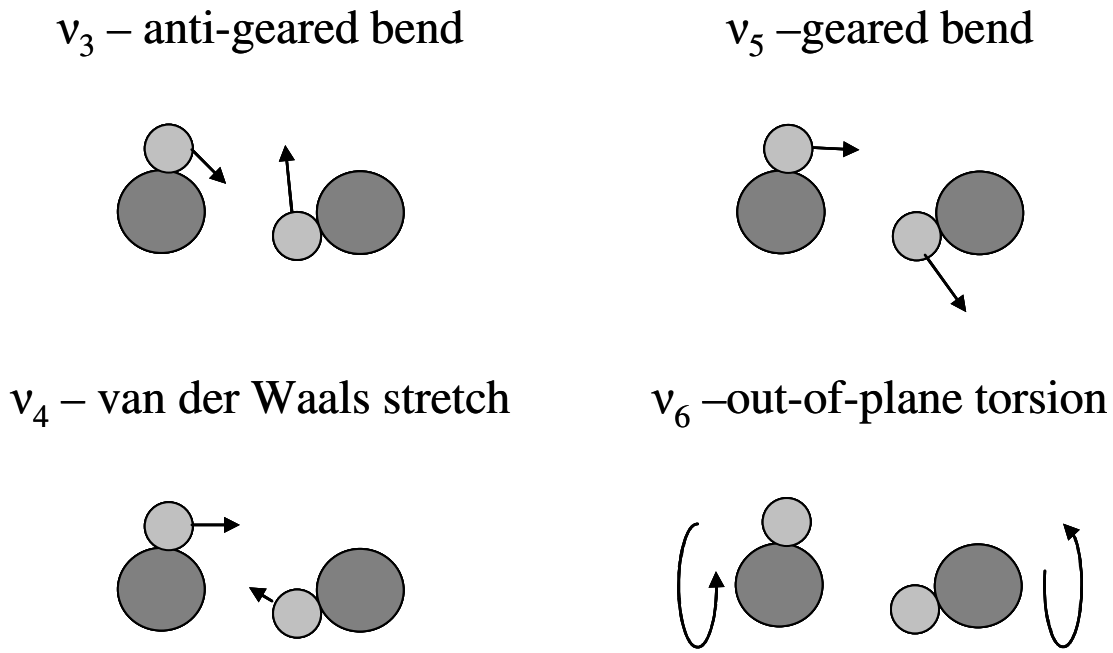

Figure 31. Intermolecular bending modes of $(HX)_2$

Previous investigations of the hydrogen fluoride and hydrogen chloride dimers dominate what is currently known about the hydrogen bond in this class of molecular complex. Not only have these two species been studied in the infrared, microwave and submillimeter spectral regions[69, 96, 99, 100], but there are a number of theoretical treatments of these dimers and higher order polymers by ab initio theory and some fitting of their potentials to spectroscopic data[90, 94, 101-104].

The first report of the direct tunneling transition in $(HF)_2$ was first observed by Klemperer and co-workers using molecular beam electric resonance spectroscopy[69, 90]. The spectra associated with the tunneling inversion, observed at 0.66 cm^{-1}, as well as transitions of ΔK=1 and dipole moments were used to determine the equilibrium structure of the complex as an "L-Shaped" complex with one hydrogen atom bonding

between the two heavy atoms of fluorine(see Figure 29). The angle of the monomer units were determined to be 63° and 10° for θ_1 and θ_2 respectively. Initially, the structure of the rotational spectrum was a puzzle, as the predicted rotational transition was expected to be at about 12 GHz, much lower then the observed value of 19 GHz. The spectrum could only be understood by invoking a tunneling between two isoenergetic structures by the exchange of the positions of the hydrogen nuclei[105] with the breaking and reformation of the hydrogen bond. Infrared combination bands of the HF stretching vibrations have also been observed[91, 93-95]. In these spectra, the free and hydrogen bound HF monomer units are excited by infrared radiation and combination bands of the low frequency bending vibrations have also been observed. Potential energy surfaces have been generated that describe the energetics of the different vibration modes of the dimer[101-103, 106]. Through these calculations the barrier between the isoenergetic structures has been estimated to be about 351±2 cm^{-1}.

Similar spectroscopic studies of $(HCl)_2$ have also been made in the far infrared and the infrared regions [92, 96-98, 107, 108], and the tunneling inversion was determined to be about 15.476680(4) cm^{-1} [96] corresponding to a significantly lower barrier of 38.5±2 cm^{-1}.

$(HBr)_2$ has also been studied although not with the same degree of detail as the previously mentioned complexes. Infrared matrix isolation spectroscopy has been used to observe the infrared spectrum of the bound and free stretch of HBr dimer in solid argon and krypton[67, 109]. The bulk properties of the HBr dimer have also been determined mainly through the determination of the second virial coefficient which was measured by speed-of-sound measurements[110] in gaseous HBr. The second virial

coefficient is directly related to the dissociation energy of the complex and has been determined to be about 415 cm^{-1}. The bound HBr stretch has been observed in supersonic slit jet FTIR spectra of HBr dimer at low resolution (1 cm^{-1}) and the assignment of the tunneling inversion combination bands made[111]. There have only been two prior notable high resolution spectroscopic studies of $(HBr)_2$. The first, a microwave analysis of the HBr-DBr complex,[4] and the near infrared spectrum[112] of the HBr stretching vibrations in $(HBr)_2$ and combination bands of the tunneling states from the broken symmetry transitions. Based on these studies, a four-dimensional ab initio potential energy surface was generated and the tunneling of about 15 cm^{-1} was predicted. This correlated with the broken symmetry results of $H^{79}Br$-$H^{81}Br$ for ν_5 of 15.03220(19) cm^{-1}.

The hydrogen iodide dimer has been observed using an infrared diode laser spectrometer[113]. The bound HI stretch was observed along with the combination bands associated with a common lower state which were not assigned at the time. As with HBr and HCl dimers, matrix isolation studies have also been used to observe the monomer stretch of HI dimer in Argon matricies[67, 114]. $(HI)_2$ has been studied via high-*n* Rydberg time-of-flight[115], and an L shaped structure was assumed from ab initio calculation[116].

The potential energy surfaces of the two hydrogen halide dimers, $(HF)_2$ and $(HCl)_2$, are known to be characterized by a two minima potential, with equivalent energy, and a barrier between them. The tunneling spectra of hydrogen halide dimers give some information concerning the potential energy surface of the dimer, such as the depth of the wells and the height of the barrier, as well as dissociation energies. The

$(HF)_2$, $(HCl)_2$ and $(HBr)_2$ are known to have an L-shaped structure as shown in Figure 29, with characteristic angles θ_1 and θ_2 and the distance between the centers of mass, R_{CM}.

The tunneling vibration of the hydrogen halide dimers is inversely dependent on the height and width of the barrier between the isoenergetic forms. From previous studies, the tunneling inversion energy for $(HCl)_2$ and $(HBr)_2$ is known to be within the submillimeter frequency range. These systems are a perfect opportunity for the use of the TAMU submillimeter spectrometer to observe the low frequency tunneling vibrations of these complexes. In addition, the low frequency bending vibration is expected to be around 14.5 cm^{-1} for $(HI)_2$ based on extrapolation using the previously observed band origins in the infrared[113]. The high resolution coupled with the frequency accuracy of which the submillimeter spectroscopic technique is capable of providing a great deal of structural and dynamical information on these complexes to be determined from experimental observations,

The generation of potential energy surfaces for these dimers affords a systematic study of the accuracy of the theoretical models that treat the dynamics of these prototypical systems. It has been demonstrated that the tunneling motion in the dimers is characterized by two isoenergetic structures which are separated by a potential energy barrier for $(HF)_2$ and $(HCl)_2$. The inversion pathway occurs through the barrier and the structure of the dimer must undergo a large amplitude anharmonic motion by which the respective hydrogen atoms interconvert between the two isoenergetic structures. As a consequence of this tunneling motion characteristic, the vibration energy levels of the

dimer is split into a pair of levels separated by the tunneling frequency. Superimposed on these we expect significant quadrupole substructure due to the presence of two quadrupole nuclei which create significant hyperfine splitting in the rotational levels, and the quadrupole transitions will become increasingly separated due to the contribution of the quadrupole moment of the monomer units. HF lacks a quadrupole moment, however HCl, HBr and HI have corresponding quadrupole moments of -66.7751(30) MHz, 532.3041(8) MHz and -1828.286(9) MHz respectively. The splitting due to these nuclei is significant for low rotational transitions and collapses and become overlapped at higher rotation transitions. Taking an effective quadrupole moment in the complex at an angle of 45° the transitions will be split to approximately 30% of the monomer quadrupole moment. However the presence of the second nuclei will split the levels further. A significant number of transitions can be observed as the degeneracy of the quadrupole sublevels and the selection rules can generate as many as 144 transitions in HI dimer compared with 48 for HBr dimer.

It is pertinent to note that in the case of HBr dimer, a barrier to tunneling inversion has been previously proposed. However in the case of HI dimer there is no direct evidence of such tunneling. This will be the topic of further discussions later in this chapter.

It is the goal of the current work to extend the treatment of the dimers through the homologous series to $(HBr)_2$ and $(HI)_2$ with the observation of the "geared bending" vibration, with quadrupole resolved rotational structure, afforded by the high resolution co-axially configured submillimeter spectrometer.

The observation and analysis of the corresponding tunneling transitions in $(HBr)_2$ and $(HI)_2$ would complete investigations of the homologous series of $(HX)_2$ and provide additional information about the dynamics involved with the hydrogen bond in these complexes. The application of theoretical models to describe the molecular dynamics involved in the hydrogen halide dimers and the potential energy surfaces that are generated are a central theme of the current studies. Such analyses will have direct relevance to the interpretation of photo-induced dynamics. Furthermore, such results will have direct relevance to the development of six dimensional morphed potential functions, important in the complete vibrational treatments of the complexes. Such well characterized pair-wise potentials will be important in characterizing the aggregation processes to form trimers and higher clusters and possibly be capable of explaining the observed differences in the structure of solid state HBr and HI.

Experimental

The HBr and HI dimer complexes are observed using the TAMU submillimeter spectrometer as described in a previous chapter of this dissertation. The complexes were formed by expanding a mixture of 2% HBr or HI seed gas in a balance of argon as carrier expanded through a solenoid valve with an orifice of 0.030". A stagnation pressure of 6-24 psi was adjusted for maximum signal intensity. The operating conditions were comparable to those used for the observation of Ar:HBr. HBr dimer was observed using an OB-32 BWO tube version which operated in the frequency range of 435 to 465 GHz. HI dimer was observed using an OB-80 tube version and operated

from 506 to 517 GHz, which is below the stated operation range of this tube but had sufficient power available for making the desired observations. Each transition center frequency was calculated as the average of the 4 Doppler components as was done previously for Ar-HBr. Transitions associated with $\Delta J=\pm1,\Delta F=0,\pm1$ of the rovibrational transitions were thus recorded with 50 kHz instrumental resolution and an estimated frequency accuracy of ~1 kHz.

Analysis

Analysis of the observed spectra of both HBr and HI dimers were made on the basis of a linear prolate rotor approximation. The ν_5^1 "geared bending" rovibrational spectrum associated with the $H^{79}Br$-$H^{79}Br$, $H^{79}Br$-$H^{81}Br$ and $H^{81}Br$-$H^{81}Br$ isotopomers of HBr dimer and HI dimer have been observed and assigned based on a complex involving two quadrupole nuclei. The HBr dimer isotopomers were observed in natural abundances with a ratio of ~1:2:1 for the $H^{79}Br$-$H^{79}Br$, $H^{79}Br$-$H^{81}Br$ and $H^{81}Br$-$H^{81}Br$ isotopomers. A similar observation was made for the isotopomers of $(HCl)_2$ but in this case the intensity ratios were appropriate to a ^{35}Cl:^{37}Cl ratio of 75:25 [96]. There are no naturally occurring isotopomers of iodine and no other isotopomers of this complex were observed. The K=0←0 rovibrational transitions of dimers were assigned as there was no evidence of a Q-branch in the observed spectra and observed transitions were restricted and did not include observation of K=1←0. Figure 32 contains the predicted stick spectrum of the three isotopomers of HBr dimer with correct intensity ratios.

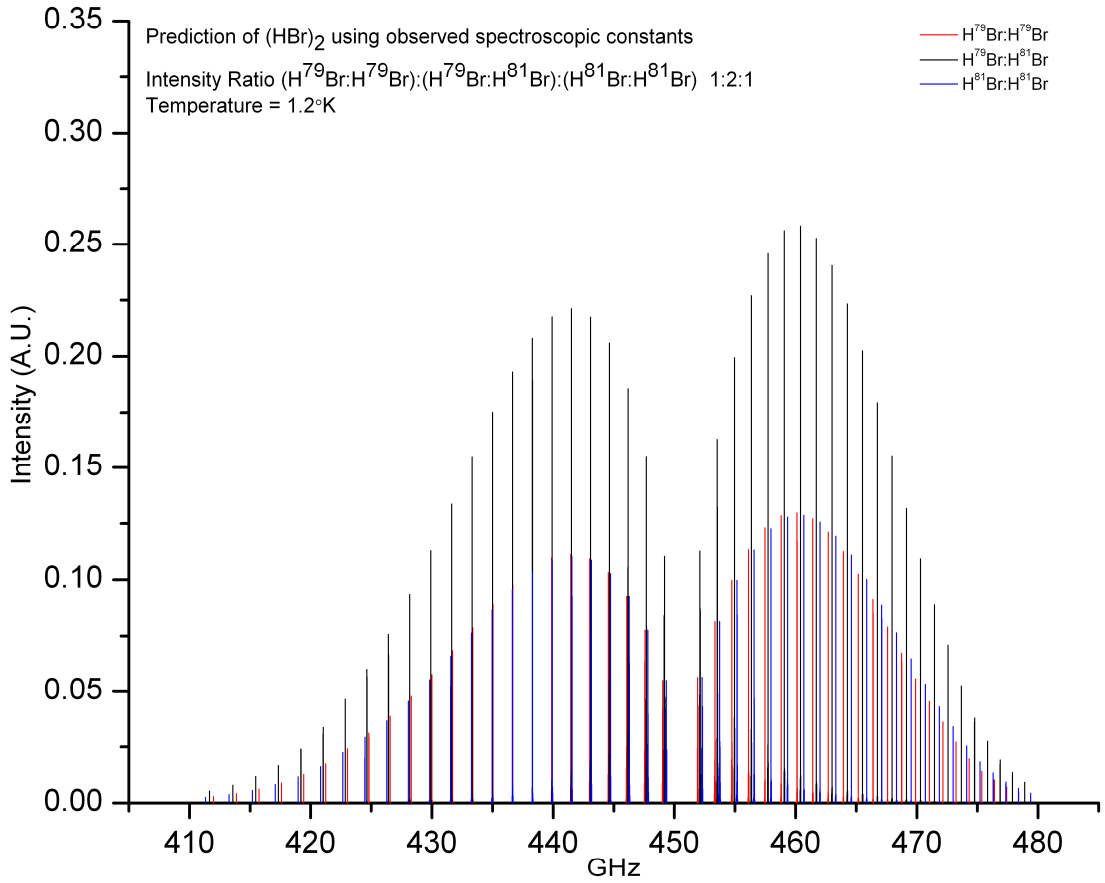

Figure 32. Predicted spectrum of HBr dimer showing the 3 possible isotopomer combinations with an intensity ratio of 1:2:1.

$(HBr)_2$

1140 lines from the three isotopomers of HBr dimer were recorded for R(10) to P(10) rovibrational transitions with an estimated effective rotational temperature of 1.2K. The extensive quadrupole substructure of the rovibrational transitions is very rich with 14 quadrupole transitions for the R(0) and P(1) transitions alone and they were almost completely resolved. Figure 33 shows the predicted stick spectrum of the $H^{79}Br:H^{79}Br$ isotopomer centered at 15.03 cm^{-1} or 450.8 GHz.

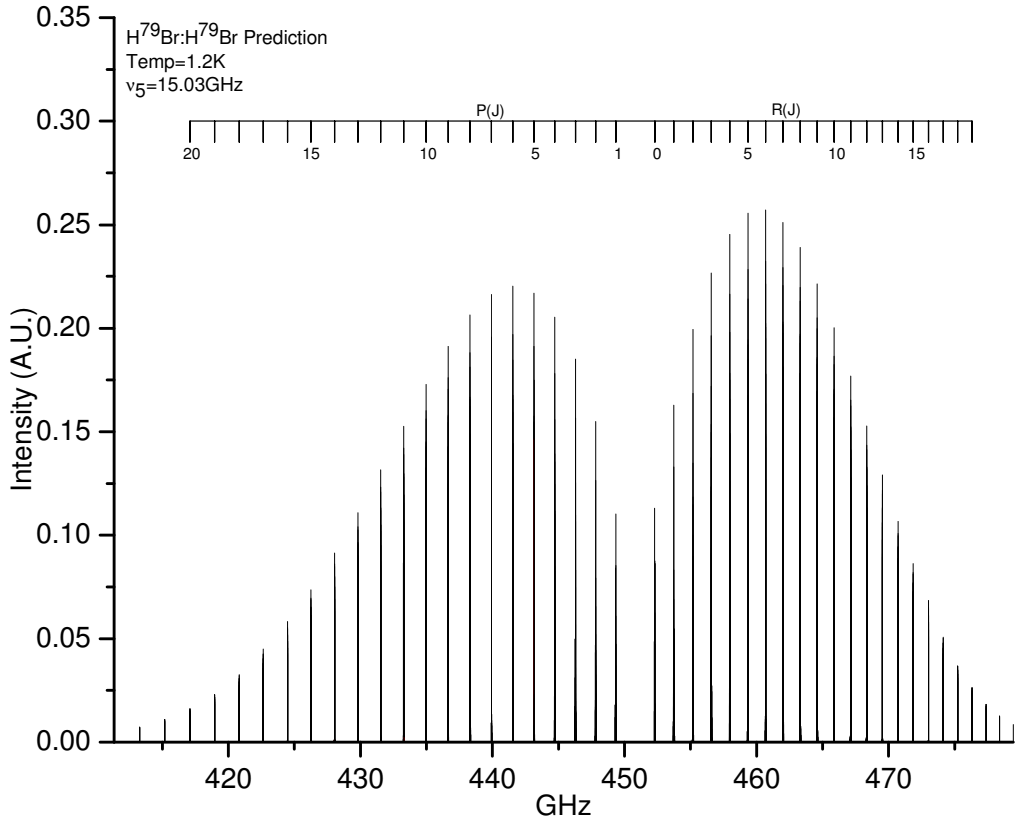

Figure 33. Predicted stick spectrum of $H^{79}Br:H^{79}Br$ with ν_5^1=15.03 cm^{-1} and a temperature of 1.2K.

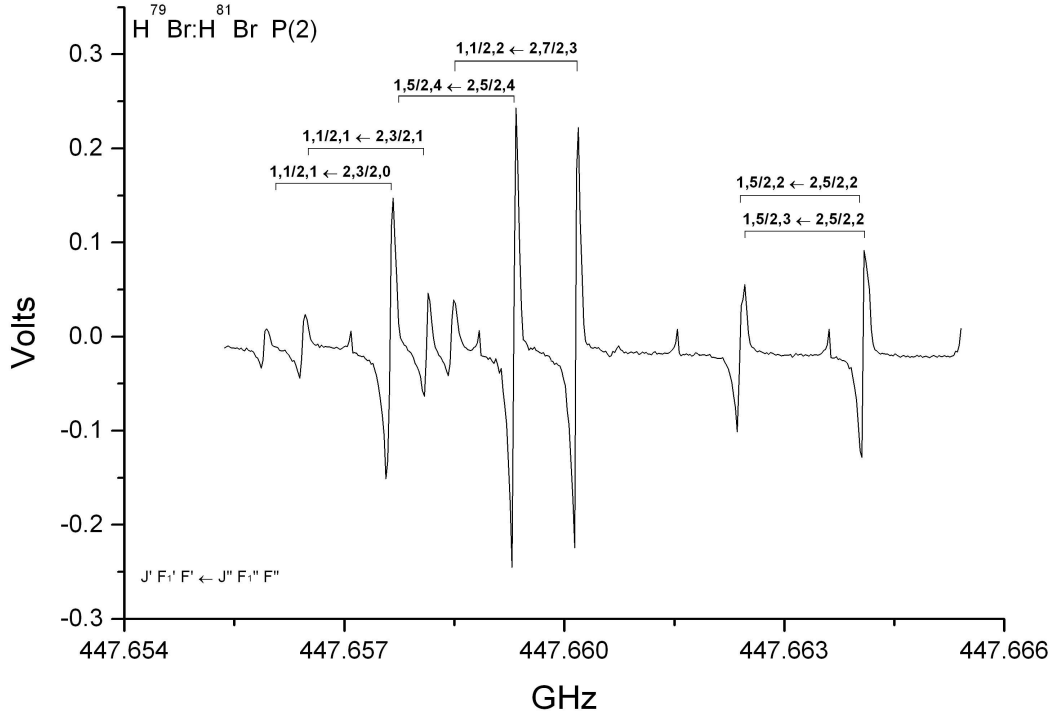

Figure 34. Portion of the P(2) rotation tunneling inversion band of $H^{79}Br:H^{81}Br$.

The observed quadrupole substructure involved with the P(2) transition of $H^{79}Br:H^{81}Br$ isotopomer is illustrated in Figure 34. This segment of the spectrum, which covers approximately 10 MHz, shows the partially resolved quadrupole substructure of 6 discrete quadrupole transitions, with the quantum numbers indicated. Although the resolution here is 50 kHz the center frequency is able to be determined with an accuracy of 1 kHz for well resolved transitions and 5 kHz transitions that had distorted line shapes due to overlap of line profiles.

As stated previously, the Hamiltonian that was used to fit the rovibrational transitions of $(HBr)_2$ was that of a linear rotor including individual contributions from the vibration, rotation and quadrupole energy components described by

$H = H_T + H_R + H_Q$. Here, H_Q follows the F_1=J+I_{Br1} and F=F_1+I_{Br2} coupling scheme. The linear rotor quanta were selected as the rovibrational band showed no Q-branch indicating the observed transitions were K=0←0 transitions. The fitting procedure was carried out using the SPFIT package[81] as discussed previously. A total of 1140 quadrupole transitions were recorded, 295 for $H^{79}Br$-$H^{79}Br$, 526 for $H^{79}Br$-$H^{81}Br$ and 319 for $H^{81}Br$-$H^{81}Br$. The determined values of ν_0, tunneling frequency, and the associated rotational constants B and D_J, as well as the quadrupole constants χ_{aa1}, $D\chi_{aa1}$, χ_{aa2} and $D\chi_{aa2}$ are determined and given in Table 16. The RMS deviation of the fits for the $H^{79}Br$-$H^{79}Br$, $H^{79}Br$-$H^{81}Br$ and $H^{81}Br$-$H^{81}Br$ were 12.0 kHz, 10.5 kHz and 10.1 kHz respectively. Table 15 contains the transition frequencies of the three isotopomers for the R(0) and P(1) rovibrational transitions and is compiled with the quantum numbers of a given state and the Observed-Calculated residuals in kHz from the fitting procedure for each isotopomer. The complete listing is given in Appendix B.

Table 15. Selected individual quadrupole component frequencies for $(HBr)_2$ including the R(0) and P(1) rotational tunneling transitions.

								$H^{79}Br$-$H^{81}Br$		$H^{79}Br$-$H^{79}Br$		$H^{81}Br$-$H^{81}Br$	
J'	V'	F1'	F'	J"	V"	F1"	F"	Observed (MHz)	O-C (kHz)	Observed (MHz)	O-C (kHz)	Observed (MHz)	O-C (kHz)
1	1	1/2	2	0	0	3/2	3	452076.0061	-4	452252.4438	-10	451899.4951	-6
1	1	1/2	2	0	0	3/2	1	452076.0061	-4	452252.4438	-10	451899.4951	-7
1	1	1/2	1	0	0	3/2	2	452080.3110	-9			451903.5914	-7
1	1	1/2	1	0	0	3/2	0	452080.7125	6	452257.7840	6	451903.9270	2
1	1	5/2	1	0	0	3/2	1	452092.3124	4	452269.8751	2	451914.0586	2
1	1	5/2	4	0	0	3/2	3	452101.7180	4	452280.3464	0	451922.8222	0
1	1	5/2	3	0	0	3/2	2	452111.2059	-15	452290.8120	6	451931.5837	7
1	1	5/2	2	0	0	3/2	2			452290.9130	9	451931.6570	10
1	1	3/2	2	0	0	3/2	3	452127.8429	5	452308.4471	5	451946.2895	3
1	1	3/2	2	0	0	3/2	1	452127.8429	5	452308.4471	5	451946.2895	3
1	1	3/2	3	0	0	3/2	3	452140.7237	-3	452322.7535	-7	451958.2480	-5
1	1	3/2	1	0	0	3/2	2	452142.0739	-9	452324.2464	-13	451959.5225	-9
1	1	3/2	1	0	0	3/2	0	452142.4735	3	452324.7234	7	451959.8594	0
1	1	3/2	0	0	0	3/2	1	452150.3151	-12	452333.3134	-17	451967.0743	-13
0	1	3/2	1	1	0	3/2	0	449145.7980	-5	449285.7410	-8	449005.6150	-3
0	1	3/2	0	1	0	3/2	1	449153.2700	-12	449293.9315	-17	449012.4900	-14
0	1	3/2	2	1	0	3/2	1	449153.7240	13	449294.4685	13	449012.8763	9
0	1	3/2	3	1	0	3/2	3	449154.9710	-5	449295.8492	-3	449014.0606	-3
0	1	3/2	1	1	0	3/2	2	449167.2810	1	449309.5392	0	449025.5050	0
0	1	3/2	3	1	0	3/2	2			449309.5392	0	449025.5050	0
0	1	3/2	2	1	0	5/2	3	449183.2490	6	449326.4260	-5	449039.5900	-3
0	1	3/2	2	1	0	5/2	2	449183.3190	-2	449326.3517	9	449039.5400	10
0	1	3/2	3	1	0	5/2	4	449192.2880	-3	449336.3813	-7	449047.9282	-6
0	1	3/2	1	1	0	5/2	1	449201.2720	0	449346.4062	1	449056.3162	-1
0	1	3/2	2	1	0	1/2	1	449212.8220	12	449358.4497	13	449066.3492	8
0	1	3/2	0	1	0	1/2	1	449212.3660	-14	449357.9110	-18	449065.9650	-13
0	1	3/2	3	1	0	1/2	2	449216.8840	-4	449363.0519	-3	449070.2286	-4
0	1	3/2	1	1	0	1/2	2	449216.8840	-4	449363.0519	-3		

HI Dimer

342 quadrupole transitions in P(6) to R(6) rovibrational transitions were recorded in the frequency range of 506 to 517 GHz. Predicted stick spectra for the rovibrational band of $(HI)_2$ which is centered at 17.1 cm^{-1} are shown in Figure 35, Figure 36, and Figure 37. The extensive quadrupole structure of the rotation transitions is more complex than that seen in $(HBr)_2$ as the nuclear spin of iodine is 5/2, and the two nuclei split the respective R(0) and P(1) transitions into 24 iodine-iodine nuclear quadrupole components. In theses cases, the quadrupole components have been resolved as illustrated by the simulated stick spectrum in Figure 37. These predictions were made assuming that the quadrupole coupling from each iodine nucleus is equivalent and that the angle is 46.40°. The center frequencies of the quadrupole transitions of the rovibrational energy levels were also fitted to the standard linear rotor Hamiltonian describing the vibration, rotation and quadrupole structure given by $H = H_T + H_R + H_Q$ where H_Q follows the $I_{Tot}=I_{I1}+I_{I2}$ and $F=J+I_{Tot}$ coupling scheme, using the SPFIT package[81]. The I_{Tot} coupling scheme was used in the case of $(HI)_2$, and will be the subject of a detailed discussion in the following section. Figure 38 shows a frequency scan of the two Doppler split components of the single transition $I',F' \leftarrow I'',F''$ 3,3←3,3 quadrupole transition of the J=1←0 rotation transition of the v_5 bending vibration in $(HI)_2$ as identified by the arrow in Figure 37. The center frequency of this transition is 512679.0404(50) MHz.

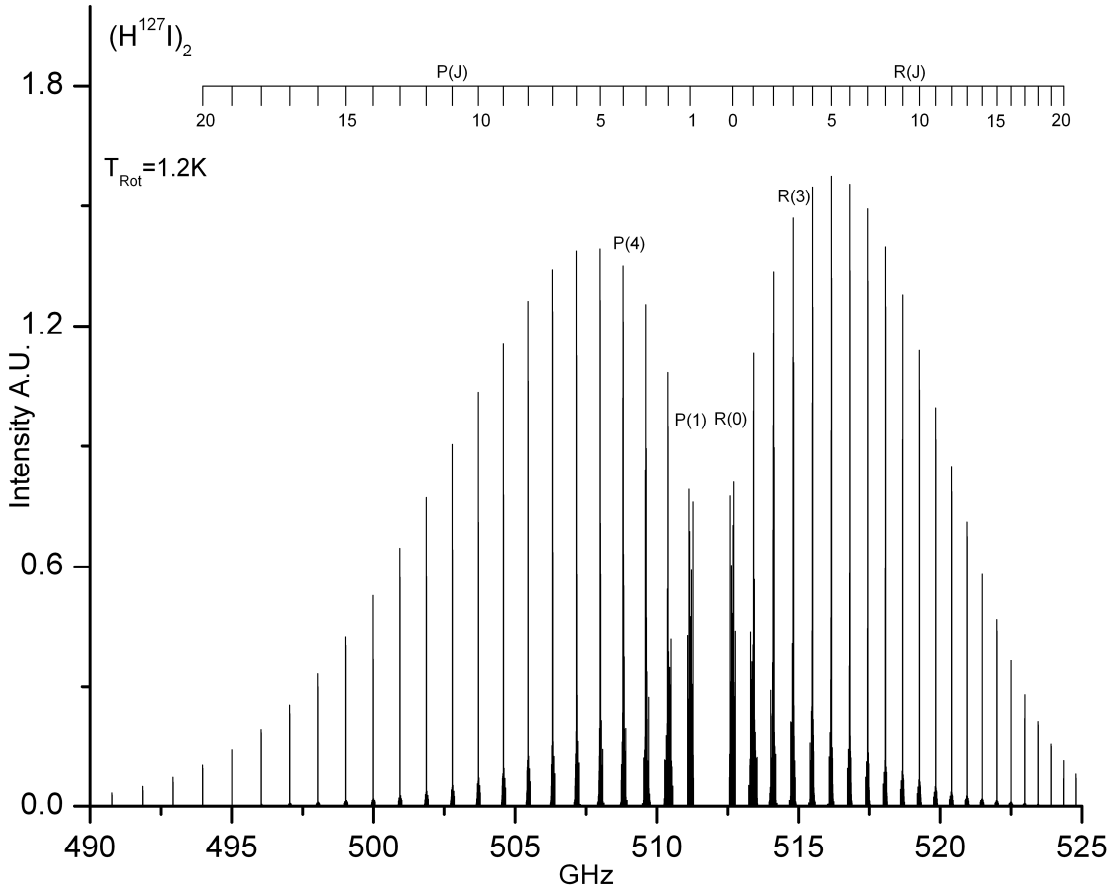

Figure 35. Predicted spectrum of the ν_5^1 "geared bending" vibration band of HI Dimer.

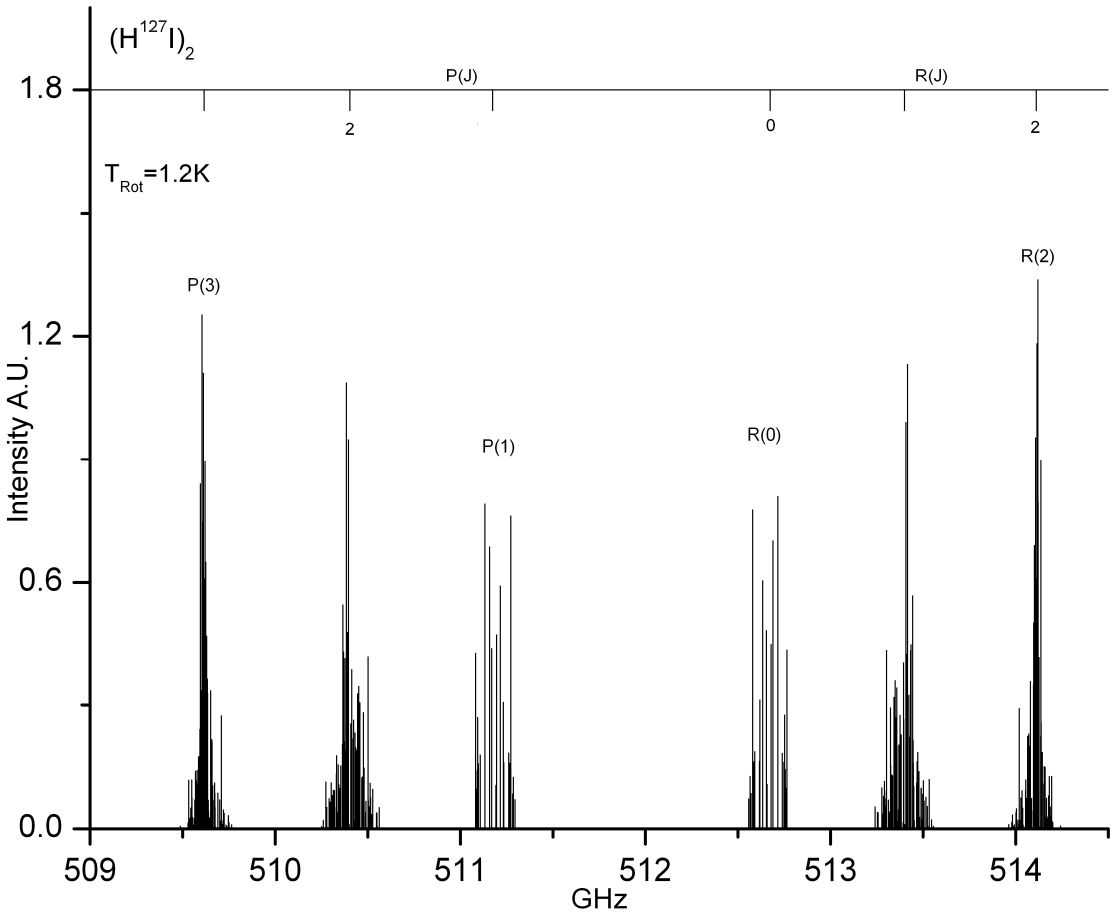

Figure 36. Predicted spectrum of the v_5^1 "Geared Bending" vibration of HI Dimer of the Low J transitions showing partially resolved quadrupole substructure. It corresponds to 5.5 GHz section (0.18346 cm^{-1}) segment of the spectrum magnified by a factor of 6 in the frequency scale relative to Figure 35.

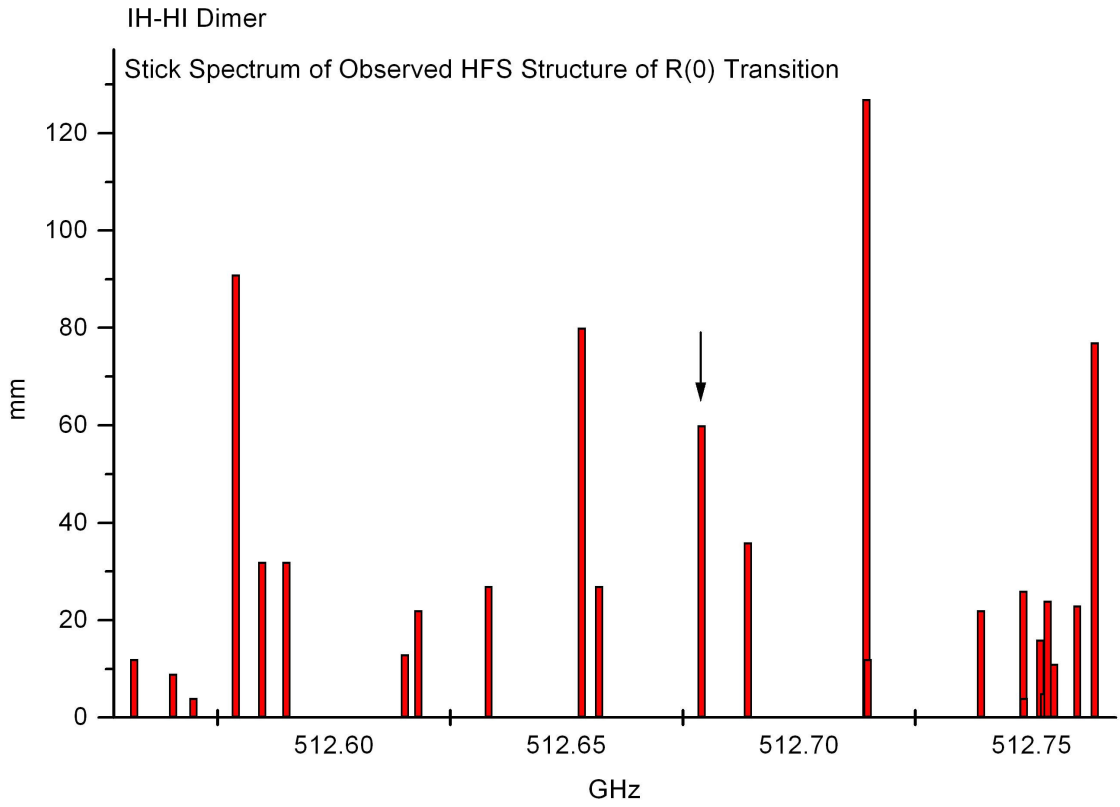

Figure 37. $(HI)_2$ Stick Spectrum of the R(0) rovibrational transition. The arrow indicates the transition shown experimentally in Figure 38. The scale of this illustration corresponds to a factor of 16 magnification in the frequency scale relative to Figure 36.

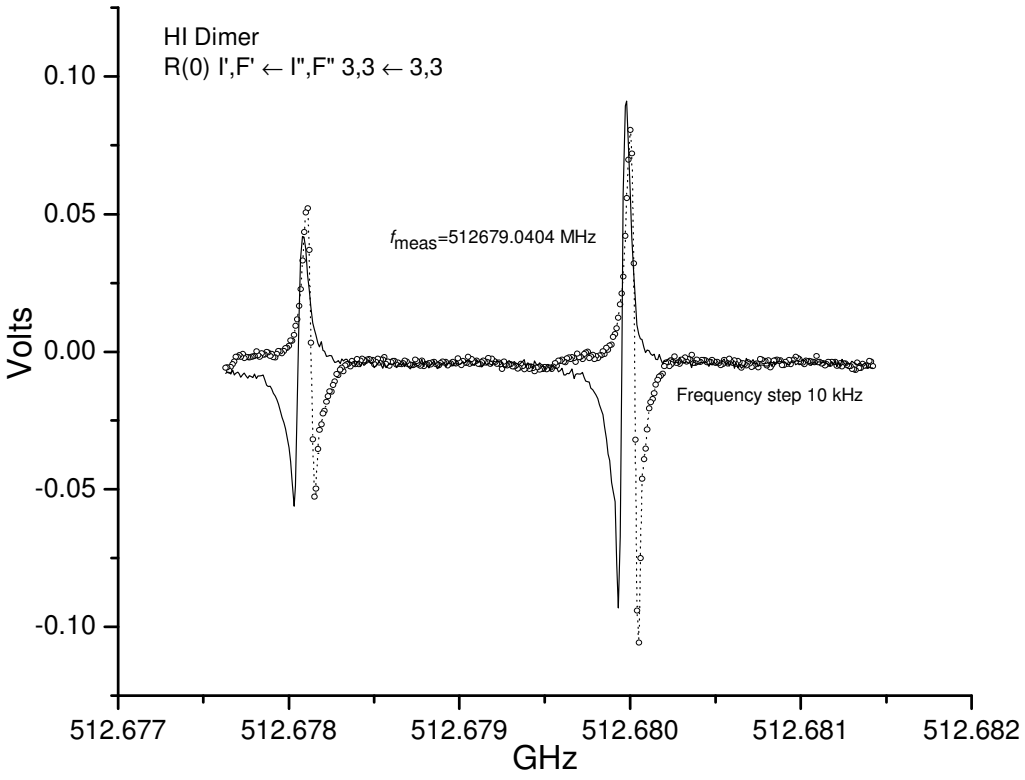

Figure 38. Experimentally recorded spectrum of R(0) *I'*,*F'*←*I''*,*F''* 3,3←3,3 transition of HI Dimer. The center frequency is 512679.0404(50) MHz. This corresponds to a factor of 60 magnification in the frequency scale relative to that of Figure 37. The ratio of the peak intensities is an instrumental artifact.

Table 16. $(HBr)_2$ and $(HI)_2$ spectroscopic constants.

	ν_0 (MHz)	B (MHz)	D_J (kHz)	$\chi_{aa}1$ (MHz)	$D\chi_{aa}1$ (kHz)	$\chi_{aa}2$ (MHz)	$D\chi_{aa}2$ (kHz)	σ (kHz)
$H^{79}Br$: $H^{81}Br$[a]	450657.48138(11)	726.913631(15)	1.07791(24)	105.6040(12)	0.421(53)	88.6280(14)	0.538(57)	10.5
$H^{79}Br$: $H^{81}Br$[b]		737.156541(17)	1.22684(28)	101.3731(13)	1.446(59)	84.3791(15)	-0.182(64)	
$H^{79}Br$:$H^{79}Br$[a]	450819.01715(12)	735.888632(17)	1.10352(22)	105.83967(42)	0.560(16)			12.0
$H^{79}Br$:$H^{79}Br$[b]		746.276056(20)	1.25329(35)	101.16259(43)	0.84(19)			
$H^{81}Br$:$H^{81}Br$[a]	450495.69107(12)	717.93898(15)	1.05308(20)	88.43842(41)	0.425(15)			10.1
$H^{81}Br$:$H^{81}Br$[b]		728.037393(20)	1.19696(33)	84.54797(45)	0.8867(21)			
$H^{127}I$: $H^{127}I$[a]	511931.43854(10)	370.809883(15)	0.29788(25)	-377.36085(42)				79.0
$H^{127}I$: $H^{127}I$[b]		378.298933(23)	0.347409(44)	-389.99342(42)				

[a] upper state

[b] lower state

Fitting $(HI)_2$ to the Hamiltonian described by a linear prolate rotor proved to be the cause of concern as the RMS deviation of the fit was ~80 kHz and was much greater than the estimated accuracy of the measurements. This was especially so when compared to the corresponding fit for transitions in $(HBr)_2$. A second fit was made using an asymmetric prolate rotor basis with the addition of second order quadrupole coupling. The *A* rotation constant was fixed to a value that is consistent with the two hydrogen atoms having a projection of 45° from the major axis of the complex, in both the ground and excited state. This assumption was considered a good approximation based on the interpretation of χ_{aa} determined. An additional quadrupole coupling term, $\chi_{bb} - \chi_{cc}$, was also included for both iodine nuclei and fixed to be the same value. This improved the fit to ~30 kHz but this was still larger than was found for either Ar-HBr or Ar-IH where the corresponding values of σ were 0.9 kHz and 7.0 kHz.

There are two different quadrupole coupling schemes that could be used in the assignment and fitting of spectra[117]. The first case is the sequential coupling scheme where the rotation quantum number is coupled to the nuclear spin of one nucleus and the resultant F quantum number is then coupled with the second nucleus to give F.

$$\begin{aligned} &J + I_1 = F_1 \\ &F_1 + I_2 = F \\ &J \text{ - Rotational angular momentum} \\ &I_N \text{ - Nuclear spin (N = 1..n)} \end{aligned} \qquad (33)$$

The second case, I_{Tot}, for equal or nearly equal coupling, first couples the nuclear spins of identical (or nearly equal) nuclei together to give I_{Tot} and then the coupling to the rotational quantum number to give F.

$$I_1 + I_2 = I_{Tot}$$
$$J + I_{Tot} = F \quad (34)$$
J - Rotational angular momentum
I_N - Nuclear spin (N = 1..n)

In the final analysis, both coupling schemes are identical but the use of I_{Tot} makes the identification of the symmetric and antisymmetric states of the quadrupole coupling readily apparent, as will be discussed below.

Improvement of Fits

A plot of the observed-calculated (O-C) residuals for the fit for the three $(HBr)_2$ isotopomers was made and shown in Figure 39. Only the P(1) and R(0) transitions are plotted for clarity. However, the general trend can still be seen. Each set of isotopomers roughly follow the same O-C values. This indicates that the Hamiltonian used to fit the measured data is not adequate to treat the data to the precision and accuracy of the measurements. The number of terms that are included into the fit generally should achieve a reduction in the standard deviation of the fit. The quality of the fit can be evaluated by plotting the O-C differences on an arbitrary axis, as done in Figure 39 for $(HBr)_2$. The important thing to note here is that the O-C residuals from the fit are grouped isotopically. The reason for this observation is that the Hamiltonian used is lacking terms specific for the quadrupole energy, as discussed earlier. This also indicates that the accuracy of the measurements is ~1 kHz.

In an effort to fit the quadrupole coupling with a higher degree of accuracy a higher level fitting procedure was undertaken with a collaborative effort with Jon Hougen (NIST, Gaithersburg, MD, USA) and Laurent Coudert (LISA, University of

Paris, France). The fit of HI dimer was improved by incorporating an asymmetric rotor Hamiltonian with the inclusion of second order quadrupole terms that involve energies of each state as well as those between the states[118]. This improved the fit of HI dimer to 18 kHz[119].

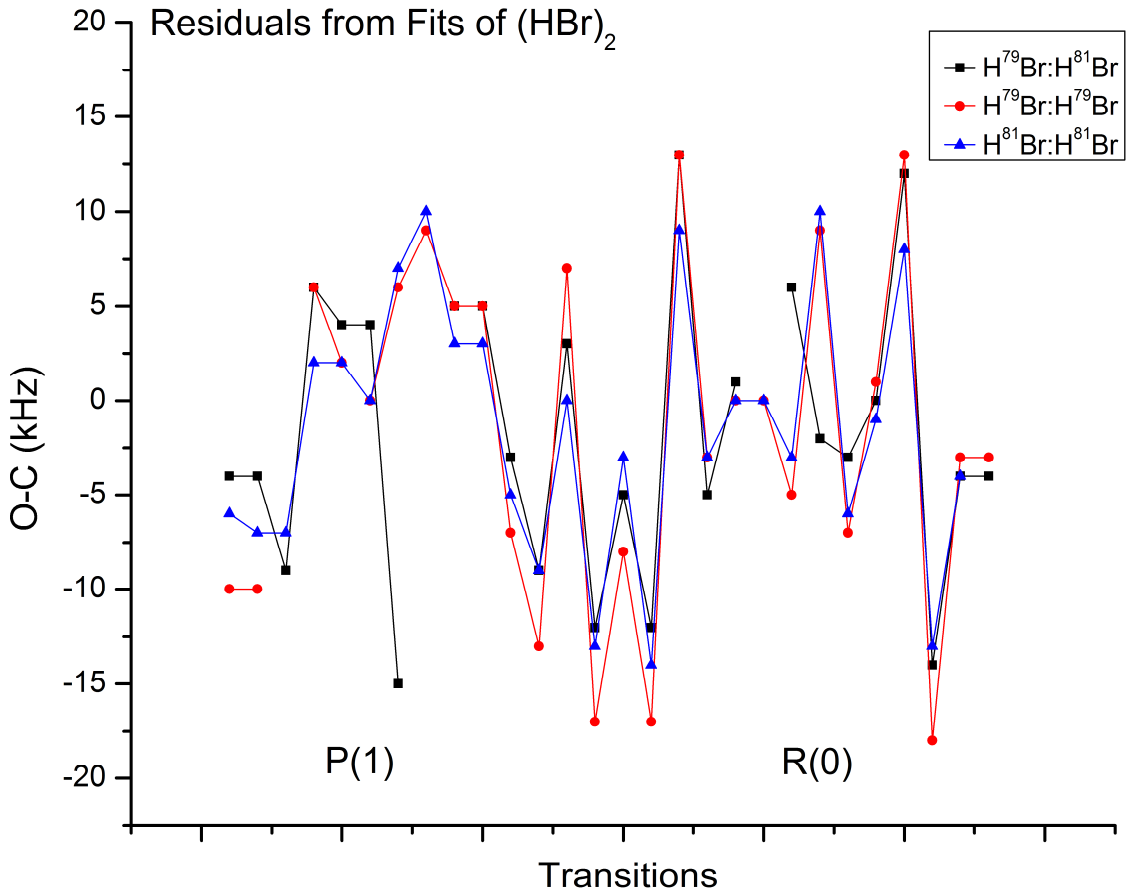

Figure 39. $(HBr)_2$ residuals plotted against the transition number for comparison. P(1) transitions are on the left and R(0) transitions are on the right.

The fit uses the I_{Tot} coupling scheme and defines the orientation of the complex in the Eulerian coordinate system. This generates slightly different constants for the quadrupole coupling but is still experimentally comparable.

Table 17. Spectroscopic parameters obtained for HI dimer from Coudert et. al.

Parameter	ν_5=0	ν_5=1
E^{v_5}	0.0	511931.090
A^{v_5}	232000.0	232000.0
$\left(B^{v_5}+C^{v_5}\right)/2$	378.29990(42)	370.81099(29)
$B^{v_5}-C^{v_5}$	2.411(1700)	10.647(7900)
$D_J^{v_5}\times 10^3$	0.36401(810)	0.29239(2300)
$\chi(S)_{xx}^{v_5}+\chi(S)_{yy}^{v_5}$	389.86103(900)	377.46485(990)
$\chi(S)_{xx}^{v_5}-\chi(S)_{yy}^{v_5}$	-864.6[b]	-178.3[b]
$\chi(S)_{xz}^{v_5}$	-778.80(610)	-175.4(380)
$\chi(A)_{xx}+\chi(A)_{yy}$	559.09(910)	
$\chi(A)_{xx}-\chi(A)_{yy}$	211.8[b]	
$\chi(A)_{xz}$	-146.7(490)	

[a] Parameters in MHz. Errors are one standard deviation in the fit.
[b] Constrained value.

The constants of the fitting procedure for HI dimer are given in Table 17 for the asymmetric rotor fit with previously discussed terms included. The constants relating the quadrupole terms and the rotational constant B are very well determined. In order to fit the A rotation constant with a higher degree of accuracy as well as B-C constant the measurement of a K=1←0 band will need to be made. The estimated band origin of this vibration rotation spectrum will be about 740 GHz, which is well within the current operation range of the spectrometer.

Structural Determination

The ground state averaged structure of both complexes can now be evaluated. Based on the observed rotation and quadrupole coupling constants given in Table 16 the center of mass distance and effective angle of the monomers can be determined in the ground and either the excited tunneling state or vibrational state. The effective angle of each monomer can be determined by using Equation 30 in Chapter III in which it is assumed that there are no structural changes of the monomer components on complexation. The vibrationally averaged angles based on the quadrupole coupling constants in the complex determined from the fitting procedure are given in Table 18. The R_{CM} distance is determined by substituting the appropriate angles and moments of inertia of the complex and monomer units into Equation 35.

$$I_D = \mu_D R_{CM}^2 + I_1\left(\frac{1+\cos^2\theta_1}{2}\right) + I_2\left(\frac{1+\cos^2\theta_2}{2}\right) + \frac{\left(I_1 \sin 2\theta_1 + I_1 \sin 2\theta_1\right)^2}{4I_D} - \frac{\left(I_1 \sin^2\theta_1 + I_1 \sin^2\theta_1\right)^2}{4I_D} \tag{35}$$

I_D – moment of inertia of the complex

μ_D – reduced mass of the complex

I_i – moment of inertia of diatomic (1 or 2)

θ_i – angle of diatomic (1 or 2)

Table 18. Vibrationally averaged ground state structural parameters for HBr and HI dimers.

	θ_1/Deg	θ_2/Deg	R_{CM}/Å	R(X-X)/Å
$H^{79}Br$:$H^{79}Br$	47.2925	47.2925	4.1075	4.1319
$H^{79}Br$:$H^{81}Br$	47.2773	47.3038	4.1077	4.1318
$H^{81}Br$:$H^{81}Br$	47.2892	47.2892	4.1079	4.1316
$H^{127}I$:$H^{127}I$	46.4020	46.4020	4.5637	4.5813

The distance between the heavy atoms in the complex, R(X-X), can be estimated through simple geometry relationships. The vibrationally averaged effective structure of the complex is dependent on the large amplitude vibrations which occur in each state of the complex. The motion of the monomer unit occurs about the center of mass of the monomer. However, by adding the projection of the distance of the heavy atom to the center of mass of the monomer onto the major axis of the complex, the R(X-X) distance can be determined and these values are given in Table 18 for comparison. As can be seen, this distance agrees within 0.0003Å which is not considered significant for the three isotopomers of HBr dimer. Most likely this is due to a difference in the amplitude of the motion and some distortional effect due to the difference in masses of the bromine nuclei which will slightly lengthen the hydrogen bond in the complex.

Morphed Potentials of HBr and HI Dimer

In the previous sections, the observation and characterization of the structure of the ground state and first excited geared bending vibration in $(HBr)_2$ and the excited vibration state of $(HI)_2$ have been related. The effective averaged angles of the 4 complexes have been determined as well as their R_{CM} and R(X-X) distances. The rotational constants and energy of the excited tunneling and geared bending vibration as well as the quadrupole coupling constants are used to generate morphed potential energy surfaces of the dimers.

The 4-D morphed potential of HBr dimer has been generated using data from the infrared, microwave and submillimeter spectroscopy[12]. This potential which uses a previously generated ab-initio potential[112] includes data form the current submillimeter

study along with the extensive data from the infrared for K>0 rotational constants and PN-FTMW data of the HBr-DBr complex. Although the ground state dissociation energy of the complex has not been determined directly, the availability of the second virial coefficient provides important information for such an estimate. The morphed potential utilizes a non-linear least squares optimization procedure[65] to modify the ab initio potential energy surface to reproduce experimental data. The ground state and the excited tunneling vibrational state constants of the $H^{79}Br$:$H^{81}Br$ isotopomer are fitted well in a 7 parameter morphed potential, the results are given in Table 19.

Representation of the potential energy surface of HBr dimer is presented in Figure 40 and Figure 41. The energy is relative to the minimum of the potential and the energy at infinite separation. In both cases, it is shown that the potential energy surface has two minima which are isoenergetic and separated by a barrier. This confirms that HBr dimer is similar to HF and HCl dimers. The barrier between the two states is determined to be 72.8 cm^{-1} above the minimum in the potential (-644.0 cm^{-1}) which is slightly larger than that in $(HCl)_2$ but significantly smaller than$(HF)_2$.

Table 19. Experimental data used in the determination of the morphed potential of $(HBr)_2$. The fits and the values obtained from the fits together with the uncertainties are indicated. The states for the various constants are referred to as (v_5, K) where all other quantum numbers are zero.

Observable	Units	Isotopomer	$N_p = 0$	$N_p = 3$	$N_p = 7$	Exp.	σ_k
$B(0,0)$	10^{-2} cm^{-1}	$H^{79}Br$:$H^{81}Br$	2.485	2.437	2.458	2.459[a]	0.003
$B(1,0)$	10^{-2} cm^{-1}	$H^{79}Br$:$H^{81}Br$	2.466	2.418	2.423	2.425[a]	0.003
$B(0,0)$	10^{-2} cm^{-1}	$H^{79}Br$:$D^{81}Br$	2.484	2.436	2.449	2.444[b]	0.003
$B(0,1)$	10^{-2} cm^{-1}	$H^{79}Br$:$H^{81}Br$	2.485	2.437	2.458	2.459[c]	0.003
$B(0,2)$	10^{-2} cm^{-1}	$H^{79}Br$:$H^{81}Br$	2.485	2.436	2.457	2.458[c]	0.003
$B(1,1)$	10^{-2} cm^{-1}	$H^{79}Br$:$H^{81}Br$	2.466	2.418	2.424	2.424[c]	0.003
$D(0,0)$	10^{-8} cm^{-1}	$H^{79}Br$:$H^{81}Br$	4.71	4.70	4.07	4.09[a]	0.01
$D(1,0)$	10^{-8} cm^{-1}	$H^{79}Br$:$H^{81}Br$	4.72	4.72	3.60	3.60[a]	0.01
$D(0,0)$	10^{-8} cm^{-1}	$H^{79}Br$:$D^{81}Br$	4.68	4.67	3.99	3.97[b]	0.01
$\langle P_2(\cos\theta)\rangle$ ($H^{79}Br$)(0,0)		$H^{79}Br$:$H^{81}Br$	0.190	0.188	0.186	0.190[a]	0.001
$\langle P_2(\cos\theta)\rangle$ ($H^{81}Br$)(0,0)		$H^{79}Br$:$H^{81}Br$	0.190	0.187	0.185	0.190[a]	0.001
$\langle P_2(\cos\theta)\rangle$ ($H^{79}Br$)(1,0)		$H^{79}Br$:$H^{81}Br$	0.202	0.201	0.202	0.198[a]	0.001
$\langle P_2(\cos\theta)\rangle$ ($H^{81}Br$)(1,0)		$H^{79}Br$:$H^{81}Br$	0.203	0.201	0.203	0.199[a]	0.001
$\langle P_2(\cos\theta)\rangle$ ($H^{79}Br$)(0,0)		$H^{79}Br$:$D^{81}Br$	-0.282	-0.273	-0.242	-0.237[b]	0.001
$\langle P_2(\cos\theta)\rangle$ ($D^{81}Br$)(0,0)		$H^{79}Br$:$D^{81}Br$	0.712	0.700	0.664	0.668[b]	0.001
v_5	cm^{-1}	$H^{79}Br$:$H^{81}Br$	14.23	14.36	15.03	15.03[a]	0.01
G			42.05	37.82	2.73		

[a] Submillimeter data from current study.
[b] HBr-DBr[120]
[c] HBr-HBr Infrared[112]

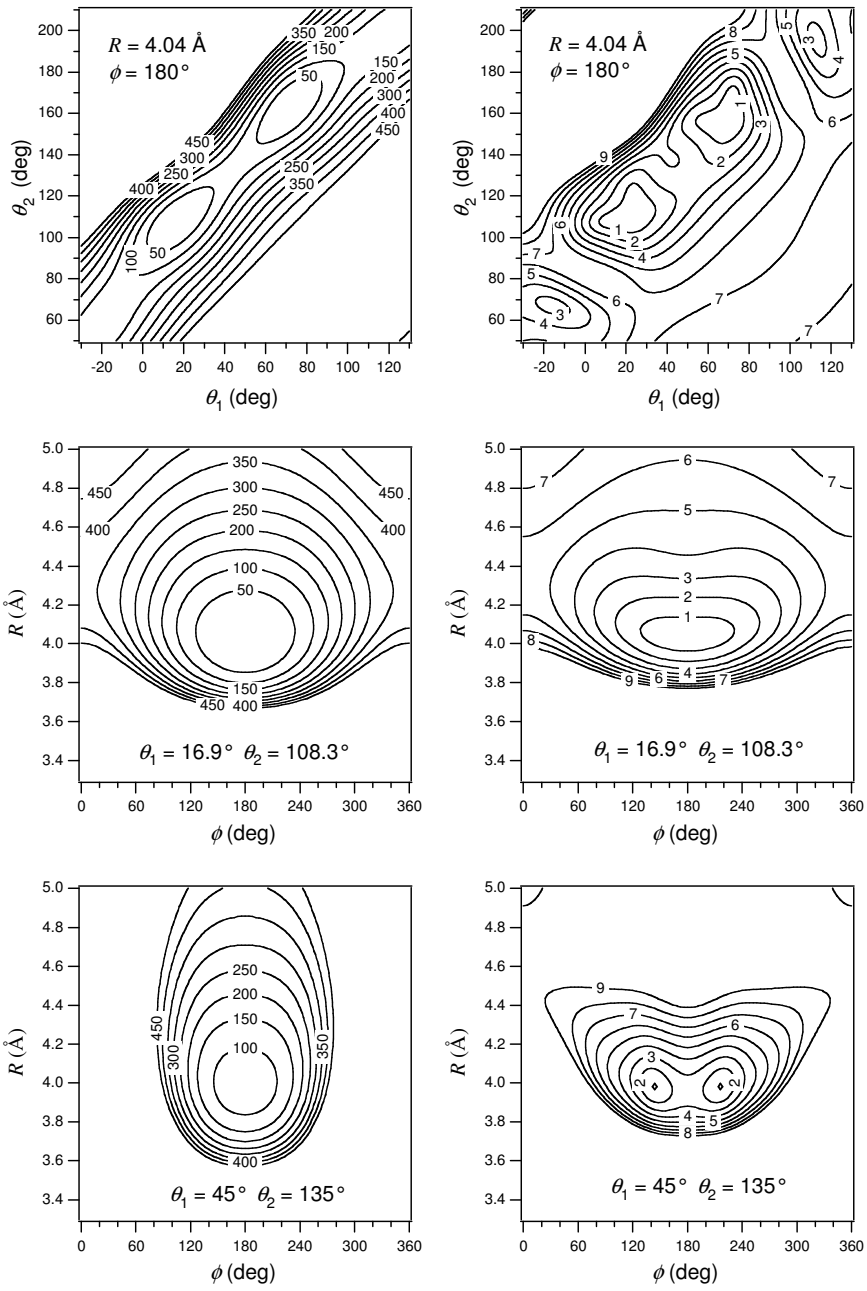

Figure 40. Morphed potential of $(HBr)_2$ (left column) with the corresponding statistical uncertainties (right column). All contours are in cm^{-1} and are relative to the minimum of the potential which occurs at R=4.04 Å, θ_1 = 16.9°, θ_2 = 108.3°, and ϕ = 180°, with V = -644.0 cm^{-1}.

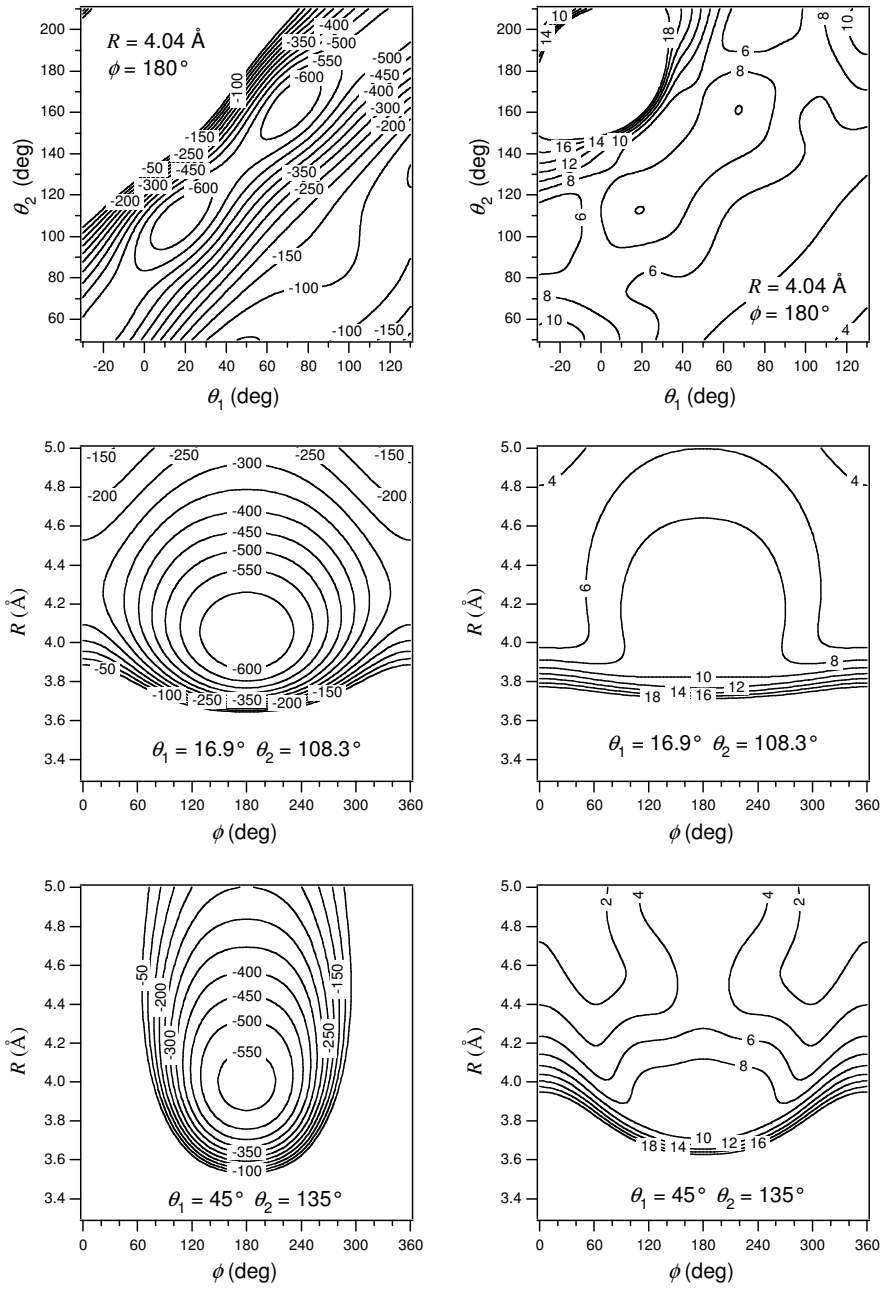

Figure 41. Morphed potential of $(HBr)_2$ (left column) with the corresponding statistical uncertainties (right column). All contours are in cm^{-1} and are relative to the value of the potential at infinite separation.

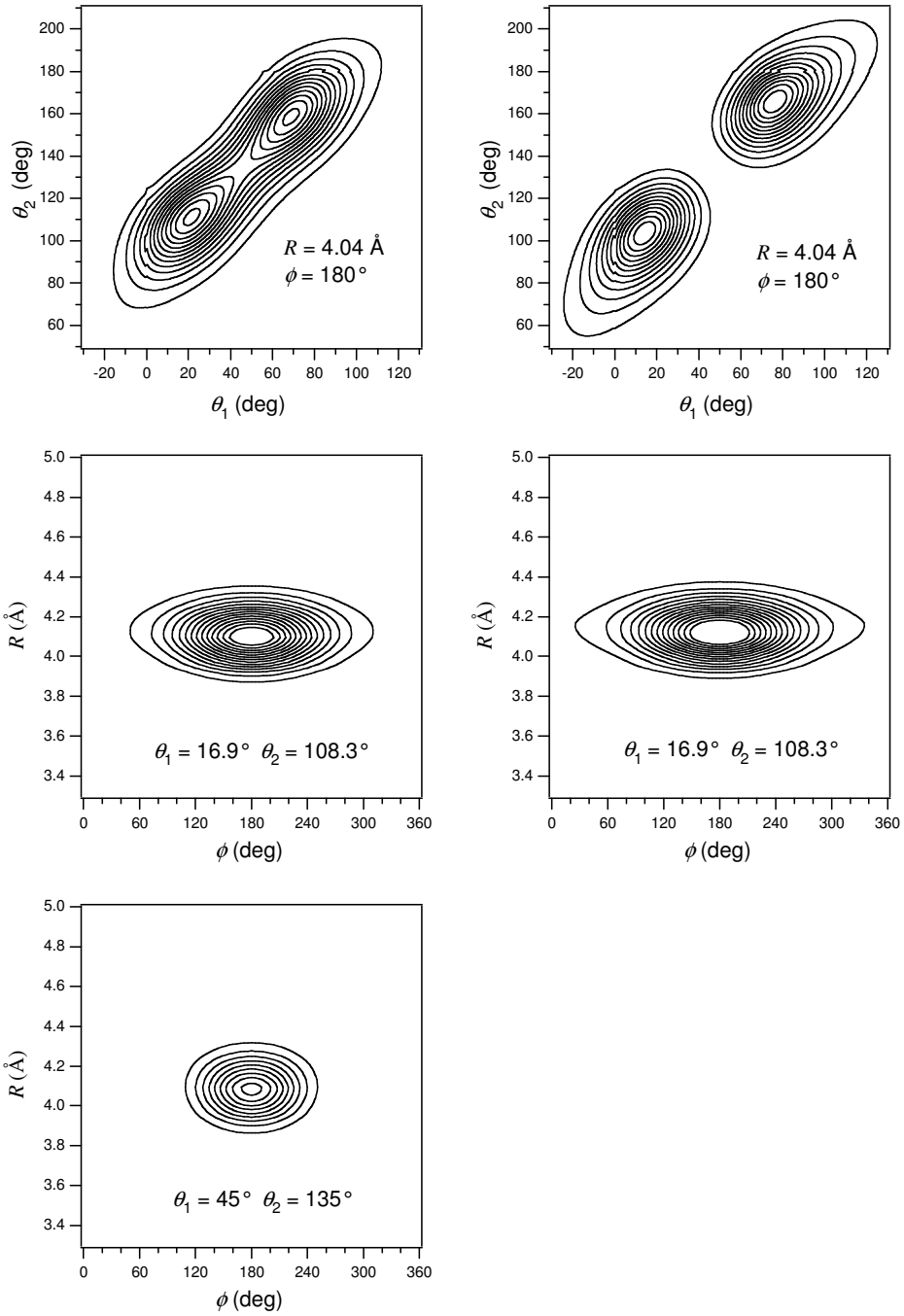

Figure 42. Vibrational wave functions of $(H^{79}Br)_2$ in the ground state (left column) with energy of E = –409.87 cm^{-1} and in the first excited state (v_5 = 1) (right column) with an energy of E = –394.83 cm^{-1}. Note that the v_5 = 1 wave function is identically zero when θ_1 = 45° and θ_2 = 135°.

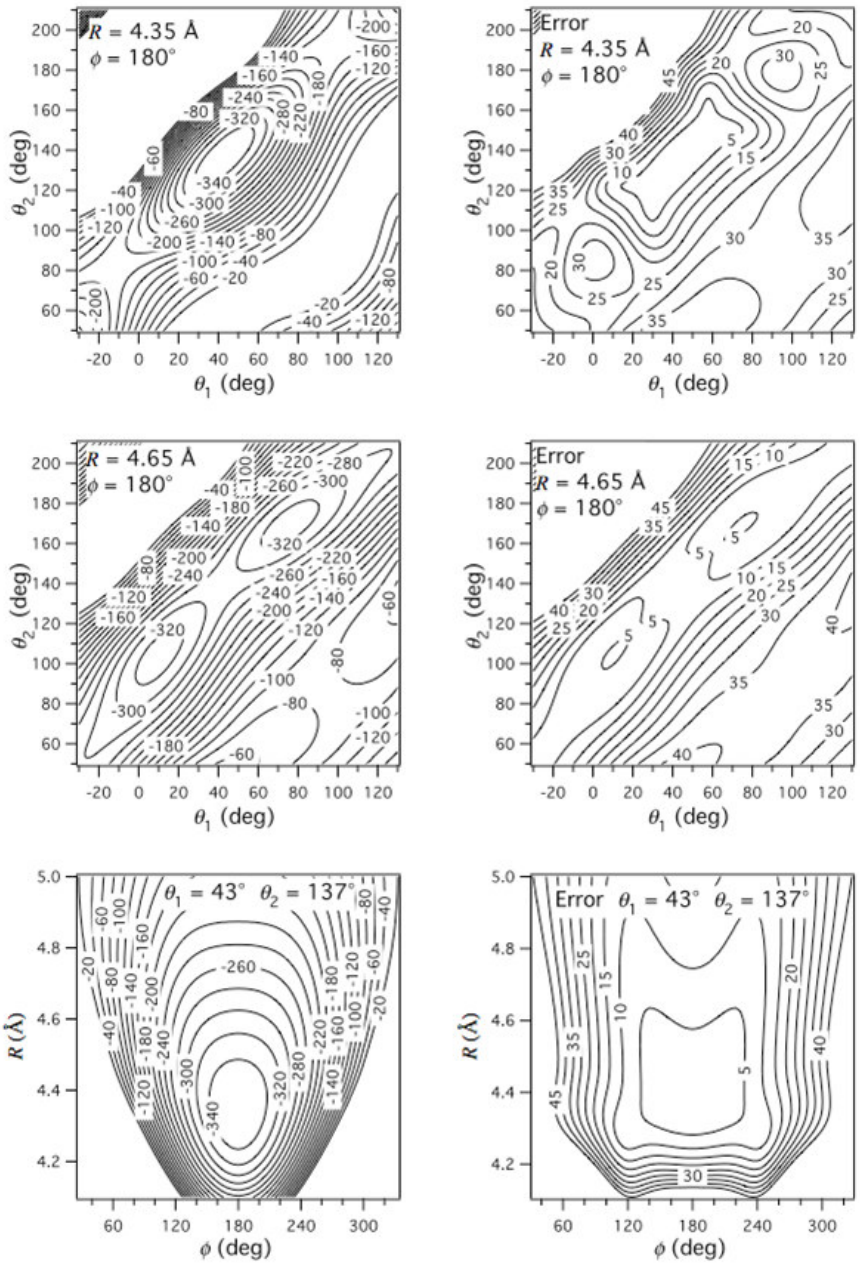

Figure 43. HI dimer potential energy surfaces generated from the morphed potential.

The geometry of $(HBr)_2$ in the ground state as determined from the morphed potential has an R_{CM} distance of 4.04 Å with θ_1=16.9° and θ_2=108.3° with ϕ=180.0°, which is consistent with HF and HCl dimers where there are L-shaped equilibrium

structures. The structure determined from the current spectroscopic data is different from the values of the morphed potential at the minimum. The ground state has a zero point energy of 234 cm^{-1} and its structure as expected is different from that of the equilibrium R_{CM} distance. This difference is 0.07Å for the R_{CM} distance. The contribution of the zero point energy to the total energy of the complex is taken into account as the vibrational energy of the other vibrational modes (ν_3, ν_4 and ν_6) is added to the potential energy surface. The R_{CM} calculated from the experimental data is an average of the internuclear separation over the tunneling mode, ν_5. The dihedral angle and angles of the monomer components to the figure axis, θ_1 and θ_2, are effective angles which are averaged over the amplitude and effectively corresponds to a linear structure due to the rapid interchange between structures. Figure 42 contains the plots of the vibrational wave functions of $(H^{79}Br)_2$ in the ground (left) and excited (right) tunneling states. The ground state is characterized by a fairly delocalized structure, with deviations from the global minimum in the potential. The excited tunneling state is more localized around the minima but is still indicative that there is some deviation from the R_{CM} distance.

The determined D_0 value, 644 cm^{-1}, from the four dimensional morphed potential can be compared with the corresponding values of 1025.6 cm^{-1} in $(HF)_2$ and 403.4 cm^{-1} in $(HCl)_2$ indicating that the bond in the $(HBr)_2$ complex is slightly stronger than the bond in $(HCl)_2$.

An initial morphed potential has also been generated for $(HI)_2$ and is reproduced in Figure 43. A slightly different picture of the structure of the complex is determined on the basis of this potential. Based on the previous IR data and that of the submillimeter

spectroscopy the barrier is notably absent in contrast to those previously determined for other members of the homologous series $(HX)_2$, X=(F, Cl and Br). This indicates that there is a symmetric structure at the minimum which is very close to a bifurcated hydrogen bound equilibrium structure that is consistent with the transition C_{2h} saddle point structure in the other hydrogen halide dimers. The lack of a significant barrier indicates that there is in essence no "tunneling" and the physical manifestation of the observed excited vibration state is thus the geared bending vibration associated with the change of vibrational energy. The possibility of a bifurcated double hydrogen bound complex was not addressed in the previous study[113] , which was reported on the basis of IR spectroscopic data. This previous work initially indicated an L shaped equilibrium structure, after the constraining of the bonding angles to 0±30° and 90±30° for the bound and free monomer units in the complex for the corresponding ground state structure determination. However, the identification of only one μ_a stretching vibration and absence of a clear tunneling pair $\nu_1^{\pm}$ and $\nu_2^{\pm}$ are indicative of this possibility. However, a tunneling barrier can not be explicitly ruled out because the perpendicular band may have a very small transition moment.

As noted in the previous study, the observation of the monodeuterated complex HBr-DBr was made. However the observation of the pure rotational spectrum of HI-DI proved to be elusive. The analysis of such a species would provide additional information on the potential energy surface of the complex. Potentially, analysis of the submillimeter spectrum of $(DI)_2$ would also provide additional information relevant to this issue. An extensive spectroscopic search is currently underway to observe the geared

bending vibration associated with the deuterated species $(DI)_2$ in the submillimeter region. The observation of this band should resolve the issue of a barrier in HI dimer. Although it is expected that the hydrogen halide dimers would have a barrier in all cases this cannot be confirmed with the currently available spectroscopic data.

Permutation-Inversion and Molecular Symmetry Wavefunctions

The spectroscopy and molecular dynamics of the hydrogen halide dimers are best considered from the perspective of Permutation-Inversion and VRT or vibration rotation tunneling theory. This describes the exchange or permutation of the HX subunits, and in particular, both pairs of identical nuclei in a complex following a change in vibronic or tunneling state. The permutation of identical nuclei in the two HX monomer units of these dimer can be described as the breaking of the hydrogen bond and the subsequent reformation of another with a rotation about an axis which is perpendicular to the major molecular axis[69]. The theory of permutation-inversion[121] has been instrumental in the understanding the spectra of molecules and weakly bound molecular complexes which have pairs of identical nuclei.

As the dimers are part of the G4 molecular symmetry group, they are isomorphic with the point group $C_{2v,}$ and have a major symmetry axis which connects the heavy atoms in the complex. The permutation inversion group, P_{12}, describes the rotation of the molecule with respect to the symmetry of the complex. The traditional Jacobian coordinates, $(R,\theta_1,\theta_2,\phi)$, shown in Figure 29, can be used to describe the vibrations and movement of the individual atoms in the complex. In addition to these, the Eulerian axes are also incorporated to describe the rotation of the molecule, decoupled from the

vibrational modes of the complex, in fixed space. The character table for the complex is included in Table 20.

Table 20. Effect of Permutation Inversion on molecular coordinates.

E	$(12)(ab)$	E^*	$(12)(ab)^*$
$\theta_1\phi_1$	$\pi-\theta_2,-\phi_2$	$\theta_1,-\phi_1$	$\pi-\theta_2,\phi_2$
$\theta_2\phi_2$	$\pi-\theta_1,-\phi_1$	$\theta_2,-\phi_2$	$\pi-\theta_1,-\phi_1$
$\alpha\beta\gamma$	$\pi+\alpha,\pi-\beta,-\gamma$	$\pi+\alpha,\pi-\beta,\pi-\gamma$	$\alpha,\beta,\pi+\gamma$

The (12)(ab), E^*, and $(12)(ab)^*$ are used to define which pertinent transformations are made in the complex after the permutation of the nuclei occur. The application of E^* and (12)(ab) are equivalent to the rotation about the axis perpendicular to the major molecular axis, that will be called $C_{Y\pi}$. The rotation about this axis induces the change in the position of all of the nuclei through the axis and the tunneling inversion effectively induces the change in the hydrogen atoms so that all atoms are changed in position through the origin, or the center of symmetry of the complex.

The nuclei that are present in the complex are characterized by a spin which is a measure of the number of unpaired electrons in the complex. As discussed previously the hydrogen atom and the halides have half integer spins ($\frac{1}{2},\frac{3}{2},\frac{5}{2}$), making them Fermions. Deuterium on the contrary, is a Boson as the spin is full integer with spin 1. The rules for the exchange of two particles must follow the Pauli symmeterization postulate, which

states that the exchange of two identical fermions (half integer spin) changes the total wavefunction from symmetric to antisymmetric and vice versa. However, the exchange of two sets of identical fermions, or one pair of bosons, the total wavefunction does not change sign. The selection rule for transitions that can occur specify that the total wave function of a complex that undergoes the exchange of two sets of identical fermions must occur from symmetric to symmetric and antisymmetric and antisymmetric states, and transitions cannot occur from symmetric to antisymmetric and vice versa.

The total spin wavefunction, which is a product of the spatial coordinate (rotation), the vibrational coordinate, and the nuclear spin wavefunction, must commute between the states for a transition to occur[122, 123]. The total spin wavefunction can thus be either symmetric or antisymmetric, depending on the state of the molecule. The symmetry of a given state is described in Gordy and Cook[123] as the complete wave function which is the product of the electric, vibronic, rotation and nuclear spin wave functions. For these purposes, an additional wave function is needed for considering the tunneling vibration to be fully accounted. Although this is analogous to a vibration in the molecule. The total spin wave function is given in the following equation.

$$\psi_{tot} = \phi_{tun}\phi_{vib}\phi_{rot}\phi_{spin} \tag{36}$$

The hydrogen halide dimers are described by the molecular symmetry group G_4 when the two monomers are of the same isotopomer.

Table 21. Group G_4 character table.

	E	(12)(34)	E^*	$(12)(34)^*$
A^1	1	1	1	1
A^2	1	1	-1	-1
B^2	1	-1	-1	1
B^1	1	-1	1	-1

Traditional descriptions defined in Table 21 for the states of the complex are A^1, A^2, B^1, and B^2, where A and B are symmetric or antisymmetric with respect to the permutation of the H and X atoms, and the 1 and 2 identifiers refer to the symmetry due to the inversion or permutation of all of the atoms in the complex by tunneling. However, as the substructure of the experimentally investigated rotation transition is resolved, further additional descriptors must also be taken into account as well as the effect on the total spin wavefunction due to the resolved structure. The vibration-rotation-tunneling symmetry of a state is the product of the symmetry of each of the parts[69, 112, 122]. The total symmetry spin wave function is given to be $\Gamma_{VRT} = \Gamma_V \otimes \Gamma_R \otimes \Gamma_T \otimes \Gamma_{NS}$, where the symmetry wavefunctions are vibration, rotation, tunneling and nuclear spin respectively. This equation defines the state with the exclusion of the nuclear spin wave function.

The Vibration Wavefunction

The vibration and tunneling wavefunctions are used to describe the parity of a given state with respect to one another. Figure 30 shows a simple potential with the identification of the vibrational states that are separated by the tunneling frequency. The lower state is referred to as + and the upper tunneling state is -. These identifiers are used to describe the parity of a state relative to another. In the case of $(HX)_2$ the + state is

always symmetric and – is antisymmetric for the vibration wavefunction under consideration. The + and – notations are the same as 1 and 2 used previously.

The Rotational Wavefunction

The rotational wave function of $(HX)_2$ also will have parity due to rotation of the complex. The rotation of the molecule or complex about an axis perpendicular to the major axis also must follow selection rules. The change in the rotation of the molecular is also defined by the parity of the rotation wavefunction. Using the J_{K_a,K_c} convention for an asymmetric rotor the symmetry of a state can be identified. If K_c is even, the rotational wave function is A, and if it is odd, then state is characterized as B, if A and B the are symmetric and antisymmetric states. For a linear molecule, where K_a=0 and J=K_c, the symmetric states are *J*=even,(0,2,4,…) and antisymmetric states are where *J*=odd,(1,3,5,…). Using the above criteria, the symmetry of any given rotational state can be determined. The change in rotation wavefunction must change sign, adhering to the selection rules of $\Delta J=\pm 1$ for a linear molecule. The case where $\Delta J=0$ occurs if there is a change in K_a but is not observed in the geared bending vibration considered here.

Nuclear Spin Wavefunction

The nuclear spin wavefunction can be determined by investigating the spin projection of the individual nuclei relative to the total nuclear spin wavefunction. The total number of spin states as determined from the nuclear spins as given by the product of the degeneracies of the spins of each nucleus, $(2I+1)$, the total number of spin wavefunction is given by

$$\prod_{i=1}^{n} 2I_i + 1 \tag{37}$$

where *i* is the nucleus of interest and I is the magnitude of the spin of the nucleus. This equation gives a total number of possible states of 16, 64, 64 and 128 for $(HF)_2$, $(HCl)_2$, $(HBr)_2$, and $(HI)_2$ respectively, as each has a different nuclear spin and different degeneracies of spin. However, this equation does not define the symmetry of the states, only the total number of the states. The symmetric and antisymmetric states are given by the following equations:

$$\begin{aligned} symmetric &= (2I_1+1)(2I_2+1)(2I_1I_2+I_1+I_2+1) \\ antisymmetric &= (2I_1+1)(2I_2+1)(2I_1I_2+I_1+I_2) \end{aligned} \tag{38}$$

where I_1 and I_2 are the nuclear spin of the identical sets of nuclei. These equations give the number of symmetric and antisymmetric states for a dimer with any given spin. The ratios are 10:6, for 1/2 and 1/2; 36:28 for 3/2 and 1/2; and finally 78:66 for 5/2 and 1/2 spins. These cases are relevant to the dimers of the homologous series $(HF)_2$; $(HCl)_2$ and $(HBr)_2$; and finally $(HI)_2$ dimer respectively. The identification of states that are symmetric and antisymmetric is analogous to that of molecular hydrogen. With the 2 spin directions, there are only 3 possible combinations, two cases where the spins are parallel (↑↑and ↓↓) and one possible configuration where they are antiparallel (↑↓). However, in the case of the antiparallel spins, there are actually two states that are defined in that case where (↑↓) and (↓↑) are indistinguishable. The interaction of these two states and their indistinguishability give one state which is symmetric, (↑↓)+(↓↑), and one which is antisymmetric, (↑↓)-(↓↑). The same state definitions can also be carried out for the other nuclei where $I>1/2$, as is the case for Cl, Br, and I.

The symmetry identifiers of the nuclear spin wavefunction for $(HBr)_2$ and $(HI)_2$ are given in Table 22 and Table 23. It should be noted that degenerate or spin states that are indistinguishable are given both a symmetric and antisymmetric spin identifier as is the case for molecular hydrogen.

Table 22. $(HBr)_2$ symmetry identifiers.

		H1,H2			
Br1,Br2	Br1,Br2	<1/2,1/2>(S)	<1/2,-1/2>+ <-1/2,1/2>(S)	<1/2,-1/2>- <-1/2,1/2>(A)	<-1/2,-1/2>(S)
3/2,3/2		S	S	A	S
3/2,1/2	1/2,3/2	S,A	S,A	A,S	S,A
3/2,-1/2	-1/2,3/2	S,A	S,A	A,S	S,A
3/2,-3/2	-3/2,3/2	S,A	S,A	A,S	S,A
1/2,1/2		S	S	A	S
1/2,-1/2	-1/2,1/2	S,A	S,A	A,S	S,A
1/2,-3/2	-3/2,1/2	S,A	S,A	A,S	S,A
-1/2,-1/2		S	S	A	S
-1/2,3/2	-3/2,-1/2	S,A	S,A	A,S	S,A
-3/2,-3/2		S	S	A	S
S(36)		10	10	6	10
A(28)		6	6	10	6
I1,I2+I1,I2 = S					
I1,I2-I1,I2 = A					

Table 23. $(HI)_2$ symmetry identifiers.

I1,I2	I1,I2	<1/2,1/2>(S)	H1,H2 <1/2,-1/2>+ <-1/2,1/2>(S)	<1/2,-1/2>- <-1/2,1/2>(A)	<-1/2,-1/2>(S)
5/2,5/2		S	S	A	S
5/2,3/2	3/2,5/2	S,A	S,A	A,S	S,A
5/2,1/2	1/2,5/2	S,A	S,A	A,S	S,A
5/2,-1/2	-1/2,5/2	S,A	S,A	A,S	S,A
5/2,-3/2	-3/2,5/2	S,A	S,A	A,S	S,A
5/2,-5/2	-5/2,5/2	S,A	S,A	A,S	S,A
3/2,3/2		S	S	A	S
3/2,1/2	1/2,3/2	S,A	S,A	A,S	S,A
3/2,-1/2	-1/2,3/2	S,A	S,A	A,S	S,A
3/2,-3/2	-3/2,3/2	S,A	S,A	A,S	S,A
3/2,-5/2	-5/2,3/2	S,A	S,A	A,S	S,A
1/2,1/2		S	S	A	S
1/2,-1/2	-1/2,1/2	S,A	S,A	A,S	S,A
1/2,-3/2	-3/2,1/2	S,A	S,A	A,S	S,A
1/2,-5/2	-5/2,1/2	S,A	S,A	A,S	S,A
-1/2,-1/2		S	S	A	S
-3/2,-1/2	-1/2,-3/2	S,A	S,A	A,S	S,A
-5/2,-1/2	-1/2,-5/2	S,A	S,A	A,S	S,A
-3/2,-3/2		S	S	A	S
-5/2,-3/2	-3/2,-5/2	S,A	S,A	A,S	S,A
-5/2,-5/2		S	S	A	S
S(78)		21	21	15	21
A(66)		15	15	21	15
I1,I2+I1,I2 = S					
I1,I2-I1,I2 = A					

The above tables can be used to identify the symmetry of the spin wavefunction for exchange of identical nuclei. However, these tables cannot be applied to molecular dimers that contain two nuclei with equivalent spins, if the magnitude of the quadrupole moment is different. If the magnitude of the quadrupole moment is different the nuclei are strictly not equivalent. This is particularly true for the isotopomers of bromine and chlorine. The mixed isotopomers have no symmetry in the nuclear spin wave function. This is even true for the hydrogen nuclei which are covalently bound to the heavy atoms.

Total Wavefunction

The total spin wavefunction is defined using the following equation:

$$\psi_{tot} = \phi_{tun}\phi_{vib}\phi_{rot}\phi_{spin} \quad (36)$$

Equation 36 gives the total spin wave function with respect to the exchange of identical pairs of nuclei that holds true for $(HX)_2$. The wavefunctions for the tunneling, vibration, rotation and spin are separable and each is assigned a sign, which are derived from the considerations described above. The ground state of a complex such as $(HF)_2$ and $(HBr)_2$ where V=0 (the lowest vibration state) and J=0 (the lowest rotation state) are characterized by a symmetric total spin wavefunction with the exclusion of nuclear spin. The nuclear spin wavefunction symmetry is defined as in the previous section. The product of all of the wavefunctions will determine the symmetry of respective states of the complex. The selection rule for the exchange of two pairs of identical Fermions must be symmetric to symmetric and antisymmetric to antisymmetric for the total wavefunction. The change in vibration or tunneling state of a complex and the associated change in rotational energy leaves the total wavefunction unchanged. For the selection rule to be satisfied, there cannot be a change in the spin wave function so only transitions that conserve this value can occur. The symmetry of a given state can thus be determined experimentally by the intensity of the observed transitions.

Determination of the Symmetry of Transitions from Experimentally Observed Intensity

The symmetry of transitions in $(HI)_2$ can be determined by comparing the directly observed intensities of the quadrupole transitions in the spectra of the respective complexes. Using Equation 38, the number of symmetric and antisymmetric states for

two identical iodine nuclei is expected to be 21:15 or 1.4. The experimentally observed intensities of the R(0) and P(1) transitions are shown in Figure 44. This figure illustrates the observed quadrupole structure of the R(0) transition with experimental intensities measured as the peak to peak height of the first derivative spectrum. The comparison is made on the basis that the transition originating from quadrupole states in J=0, V=0 to those in J=1, V=1 are opposite from transition from the J=1,V=0 state to J=0, V=1. Due to the change in rotational and vibrational energy the P(1) quadrupole structure is the mirror image of the R(0) and this is taken into account in Figure 44, so that a direct comparison of intensity can be made for similar quadrupole states, which are a mirror image.

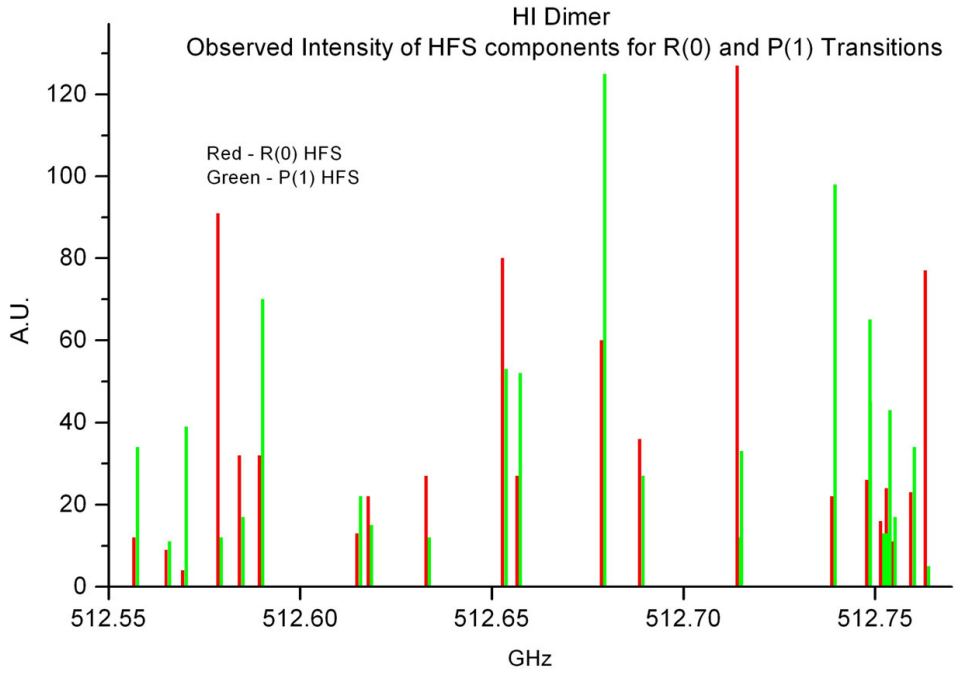

Figure 44. Observed intensities of the R(0) transitions of HI dimer with those of the same quadrupole transitions in the P(1) rotational transition.

Table 24. Observed intensities of HI dimer measured for R(0) quadrupole transitions.

Frequency(GHz)	*Jv,Itot,F* ← *Jv,Itot,F*	Exp. Intensity(mV)
512557.1724	1110 S ← 0011 S	12
512565.4390	1121 A ← 0022 A	9.64
512569.9796	1121 A ← 0000 A	4.39
512579.0021	1155 S ← 0055 S	97.7
512584.5271	1112 S ← 0033 S	38.11
512589.9444	1112 S ← 0011 S	35.88
512615.1986	1123 A ← 0044 A	15.83
512618.2403	1123 A ← 0022 A	20.71
512633.2140	1144 A ← 0044 A	29.93
512653.2445	1134 S ← 0033 S	88.12
512657.1485	1134 S ← 0055 S	38.78
512679.0404	1133 S ← 0033 S	65.04
512688.9916	1145 A ← 0044 A	39.35
512714.5617	1156 S ← 0055 S	136.81
512714.8160	1122 A ← 0022 A	16.38
512739.3156	1111 S ← 0011 S	26.23
512748.1820	1132 S ← 0033 S	33.73
512748.3820	1101 A ← 0022 A	4.87
512751.8212	1143 A ← 0044 A	15.00
512752.9200	1101 A ← 0000 A	4.47
512753.5983	1132 S ← 0011 S	28.3
512754.8620	1143 A ← 0022 A	13.17
512759.7410	1154 S ← 0033 S	28.15
512763.6443	1154 S ← 0055 S	84.7

The observed intensities are given in Table 24 along with the respective quantum numbers of each state. The quantum numbers are defined as J,V,I_{Tot},F in both the ground and excited vibrational state. The transitions for R(0) originate in the J=0, V=0 state, both symmetric. The excited state is J=1,V=1 which are both antisymmetric the product of which is symmetric. The transition there for follows directly the selection rules stated before, symmetric to symmetric. Therefore the symmetry of the spin wave function can be determined directly. From the treatment given in Table 23 of HI dimer the symmetric

states are those that have I_{Tot} which are odd, where the spins are parallel, and the antisymmetric states have I_{Tot} = even. From the labeling it can be seen that all of the observed transitions occur from symmetric to symmetric or antisymmetric to antisymmetric. There are no transitions between symmetry states observed. The total of all of the observed transitions from each state will thus give the integrated intensity of the respective symmetry states. The integrated intensity of the symmetric to antisymmetric can be calculated as $\frac{\sum \text{Exp. Int.}_s}{\sum \text{Exp. Int.}_a} = \frac{713.55}{173.74} = 4.107$. This is significantly greater than the expected intensity ratio of 1.4 for two identical iodine nuclei. This can be understood if the symmetry of the hydrogen nuclei (I=1/2) are also taken into account (specifically symmetric:antisymmetric = 3:1) and the factor multiplied into the expected intensity due to iodine. This gives 3*21/15*1 or 4.2 which is quite close to the observed value. This factor is derived by the inclusion of the hydrogen spin wave function with the iodine spin wave function where the symmetric triplet state of the hydrogen spin wavefunction couples with the symmetric iodine spin wave function (loosely the quintet, triplet and singlet) and the singlet hydrogen antisymmetric spin wavefunction couples with the doublet and quadruplet antisymmetric spin wavefunctions of iodine. The same factors can be considered for the P(1) transition where the observed intensities and quantum numbers in included in Table 25.

Table 25. Observed Intensities of HI Dimer for P(1) transitions of HI dimer.

Frequency(GHz)	$JVI_{Tot}F \leftarrow JVI_{Tot}F$	Exp. Intensity(mV)
512557.1724	0111 S ← 1010 S	4.90
512565.4390	0122 A ← 1021 A	33.49
512569.9796	0120 A ← 1001 A	15.61
512579.0021	0155 S ← 1055 S	42.06
512584.5271	0113 S ← 1032 S	13.12
512589.9444	0111 S ← 1012 S	12.93
512615.1986	0124 A ← 1043 A	44.06
512618.2403	0122 A ← 1023 A	63.76
512633.2140	0144 A ← 1044 A	98.00
512653.2445	0133 S ← 1034 S	32.51
512657.1485	0135 S ← 1054 S	11.12
512679.0404	0133 S ← 1033 S	26.28
512688.9916	0144 A ← 1045 A	124.11
512714.5617	0155 S ← 1056 S	51.51
512714.8160	0122 A ← 1022 A	54.69
512739.3156	0111 S ← 1011 S	11.31
512748.1820	0133 S ← 1032 S	14.16
512748.3820	0102 A ← 1021 A	21.24
512751.8212	0144 A ← 1043 A	68.48
512752.9200	0100 A ← 1001 A	14.83
512753.5983	0131 S ← 1012 S	11.34
512754.8620	0142 A ← 1023 A	38.38
512759.7410	0153 S ← 1034 S	10.83
512763.6443	0155 S ← 1054 S	34.00

$\frac{\sum \text{Exp. Int.}_s}{\sum \text{Exp. Int.}_a} = \frac{276.06}{576.65} = 0.479$ where the expected ratio is 0.4667 or 21/45 very close to the observed ratio. However, here the J=1 state is where the rotational quantum number is odd so the state is antisymmetric with respect to rotation and V=0 is symmetric so the spin wavefunctions of hydrogen and iodine must be chosen so that the total spin wave function of the ground state is symmetric. This means that the spin wave function due to the nuclear spin must couple symmetric to antisymmetric and vice versa for iodine

and hydrogen respectively. Although we know that the splitting due to hydrogen is small (<2 kHz) and consequently unresolved, we still see evidence of its intensity contributions through the determined quadrupole substructure intensity. Evidence for intensity alternation was also observed in the previous microwave work on $(HF)_2$[69] and the submillimeter spectrum of $(HCl)_2$ [97].

The previously described treatment can be extended to HBr where the ratio of two quadrupole nuclei with spin 3/2 should be 10:6 for symmetric and antisymmetric states respectively. Table 26 contains the measured intensity for the observed lines for the R(0) and P(1) transitions. Color has been added to identify the symmetric and antisymmetric states of the $(H^{79}Br)_2$ and $(H^{81}Br)_2$ as were identified in HI dimer. It can be seen here that the intensity of the homodimers are about the same for like transitions but there are significant differences for the mixed $H^{79}Br$:$H^{81}Br$. By taking the integrated intensity of the I_{Tot} = Odd and I_{Tot} = Even states, we find the ratios given in Table 27.

Table 26. Observed intensities (Volts) of HBr dimer for the R(0) and P(1) transitions.

J	K_a	K_c	V	I_{tot}	F	J	K_a	K_c	V	I_{Tot}	F	$H^{79}Br:H^{79}Br$	$H^{79}Br:H^{81}Br$	$H^{81}Br:H^{81}Br$
0	0	0	1	1	1	1	0	1	0	1	0	0.027	0.105	0.024
0	0	0	1	0	0	1	0	1	0	2	1	0.051	0.16	0.066
0	0	0	1	2	2	1	0	1	0	2	1	0.16	0.182	0.075
0	0	0	1	3	3	1	0	1	0	3	3	0.146	0.57	0.1
0	0	0	1	1	1	1	0	1	0	1	2	0.0565	0.265	0.0455
0	0	0	1	3	3	1	0	1	0	1	2	0.0565	0.265	0.0455
0	0	0	1	2	2	1	0	1	0	1	2		0.026	
0	0	0	1	1	1	1	0	1	0	2	2		0.08	
0	0	0	1	2	2	1	0	1	0	2	3	0.3	0.49	0.36
0	0	0	1	2	2	1	0	1	0	2	2	0.15	0.465	0.165
0	0	0	1	3	3	1	0	1	0	3	4	0.12	0.5	0.159
0	0	0	1	0	0	1	0	1	0	1	1		0.02	
0	0	0	1	1	1	1	0	1	0	1	1	0.066	0.174	0.056
0	0	0	1	0	0	1	0	1	0	0	1	0.1	0.14	0.072
0	0	0	1	2	2	1	0	1	0	0	1	0.12	0.17	0.162
0	0	0	1	1	1	1	0	1	0	3	2	0.0615	0.25	0.0615
0	0	0	1	3	3	1	0	1	0	3	2	0.0615	0.25	0.0615
1	0	1	1	3	2	0	0	0	0	1	1	0.2055	0.2765	0.24
1	0	1	1	3	2	0	0	0	0	3	3	0.2055	0.2765	0.24
1	0	1	1	0	1	0	0	0	0	2	2	0.066	0.273	0.05
1	0	1	1	0	1	0	0	0	0	1	1		0.017	
1	0	1	1	0	1	0	0	0	0	0	0	0.025	0.122	0.045
1	0	1	1	1	1	0	0	0	0	1	1	0.174	0.276	0.12
1	0	1	1	1	1	0	0	0	0	0	0		0.02	
1	0	1	1	3	4	0	0	0	0	3	3	0.528	0.702	0.215
1	0	1	1	2	3	0	0	0	0	2	2	0.086	0.3395	0.029
1	0	1	1	2	2	0	0	0	0	2	2	0.07	0.3395	0.029
1	0	1	1	2	2	0	0	0	0	1	1		0.02	
1	0	1	1	1	2	0	0	0	0	2	2		0.02	
1	0	1	1	1	2	0	0	0	0	1	1	0.12	0.2635	0.12
1	0	1	1	1	2	0	0	0	0	3	3	0.12	0.2635	0.12
1	0	1	1	3	3	0	0	0	0	3	3	0.332	0.65	0.183
1	0	1	1	2	1	0	0	0	0	2	2	0.051	0.3	0.06
1	0	1	1	2	1	0	0	0	0	0	0	0.021	0.12	0.04
1	0	1	1	1	0	0	0	0	0	1	1	0.064	0.1	0.03

Table 27. Integrated Intensities of the isotopomers of HBr Dimer.

	$H^{79}Br:H^{79}Br$	$H^{79}Br:H^{81}Br$	$H^{81}Br:H^{81}Br$
R(0),I_{Tot}(Odd)	1.749	2.845	1.268
R(0),I_{Tot}(Even)	0.319	1.534	0.253
P(1),I_{Tot}(Odd)	0.595	2.428	0.553
P(1),I_{Tot}(Even)	0.881	1.687	0.900
R(0),(Odd/Even)	*5.483*	*1.855*	*5.012*
P(1),(Odd/Even)	*0.675*	*1.439*	*0.614*

Intensities are in Volts

The observed ratios of I_{Tot}(Odd)/ I_{Tot}(Even) are expected to be 10/6 for R(0) and P(1) or 1.666. The mixed isotopomer $H^{79}Br:H^{81}Br$ which lacks identical nuclei has the intensity ratio of 10:6 as is expected for the intensity of two different nuclei with spin 3/2. However, in the case of the homodimers, the statistical weight of the symmetric or antisymmetric state must be divided or multiplied by 3 to get the experimental ratios of 5.483, 5.012 in R(0) for the $(H^{79}Br)_2$ and $(H^{81}Br)_2$ homodimers respectively. The respective ratios of the P(1) transitions is 0.675 and 0.614.

Conclusion

The total spin wavefunctions given with equivalent quadrupole nuclei have been confirmed in the case of hydrogen bound homomolecular dimers of hydrogen bromide and hydrogen iodide. Although the observed intensities are consistent within 10-15%, the statistical weights can still be determined with integrated intensities of rotational levels with resolved quadrupole substructure. This is opposite to the nearly equal coupling of ($H^{79}Br:H^{81}Br$) where the two nuclei with spin 3/2 do not have a symmetry axis but still couple together and give an intensity ratio of 10:6 that can be accounted for with standard intensity considerations, as given by the SPFIT package referred to

previously. The hydrogen hyperfine splitting will be extremely small and is unresolvable with the current experimental capabilities.

The generation of experimental data that can be included into morphed potential energy surfaces of the $(HBr)_2$ and $(HI)_2$ has been discussed. We have determined that the potential of $(HBr)_2$ is characteristic of a tunneling inversion similar to that observed previously in $(HF)_2$ and $(HCl)_2$. We estimate the barrier to be 72 cm^{-1} which is less than that of $(HF)_2$ at 351 cm^{-1} but more than $(HCl)_2$ at 35 cm^{-1}. We also note that the barrier in the case of $(HI)_2$ is very small or non-existent. The observation and analysis of $(DI)_2$ may provide the needed data to confirm this assumption.

The Hamiltonian describing the quadrupole coupling of the large electric quadrupole moment of Br and I has been proven to be inadequate for the high resolution measurement related here. The need for further development of additional terms to be included for this purpose is being pursued. It is the ultimate goal of a collaboration with L. Coudert and J. Hougen that the theory describing the quadrupole coupling can be enhanced so that the observed structure can be fitted to the estimated accuracy of the measurements.

CHAPTER V

GROUND STATE ISOTOPIC ISOMERIZATION OC-HI AND OC-ID

Isotopic substitution frequently provides powerful and widely applied approaches to the investigation of a large range of physical and chemical phenomena[124]. These have greatly enhanced fundamental understanding, characterization and prediction of the properties of matter and played a major role in rapidly developing fields such as structural biology, nanotechnology and biotechnology [124-129]. The latter have varied from structural effects in biologically significant interactions, isotopic effects in atmospheric ozonolysis to enzymatic rate effects [130-132]. Considerable attention has concentrated on the influence of deuterium and tritium isotopic substitution due to the inherently light mass of hydrogen and the consequent influence of relatively large mass substitution dependence particularly related to zero point energy effects. As a consequence of such extensive applications, investigations of anomalous isotope effects have now become the subject of intense interest and considerable focus [133-136]. Such effects are particularly prominent when involved in non-covalent interactions where the influence of large amplitude anharmonic vibrations and the frequent existence of different low energy isomeric configurations can manifest themselves in many phenomena whether in the gas or condensed phases. The initial investigations of deuterium substitution effects in hydrogen bonded materials by Ubbelohde and his coworkers [137] have long been the subject of study, particularly with respect to the isotopic dependence on the hydrogen bond length and the influence of multidimensional quantum

dynamics [138-140]. Moreover, application of high resolution spectroscopic techniques to the systematic study of a range of prototypical isolated gas phase systems have proven particularly effective in giving more detailed insight following deuterium substitution in medium to weakly bound hydrogen bound dimers [141]. In-depth investigation of relatively small isolated molecular interactions are well known to provide definitive and accurate experimental data on phenomena that have wide ranging relevance but are inherently dependent on quantal effects even under macroscopic conditions. A combination of high resolution gas phase and supersonic jet/molecular beam spectroscopic methods and application of theoretical and modeling approaches [142-144] can be particularly effective for phenomenologically more detailed investigations. This is especially so when extraneous complications characteristic of condensed phase or matrix interactions are minimized and many properties can be measured with exquisite accuracy and facilitate direct comparison with theoretical and molecular computational methods. The interplay between these and condensed phase investigations can thus give important new insights into fundamental characteristics of non-covalent interactions. Indeed, such approaches can suggest new directions in investigations of related structural changes associated with isotopic substitution in isolated non-covalent interactions. A particularly unique example is the anomalous isotopic structural change on condensed phase deuteration that has been reported by Mootz and Schilling [145]. Here, deuterium substitution has been proposed to fundamentally change hydrogen bonding in trifluoroacetic acid tetrahydrate from a cationic layer structure of hydrogen bonded ($H_3O^+.3H_2O$) enclosing $F_3C.COO^-$ anions to a molecular hydrogen bonded $(D_2O)_n$ layer enclosing F_3CCO_2H [145].

This result suggests potential investigations of related structural changes associated with isotopic substitution in isolated non-covalent interactions. Specifically, the possibility that isotopic substitution can induce a change in the ground state structure of a non-covalent interaction appears worthy of investigation. Such an example would be a ground state hydrogen bound molecular system being converted on deuteration to a deuterated ground state with van der Waals structure. In this case, at absolute zero temperature, the protonated ground state structure would then be hydrogen bound whereas the corresponding deuterated structure would be van der Waals giving rise to a profound anomalous geometric isotope effect. Differential zero point energy effects have the possibility of initiating such a significant change in structure in the weakly bound limit as a consequence of the shallower nature of the hydrogen bound interaction at its potential minimum (frequently a consequence of greater quartic character of the potential) relative to corresponding to van der Waals minimum [82]. Demonstration of this phenomena should be most possible in the case of using deuterium for stable isotopic substitution.

In the specific case of Ar-HBr, however, the isomerization energy could be determined with great precision from observation of direct spectroscopic transitions between states in the different isomeric structures. Using submillimeter spectroscopy the isomerization energy was found to be reduced from 10.99465379(3) cm^{-1} in Ar-HBr to 7.123429433(17) cm^{-1} in Ar-DBr. This analysis furthermore independently confirmed that the ground state structure remained hydrogen bound with both the proton or

deuterium atoms located between the Ar and Br heavy atoms for the barrier between the minima of the isomers being 54 cm^{-1}.

The specific case of OC-HI appeared to be a more favorable candidate for a comparable analysis and for investigating the proposed ground state isotope effect. In this case, there is the possibility of four stable linear equilibrium isomeric structures OC-HI, OC-IH, CO-HI and CO-IH, which are shown in Figure 45.

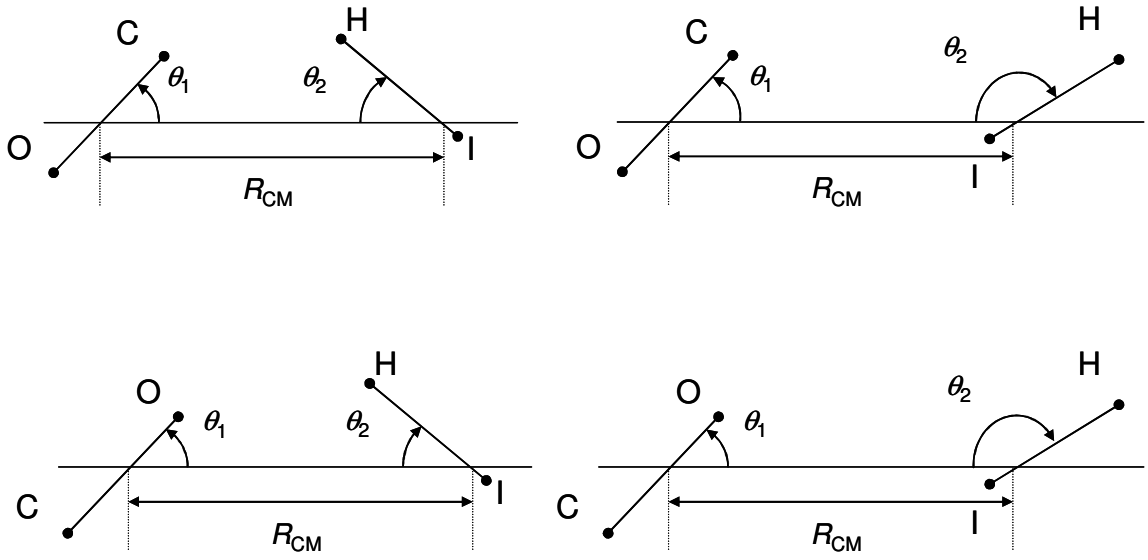

Figure 45. Isomeric structures of OC:HI.

A microwave analysis of the complex using pulsed-nozzle FT microwave spectroscopy at an assumed effective rotational temperature of 1-2K has indicated a ground state hydrogen bound structure for the $^{16}O^{12}C$ -$^{1}H^{127}I$ common isotopic species [146] but no other structural isomer was detected in this initial study. Subsequent application of high frequency wavelength modulation infrared diode laser cw supersonic

spectroscopy which was carried out at an effective rotational temperature of 13 K showed that both OC-HI and OC-IH were populated in this expansion and were energetically the most stable isomers that existed [147] having an approximate isomerization energy of 2 to 5 cm^{-1} based on observed relative intensity measurements. This is consistent with preliminary ab-initio calculations [148] associated with a significantly larger tunneling barrier (~ 400 cm^{-1}) than in Ar-HBr and consequently a significantly smaller energy difference between the OC-HI and OC-IH isomeric structures. These factors enhance the possibility that the zero point energy change on deuteration of these two protonated isomers would be negative and sufficiently large in magnitude to result in ground state isotopic isomerization to the van der Waals structural form. Such a determination would necessitate further investigations of whether the zero point energy shift on deuteration would be sufficient to bring about the effect from ground state OC-HI to the corresponding structure OC-ID as shown in .

Experimental

The spectra associated the isomeric structures of OC:HI as well as isotopomers have been observed using pulsed jet Fourier transform microwave spectrometers at NIST, Gaithersburg, MD and the Chemistry Department, University of North Texas, Denton, TX.. This is an extension of the previous two studies using PN-FTMW and slit jet infrared spectroscopies[146, 147]. In general a mixture comprising 1-2% HI and 5% CO was made in either Ar or a mixture of Ne/He (80:20) was used to produce the molecular complexes through a supersonic expansion. The PN-FTMW utilized a solenoid valve with a 0.8mm orifice and a pulse rate of 3-5 Hz to generate the expansion with a 2 ATM

backing pressure. The CW slit jet expansion used similar conditions through a 50 mm by 25μm and a 1.7 atmospheres backing pressure. The later PN-FTMW study using the NIST spectrometer and the one located at the University of North Texas was made to identify isotopically substituted complexes using ^{13}CO and $^{13}C^{18}O$ as well as DI. The backing pressures used in the expansions were changed to increase the signal for the complexes. Additionally, significant efforts were made to enrich DI as this component rapidly converts to HI in the presence of water. Samples containing DI were purged through the valve into the spectrometer for 1-4 hours before the OC:DI complex could be observed. The temperature of the expansion is estimated to be between 1 and 2 K for expansions with Ar and 3-5 K for the Ne/He carrier gases.

Results and Discussion

Analysis of observed rotational transitions ΔJ=1 for J=4←3, 5←4, 6←5, 7←6, 8←7, 9←8 and ΔF=1 or 0 following application of pulsed-nozzle FT microwave spectroscopic methods are given in Table 1. The results for $^{16}O^{12}C$-HI and $^{16}O^{13}C$-HI ground state molecular parameters were determined as described previously [146]. The remaining isotopomers were recorded at NIST Gaithersburg and at the Chemistry Department, University of North Texas. All frequencies used in the analysis are listed in Table A 10.

All data were analyzed similarly to the initial $^{16}O^{12}C$-HI and $^{16}O^{13}C$-HI investigation [146] using the JPL SPFIT Package of Pickett [81] to provide the molecular parameters for three different isomeric structures given in Table 28. The fourth isomeric structure, that of CO-IH, was not detected in these experiments presumably because its

ground state is depopulated sufficiently that it could not be detected under the temperature conditions of these experiments.

This project was first initiated by completing the recording and analysis of the microwave spectra of the ground states of the two lowest common isomeric forms OC-HI, OC-IH, their deuterated isotopomers OC-DI, OC-ID, and as well as that of the less stable isomeric form CO-DI. The concentrations of the different isomers were found to be very sensitive to the effective temperature conditions associated with supersonic jet expansions in different carriers used in the supersonic expansions. Such spectra were recorded with both Ar and Ne/He as carrier gases for this purpose. The Ne/He expansions are known to give somewhat higher rotational temperature (3-5 Kelvin) than corresponding argon expansions (1-2 Kelvin). Indeed, the OC-IH isomer could not be detected with Ar carrier expansions but could be detected when expanded in the warmer Ne/He carrier gas expansions. In a similar manner, the CO-HI isomer could not be detected in its protonated configuration either in Ar or Ne/He carrier expansions due to depopulation of this isotopomer. However, the CO-DI isomer, which is expected to occur at lower energies relative to the ground state was detected using the Ne/He carrier.

Table 28. Ground state molecular parameters of different isotopomers and isomers of OC-HI recorded using pulsed nozzle FT microwave spectroscopy.

Spectroscopic constant	B_0/MHz	D_J/kHz	C_N/kHz	χ_{aa}/MHz	χ_J/kHz
OC–HI[a]	900.952316(59)	2.521(64)	1.420(89)	-1346.237(11)	-8.16(19)
$O^{13}C$–HI[a]	882.599761(80)	2.4042(10)	1.74(12)	-1349.540(12)	-8.03(21)
$^{18}O^{13}C$–HI[b]	825.787281(95)	2.07329(72)	1.62(28)	-1350.47(10)	-7.66(17)
OC–DI[b]	899.47512(15)	2.2354(13)	1.67(32)	-1466.64(11)	-6.51(21)
$O^{13}C$–DI[b]	881.34120(13)	2.14004(91)	1.93(32)	-1468.84(16)	-6.15(18)
OC–IH[b]	1158.673722(56)	4.51639(65)	1.992(87)	-1494.2681(99)	2.63(19)
$O^{13}C$–IH[b]	1136.54593(12)	4.3399(18)	2.35(27)	-1497.391(42)	1.93(27)
OC–ID[c]	1159.93107(15)	3.9560(23)	2.25(31)	-1591.496(66)	-0.83(28)
CO–DI[b]	966.85148(80)	1.57836(55)	2.28(28)	-1518.106(10)	-2.33(18)

[a] Wang, Z.; Lucchese, R. R.; Bevan, J. W.; Suckley, A. P.; Rego, C. A.; Legon, A. C. Journal of Chemical Physics 1993, 98, 1761

[b] NIST, Gaithersburg, MD.

[c] S. A. Cooke, University of North Texas, Denton, TX.

Structural Properties of OC:HI

The structure and geometry of the observed isomers of OC:HI has been determined from the observed spectroscopic constants. The general picture of the isomers is shown in Figure 45. In the Jacobi coordinate system there are 4 geometric variables, angles of the monomer units to the major axis, θ_1 and θ_2, the CO and HI angles respectively, the dihedral angle ϕ, which is an angle of the monomers relative to one another about the major molecular axis, and R_{CM}, the distance between the centers of mass of the respective monomer units. The dihedral angle, the angle of the monomer units relative to one another, is fixed to 0° in the following structural interpretation.

The quadrupole coupling constant from the fitting procedure and given in Table 28 is used to determine θ_2, the HI monomer angle, using Equation 39.

$$\chi_{complex} = \frac{\chi_0}{2}\left(3\cos^2\theta - 1\right) \tag{39}$$

R_{CM} is the distance between the center-of-mass of the OC and the center-of-mass distance of the HI moieties respectively as determined using the relationship

$$R_{cm}^2 = \frac{1}{\mu}\left[I_{OC-HI} - \frac{1}{2} I_{CO}\left(1+\cos^2\theta_1\right) - \frac{1}{2} I_{HI}\left(1+\cos^2\theta_2\right)\right]$$

where

$$I_A = \frac{h}{8\pi^2 B_A} \quad \mathrm{A} = \{\mathrm{OC}, \mathrm{HI}, \mathrm{OC:HI}\} \tag{40}$$

$$\mu = \frac{m_{CO} m_{HI}}{m_{CO} + m_{HI}}$$

It is interesting to compare the characteristic values of R_{CM} and θ_2 for the different isomers and their isotopomers in a similar manner to that described previously [141][18].

The angle of the CO monomer, θ_1 is fixed at 20° as indicated by a preliminary morphed potential[148]. The R_{CM} and θ_2 are used to calculate the r(B…I), this distance is used for comparison as the R_{CM} is isotopically dependent.

$$r(B...X) = R_{CM} + r(\cos\theta_1) + r'(\cos\theta_2) \quad (41)$$

where r and r' are the distances of the acceptor atom in B to the center of mass of the monomer and the distance of the iodine atom to the center of mass in either HI or DI, respectively. The contribution of each monomer to *r(B…X)* can be positive or negative depending on the orientation of the monomer under consideration. The results of this analysis are given in Table 29 and a graphical representation is made in Figure 46.

Table 29. Ground state structures of OC:HI

	θ_{HI}/Deg	θ_{CO}/Deg	R_{CM}/Å	R(B…I) /Å
OC-HI	24.7875	20	4.8948	4.2992
OC^{13}-HI	24.6935	20	4.8740	4.2995
$^{18}O^{13}C$-HI	24.6753	20	4.9056	4.3003
OC-DI	21.1690	20	4.8845	4.3009
OC^{13}-DI	21.0710	20	4.8634	4.3008
OC-IH	159.5851	20	4.3039	3.7087
OC^{13}-IH	159.6733	20	4.2826	3.7085
OC-ID	163.0237	20	4.2859	3.7029
CO-DI	19.5195	20	4.7068	4.2751

As expected the *r(B…I)* value of the OC-HI isomer is significantly longer than that for the corresponding OC-IH isomer, a reflection of the significantly larger B_0 value for the later. This indicates that the bond between the monomers is significantly smaller, by 0.5905 Å, which is consistent with a van der Waals structure where the hydrogen atom is not involved in the bond.

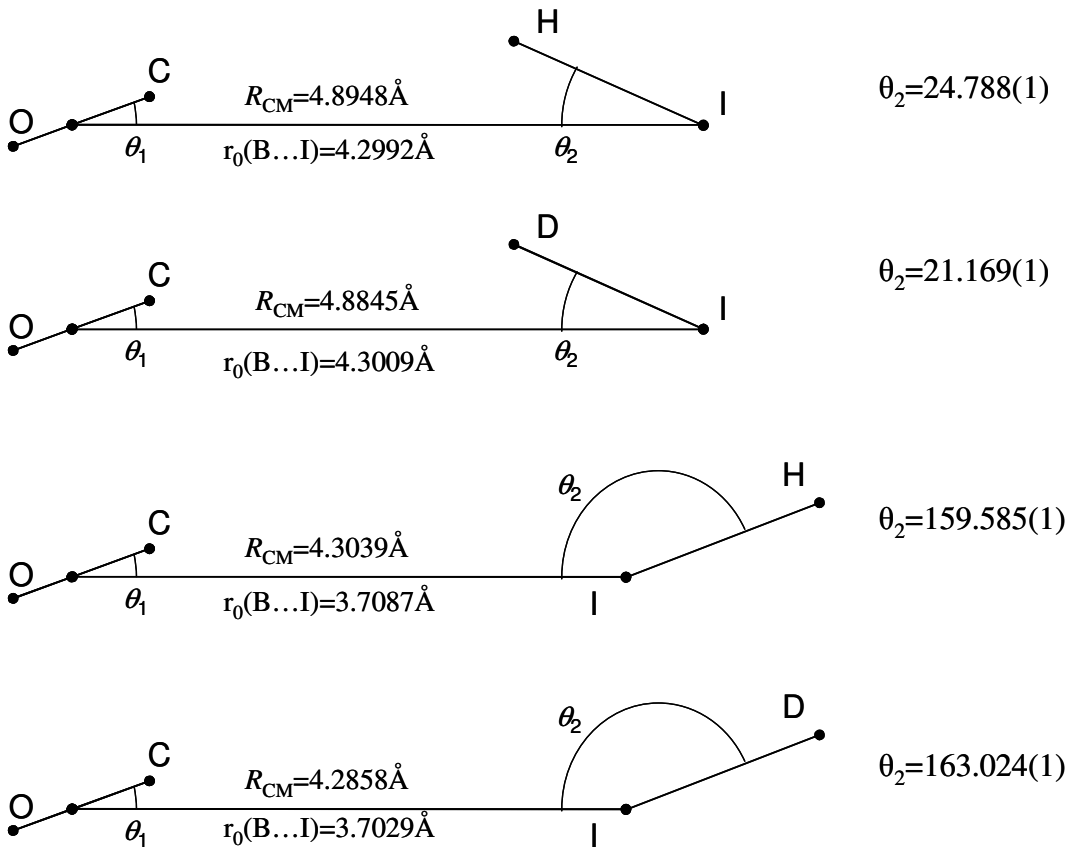

Figure 46. Geometry and structures of OC:H(D)I isomers.

The hydrogen bond length of the deuterated complex OC-DI is slightly longer and the magnitude of the angle, θ_2, is smaller, this is consistent with a smaller amplitude of motion of the deuterium due to the mass effect in that the large amplitude motion is suppressed by the larger inertia of the deuterium atom. This effect is not attributable completely to the Ubbelohde effect as discussed earlier but an apparent structural effect none the less. The Ubbelohde effect is interpreted as a decrease in the bond energy of the hydrogen bond on deuteration. A lower bond energy leads to a larger intermolecular separation if all other interactions are identical. However, the effects leading to the

nature of the hydrogen bond especially zero point energy and dipole-dipole interactions are not independent of isotopic substitution. It was noted that in the case of isolated complexes especially OC-H(D)F and OC-H(D)Cl that the deuterated species is characterized by a shorter R(B…D-X) distance than the corresponding hydrogen species. This supports in interpretation that the deuterated hydrogen bond is slightly stronger in the deuterated species contradicting the effects found by Ubbelohde as discussed in the introduction of this chapter, and are in direct contrast to the effect in OC-H(D)I where the hydrogen bond increases by 0.0017Å.

Relative Intensity and Energy of Isomers

Intensity measurements were made by carefully normalization of transition signal corrected for power dependence and other instrumental factors with frequency. The estimated accuracy for the measurements of this data was 2 kHz except for the deuterated results which were estimated to be 6 kHz. As the data was recorded using both Ar and Ne/He carrier gases in the expansions the effective temperatures are typically expected to be 1 to 2 Kelvin and 3-5 Kelvin respectively under the conditions of the current investigations. If it is assumed that the different isomeric forms are in effective rotational equilibrium temperatures, the intensities of the observed spectra when corrected for instrumental factors and effective μ_{aa} dipole moments are consistent with a ground state OC-HI isomeric structure and an approximate isomerization energy of 3.9 +/- 1.3 cm^{-1} relative to the isomer OC-IH. Corresponding intensity measurements on the OC-DI and OC-IH isomers are consistent with an OC-ID ground state isomeric structure and an approximate isomerization energy of 1.0 +/- 0.3 cm^{-1} relative to the OC-DI isomeric

structure. This indicates that the ground state structure of the complex will change upon deuteration, from a hydrogen bound OC-HI isomer to a van der Waals OC-ID structure.

Summary

Efforts are currently underway to generate a 4D and 6D morphed potential energy surface with the inclusion of all spectroscopic data which is available. Not only will this provide information that will support the ground state isotopic isomerization, but will enable the prediction of isomerization energies that can be observed in the submillimeter spectral region as well as combination bands in the infrared. If the barrier is high enough the search for transitions in the submillimeter will be prohibitive as the Franck-Condon factor and the cross section for the transition be too weak to observe. This might necessitate a search in the overtone region of the HI or CO stretching vibrations in the infrared to find the direct isomerization energy through combination differences. However, this will not provide conclusive information as there will be no quadrupole substructure to determine the structure accurately and combination bands are difficult to assign with a high degree of confidence. In addition, plans are being made to observe the complexes in colder expansions, namely krypton as a carrier, which has an effective temperature of 0.6 – 0.8 K and will serve to depopulate the higher energy isomer preferentially. By comparing relative intensities of the OC-HI, OC-IH OC-DI and OC-ID isomers the ground state of the respective isotopomers can then be more accurately ascertained. These planned observations can also be included to provide a vibrationally complete morphed potential energy surface of OC:H(D)I. Application of these

methodologies will hopefully lead to investigations of other complexes that can demonstrate a similar isotopic isomerization effect.

CHAPTER VI

CONCLUSION

Properties of weakly bound dimer interactions have been studied using pulsed nozzle FT microwave and submillimeter spectroscopic techniques to yield fundamentally new information for characterizing structures and molecular dynamics. In particular, a newly developed co-axially configured supersonic jet submillimeter spectrometer has been used to investigate low frequency vibrations in Ar-HBr, Ar-HI, $(HBr)_2$, $(HI)_2$ and the heterogeneous dimer OC-HI at ultra high instrumental resolution with frequency precision less than 1 kHz. Analysis of this data has provided the basis for generating model potential energy surfaces for the systems studied.

The spectrometer and the experimental methods involved in the studies set a new paradigm in the application of broadband tunable submillimeter spectroscopy to the investigation of weakly bound dimers. This is demonstrated by a critical evaluation of the operational capabilities of this spectrometer through applications to both monomeric diatomic molecules and the molecular complexes previously discussed. The estimated absolute RMS frequency accuracy of 380 Hz and an instrumental line width of 40 kHz are demonstrated through a comparison of the results with those from a state-of-the-art PN-FTMW spectrometer. Specifically, rovibrational spectroscopic constants are generated from these experimental data demonstration that such molecular constants are determined to microwave accuracy. The fact that the operational frequency in the

submillimeter is near 30 times higher than the latter indicates some of the impressive new capabilities for the instrument.

The previously discussed dimers include analyses of the Σ bending vibration of the molecular complexes Rg:HX (X=Br and I). The energy of the ground state isomerization of Ar-H^{79}Br, Ar-H^{81}Br, Ar-D^{79}Br, Ar-D^{81}Br and Ar-H^{79}Br (v=1) have been determined directly using the TAMU submillimeter spectrometer. An evaluation of the structure of each complex, characterized by the R_{CM} and angle of the monomer unit, θ, is made so that detailed information can be determined from isotopic substitution. The ground state in Ar-HBr is demonstrated to be hydrogen bound Ar-HBr while in contrast the next excited state is van der Waals and has the Ar-BrH structure. In addition, it is found that the magnitude of the large amplitude bending motion is decreased upon substitution of the proton with deuterium. The substitution also increases the hydrogen bond length, as shown by the change in the R_{CM} distance (Ar-H^{79}Br=4.1331Å and Ar-D^{79}Br=4.1528Å), while also effecting a decrease in the isomerization energy by 3.871224(1) cm^{-1}. Changes in the isomerization energy following excitation to the vibrational state of the monomer HBr in the complex has been determined and the energy shown to decrease by 1.7978011(1) cm^{-1}, also a value indicative of a decrease in the hydrogen bond strength. The change in the R_{CM} is characteristic of a 0.0149 Å increase. This effect is most likely a consequence of additional moment of inertia as well as vibrational energy that is contributed by the excited state of HBr to the complex.

Ar-IH demonstrates different properties as it is the van der Waals form in the ground state. The isomerization energy of the complex has been directly determined by

the application of submillimeter spectroscopy. The difference in the ground state and the excited hydrogen bound complex in this dimer is 8.7700748(1) cm^{-1}. The observed rotation and quadrupole constants are used to determine the structure of both the ground state (R_{CM}=3.9975(1) Å and θ=149.33(1)°) and the first excited Σ bending state (R_{CM}=4.3440 (1) Å and θ=43.362(1)°). The temperature of the expansion is determined experimentally to be 1.2 K based on the relative intensity ratios of the rotational quadrupole components in different rotational levels. Additionally, the accuracy of the intensity measurements is estimated to be better than 10% for well resolved transitions that have been studied.

The investigations of $(HX)_2$ (X=F or Cl) represent investigations of one of the most important prototypical hydrogen bonded systems that involves tunneling interconversion. Extensive studies of the corresponding hydrogen bromide and hydrogen iodide dimers give unique perspectives on the influence of competing intermolecular forces on both structure and dynamics. The utility of the TAMU spectrometer to resolve and determine the quadrupole substructure of the rotation transitions in these complexes has also been demonstrated to be a key factor in these analyses. Rotation tunneling has been observed in the three isotopomers of HBr dimer ($H^{79}Br:H^{79}Br$, $H^{79}Br:H^{81}Br$ and $H^{81}Br:H^{81}Br$) but in $H^{127}I:H^{127}I$ geared bending vibration, ν_5^1 is demonstrated to occur illustrating a fundamentally different symmetrical structure in this complex. The evaluated structures of each set of complexes have been determined and are presented in Table 21.

The analyses of the symmetry associated with each state have also been studied and the compliance with the symmeterization postulate verified using intensity measurements. In the case of the homogeneous dimers $(H^{79}Br)_2$, $(H^{81}Br)_2$ and $(H^{127}I)_2$, we see evidence that the exchange of two sets of identical fermions (the halogen and hydrogen) create intensity alternation due to the nuclear statistics and the symmetry of the component vibration, rotation, tunneling and nuclear spin wavefunction. The heterodimer of $H^{79}Br:H^{81}Br$ does not follow this trend and no intensity alternation is observed.

Results for an additional four atom complex, OC:HI are also presented. The microwave and infrared spectra associated with the isomers and isotopomers of OC:HI has been analyzed and an isotopic ground state isomerization effect has been identified. Over a period of 15 years the spectra associated with 9 isotopomers and isomers of the complex have been observed. Combination bands in the infrared and associated relative intensity measurements of the complex in the microwave lead to an estimate of the isomerization energy of OC-HI and OC-IH isomers. This separation is approximately 3.9 cm^{-1} with the hydrogen bound form being the most stable. However, in the case of OC-DI and OC-ID the ground state isomer is van der Waals and the hydrogen bound OC-DI is approximately 1.0(3) cm^{-1} higher in energy.

The use of methodologies to generate morphed potential energy surfaces that are based on ab initio potentials has been stringently evaluated in the Ar-HBr molecular complex. Through the aforementioned measurements a CCCC (Coupled Cluster Correlation Consistent) morphed potential in the CCSD(T) limit has been generated that

predicts experimental observations of Ar-DBr and Ar-HBr (v=1) to near spectroscopic accuracy. The evaluation of this potential is now believed to be fully converged in the CCSD(T) limit. Applications of this methodology to the intermolecular potentials of HBr dimer and HI dimer have also made. The identification that the excited tunneling state of HBr dimer lies just below the barrier is an important observation. The dissociation energy has also been evaluated and seen to follow the other members HF dimer and HCl dimer with decreasing dissociation energy (1025.6 cm^{-1} and 403.4 cm^{-1} respectively) to 644 cm^{-1}. The barrier in the case of HI dimer is predicted not to exist in a preliminary morphed potential, and the geared motion bending vibration is observed directly at 17.076183(1) cm^{-1}. In order to confirm the lack of a barrier, and associated with that a bifurcated structure, a further analysis of DI dimer is needed.

In conclusion, the TAMU submillimeter spectrometer has provided a significant amount of new experimental information that is used to improve the quantitative evaluation of the non-covalent interactions in Rg:HX, HX dimers and especially OC-HI. It is hoped that the methodologies currently being developed and presented in this dissertation can be used in the future. With further development it is hoped that morphed potentials based on such data will be able to predict the properties of weakly bound system with spectroscopic accuracy.

REFERENCES

1 A. Weber and North Atlantic Treaty Organization. Scientific Affairs Division, *Structure and Dynamics of Weakly Bound Molecular Complexes*, D. Reidel Pub. Co., Boston, MA., 1987.

2 J. D. Watson and F. H. C. Crick, *Nature*, 1953, **171**, 737-738.

3 K. A. Dill, *Biochemistry*, 1990, **29**, 7133-7155.

4 B. N. Chen, S. Piletsky and A. P. F. Turner, *Combinatorial Chemistry & High Throughput Screening*, 2002, **5**, 409-427.

5 A. C. Legon, *Chem. Soc. Rev.*, 1990, **19**, 197-237.

6 I. G. Kaplan, *Intermolecular Interactions: Physical Picture, Computational Methods, Model Potentials*, Wiley, Hoboken, NJ, 2006.

7 M. Rigby, *The Forces Between Molecules*, Clarendon Press; Oxford University Press, New York, 1986.

8 S. E. Novick, Bibliography of Rotational Spectra of Weakly Bound Complexes, http://www.wesleyan.edu/chem/faculty/novick/vdw.html, 2007.

9 S. P. Belov, B. A. McElmurry, R. R. Lucchese, J. W. Bevan and I. Leonov, *Chem. Phys. Lett.*, 2003, **370**, 528-534.

10 B. A. McElmurry, R. R. Lucchese, J. W. Bevan, I. I. Leonov, S. P. Belov and A. C. Legon, *J. Chem. Phys.*, 2003, **119**, 10687-10695.

11 B. A. McElmurry, R. R. Lucchese, J. W. Bevan and S. P. Belov, *Physical Chemistry Chemical Physics*, 2004, **6**, 5318-5323.

12 B. A. McElmurry, R. R. Lucchese, J. W. Bevan, S. P. Belov and I. I. Leonov, *Chem. Phys. Lett.*, 2005, **407**, 40-47.

13 S. P. Belov, B. A. McElmurry, R. R. Lucchese and J. W. Bevan, Relative Intensity Measurements with the TAMU Fast Scan BWO Spectrometer: Ortho-Para HI Dimer., in *The 60th International Symposium on Molecular Spectroscopy*, The Ohio State University, Columbus, OH., 2005.

14 J. W. Bevan, B. A. McElmurry, S. P. Belov and R. R. Lucchese, Application of a Coaxially Configured Sub-millimeter Pulse Jet Spectrometer for Investigation of Weakly Bound Dimers, in *The 60th International Symposium on Molecular Spectroscopy*, The Ohio State University, 2005.

15 B. A. McElmurry, S. P. Belov, R. R. Lucchese and J. W. Bevan, Observation and Analysis of the K=0←0 Rotation-Tunneling Transitions in $(HI)_2$, in *The 60th International Symposium on Molecular Spectroscopy*, The Ohio State University, 2005.

16 A. D. Buckingham, P. W. Fowler and J. M. Hutson, *Chemical Reviews*, 1988, **88**, 963-988.

17 L. Pauling, *The Nature of the Chemical Bond and the Structure of Molecules and Crystals; An Introduction to Modern Structural Chemistry*, Cornell University Press, Ithaca, NY, 1960.

18 R. Chauvin, *J. Phys. Chem.*, 1992, **96**, 9194-9197.

19 Z. Kisiel, *J. Phys. Chem.*, 1991, **95**, 7605-7612.

20 P. K. Mandal and E. Arunan, *J. Chem. Phys.*, 2001, **114**, 3880-3882.

21 A. Bondi, *J. Phys. Chem.*, 1964, **68**, 441-451.

22 T. J. Balle, E. J. Campbell, M. R. Keenan and W. H. Flygare, *J. Chem. Phys.*, 1980, **72**, 922-932.

23 M. R. Keenan, E. J. Campbell, T. J. Balle, L. W. Buxton, T. K. Minton, P. D. Soper and W. H. Flygare, *J. Chem. Phys.*, 1980, **72**, 3070-3080.

24 K. C. Jackson, P. R. R. Langridge-Smith and B. J. Howard, *Mol. Phys.*, 1980, **39**, 817-838.

25 Z. Kisiel, *J. Mol. Spectrosc.*, 2003, **218**, 58-67.

26 C. A. Burrus and W. Gordy, *Physical Review*, 1953, **92**, 274-277.

27 C. A. Burrus and W. Gordy, *Physical Review*, 1953, **92**, 1437-1439.

28 W. C. King and W. Gordy, *Physical Review*, 1953, **90**, 319-320.

29 A. F. Krupnov, *Spectrochimica Acta Part A:Molecular and Biomolecular Spectroscopy*, 1996, **52**, 967-993.

30 G. Winnewisser, A. F. Krupnov, M. Y. Tretyakov, M. Liedtke, F. Lewen, A. H. Saleck, R. Schieder, A. P. Shkaev and S. V. Volokhov, *J. Mol. Spectrosc.*, 1994, **165**, 294-300.

31 G. Winnewisser, *Vibrational Spectroscopy*, 1995, **8**, 241-253.

32 M. Bogey, S. Civis, B. Delcroix, C. Demuynck, A. F. Krupnov, J. Quiguer, M. Y. Tretyakov and A. Walters, *J. Mol. Spectrosc.*, 1997, **182**, 85-97.

33 I. Morino, M. Fabian, H. Takeo and K. M. T. Yamada, *J. Mol. Spectrosc.*, 1997, **185**, 142-146.

34 K. A. Walker and A. R. W. McKellar, *J. Mol. Spectrosc.*, 2001, **205**, 331-337.

35 D. T. Petkie, T. M. Goyette, R. P. A. Bettens, S. P. Belov, S. Albert, P. Helminger and F. C. DeLucia, *Rev. Sci. Instrum.*, 1997, **68**, 1675-1683.

36 S. P. Belov, G. Winnewisser and E. Herbst, *J. Mol. Spectrosc.*, 1995, **174**, 253-269.

37 S. P. Belov and M. Y. Tretyakov, in *Spectroscopy from Space*, ed. J. Demaison, K. Sarka and E. A. Cohen, Kluwer Academic Publishers, Boston, 2001.

38 J. Koperski and E. S. Fry, *Journal of Physics B-Atomic Molecular and Optical Physics*, 2006, **39**, S1125-S1150.

39 T. A. Miller, *Science*, 1984, **223**, 545-553.

40 R. B. Nerf and M. A. Sonnenberg, *J. Mol. Spectrosc.*, 1975, **58**, 474-478.

41 G. W. Chantry, *Modern Aspects of Microwave Spectroscopy*, Academic Press, New York, 1979.

42 G. Winnewisser, S. P. Belov, T. Klaus and R. Schieder, *J. Mol. Spectrosc.*, 1997, **184**, 468-472.

43 F. A. Vandijk and A. Dymanus, *Chem. Phys.*, 1974, **6**, 474-478.

44 J. Andzelm, S. Huzinaga, M. Klobukowski and E. Radzio, *Chem. Phys.*, 1985, **100**, 1-11.

45 R. C. Cohen and R. J. Saykally, *J. Phys. Chem.*, 1992, **96**, 1024-1040.

46 J. M. Hutson, *J. Chem. Phys.*, 1988, **89**, 4550-4551.

47 J. M. Hutson, *J. Chem. Phys.*, 1989, **91**, 4455-4461.

48 J. M. Hutson, A. E. Barton, P. R. R. Langridgesmith and B. J. Howard, *Chem. Phys. Lett.*, 1980, **73**, 218-223.

49 J. M. Hutson and B. J. Howard, *Mol. Phys.*, 1981, **43**, 493-516.

50 A. C. Legon, *J. Phys. Chem.*, 1983, **87**, 2064-2072.

51 S. E. Novick, P. Davies, S. J. Harris and W. Klemperer, *J. Chem. Phys.*, 1973, **59**, 2273-2279.

52 S. E. Novick, K. C. Janda, S. L. Holmgren, M. Waldman and W. Klemperer, *J. Chem. Phys.*, 1976, **65**, 1114-1116.

53 S. J. Harris, S. E. Novick and W. Klemperer, *J. Chem. Phys.*, 1974, **60**, 3208-3209.

54 L. Oudejans, K. Nauta and R. E. Miller, *J. Chem. Phys.*, 1996, **105**, 10410-10415.

55 J. Han, A. L. McIntosh, Z. Wang, R. R. Lucchese and J. W. Bevan, *Chem. Phys. Lett.*, 1997, **265**, 209-216.

56 A. McIntosh, Z. Wang, J. Castillo-Chara, R. R. Lucchese, J. W. Bevan, R. D. Suenram and A. C. Legon, *J. Chem. Phys.*, 1999, **111**, 5764-5770.

57 D. G. Melnik, S. Gopalakrishnan, T. A. Miller, F. C. De Lucia and S. Belov, *J. Chem. Phys.*, 2001, **114**, 6100-6106.

58 M. Hepp, R. Gendriesch, I. Pak, F. Lewen and G. Winnewisser, *J. Mol. Spectrosc.*, 1997, **183**, 295-299.

59 R. Gendriesch, I. Pak, F. Lewen, L. Surin, D. A. Roth and G. Winnewisser, *J. Mol. Spectrosc.*, 1999, **196**, 139-145.

60 D. W. Firth, M. A. Dvorak, S. W. Reeve, R. S. Ford and K. R. Leopold, *Chem. Phys. Lett.*, 1990, **168**, 161-167.

61 R. L. Robinson, D. H. Gwo and R. J. Saykally, *J. Chem. Phys.*, 1987, **87**, 5156-5160.

62 D. Ray, R. L. Robinson, D. H. Gwo and R. J. Saykally, *J. Chem. Phys.*, 1986, **84**, 1171-1180.

63 K. L. Busarow, G. A. Blake, K. B. Laughlin, R. C. Cohen, Y. T. Lee and R. J. Saykally, *J. Chem. Phys.*, 1988, **89**, 1268-1276.

64 M. Meuwly and J. M. Hutson, *J. Chem. Phys.*, 1999, **110**, 8338-8347.

65 J. Castillo-Chara, R. R. Lucchese and J. W. Bevan, *J. Chem. Phys.*, 2001, **115**, 899-911.

66 D. H. Rank, B. S. Rao and T. A. Wiggins, *J. Chem. Phys.*, 1962, **37**, 2511-2515.

67 M. T. Bowers and W. H. Flygare, *J. Mol. Spectrosc.*, 1966, **19**, 325-331.

68 M. T. Bowers and W. H. Flygare, *J. Chem. Phys.*, 1966, **44**, 1389-1404.

69 T. R. Dyke, B. J. Howard and W. Klemperer, *J. Chem. Phys.*, 1972, **56**, 2442-2454.

70 H. K. Hughes, *Physical Review*, 1947, **72**, 614-623.

71 C. A. Lee, B. P. Fabricand, R. O. Carlson and I. I. Rabi, *Physical Review*, 1953, **91**, 1395.

72 E. Arunan, S. Dev and P. K. Mandal, *Applied Spectroscopy Reviews*, 2004, **39**, 131-181.

73 T. J. Balle, E. J. Campbell, M. R. Keenan and W. H. Flygare, *J. Chem. Phys.*, 1979, **71**, 2723-2724.

74 R. D. Suenram, J. U. Grabow, A. Zuban and I. Leonov, *Rev. Sci. Instrum.*, 1999, **70**, 2127-2135.

75 J. U. Grabow, E. S. Palmer, M. C. McCarthy and P. Thaddeus, *Rev. Sci. Instrum.*, 2005, **76**, 093106.

76 J. W. Bevan, A. C. Legon and C. A. Rego, *Chem. Phys. Lett.*, 1993, **204**, 551-555.

77 J. W. Bevan, A. C. Legon, C. A. Rego and J. Roach, *Chem. Phys. Lett.*, 1992, **198**, 347-354.

78 Y. Endo, H. Kohguchi and Y. Ohshima, *Faraday Discussions*, 1994, **97**, 341-350.

79 Y. Ohshima and Y. Endo, *J. Mol. Spectrosc.*, 1993, **159**, 458-467.

80 J. U. Grabow, W. Stahl and H. Dreizler, *Rev. Sci. Instrum.*, 1996, **67**, 4072-4084.

81 H. M. Pickett, *J. Mol. Spectrosc.*, 1991, **148**, 371-377.

82 Z. Wang, A. L. McIntosh, B. A. McElmurry, J. R. Walton, R. R. Lucchese and J. W. Bevan, *Journal of Physical Chemistry A*, 2005, **109**, 8168-8179.

83 M. R. Keenan, L. W. Buxton, E. J. Campbell, A. C. Legon and W. H. Flygare, *J. Chem. Phys.*, 1981, **74**, 2133-2137.

84 K.-P. Huber and G. Herzberg, *Molecular Spectra and Molecular Structure IV. Constants of Diatomic Molecules*, Van Nostrand Reinhold, New York, 1979.

85 R. Prosmiti, S. Lopez-Lopez and A. Garcia-Vela, *J. Chem. Phys.*, 2004, **120**, 6471-6477.

86 C. Jaques, L. Valachovic, S. Ionov, E. Bohmer, Y. Wen, J. Segall and C. Wittig, *Journal of the Chemical Society-Faraday Transactions*, 1993, **89**, 1419-1425.

87 T. Suzuki, H. Katayanagi and M. C. Heaven, *Journal of Physical Chemistry A*, 1997, **101**, 6697-6701.

88 J. M. Hutson, *The Journal of Chemical Physics*, 1992, **96**, 6752-6767.

89 K. Liu, J. D. Cruzan and R. J. Saykally, *Science*, 1996, **271**, 929-933.

90 B. J. Howard, T. R. Dyke and W. Klemperer, *J. Chem. Phys.*, 1984, **81**, 5417-5425.

91 A. S. Pine and W. J. Lafferty, *J. Chem. Phys.*, 1983, **78**, 2154-2162.

92 N. Ohashi and A. S. Pine, *J. Chem. Phys.*, 1984, **81**, 73-84.

93 A. S. Pine and B. J. Howard, *J. Chem. Phys.*, 1986, **84**, 590-596.

94 A. S. Pine, W. J. Lafferty and B. J. Howard, *J. Chem. Phys.*, 1984, **81**, 2939-2950.

95 A. S. Pine and G. T. Fraser, *J. Chem. Phys.*, 1988, **89**, 6636-6643.

96 M. D. Schuder, C. M. Lovejoy, R. Lascola and D. J. Nesbitt, *J. Chem. Phys.*, 1993, **99**, 4346-4362.

97 G. A. Blake, K. L. Busarow, R. C. Cohen, K. B. Laughlin, Y. T. Lee and R. J. Saykally, *J. Chem. Phys.*, 1988, **89**, 6577-6587.

98 M. D. Schuder, D. D. Nelson and D. J. Nesbitt, *J. Chem. Phys.*, 1993, **99**, 5045-5060.

99 M. J. Elrod and R. J. Saykally, *J. Chem. Phys.*, 1995, **103**, 921-932.

100 M. J. Elrod and R. J. Saykally, *J. Chem. Phys.*, 1995, **103**, 933-949.

101 A. E. Barton and B. J. Howard, *Faraday Discussions*, 1982, 45-62.

102 Z. Latajka and S. Scheiner, *Chem. Phys.*, 1988, **122**, 413-430.

103 M. Quack and M. A. Suhm, *Mol. Phys.*, 1990, **69**, 791-801.

104 P. R. Bunker, V. C. Epa, P. Jensen and A. Karpfen, *J. Mol. Spectrosc.*, 1991, **146**, 200-219.

105 K. K. Lehmann, S. E. Novick, R. W. Field and A. J. Merer, *J. Mol. Spectrosc.*, 2003, **222**, 1-2.

106 M. Quack and M. A. Suhm, *J. Chem. Phys.*, 1991, **95**, 28-59.

107 M. D. Schuder, C. M. Lovejoy, D. D. Nelson and D. J. Nesbitt, *J. Chem. Phys.*, 1989, **91**, 4418-4419.

108 M. D. Schuder and D. J. Nesbitt, *J. Chem. Phys.*, 1994, **100**, 7250-7267.

109 D. Maillard, A. Schriver, J. P. Perchard and C. Girardet, *J. Chem. Phys.*, 1979, **71**, 505-516.

110 J. J. Hurly, *International Journal of Thermophysics*, 2000, **21**, 805-829.

111 T. Haber, *Physical Chemistry Chemical Physics*, 2003, **5**, 1365-1369.

112 J. Castillo-Chara, A. L. McIntosh, Z. Wang, R. R. Lucchese and J. W. Bevan, *J. Chem. Phys.*, 2004, **120**, 10426-10441.

113 A. L. McIntosh, Z. Wang, R. R. Lucchese and J. W. Bevan, *Chem. Phys. Lett.*, 2000, **328**, 153-159.

114 A. Engdahl and B. Nelander, *J. Phys. Chem.*, 1986, **90**, 6118-6121.

115 J. Zhang, M. Dulligan, J. Segall, Y. Wen and C. Wittig, *J. Phys. Chem.*, 1995, **99**, 13680-13690.

116 A. D. Buckingham and P. W. Fowler, *J. Mol. Struct.*, 1988, **189**, 203-210.

117 R. L. Cook and F. C. DeLucia, *American Journal of Physics*, 1971, **39**, 1433-1454.

118 I. Merke and L. H. Coudert, *J. Mol. Spectrosc.*, 2006, **237**, 174-204.

119 S. P. Belov, F. F. Willaert, B. A. McElmurry, R. R. Lucchese, J. W. Bevan, L. H. Coudert and J. T. Hougen, Vibration and Hyperfine Coupling Effects in $(HI)_2$ Manuscript in Preparation, 2008.

120 W. Chen, A. R. H. Walker, S. E. Novick and F. M. Tao, *J. Chem. Phys.*, 1997, **106**, 6240-6247.

121 H. C. Longuet-Higgins, *Mol. Phys.*, 1963, **6**, 445-460.

122 P. R. Bunker and P. Jensen, *Molecular Symmetry and Spectroscopy*, NRC Research Press, Ottawa, 1998.

123 W. Gordy and R. L. Cook, *Microwave Molecular Spectra*, Wiley, New York, 1984.

124 A. Kohen and H.-H. Limbach, *Isotope Effects in Chemistry and Biology*, Taylor & Francis, Boca Raton, 2006.

125 M. Boudart, *Annual Review of Physical Chemistry*, 1962, **13**, 241-&.

126 J. M. de Souza, P. T. C. Freire, H. N. Bordallo and D. N. Argyriou, *Journal of Physical Chemistry B*, 2007, **111**, 5034-5039.

127 S. Koval, J. Kohanoff, J. Lasave, G. Colizzi and R. L. Migoni, *Physical Review B*, 2005, **71**, -.

128 M. I. Mcmahon, R. J. Nelmes, W. F. Kuhs, R. Dorwarth, R. O. Piltz and Z. Tun, *Nature*, 1990, **348**, 317-319.

129 A. P. Zhernov and A. V. Inyushkin, *Physics-Uspekhi*, 2001, **44**, 785-811.

130 R. Guzzi, C. Arcangeli and A. R. Bizzarri, *Biophysical Chemistry*, 1999, **82**, 9-22.

131 H. Sugimoto, *Journal of Physics-Condensed Matter*, 1998, **10**, 1237-1246.

132 D. H. Williams, E. Stephens, D. P. O'Brien and M. Zhou, *Angewandte Chemie-International Edition*, 2004, **43**, 6596-6616.

133 S. I. Chan, L. Lin, D. Clutter and P. Dea, *Proceedings of the National Academy of Sciences of the United States of America*, 1970, **65**, 816-822.

134 R. R. Choudhury, R. Chitra and M. Ramanadham, *Physica B-Condensed Matter*, 2005, **366**, 116-121.

135 K. Giese, M. Petkovic, H. Naundorf and O. Kuhn, *Physics Reports-Review Section of Physics Letters*, 2006, **430**, 211-276.

136 V. A. Jaravine, F. Cordier and S. Grzesiek, *Journal of Biomolecular NMR*, 2004, **29**, 309-318.

137 E. M. T. Robertson and A. R. Ubbelohde, *Proceedings of the Royal Society of London Series a-Mathematical and Physical Sciences*, 1939, **170**, 0222-0240.

138 H. H. Limbach, M. Pietrzak, H. Benedict, P. M. Tolstoy, N. S. Golubev and G. S. Denisov, *Journal of Molecular Structure*, 2004, **706**, 115-119.

139 T. R. Singh and J. L. Wood, *Journal of Chemical Physics*, 1969, **50**, 3572-3576.

140 M. Z. Zgierski, *Chemical Physics Letters*, 1975, **33**, 165-167.

141 A. C. Legon and D. J. Millen, *Chemical Physics Letters*, 1988, **147**, 484-489.

142 P. Hobza, in *Annual Reports on the Progress of Chemistry, Section C, Physical Chemistry, Vol 100*, Royal Soc Chemistry, Cambridge, 2004, vol. 100, pp. 3-27.

143 P. Hobza, R. Zahradnik and K. Muller-Dethlefs, *Collection of Czechoslovak Chemical Communications*, 2006, **71**, 443-531.

144 A. J. Stone, *Science*, 2008, **321**, 787-789.

145 D. Mootz and M. Schilling, *Journal of the American Chemical Society*, 1992, **114**, 7435-7439.

146 Z. Wang, R. R. Lucchese, J. W. Bevan, A. P. Suckley, C. A. Rego and A. C. Legon, *Journal of Chemical Physics*, 1993, **98**, 1761-1767.

147 A. L. McIntosh, Z. Wang, R. R. Lucchese, J. W. Bevan and A. C. Legon, *Chemical Physics Letters*, 1999, **305**, 57-62.

148 L. A. Rivera-Rivera, R. R. Lucchese and J. W. Bevan, Unpublished Results, 2008.

149 C. H. Townes and A. L. Schawlow, *Microwave Spectroscopy*, Dover Publications, New York, 1975.

APPENDIX

The structure of a molecular complex can be determined directly through the fitted spectroscopic constants which are unique to the complex under study. Each individual transition is fitted with an equation describing how the structure of the molecule or molecular complex affects the spacing of the rotationally resolved transitions. Accurate parameters are determined for these complexes through fitting the transitions to a Hamiltonian describing the energy dependence to the rotational quantum numbers. The total energy of a molecular complex can be described by a Hamiltonian comprising the vibrational, rotational and quadrupole terms.

The nuclear quadrupole coupling constants for HCl, HBr and HI are -67.6, 532.3, -1828.3 MHz respectively. Therefore it, is expected that the quadrupole structure afforded by the coupling of the two nuclei with the rotation of the molecule will lead to extensive quadrupole substructure of the rotational transitions which give precise information about the structure of the dimers. The spectroscopic constants including the vibration energy, rotational constants and quadrupole constants, will then be used to generate a morphed potential energy surface that will be able to reproduce the experimental data, and subsequent prediction of other experimentally observable quantities. The treatment of the dimers with respect to the spin wave function and nuclear statistics with intensity alternation will also be presented in these analyses.

The equation describing the rotational energy levels is as follows

$$H_{rot} = BJ(J+1) - D_J J^2 (J+1)^2 + H_J J^3 (J+1)^3$$

J – Rotational quantum number

B – Rotation constant

D_J – Centrifugal Distortion Rotation Constant

H_J – Cubic Distortion Constant

The rotational transitions are then split by the quadrupole moment of a quadrupole nucleus in the complex by

$$H_{quad} = [\chi_{aa} + D_{\chi} J(J+1)] \times \left\{ \frac{\frac{3}{4} C(C+1) - I(I+1)J(J+1)}{2I(I-1)(2J-1)(2J+3)} \right\} + \frac{\left[\chi_{aa} + D_{\chi} J(J+1)\right]^2}{B} g \times 10^{-3}$$

I – Spin quantum number

F- Quadrupole coupling constant

χ_{aa} – Quadrupole coupling constant

$D\chi_{aa}$ – Quadrupole distortion constant

g – Second-order quadrupole correction energy[149]

where the valid quantum numbers are given by

$$F = J + I, J + I - 1, J + I - 2, \ldots, |J - I|$$

and

$$C = F(F+1) - J(J+1) - I(I+1)$$

where I is the value of the quadrupole moment (Br and Cl = 3/2 and I = 5/2)

$$H_{SR}(X) = \mathbf{I}_X \bullet \mathbf{M}(X) \bullet \mathbf{J}$$
$$= M_{bb}(X)\frac{1}{2}\left[F(F+1) - I(I+1) - J(J+1)\right]$$

The Energy difference between 2 states is given by the following equation.

$$H = H_{vib} + H'_{rot} - H''_{rot} + H'_{quad} - H''_{quad} + H'_{SR} - H''_{SR}$$

The fitting of vibration, rovibrational and pure rotational transitions can be achieved by the use of the above equation. The results of these fits are then used to determine the precise value of the structural parameters of the complex via the Jacobi coordinates, R_{CM} and θ, or the center of mass distance and the angle of the diatomic hydrogen to the major axis.

The rotational constant is related to the moment of inertia of the complex by

$$B = \frac{h}{8\pi^2 I}$$

B – Rotational Constant

I – Moment of inertia

h – Planck's constant

a simplified form of this equation for units that are pertinent to spectroscopy is

$$B(MHz) = \frac{505379.006(51)}{I(amu\text{Å}^2)}$$
$$I(amu\text{Å}^2) = \frac{505379.006(51)}{B(MHz)}$$

The moment of inertia is related to the distance between masses by

$$I = \mu r^2$$

Where *r* is in units of angstroms (Å) and the reduced mass is given by

$\mu = \frac{m_1 m_2}{m_1 + m_2}$ if the units of the masses are in atomic mass units.

For example the bond distance in $H^{79}Br$ is determined by the above equations in the following steps

$$\frac{505379.006}{250357.599} = \mu r^2 = 2.01862286 \text{amu} \text{Å}^2$$
$$\mu = \frac{1.00782519 \times 78.918329}{1.00782519 + 78.918329} = 0.99511706$$
$$r^2 = \frac{2.01862286}{0.99511706} = 2.02852804 \text{Å}^2$$
$$r = 1.42426403 \text{Å}$$

In order to calculate the R_{CM} distance in the Rg:HX complex Ar:HBr the equation must be changed to incorporate the relative change in the center of mass of the diatomic as the molecular angle is changed

$$I_{complex} = \mu R_{cm}^2 + (I_{HBr} / 2)\left(1 + \left\langle \cos^2 \theta \right\rangle\right)$$

$$\chi_{aa} = \frac{1}{2}\chi_0 \left(3\left\langle \cos^2 \theta \right\rangle - 1\right)$$

χ_{aa} – Quadrupole coupling constant as determined from the fitting procedure

χ_0 – Quadrupole constant of the free monomer unit

θ – Angle of projection of quadrupole moment to the major axis of the complex

Table A 1. HBr and HI Reference Data.

	$H^{79}Br$	$H^{81}Br$	$D^{79}Br$	$D^{81}Br$	$H^{127}I$	$D^{127}I$
B_0 /MHz	250357.599(20)	250250.202(20)	123357.6343(60)	127279.7614(60)	192657.577(19)	97.537.092(9)
D_0 /MHz	12.320(10)	10.315(10)	2.6529(14)	2.6479(20)	6.023(3)	1.578(1)
$eQq_0(X)$ /MHz	532.3041(8)	444.6793(8)	530.6315(21)	443.2799(21)	-1828.286(9)	-1823.36535(91)
$eQq_0(D)$ /MHz			0.1469(19)	0.1461(19)		98.5(92)
c_X /kHz	290.83(8)	313.25(8)	145.82(24)	157.26(24)	351.1(3)	170.45(54)
c_H /kHz	-41.27(31)	-41.23(31)	-3.25(57)	-3.55(57)	-49.22(22)	8.8(17)

Reference Data taken from Diatomic Spectra Database

F.J. Lovas, E. Tiemann, J.S. Coursey, S.A. Kotochigova, J. Chang, K. Olsen, and R.A. Dragoset (2003), *Diatomic Spectral Database* (version 2.0). [http://physics.nist.gov/Diatomic [2008, April 2]. National Institute of Standards and Technology, Gaithersburg, MD.

Table A 2. Observed submillimeter data for Ar-H^{79}Br and Ar-H^{81}Br with the observed-calculated values from the fit.

v=1		v=0		Ar:H^{79}Br		Ar-H^{81}Br	
J'	F'	J"	F"	ν_{obs}/MHz[a]	$\Delta\nu$/kHz[a]	ν_{obs}/MHz[a]	$\Delta\nu$/kHz[a]
1	5/2	0	3/2	332071.1183	-0.6	331668.2525	-3.0
1	3/2	0	3/2	332136.5361	-1.3	331722.8547	-1.2
1	1/2	0	3/2	332019.2662	0.5	331624.9094	-0.4
0	3/2	1	5/2	327406.3879	-0.8	327037.5167	-0.3
0	3/2	1	3/2	327362.9727	-0.6	327001.2372	-0.9
0	3/2	1	1/2	327440.8795	-1.5	327066.372	-0.4
2	7/2	1	5/2	334806.149	-0.2	334382.4131	0.7
2	5/2	1	3/2	334828.0181	-0.2	334400.6345	-0.4
2	3/2	1	1/2	334860.0529	-0.2	334427.37	0.3
2	5/2	1	5/2	334871.4331	-0.6	334436.9142	0.4
2	3/2	1	3/2	334782.146	0.6	334362.2354	0.0
2	1/2	1	1/2	334794.29	0.0	334372.5292	0.6
2	3/2	1	5/2	334825.5612	0.4	334398.514	-0.1
2	1/2	1	3/2	334716.3839	1.6	334307.3963	1.9
1	5/2	2	7/2	325443.7485	-0.4	325093.4327	0.3
1	3/2	2	5/2	325465.7851	0.3	325111.7748	-0.3
1	1/2	2	3/2	325379.1254	0.8	325039.4642	0.5
1	5/2	2	5/2	325400.367	0.6	325057.1749	0.2
1	3/2	2	3/2	325496.3966	0.3	325137.4095	-0.2
1	1/2	2	1/2	325422.7421	0.8	325075.8882	0.6
1	5/2	2	3/2	325430.9788	1.0	325082.81	0.6
1	3/2	2	1/2	325540.013	0.0	325173.8335	-0.1
3	9/2	2	7/2	337797.6296	-0.5	337352.3195	0.1
3	7/2	2	5/2	337819.4418	0.2	337370.4929	0.1
3	5/2	2	3/2	337820.0836	0.3	337371.0415	-0.3
3	3/2	2	1/2	337798.3503	-0.8	337352.9207	-0.3
3	7/2	2	7/2	337862.8236	-0.5	337406.7516	1.1
3	5/2	2	5/2	337789.4712	-0.5	337345.4072	0.0
3	3/2	2	3/2	337754.7343	0.0	337316.4972	0.0
3	5/2	2	7/2	337832.8543	0.0	337381.6652	0.3
3	3/2	2	5/2	323746.8924	-1.1	337290.8637	1.1
2	7/2	3	9/2	323768.7896	-0.5	323413.0936	-0.2
2	5/2	3	7/2	323742.9371	-1.1	323431.3305	-0.3
2	3/2	3	5/2	323720.637	-0.2	323409.6963	-0.1
2	1/2	3	3/2	323703.5066	0.9	323391.1743	0.2
2	7/2	3	7/2	323788.8117	0.4	323376.8297	0.3
2	5/2	3	5/2	323786.4009	0.5	323448.0961	0.0
2	3/2	3	3/2	323723.5261	-0.7	323446.0155	0.3
2	7/2	3	5/2	323832.2752	1.8	323393.595	0.3
2	5/2	3	3/2	341047.18	-0.3	323484.4161	1.3
4	11/2	3	9/2	341068.9003	-0.3	340579.2856	0.1
4	9/2	3	7/2	341066.4112	-0.4	340597.3825	-0.4
4	7/2	3	5/2	341044.6861	-0.6	340595.3066	-0.3

ν=1		ν=0		Ar:H^{79}Br		Ar-H^{81}Br	
J'	F'	J"	F"	ν_{obs}/MHz[a]	Δν/kHz[a]	ν_{obs}/MHz[a]	Δν/kHz[a]
4	5/2	3	3/2	341112.2883	-0.1	340577.2026	0.4
4	9/2	3	9/2	341046.3908	0.3	340633.6479	0.5
4	5/2	3	5/2	341001.2237	-0.9	340540.885	1.4
3	9/2	4	11/2	322312.123	0.0	321993.4448	0.3
3	7/2	4	9/2	322333.9053	0.2	322011.5889	-1.0
3	5/2	4	7/2	322318.997	0.3	321999.1158	-0.3
3	3/2	4	5/2	322297.096	0.1	321980.8838	-1.1
3	9/2	4	9/2	322268.7117	0.5	321957.1597	0.8
3	7/2	4	7/2	322348.9677	1.2	322024.2022	0.4
3	5/2	4	5/2	322362.4451	0.3	322035.4298	0.2
5	13/2	4	11/2	344554.8511	-1.1	344063.3031	-0.8
5	11/2	4	9/2	344576.4543	-1.3	344081.3036	-0.5
5	9/2	4	7/2	344573.4231	-1.4	344078.7711	-0.9
5	7/2	4	5/2	344551.802	-1.9	344060.7539	-0.9
5	11/2	4	11/2	344619.8673	-0.1	344117.5909	1.1
5	9/2	4	9/2	344558.3615	-1.7	344066.1605	0.1
5	7/2	4	7/2	344508.3555	-0.3	344024.4404	-1.0
4	11/2	5	13/2	321138.7307	0.3	320833.9299	-0.3
4	9/2	5	11/2	321160.3902	0.7	320851.9751	0.0
4	7/2	5	9/2	321150.0103	0.7	320843.2911	-0.1
4	5/2	5	7/2	321128.2946	0.1	320825.2034	-0.6
4	11/2	5	11/2	321095.2821	0.6	320797.6135	0.2
4	9/2	5	9/2	321172.5208	1.1	320862.1333	0.7
4	7/2	5	7/2	321193.4819	0.4	320879.628	0.6
6	15/2	5	13/2	348320.4007	1.4	347804.1123	-0.5
6	13/2	5	11/2	348341.8615	0.1	347821.9953	-0.2
6	11/2	5	9/2	348338.8466	0.6	347819.4752	0.1
6	9/2	5	7/2	348317.3638	0.8	347801.5713	-0.7
6	13/2	5	13/2			347858.3127	0.0
6	11/2	5	11/2	348326.7149	-0.9	347809.3176	-0.1
6	9/2	5	9/2	348273.8904	-0.6	347765.2348	-1.1
5	13/2	6	15/2	320226.6206	-0.7	319934.5048	-0.9
5	11/2	6	13/2	320248.1391	-0.4	319952.4333	-0.9
5	9/2	6	11/2	320240.2263	-0.4	319945.8133	-1.3
5	7/2	6	9/2	320218.6725	-0.1	319927.8561	-1.0
5	13/2	6	13/2	320183.1241	-0.2	319898.1489	0.5
5	11/2	6	11/2	320258.3198	0.6	319960.9591	0.6
5	9/2	6	9/2	320283.742	0.6	319982.1878	0.0
7	17/2	6	15/2	352343.4658	-0.2	351801.3523	0.3
7	15/2	6	13/2	352364.7626	0.0	351819.0968	-0.2
7	13/2	6	11/2	352361.9118	-0.2	351816.7131	-0.3
7	11/2	6	9/2	352340.5927	0.3	351798.9453	-0.5
7	15/2	6	15/2	352408.2599	0.2	351855.4545	0.1
7	13/2	6	13/2	352351.7327	0.3	351808.189	-0.2
7	11/2	6	11/2	352297.079	1.2	351762.5726	0.0

ν=1		ν=0		Ar:H^{79}Br		Ar-H^{81}Br	
J'	F'	J"	F"	ν_{obs}/MHz[a]	Δν/kHz[a]	ν_{obs}/MHz[a]	Δν/kHz[a]
6	15/2	7	17/2	319575.8626	-0.3	319295.2542	-0.5
6	13/2	7	15/2	319597.2199	0.9	319313.049	0.2
6	11/2	7	13/2	319590.857	0.2	319307.7263	0.1
6	9/2	7	11/2	319569.4724	0.1	319289.9071	-0.4
6	15/2	7	15/2	319532.3099	1.9	319258.85	1.0
6	13/2	7	13/2	319606.004	1.6	319320.406	2.0
6	11/2	7	11/2	319634.428	0.8	319344.147	0.2
8	19/2	7	17/2	356623.6196	-0.6	356054.5883	0.3
8	17/2	7	15/2	356644.7255	-1.6	356072.1758	0.7
8	15/2	7	13/2	356642.0755	-1.3	356069.9587	0.3
8	13/2	7	11/2	356620.9454	0.3	356052.3479	1.4
8	17/2	7	17/2			356108.582	1.1
8	15/2	7	15/2			356062.606	2.9
7	17/2	8	19/2	319186.5474	-0.4	318916.274	-1.4
7	15/2	8	17/2	319207.7194	0.4	318933.9167	0.8
7	13/2	8	15/2	319202.4212	-0.3	318929.4844	0.5
7	11/2	8	13/2	319181.2237	-0.7	318911.8192	-0.6
9	21/2	8	19/2	361160.3492	0.2	360563.3083	-0.5
9	19/2	8	17/2	361181.2416	0.0	360580.716	-1.6
9	17/2	8	15/2	361178.7913	0.2	360578.6656	-1.8
9	15/2	8	13/2	361157.8724	1.1	360561.2303	-1.2
10	23/2	9	21/2	365953.0427	-0.5	365326.9118	0.7
10	21/2	9	19/2	365973.6978	0.3	365344.1201	-1.4
10	19/2	9	17/2	365971.4344	0.2	365342.227	-0.3
10	17/2	9	15/2	365950.7504	-0.2	365324.9898	2.1

[a] $\Delta\nu = \nu_{obs}-\nu_{calc}$

Table A 3. Ar-HBr microwave transition frequencies.

Transition	Ar-H^{79}Br		Ar-H^{81}Br	
$J' F_1' F \leftarrow J'' F_1'' F$	ν_{obs}/MHz[a]	Δν/kHz[a]	ν_{obs}/MHz[a]	Δν /kHz[a]
$3\ \frac{3}{2}\ 2 \leftarrow 2\ \frac{3}{2}\ 2$	6603.76932	0.36	6555.01117	0.44
$3\ \frac{5}{2}\ 3 \leftarrow 2\ \frac{5}{2}\ 3$	6616.61878	-0.14	6565.69394	-0.42
$3\ \frac{5}{2}\ 2 \leftarrow 2\ \frac{5}{2}\ 2$	6616.62136	-0.03	6565.69709	0.26
$3\ \frac{9}{2}\ 5 \leftarrow 2\ \frac{7}{2}\ 4$	6636.63598	-0.45	6582.45389	-0.31
$3\ \frac{7}{2}\ 3 \leftarrow 2\ \frac{5}{2}\ 2$	6636.64078	0.44	(6582.46135)[b]	(1.60)[b]
$3\ \frac{7}{2}\ 4 \leftarrow 2\ \frac{5}{2}\ 3$	6636.64208	0.11	6582.46135	0.05
$3\ \frac{5}{2}\ 3 \leftarrow 2\ \frac{3}{2}\ 2$	6647.23115	-0.48	6591.32986	-0.36
$3\ \frac{3}{2}\ 2 \leftarrow 2\ \frac{1}{2}\ 1$	6647.38505	-0.07	6591.43450	0.04
$3\ \frac{7}{2}\ 4 \leftarrow 2\ \frac{7}{2}\ 4$	6680.02075	0.03	6618.71607	0.25

Transition	Ar-H^{79}Br		Ar-H^{81}Br	
$J' F_1' F \leftarrow J'' F_1'' F$	ν_{obs}/MHz[a]	$\Delta\nu$/kHz[a]	ν_{obs}/MHz[a]	$\Delta\nu$ /kHz[a]
$3\ \frac{7}{2}\ 3 \leftarrow 2\ \frac{7}{2}\ 3$	6680.02808	0.47	6618.72256	-0.15
$4\ \frac{5}{2}\ 3 \leftarrow 3\ \frac{5}{2}\ 3$	8810.40605	-0.11	8744.28174	0.35
$4\ \frac{5}{2}\ 2 \leftarrow 3\ \frac{5}{2}\ 2$	8810.40828	-0.02	8744.28358	0.06
$4\ \frac{7}{2}\ 4 \leftarrow 3\ \frac{7}{2}\ 4$	8833.83252	0.14	8763.82893	-0.14
$4\ \frac{7}{2}\ 3 \leftarrow 3\ \frac{7}{2}\ 3$	8833.83569	-0.16	8763.83242	-0.12
$4\ \frac{11}{2}\ 5 \leftarrow 3\ \frac{9}{2}\ 4$	8848.87174	0.39	8776.42134	0.19
$4\ \frac{11}{2}\ 6 \leftarrow 3\ \frac{9}{2}\ 5$	8848.87174	0.18	8776.42134	-0.02
$4\ \frac{9}{2}\ 4 \leftarrow 3\ \frac{7}{2}\ 3$	8848.89485	-0.03	8776.44223	0.44
$4\ \frac{9}{2}\ 5 \leftarrow 3\ \frac{7}{2}\ 4$	(8848.89485)[b]	(-0.88)[b]	8776.44223	-0.43
$4\ \frac{7}{2}\ 3 \leftarrow 3\ \frac{5}{2}\ 2$	8853.85479	0.19	8780.59557	0.20
$4\ \frac{7}{2}\ 4 \leftarrow 3\ \frac{5}{2}\ 3$	8853.85479	-0.44	8780.59557	-0.43
$4\ \frac{5}{2}\ 2 \leftarrow 3\ \frac{3}{2}\ 1$	8853.86890	0.29	8780.60089	0.25
$4\ \frac{5}{2}\ 3 \leftarrow 3\ \frac{3}{2}\ 2$	8853.86890	0.06	8780.60089	0.02
$4\ \frac{9}{2}\ 5 \leftarrow 3\ \frac{9}{2}\ 5$	8892.27978	-0.25	8812.70432	0.04
$4\ \frac{9}{2}\ 4 \leftarrow 3\ \frac{9}{2}\ 4$	8892.28615	-0.35	8812.71084	0.08
$5\ \frac{7}{2}\ 4 \leftarrow 4\ \frac{7}{2}\ 4$	11019.07375	-0.13	10935.08312	-0.45
$5\ \frac{7}{2}\ 3 \leftarrow 4\ \frac{7}{2}\ 3$	11019.07647	-0.05	10935.08625	0.04
$5\ \frac{9}{2}\ 5 \leftarrow 4\ \frac{9}{2}\ 5$	11047.48389	0.14	10958.80745	0.05
$5\ \frac{9}{2}\ 4 \leftarrow 4\ \frac{9}{2}\ 4$	11047.48775	0.08	10958.81126	-0.06
$5\ \frac{13}{2}\ 6 \leftarrow 4\ \frac{11}{2}\ 5$	11059.57903	0.25	10968.93516	0.20
$5\ \frac{13}{2}\ 7 \leftarrow 4\ \frac{11}{2}\ 6$	11059.57903	0.16	10968.93516	0.11
$5\ \frac{11}{2}\ 5 \leftarrow 4\ \frac{9}{2}\ 4$	11059.61582	0.24	10968.96638	0.27
$5\ \frac{11}{2}\ 6 \leftarrow 4\ \frac{9}{2}\ 5$	11059.61582	-0.25	10968.96638	-0.23
$5\ \frac{7}{2}\ 3 \leftarrow 4\ \frac{5}{2}\ 2$	11062.52297	0.15	10971.39811	0.05
$5\ \frac{7}{2}\ 4 \leftarrow 4\ \frac{5}{2}\ 3$	11062.52297	0.03	10971.39811	-0.07
$5\ \frac{9}{2}\ 4 \leftarrow 4\ \frac{7}{2}\ 3$	11062.54665	-0.06	10971.42077	0.19
$5\ \frac{9}{2}\ 5 \leftarrow 4\ \frac{7}{2}\ 4$	11062.54665	-0.46	10971.42077	-0.22
$5\ \frac{11}{2}\ 6 \leftarrow 4\ \frac{11}{2}\ 6$	11103.02469	0.14	11005.24943	-0.10
$5\ \frac{11}{2}\ 5 \leftarrow 4\ \frac{11}{2}\ 5$	11103.03080	0.07	11005.25584	0.12
$6\ \frac{15}{2}\ 7 \leftarrow 5\ \frac{13}{2}\ 6$	13268.65252	0.05	13159.86450	0.19
$6\ \frac{15}{2}\ 8 \leftarrow 5\ \frac{13}{2}\ 7$	13268.65252	0.03	13159.86450	0.16

Transition	Ar-H^{79}Br		Ar-H^{81}Br	
$J' F_1' F \leftarrow J'' F_1'' F$	ν_{obs}/MHz[a]	$\Delta\nu$/kHz[a]	ν_{obs}/MHz[a]	$\Delta\nu$ /kHz[a]
$6\ \frac{13}{2}\ 6 \leftarrow 5\ \frac{11}{2}\ 5$	13268.70014	-0.15	13159.90448	0.12
$6\ \frac{13}{2}\ 7 \leftarrow 5\ \frac{11}{2}\ 6$	13268.70014	-0.45	13159.90448	-0.18
$6\ \frac{9}{2}\ 4 \leftarrow 5\ \frac{7}{2}\ 3$	13270.60808	-0.03	13161.50072	0.04
$6\ \frac{9}{2}\ 5 \leftarrow 5\ \frac{7}{2}\ 4$	13270.60808	-0.08	13161.50072	-0.01
$6\ \frac{11}{2}\ 5 \leftarrow 5\ \frac{9}{2}\ 4$	13270.65116	0.38	13161.53756	0.02
$6\ \frac{11}{2}\ 6 \leftarrow 5\ \frac{9}{2}\ 5$	13270.65116	0.12	13161.53756	-0.24

[a] $\Delta\nu = \nu_{obs}-\nu_{calc}$ from final cycle of fit.
[b] Excluded from fit.

Table A 4. Observed submillimeter frequencies of Ar-D^{79}Br and Ar-D^{81}Br.

						Ar-D^{79}Br		Ar-D^{81}Br	
J'	V'	F'	J"	V"	F"	Observed (MHz)	O-C (kHz)	Observed (MHz)	O-C (kHz)
1	1	1/2	0	0	3/2	216000.087	1.1	215576.085	1.8
1	1	5/2	0	0	3/2	216069.031	2.3	215633.78	-1.6
1	1	3/2	0	0	3/2	216156.268	-2.2	215706.643	-2.1
0	1	3/2	1	0	3/2	211323.975	1.9	210931.702	0.8
0	1	3/2	1	0	5/2	211393.299	2.7	210989.608	0.4
0	1	3/2	1	0	1/2	211448.131	1.8	211035.498	1.8
2	1	1/2	1	0	3/2	218831.399	-2.0	218397.201	2.8
2	1	3/2	1	0	3/2	218919.268	1.2	218470.502	-0.5
2	1	1/2	1	0	1/2	218955.556	-1.1	218500.993	-0.2
2	1	7/2	1	0	5/2	218962.391	1.7	218506.699	-1.4
2	1	5/2	1	0	3/2	218980.116	1.1	218521.517	-1.2
2	1	3/2	1	0	1/2	219043.423	0.1	218574.298	0.5
2	1	5/2	1	0	5/2	219049.439	1.0	218579.426	1.3
1	1	1/2	2	0	3/2	209473.88	0.7	209103.8	2.2
1	1	5/2	2	0	5/2	209494.367	2.3	209120.878	1.9
1	1	1/2	2	0	1/2	209543.69	0.3	209162.054	2.1
1	1	5/2	2	0	7/2	209563.576	1.9	209178.705	1.6
1	1	3/2	2	0	5/2	209581.606	-0.2	209193.738	-1.7
1	1	3/2	2	0	3/2	209630.063	-0.7	209234.361	1.3
3	1	5/2	2	0	5/2	222184.744	-2.4		
3	1	9/2	2	0	7/2	222206.782	2.3	221730.577	0.1
3	1	3/2	2	0	1/2	222215.813	-2.5	221738.093	-3.5
3	1	7/2	2	0	5/2	222224.52	0.2	221745.398	-1.3
3	1	5/2	2	0	3/2	222233.201	-2.8	221752.675	-0.3
2	1	7/2	3	0	7/2	208028.333	3.1	207671.691	0.0
2	1	1/2	3	0	3/2	208067.718	-1.5	207704.601	-1.0
2	1	3/2	3	0	5/2	208086.221	-1.8	207719.963	-1.0
2	1	7/2	3	0	9/2	208097.506	-2.4	207729.496	-2.4
2	1	5/2	3	0	7/2	208115.376	-2.7	207744.415	-0.3
2	1	5/2	3	0	5/2	208147.07	-0.9	207770.982	2.3
2	1	3/2	3	0	3/2	208155.586	0.7	207777.909	2.6
4	1	5/2	3	0	5/2	225737.587	-2.9	225251.358	-1.2
4	1	7/2	3	0	7/2	225792.885	-1.5	225297.477	0.8
4	1	11/2	3	0	9/2	225805.082	3.4	225307.749	-0.3
4	1	5/2	3	0	3/2	225806.951	-1.4	225309.301	-0.6
4	1	9/2	3	0	7/2	225822.775	-1.4	225322.535	0.8
4	1	7/2	3	0	5/2	225824.578	-0.7	225324.04	-0.6
4	1	9/2	3	0	9/2	225891.954	-0.9	225380.345	3.4
3	1	3/2	4	0	5/2	206973.931	-4.1	206624.259	-3.6
3	1	9/2	4	0	11/2	206990.037	-1.2	206637.744	-1.4
3	1	5/2	4	0	7/2	206991.868	-1.3	206639.217	-1.0
3	1	7/2	4	0	9/2	207007.805	-1.8	206652.582	-1.2
3	1	7/2	4	0	7/2	207031.647	4.3	206672.563	1.0
5	1	9/2	4	0	9/2	229750.981	-3.9		

						Ar-D^{79}Br		Ar-D^{81}Br	
J'	V'	F'	J"	V"	F"	Observed (MHz)	O-C (kHz)	Observed (MHz)	O-C (kHz)
5	1	7/2	4	0	5/2	229757.211	-1.9	229238.052	-0.1
5	1	13/2	4	0	11/2	229757.399	4.3	229238.217	-0.4
5	1	9/2	4	0	7/2	229774.82	-0.7	229252.767	-2.2
5	1	11/2	4	0	9/2	229775.025	1.8	229252.939	-4.7
4	1	5/2	5	0	7/2	206229.074	-1.0	205893.294	-2.3
4	1	11/2	5	0	13/2	206239.841	0.3	205902.316	-1.3
4	1	7/2	5	0	9/2	206246.813	-1.5	205908.105	-0.8
4	1	9/2	5	0	11/2	206257.514	-1.2	205917.079	-0.2
6	1	9/2	5	0	7/2	234062.283	-1.4	233520.65	-0.8
6	1	15/2	5	0	13/2	234063.229	3.4	233521.451	-0.5
6	1	11/2	5	0	9/2	234079.816	-1.2	233535.305	1.2
6	1	13/2	5	0	11/2	234080.766	1.3	233536.104	1.0
5	1	7/2	6	0	9/2	205838.303	-1.6	205515.96	-0.6
5	1	13/2	6	0	15/2	205846.282	2.2	205522.647	0.0
5	1	9/2	6	0	11/2	205855.91	0.5	205530.664	-0.3
5	1	11/2	6	0	13/2	205863.853	-0.3	205537.327	0.8
7	1	11/2	6	0	9/2	238720.569	-3.6	238155.641	2.5
7	1	17/2	6	0	15/2	238721.82	5.7	238156.693	1.6
7	1	13/2	6	0	11/2	238738.003	-0.2	238170.208	1.7
7	1	15/2	6	0	13/2	238739.249	2.8	238171.255	1.7
6	1	9/2	7	0	11/2	205802.572	0.0	205492.996	2.1
6	1	15/2	7	0	17/2	205808.853	4.5	205498.259	0.0
6	1	11/2	7	0	13/2	205820.05	0.1	205507.596	0.8
6	1	13/2	7	0	15/2	205826.311	2.0	205512.846	1.1
8	1	13/2	7	0	11/2	243730.883	-1.4	243141.874	2.3
8	1	19/2	7	0	17/2	243732.239	5.0	243143.016	0.3
8	1	15/2	7	0	13/2	243748.191	-1.7	243156.339	0.9
8	1	17/2	7	0	15/2	243749.542	0.5	243157.474	-0.1
7	1	11/2	8	0	13/2	206121.87	-3.3	205824.325	1.8
7	1	17/2	8	0	19/2	206127.017	3.6	205828.637	-0.5
7	1	13/2	8	0	15/2	206139.217	-0.4		
7	1	15/2	8	0	17/2	206144.347	0.1	205843.119	0.8
9	1	15/2	8	0	13/2	249092.037	-3.6	248478.198	-0.4
9	1	21/2	8	0	19/2	249093.415	6.2		
9	1	17/2	8	0	15/2	249109.206	-2.7	248492.548	-0.7
9	1	19/2	8	0	17/2	249110.574	-1.3	248493.699	-0.8
8	1	13/2	9	0	15/2	206795.824	-3.3	206509.539	-1.8
8	1	19/2	9	0	21/2	206800.158	1.7	206513.177	0.3
8	1	15/2	9	0	17/2	206813.022	-3.5	206523.913	0.0
8	1	17/2	9	0	19/2	206817.349	1.3	206527.539	-0.4
10	1	17/2	9	0	15/2	254802.767	-5.5	254163.368	-2.7
10	1	23/2	9	0	21/2			254164.511	-0.4
10	1	19/2	9	0	17/2			254177.588	-2.9
10	1	21/2	9	0	19/2			254178.72	-1.1
9	1	15/2	10	0	17/2			207548.025	-1.5

						Ar-D^{79}Br		Ar-D^{81}Br	
J'	V'	F'	J"	V"	F"	Observed (MHz)	O-C (kHz)	Observed (MHz)	O-C (kHz)
9	1	21/2	10	0	23/2	207827.546	0.9	207551.156	1.1
9	1	17/2	10	0	19/2			207562.269	2.1
9	1	19/2	10	0	21/2	207844.579	0.3	207565.385	-1.7
11	1	19/2	10	0	17/2	260861.681	-2.3	260196.013	1.9
11	1	25/2	10	0	23/2	260862.986	5.2	260197.114	-0.1
11	1	21/2	10	0	19/2			260210.089	1.8
11	1	23/2	10	0	21/2			260211.179	0.1

Table A 5. Observed submillimeter frequencies of Ar-H^{79}Br v=1 state.

J'	V'	F'	J"	V"	F"	Observed (MHz)	O-C (kHz)
0	1	3/2	1	0	5/2	273525.618	9.0
1	1	5/2	0	0	3/2	278174.598	-2.9
2	1	7/2	1	0	5/2	280927.299	1.1
3	1	9/2	2	0	7/2	283953.873	3.3
3	1	5/2	4	0	7/2	268590.702	-7.4
3	1	7/2	4	0	9/2	268607.233	2.5
3	1	9/2	4	0	11/2	268581.843	3.9
4	1	5/2	3	0	3/2	287252.5	-10.1
4	1	7/2	3	0	5/2	287277.842	-5.6
4	1	9/2	3	0	7/2	287281.574	-3.0
4	1	11/2	3	0	9/2	287256.243	4.7
4	1	5/2	5	0	7/2	267483.071	-12.5
4	1	7/2	5	0	9/2	267508.375	-10.7
4	1	9/2	5	0	11/2	267519.977	3.3
4	1	11/2	5	0	13/2	267494.73	6.0
5	1	7/2	4	0	5/2	290830.925	-9.2
5	1	9/2	4	0	7/2	290856.138	-8.2
5	1	11/2	4	0	9/2	290860.164	-0.4
5	1	13/2	4	0	11/2	290834.97	11.8
5	1	9/2	6	0	11/2	266704.072	-5.1
5	1	11/2	6	0	13/2	266712.958	2.2
5	1	13/2	6	0	15/2	266687.873	4.5
6	1	9/2	5	0	7/2	294686.588	-11.6
6	1	11/2	5	0	9/2	294711.648	-3.1
6	1	13/2	5	0	11/2	294715.488	3.1
6	1	15/2	5	0	13/2	294690.454	15.2
7	1	11/2	6	0	9/2	298819.552	-8.1
7	1	13/2	6	0	11/2	298844.423	0.4
7	1	15/2	6	0	13/2	298847.975	5.0
7	1	17/2	6	0	15/2	298823.135	23.2
8	1	13/2	7	0	11/2	303230.169	-16.5
8	1	19/2	7	0	17/2	303233.463	19.6
9	1	15/2	8	0	13/2	307918.899	-25.0
9	1	17/2	8	0	15/2	307943.315	-10.7
9	1	19/2	8	0	17/2	307946.308	0.3
9	1	21/2	8	0	19/2	307921.92	11.4
10	1	23/2	9	0	21/2	312888.961	9.6
1	1	5/2	2	0	7/2	271595.39	1.8
2	1	7/2	3	0	9/2	269948.652	1.5
6	1	15/2	7	0	17/2	266162.148	11.7
6	1	13/2	7	0	15/2	266187.041	4.4
6	1	11/2	7	0	13/2	266179.864	-7.5
8	1	19/2	9	0	21/2	265958.108	-1.9
7	1	17/2	8	0	19/2	265918.53	-0.2

Table A 6. Ar-IH observed frequencies of the Σ bending vibration.

J"	V'	F'	J"	V"	F"	Observed (MHz)	O-C (kHz)
1	1	5/2	0	0	5/2	264801.7110	2.5
1	1	7/2	0	0	5/2	264913.9157	-0.3
1	1	3/2	0	0	5/2	264962.8925	-1.8
0	1	5/2	1	0	3/2	260902.6824	2.4
0	1	5/2	1	0	7/2	261005.8299	1.6
0	1	5/2	1	0	5/2	261238.7528	-2.1
1	1	5/2	2	0	3/2	258511.1896	6.6
1	1	3/2	2	0	1/2	258528.9152	-5.4
1	1	7/2	2	0	9/2	258625.3319	0.4
1	1	5/2	2	0	5/2	258664.0380	-0.1
1	1	3/2	2	0	3/2	258672.3712	2.5
1	1	5/2	2	0	7/2	258727.9150	2.5
1	1	3/2	2	0	5/2	258825.2196	-4.3
1	1	7/2	2	0	7/2	258840.1185	-1.5
2	1	7/2	1	0	7/2	266200.7494	-0.9
2	1	3/2	1	0	3/2	266201.4860	-16.7
2	1	1/2	1	0	3/2	266270.5056	18.8
2	1	9/2	1	0	7/2	266304.1330	-0.1
2	1	7/2	1	0	5/2	266433.6730	-3.9
2	1	5/2	1	0	5/2	266462.7086	8.6
2	1	1/2	3	0	1/2	255863.8232	10.4
2	1	3/2	3	0	3/2	255894.3636	-19.6
2	1	9/2	3	0	11/2	255925.7252	-0.9
2	1	5/2	3	0	5/2	255947.9299	11.9
2	1	1/2	3	0	3/2	255963.3845	17.2
2	1	7/2	3	0	7/2	256022.4662	-5.4
2	1	3/2	3	0	5/2	256022.7774	-18.3
2	1	7/2	3	0	9/2	256026.6943	-1.3
2	1	5/2	3	0	7/2	256051.5035	8.8
2	1	9/2	3	0	9/2	256130.0778	-0.6
3	1	5/2	2	0	3/2	267358.6006	-3.7
3	1	11/2	2	0	9/2	267407.8588	0.7
3	1	3/2	2	0	3/2	267420.8049	-2.0
3	1	7/2	2	0	5/2	267461.4584	8.0
3	1	5/2	2	0	5/2	267511.4486	-10.8
3	1	9/2	2	0	7/2	267524.1751	-5.2
3	1	7/2	2	0	7/2	267525.3362	11.4
3	1	3/2	4	0	3/2	252827.9020	-13.1
3	1	1/2	4	0	3/2	252876.0526	14.0
3	1	5/2	4	0	5/2	252884.1086	-6.6
3	1	11/2	4	0	13/2	252911.9450	-0.7
3	1	3/2	4	0	5/2	252946.3112	-6.6
3	1	7/2	4	0	7/2	252954.7551	11.7
3	1	5/2	4	0	7/2	253004.7443	-8.1

J"	V'	F'	J"	V"	F"	Observed (MHz)	O-C (kHz)
3	1	9/2	4	0	11/2	253011.0374	-3.4
3	1	9/2	4	0	9/2	253032.2104	-7.2
3	1	7/2	4	0	9/2	253033.3709	8.8
3	1	11/2	4	0	11/2	253109.5094	2.4
4	1	5/2	3	0	3/2	268163.5957	-8.0
4	1	13/2	3	0	11/2	268205.3533	1.5
4	1	7/2	3	0	5/2	268233.5798	-2.1
4	1	5/2	3	0	5/2	268292.0100	-6.1
4	1	9/2	3	0	7/2	268299.3042	7.3
4	1	11/2	3	0	9/2	268314.3110	-5.8
4	1	3/2	5	0	5/2	249553.0238	8.0
4	1	13/2	5	0	15/2	249585.1640	-0.2
4	1	5/2	5	0	7/2	249624.6248	-8.5
4	1	7/2	5	0	9/2	249681.3002	-2.9
4	1	11/2	5	0	13/2	249682.5372	-3.9
4	1	9/2	5	0	11/2	249706.9308	9.2
5	1	5/2	4	0	3/2	268631.1728	9.5
5	1	7/2	4	0	5/2	268686.9234	-7.6
5	1	15/2	4	0	13/2	268691.7913	1.3
5	1	9/2	4	0	7/2	268751.7330	-1.0
5	1	13/2	4	0	11/2	268796.0206	-5.4
5	1	11/2	4	0	9/2	268799.7673	7.8
5	1	9/2	4	0	9/2	268830.3500	-2.7
5	1	5/2	6	0	7/2	245917.7624	6.4
5	1	15/2	6	0	17/2	245946.1869	0.5
5	1	7/2	6	0	9/2	245990.8124	-8.3
5	1	13/2	6	0	15/2	246042.0250	-4.1
5	1	9/2	6	0	11/2	246045.9187	-0.5
5	1	11/2	6	0	13/2	246068.6108	9.7
6	1	7/2	5	0	5/2	268818.2870	7.9
6	1	17/2	5	0	15/2	268865.7332	1.6
6	1	9/2	5	0	7/2	268881.1689	-8.3
6	1	11/2	5	0	9/2	268942.3321	0.6
6	1	15/2	5	0	13/2	268966.5990	-4.7
6	1	13/2	5	0	11/2	268980.0870	8.5
6	1	7/2	7	0	9/2	241970.6392	5.3
6	1	17/2	7	0	19/2	241995.9014	0.7
6	1	9/2	7	0	11/2	242044.8342	-9.2
6	1	15/2	7	0	17/2	242090.3493	-5.2
6	1	11/2	7	0	13/2	242098.5596	0.2
6	1	13/2	7	0	15/2	242118.7429	7.9
7	1	9/2	6	0	7/2	268687.9950	3.8
7	1	19/2	6	0	17/2	268726.9196	1.1
7	1	11/2	6	0	9/2	268755.1116	-7.6
7	1	13/2	6	0	11/2	268813.5114	3.0

J"	V'	F'	J"	V"	F"	Observed (MHz)	O-C (kHz)
7	1	17/2	6	0	15/2	268825.2023	-3.3
7	1	15/2	6	0	13/2	268844.5453	10.1
7	1	19/2	8	0	21/2	237735.3682	1.1
7	1	17/2	8	0	19/2	237828.5269	-7.3
7	1	13/2	8	0	15/2	237840.2518	-1.2
7	1	15/2	8	0	17/2	237858.3423	6.7
8	1	11/2	7	0	9/2	268242.7307	2.3
8	1	21/2	7	0	19/2	268275.6669	-0.6
8	1	13/2	7	0	11/2	268312.5266	-8.4
8	1	15/2	7	0	13/2	268368.7312	5.1
8	1	19/2	7	0	17/2	268371.8382	-3.0
9	1	13/2	8	0	11/2	267484.1721	-2.7
9	1	21/2	8	0	19/2	267607.0196	-1.7
10	1	15/2	9	0	13/2	266413.8498	0.8
10	1	25/2	9	0	23/2	266438.8983	1.7

Table A 7. Ar-IH intensities for selected transitions.

Frequency	Log Int.	Linear Intensity (mV)	J'	V'	F'	J''	V''	F''	mV
255963.367	-0.8081	**13**	2	1	1/2	3	0	3/2	12
256022.473	-0.4846	**28**	2	1	7/2	3	0	7/2	32
256022.796	-0.4417	**31**	2	1	3/2	3	0	5/2	28
256026.696	0.0036	**86**	2	1	7/2	3	0	9/2	100
256051.495	-0.1915	**55**	2	1	5/2	3	0	7/2	n/a
256130.078	-0.6323	**20**	2	1	9/2	3	0	9/2	21
258511.186	-0.7462	**15**	1	1	5/2	2	0	3/2	18
258528.918	-0.5181	**26**	1	1	3/2	2	0	1/2	25
267358.603	-0.3052	**42**	3	1	5/2	2	0	3/2	44
267407.858	0.31	**174**	3	1	11/2	2	0	9/2	180
267420.806	-0.4129	**33**	3	1	3/2	2	0	3/2	35
267461.45	-0.053	**75**	3	1	7/2	2	0	5/2	80
267468.929	-1.1291	**6**	3	1	1/2	2	0	3/2	n/a
267484.146	-0.9527	**9**	9	1	13/2	8	0	11/2	25
267511.459	-0.324	**40**	3	1	5/2	2	0	5/2	40
267512.642	-0.699	**17**	9	1	23/2	8	0	21/2	40
267524.181	0.1457	**119**	3	1	9/2	2	0	7/2	120
267525.325	-0.3305	**40**	3	1	7/2	2	0	7/2	40

Table A 8. Observed frequencies (MHz) and residual (kHz) from fit to a linear molecule for the three isotopomers of $(HBr)_2$

								$H^{79}Br$-$H^{81}Br$		$H^{79}Br$-$H^{79}Br$		$H^{81}Br$-$H^{81}Br$	
J'	V'	F_1'	F'	J"	V"	F_1"	F"	Observed (MHz)	O-C (kHz)	Observed (MHz)	O-C (kHz)	Observed (MHz)	O-C (kHz)
1	1	1/2	2	0	0	3/2	3	452076.0061	-4	452252.4438	-10	451899.4951	-6
1	1	1/2	2	0	0	3/2	1	452076.0061	-4	452252.4438	-10	451899.4951	-7
1	1	1/2	1	0	0	3/2	2	452080.3110	-9			451903.5914	-7
1	1	1/2	1	0	0	3/2	0	452080.7125	6	452257.7840	6	451903.9270	2
1	1	5/2	1	0	0	3/2	1	452092.3124	4	452269.8751	2	451914.0586	2
1	1	5/2	4	0	0	3/2	3	452101.7180	4	452280.3464	0	451922.8222	0
1	1	5/2	3	0	0	3/2	2	452111.2059	-15	452290.8120	6	451931.5837	7
1	1	5/2	2	0	0	3/2	2			452290.9130	9	451931.6570	10
1	1	3/2	2	0	0	3/2	3	452127.8429	5	452308.4471	5	451946.2895	3
1	1	3/2	2	0	0	3/2	1	452127.8429	5	452308.4471	5	451946.2895	3
1	1	3/2	3	0	0	3/2	3	452140.7237	-3	452322.7535	-7	451958.2480	-5
1	1	3/2	1	0	0	3/2	2	452142.0739	-9	452324.2464	-13	451959.5225	-9
1	1	3/2	1	0	0	3/2	0	452142.4735	3	452324.7234	7	451959.8594	0
1	1	3/2	0	0	0	3/2	1	452150.3151	-12	452333.3134	-17	451967.0743	-13
0	1	3/2	1	1	0	3/2	0	449145.7980	-5	449285.7410	-8	449005.6150	-3
0	1	3/2	0	1	0	3/2	1	449153.2700	-12	449293.9315	-17	449012.4900	-14
0	1	3/2	2	1	0	3/2	1	449153.7240	13	449294.4685	13	449012.8763	9
0	1	3/2	3	1	0	3/2	3	449154.9710	-5	449295.8492	-3	449014.0606	-3
0	1	3/2	1	1	0	3/2	2	449167.2810	1	449309.5392	0	449025.5050	0
0	1	3/2	3	1	0	3/2	2			449309.5392	0	449025.5050	0
0	1	3/2	2	1	0	5/2	3	449183.2490	6	449326.4260	-5	449039.5900	-3
0	1	3/2	2	1	0	5/2	2	449183.3190	-2	449326.3517	9	449039.5400	10
0	1	3/2	3	1	0	5/2	4	449192.2880	-3	449336.3813	-7	449047.9282	-6
0	1	3/2	1	1	0	5/2	1	449201.2720	0	449346.4062	1	449056.3162	-1
0	1	3/2	2	1	0	1/2	1	449212.8220	12	449358.4497	13	449066.3492	8
0	1	3/2	0	1	0	1/2	1	449212.3660	-14	449357.9110	-18	449065.9650	-13
0	1	3/2	3	1	0	1/2	2	449216.8840	-4	449363.0519	-3	449070.2286	-4
0	1	3/2	1	1	0	1/2	2	449216.8840	-4	449363.0519	-3		
2	1	1/2	1	1	0	3/2	0	453473.7290	-8				

								$H^{79}Br$-$H^{81}Br$		$H^{79}Br$-$H^{79}Br$		$H^{81}Br$-$H^{81}Br$	
J'	V'	F_1'	F'	J"	V"	F_1"	F"	Observed (MHz)	O-C (kHz)	Observed (MHz)	O-C (kHz)	Observed (MHz)	O-C (kHz)
2	1	1/2	2	1	0	3/2	1	453486.5285	4				
2	1	1/2	2	1	0	3/2	3	453488.0059	3	453681.2178	0		
2	1	7/2	2	1	0	3/2	1	453490.1636	-5	453681.5805	0		
2	1	7/2	2	1	0	3/2	3	453491.6465	-1				
2	1	1/2	1	1	0	3/2	2	453495.2102	-4	453688.5042	-2		
2	1	1/2	2	1	0	3/2	2	453500.3104	3	453694.9098	5		
2	1	7/2	3	1	0	3/2	3	453509.8929	-7	453704.1476	-9	453315.7477	-5
2	1	3/2	2	1	0	3/2	1	453515.2861	15				
2	1	3/2	1	1	0	3/2	1	453515.2861	10	453709.8841	10	453320.5626	9
2	1	3/2	0	1	0	3/2	1	453515.7989	-8	453710.4983	-10		
2	1	1/2	2	1	0	5/2	3	453516.0480	-7				
2	1	1/2	2	1	0	5/2	2	453516.1295	-4				
2	1	3/2	2	1	0	3/2	3	453516.7618	12	453711.5380	13	453321.9410	9
2	1	3/2	3	1	0	3/2	3	453516.7618	6				
2	1	7/2	2	1	0	5/2	3	453519.6910	-9	453713.5485	-8	453323.6340	-5
2	1	7/2	2	1	0	5/2	2	453519.7720	-6	453713.4636	-5	453323.5690	-7
2	1	7/2	3	1	0	3/2	2	453522.1980	-6	453717.8367	-7	453327.1899	-3
2	1	5/2	1	1	0	3/2	0	453527.7611	-13	453723.2824	-17	453331.7370	-12
2	1	3/2	2	1	0	3/2	2	453529.0670	13	453725.2260	14	453333.3820	9
2	1	1/2	2	1	0	5/2	1	453534.3010	1	453731.7449	-25	453338.8703	1
2	1	5/2	4	1	0	3/2	3	453537.6423	1	453734.0998	0	453340.8082	0
2	1	7/2	2	1	0	5/2	1	453537.9428	-1				
2	1	7/2	3	1	0	5/2	2	453538.0230	-7				
2	1	7/2	5	1	0	5/2	4	453540.0714	-1	453736.8079	1	453343.0744	2
2	1	5/2	2	1	0	3/2	1	453541.2837	-2	453738.1517	-3	453344.1843	-1
2	1	3/2	1	1	0	5/2	2			453741.7774	15	453347.2265	9
2	1	7/2	4	1	0	5/2	3	453544.5624	9	453741.7774	5	453347.2265	2
2	1	5/2	3	1	0	3/2	3	453544.5624	-9	453741.7774	-7	453347.2265	12
2	1	3/2	3	1	0	5/2	3	453544.8180	10				
2	1	1/2	1	1	0	1/2	2	453544.8180	-4	453742.0154	-6	453347.4130	-1

								$H^{79}Br$-$H^{81}Br$		$H^{79}Br$-$H^{79}Br$		$H^{81}Br$-$H^{81}Br$	
J'	V'	F_1'	F'	J"	V"	F_1"	F"	Observed (MHz)	O-C (kHz)	Observed (MHz)	O-C (kHz)	Observed (MHz)	O-C (kHz)
2	1	3/2	3	1	0	5/2	2	453544.8990	13	453741.7774	15	453347.2265	9
2	1	1/2	2	1	0	1/2	1	453545.6206	-2				
2	1	7/2	3	1	0	5/2	4	453547.2067	-8	453744.6850	-7	453349.6330	11
2	1	7/2	2	1	0	1/2	1	453549.2607	-6	453745.5574	-5	453350.3822	-4
2	1	1/2	2	1	0	1/2	2	453549.9131	-2	453748.4176	-2	453352.7840	-1
2	1	7/2	2	1	0	1/2	2	453553.5569	-3				
2	1	7/2	4	1	0	5/2	4	453553.8300	13				
2	1	5/2	2	1	0	3/2	2	453555.0750	6				
2	1	5/2	1	1	0	3/2	2					453351.6380	2
2	1	5/2	3	1	0	3/2	2	453556.8769	2	453755.4738	2	453358.6566	1
2	1	3/2	2	1	0	5/2	1	453563.0571	11	453762.0930	16	453364.1964	10
2	1	5/2	2	1	0	5/2	3	453570.8160	-1	453770.1190	-12	453370.9100	-2
2	1	5/2	2	1	0	5/2	2	453570.8907	-4	453770.0385	-4	453370.8461	-3
2	1	7/2	3	1	0	1/2	2	453571.8011	-10	453771.3471	-12	453371.9138	-8
2	1	3/2	2	1	0	1/2	1	453574.3830	14				
2	1	3/2	1	1	0	1/2	1	453574.3830	9	453773.8676	12	453374.0349	7
2	1	3/2	0	1	0	1/2	1	453574.9000	-5	453774.4796	-10	453374.4728	-9
2	1	5/2	4	1	0	5/2	4	453574.9542	-3	453774.6327	-3	453374.6751	-3
2	1	3/2	2	1	0	1/2	2	453578.6718	10	453778.7380	11		
2	1	3/2	3	1	0	1/2	2	453578.6718	5				
2	1	5/2	3	1	0	5/2	4	453581.8859	0	453782.3220	2	453381.0846	0
2	1	5/2	1	1	0	5/2	1	453583.2382	-5	453783.9470	-9	453382.4425	-6
2	1	5/2	2	1	0	5/2	1	453589.0670	6				
2	1	5/2	2	1	0	1/2	1	453600.3849	1	453802.1367	0	453397.6590	0
2	1	5/2	3	1	0	1/2	2	453606.4850	2				
1	1	1/2	1	2	0	5/2	2			447752.5520	-11	447512.7386	-3
1	1	5/2	1	2	0	5/2	1	447649.7925	0	447771.0112	-4	447528.1768	0
1	1	5/2	4	2	0	5/2	3	447651.9017	-6	447773.4590	-12	447530.2221	-3
1	1	1/2	2	2	0	3/2	2	447652.8308	15	447774.5203	21	447531.0921	17
1	1	1/2	1	2	0	3/2	0	447656.8172	-20				

								$H^{79}Br$-$H^{81}Br$		$H^{79}Br$-$H^{79}Br$		$H^{81}Br$-$H^{81}Br$	
J'	V'	F_1'	F'	J"	V"	F_1"	F"	Observed (MHz)	O-C (kHz)	Observed (MHz)	O-C (kHz)	Observed (MHz)	O-C (kHz)
1	1	1/2	1	2	0	3/2	1	447657.3255	11	447779.6030	8	447535.3390	4
1	1	5/2	4	2	0	5/2	4	447658.5212	3	447780.8119	3	447536.3490	4
1	1	1/2	2	2	0	7/2	3	447659.3624	-20	447781.5315	-22	447536.9774	-13
1	1	5/2	2	2	0	5/2	2	447663.2846	14	447786.1596	13	447540.7985	8
1	1	5/2	3	2	0	5/2	2	447663.3540	20	447786.0560	7	447540.7290	9
1	1	5/2	1	2	0	3/2	2	447669.1423	29	447791.9526	33	447545.6556	25
1	1	1/2	2	2	0	7/2	2	447676.7530	-9				
1	1	3/2	2	2	0	5/2	3	447678.0293	-3	447801.5580	-8	447553.6838	-6
1	1	5/2	4	2	0	7/2	4	447678.7420	-27				
1	1	3/2	2	2	0	5/2	2	447679.7580	0				
1	1	1/2	2	2	0	1/2	2	447680.3639	-7	447803.4548	-10	447555.2700	-6
1	1	1/2	1	2	0	7/2	2	447681.2565	-10	447806.6256	-13	447557.9254	-11
1	1	1/2	1	2	0	1/2	2	447684.8707	-4				
1	1	5/2	4	2	0	7/2	3	447685.0810	-5	447809.4359	-10	447560.3070	-4
1	1	3/2	2	2	0	5/2	1			447809.5727	-12		
1	1	1/2	2	2	0	1/2	1	447685.1834	-15	447809.5727	-19	447560.4048	-13
1	1	5/2	2	2	0	3/2	3	447688.1650	14				
1	1	5/2	3	2	0	3/2	3	447688.2150	0				
1	1	5/2	3	2	0	7/2	4	447688.4674	-3			447563.3664	3
1	1	3/2	3	2	0	5/2	3	447690.9073	-14	447815.8655	-19	447565.6440	-12
1	1	5/2	4	2	0	7/2	5	447691.8902	-6	447816.9589	-6	447566.5543	-6
1	1	5/2	1	2	0	7/2	2	447693.0572	-3				
1	1	3/2	1	2	0	5/2	2	447694.1905	-6	447819.4875	-15	447568.6662	-9
1	1	5/2	2	2	0	7/2	3	447694.7383	15				
1	1	5/2	1	2	0	1/2	2	447696.6726	4	447820.8885	4	447569.8346	3
1	1	3/2	3	2	0	5/2	4	447697.5294	-2	447823.2181	-5	447571.7719	-4
1	1	3/2	2	2	0	3/2	2	447704.6706	27	447830.5216	34	447577.8848	25
1	1	3/2	0	2	0	5/2	1	447707.7939	-18	447834.4485	-24	447581.1869	-20
1	1	3/2	2	2	0	7/2	3	447711.2066	-4	447837.5357	-6	447583.7704	-5
1	1	5/2	2	2	0	7/2	2	447712.1162	13	447840.2343	12	447585.9922	7

								$H^{79}Br$-$H^{81}Br$		$H^{79}Br$-$H^{79}Br$		$H^{81}Br$-$H^{81}Br$	
J'	V'	F_1'	F'	J"	V"	F_1"	F"	Observed (MHz)	O-C (kHz)	Observed (MHz)	O-C (kHz)	Observed (MHz)	O-C (kHz)
1	1	5/2	3	2	0	7/2	2	447712.1840	17	447840.1305	6	447585.9170	2
1	1	5/2	2	2	0	1/2	2	447715.7281	17				
1	1	3/2	3	2	0	3/2	2	447717.5510	19	447844.8314	25	447589.8434	17
1	1	3/2	1	2	0	3/2	0	447718.5619	-38				
1	1	3/2	1	2	0	3/2	1	447719.0873	10	447846.5390	5	447591.2729	4
1	1	3/2	3	2	0	7/2	3			447851.8436	-16	447595.7304	-12
1	1	3/2	2	2	0	1/2	2	447732.2036	4	447859.4592	6	447602.0656	5
1	1	3/2	2	2	0	1/2	1	447737.0240	-3	447865.5752	-4	447607.2013	-2
1	1	3/2	3	2	0	7/2	2	447741.4695	-10				
1	1	3/2	1	2	0	7/2	2	447743.0207	-9	447873.5667	-11	447613.8646	-6
1	1	3/2	3	2	0	1/2	2	447745.0840	-4	447873.7666	-5	447614.0241	-3
1	1	3/2	0	2	0	1/2	1			447890.4400	-28		
3	1	3/2	3	2	0	5/2	2	454906.2700	-1				
3	1	9/2	3	2	0	5/2	2	454908.2590	-5				
3	1	3/2	1	2	0	5/2	1	454908.9020	-9				
3	1	3/2	3	2	0	5/2	4	454911.1590	2				
3	1	3/2	2	2	0	5/2	3	454916.0194	-8	455127.3918	-10	454705.4219	-7
3	1	3/2	2	2	0	5/2	1	454923.3145	-3	455135.4164	-4	454712.1422	-3
3	1	9/2	4	2	0	5/2	3	454926.9032	-10	455139.1740	-16	454715.2630	-9
3	1	3/2	1	2	0	3/2	2	454928.2532	21	455140.2728	25	454716.1756	17
3	1	3/2	3	2	0	3/2	3	454931.1544	3			454719.5602	25
3	1	3/2	3	2	0	3/2	2	454931.1544	-3	455144.3066	31	454719.5602	25
3	1	5/2	1	2	0	5/2	2	454932.7950	-3	455145.1026	-5		
3	1	7/2	2	2	0	5/2	2	454932.8738	8	455144.8880	9	454720.0400	7
3	1	9/2	3	2	0	3/2	3	454933.1442	0	455144.5756	-4	454719.7864	-3
3	1	9/2	3	2	0	3/2	2	454933.1442	-6			454719.7864	-3
3	1	9/2	3	2	0	7/2	4	454933.3860	-14				
3	1	9/2	4	2	0	5/2	4	454933.5239	0	455146.5275	-1	454721.3931	1
3	1	3/2	3	2	0	7/2	3	454937.7209	-3	455151.3180	-11	454725.4438	-7
3	1	5/2	4	2	0	5/2	4	454937.7730	29				

								$H^{79}Br$-$H^{81}Br$		$H^{79}Br$-$H^{79}Br$		$H^{81}Br$-$H^{81}Br$	
J'	V'	F_1'	F'	J"	V"	F_1"	F"	Observed (MHz)	O-C (kHz)	Observed (MHz)	O-C (kHz)	Observed (MHz)	O-C (kHz)
3	1	9/2	3	2	0	7/2	3	454939.7077	-9				
3	1	3/2	2	2	0	3/2	2	454942.6618	24	455156.3538	30	454729.6208	22
3	1	5/2	3	2	0	5/2	3	454943.2076	-5	455156.5692	-9	454729.7969	-5
3	1	5/2	2	2	0	5/2	3	454948.5110	-10			454734.5163	-10
3	1	3/2	2	2	0	7/2	3	454949.1990	-6	455163.3684	-9	454735.5076	-7
3	1	5/2	3	2	0	5/2	4	454949.8334	10	455163.9284	12	454735.9272	5
3	1	3/2	0	2	0	1/2	1	454951.0210	-21	455164.7785	-24	454736.6726	-18
3	1	9/2	4	2	0	3/2	3	454953.5040	-15				
3	1	7/2	5	2	0	5/2	4	454953.7538	7	455167.8874	5	454739.2594	5
3	1	9/2	6	2	0	7/2	5	454954.4944	-1	455168.7417	-2	454739.9794	0
3	1	3/2	3	2	0	7/2	2	454955.1030	-1				
3	1	3/2	1	2	0	1/2	2			455169.2114	-2	454740.3560	-3
3	1	5/2	2	2	0	5/2	1	454955.7949	-16	455170.2360	-20	454741.2309	-13
3	1	9/2	3	2	0	7/2	2	454957.0920	-5				
3	1	9/2	5	2	0	7/2	4	454957.3400	0				
3	1	7/2	3	2	0	5/2	2	454957.6480	0				
3	1	5/2	4	2	0	3/2	3	454957.7520	13				
3	1	5/2	4	2	0	7/2	4	454958.0000	5				
3	1	3/2	3	2	0	1/2	2	454958.7100	-3				
3	1	9/2	4	2	0	7/2	3	454960.0815	-10				
3	1	7/2	4	2	0	5/2	3	454960.2298	-9				
3	1	3/2	1	2	0	1/2	1	454960.6040	-12				
3	1	9/2	3	2	0	1/2	2	454960.7190	14				
3	1	5/2	4	2	0	7/2	3	454964.3182	7				
3	1	3/2	2	2	0	7/2	2	454966.5825	-3				
3	1	7/2	4	2	0	5/2	4	454966.8534	4	455182.4132	2	454751.3889	2
3	1	5/2	3	2	0	3/2	2	454969.8527	29	455185.5305	30	454753.9933	21
3	1	3/2	2	2	0	1/2	2	454970.1943	1	455185.2902	1	454753.7998	0
3	1	9/2	4	2	0	7/2	5			455182.6750	-10		
3	1	9/2	5	2	0	7/2	5	454970.4690	3				

								$H^{79}Br$-$H^{81}Br$		$H^{79}Br$-$H^{79}Br$		$H^{81}Br$-$H^{81}Br$	
J'	V'	F_1'	F'	J"	V"	F_1"	F"	Observed (MHz)	O-C (kHz)	Observed (MHz)	O-C (kHz)	Observed (MHz)	O-C (kHz)
3	1	3/2	2	2	0	1/2	1	454975.0145	-7	455191.4032	-12	454758.9339	-8
3	1	5/2	2	2	0	3/2	2	454975.1534	21	455191.1832	23	454758.7138	17
3	1	5/2	3	2	0	7/2	3	454976.3868	-4	455192.5504	-3	454759.8837	-5
3	1	5/2	1	2	0	7/2	2	454981.6240	-7				
3	1	7/2	2	2	0	7/2	2	454981.7044	6	455198.9642	10	454765.2325	5
3	1	7/2	3	2	0	3/2	3	454982.5256	-3	455199.2341	-4	454765.4563	-4
3	1	7/2	3	2	0	7/2	4	454982.7720	-12				
3	1	7/2	2	2	0	1/2	2	454985.3200	13				
3	1	7/2	5	2	0	7/2	5	454987.1216	-3	455204.0365	-2	454769.4674	-3
3	1	7/2	3	2	0	7/2	3	454989.0930	-7				
3	1	5/2	2	2	0	7/2	2	454999.0690	-10				
3	1	7/2	4	2	0	7/2	5	455000.2200	-6	455218.5622	-4	454781.5978	-4
3	1	5/2	2	2	0	1/2	2	455002.6820	-6	455220.1204	-4	454782.8944	-4
3	1	7/2	3	2	0	7/2	2	455006.4780	-2				
2	1	7/2	2	3	0	7/2	3	446124.0660	-6				
2	1	1/2	2	3	0	5/2	2	446127.5000	-9	446230.4651	-11	446026.3305	-3
2	1	7/2	5	3	0	7/2	4	446131.0500	-7			446028.6420	-5
2	1	7/2	2	3	0	5/2	2	446131.1450	-9				
2	1	7/2	5	3	0	7/2	5	446143.5683	5	446247.1448	6	446040.2498	7
2	1	7/2	2	3	0	5/2	1			446250.6542	-23	446043.2077	-15
2	1	1/2	2	3	0	7/2	2	446144.1080	6				
2	1	7/2	4	3	0	7/2	4	446144.7890	-13				
2	1	7/2	2	3	0	7/2	2	446147.7500	3	446250.8873	4	446043.3748	5
2	1	7/2	4	3	0	7/2	3	446148.9290	3				
2	1	3/2	3	3	0	7/2	3	446149.1897	10	446253.0654	10	446045.1862	7
2	1	1/2	1	3	0	3/2	2	446153.5480	11	446257.3833	12	446048.7902	11
2	1	7/2	3	3	0	5/2	3	446154.4981	6	446258.8230	0	446049.9867	1
2	1	3/2	2	3	0	5/2	2	446156.2581	2	446260.7863	3	446051.6548	5
2	1	1/2	2	3	0	3/2	2	446158.6476	17	446263.7882	19	446054.1648	15
2	1	3/2	2	3	0	5/2	3	446161.3608	18	446266.2100	19	446056.1812	16

								$H^{79}Br$-$H^{81}Br$		$H^{79}Br$-$H^{79}Br$		$H^{81}Br$-$H^{81}Br$	
J'	V'	F_1'	F'	J"	V"	F_1"	F"	Observed (MHz)	O-C (kHz)	Observed (MHz)	O-C (kHz)	Observed (MHz)	O-C (kHz)
2	1	7/2	2	3	0	3/2	2	446162.2930	18				
2	1	5/2	4	3	0	7/2	4	446165.9305	-11	446271.0644	-19	446060.2412	-11
2	1	7/2	3	3	0	5/2	4	446166.0030	-6				
2	1	1/2	1	3	0	3/2	1	446167.2768	-9	446272.7340	-7	446061.6250	-7
2	1	1/2	2	3	0	9/2	3	446167.6171	-2				
2	1	1/2	2	3	0	3/2	3	446169.6028	-13	446275.2817	-3	446063.7603	-10
2	1	7/2	3	3	0	9/2	4	446170.0885	-20	446275.4184	-25	446063.8598	-17
2	1	7/2	2	3	0	9/2	3					446065.1937	-10
2	1	1/2	2	3	0	3/2	1	446172.3782	-1			446067.0008	-2
2	1	3/2	1	3	0	7/2	2					446067.0008	-10
2	1	7/2	4	3	0	5/2	4	446172.6163	5				
2	1	7/2	4	3	0	9/2	5	446173.2800	-6				
2	1	3/2	3	3	0	5/2	4					446067.0008	-10
2	1	3/2	3	3	0	7/2	2					446067.0008	-10
2	1	3/2	0	3	0	5/2	1	446173.4670	-16			446067.2902	-27
2	1	7/2	5	3	0	9/2	6	446174.7806	-10			446068.4290	-8
2	1	5/2	2	3	0	7/2	3	446175.1770	-12			446068.8000	-11
2	1	7/2	4	3	0	9/2	4	446176.7180	8				
2	1	5/2	1	3	0	5/2	2	446176.4310	-22			446069.8969	-15
2	1	3/2	3	3	0	9/2	4	446176.9750	11				
2	1	1/2	1	3	0	3/2	0					446070.0290	-29
2	1	5/2	4	3	0	7/2	5	446178.4453	-3	446284.9630	-4	446071.8462	-3
2	1	7/2	3	3	0	3/2	2	446180.5420	15			446073.2940	8
2	1	5/2	4	3	0	5/2	3	446182.2423	8	446288.7774	11		
2	1	5/2	3	3	0	5/2	2	446184.0730	-4				
2	1	3/2	2	3	0	3/2	2	446187.4060	29	446294.1075	31	446079.4901	24
2	1	5/2	3	3	0	5/2	3	446189.1730	10	446296.4612	10	446081.4549	7
2	1	7/2	3	3	0	9/2	3	446189.5010	-14				
2	1	7/2	3	3	0	3/2	3	446191.4953	-17	446298.2038	-20	446082.8940	-13
2	1	5/2	4	3	0	5/2	4	446193.7422	-9				

								$H^{79}Br$-$H^{81}Br$		$H^{79}Br$-$H^{79}Br$		$H^{81}Br$-$H^{81}Br$	
J'	V'	F_1'	F'	J"	V"	F_1"	F"	Observed (MHz)	O-C (kHz)	Observed (MHz)	O-C (kHz)	Observed (MHz)	O-C (kHz)
2	1	3/2	2	3	0	9/2	3	446196.3757	10				
2	1	3/2	3	3	0	9/2	3	446196.3757	5	446305.3149	14	446088.8540	10
2	1	5/2	4	3	0	9/2	4	446197.8427	-8	446305.3760	-11	446088.9290	-4
2	1	3/2	2	3	0	3/2	3	446198.3720	9	446305.5920	0	446089.0920	5
2	1	3/2	3	3	0	3/2	3	446198.3720	4				
2	1	5/2	2	3	0	7/2	2	446198.8693	6	446307.4613	4	446090.6450	3
2	1	5/2	2	3	0	5/2	1	446198.9660	4	446307.2250	-27	446090.4800	-15
2	1	3/2	2	3	0	3/2	1	446201.1332	7	446309.4527	6	446092.3240	5
2	1	5/2	3	3	0	9/2	4	446204.7720	-8				
2	1	5/2	1	3	0	3/2	2	446207.5830	9			446097.7390	10
2	1	5/2	3	3	0	3/2	2	446215.2177	20	446324.3573	21	446104.7652	17
2	1	5/2	4	3	0	3/2	3	446219.2500	-4				
2	1	5/2	2	3	0	9/2	3	446222.3700	-10				
4	1	5/2	2	3	0	5/2	2	456311.7105	-8				
4	1	5/2	4	3	0	5/2	3	456312.2070	12	456541.1750	11		
4	1	5/2	3	3	0	7/2	4	456313.1594	-11	456542.4153	-14		
4	1	11/2	4	3	0	5/2	3	456313.6810	13				
4	1	5/2	2	3	0	5/2	3	456316.8126	7	456545.6274	13	456088.0300	8
4	1	5/2	3	3	0	7/2	3	456317.2890	-6				
4	1	5/2	4	3	0	5/2	4	456323.7079	-4				
4	1	5/2	3	3	0	5/2	2	456324.3733	-3	456554.7000	-4	456095.6200	-5
4	1	11/2	4	3	0	5/2	4	456325.1840	-1	456554.2413	-1	456095.2348	0
4	1	9/2	3	3	0	7/2	3	456326.3528	6	456555.1084	13	456095.9466	5
4	1	5/2	4	3	0	9/2	4	456327.8030	-9	456557.7690	-15	456098.2000	-3
4	1	5/2	2	3	0	7/2	2	456328.3200	8				
4	1	5/2	1	3	0	3/2	2	456329.1660	9			456098.7100	7
4	1	11/2	4	3	0	9/2	4	456329.2807	-4				
4	1	5/2	3	3	0	5/2	3	456329.4741	11	456560.1272	15	456100.1510	10
4	1	11/2	5	3	0	7/2	5	456331.0180	-2	456561.9988	2	456101.6980	2
4	1	9/2	3	3	0	5/2	2	456333.4390	11				

								$H^{79}Br$-$H^{81}Br$		$H^{79}Br$-$H^{79}Br$		$H^{81}Br$-$H^{81}Br$	
J'	V'	F_1'	F'	J"	V"	F_1"	F"	Observed (MHz)	O-C (kHz)	Observed (MHz)	O-C (kHz)	Observed (MHz)	O-C (kHz)
4	1	7/2	5	3	0	7/2	5	456334.6553	20				
4	1	9/2	3	3	0	5/2	3	456338.5400	26				
4	1	7/2	4	3	0	7/2	4	456338.7028	-10	456569.4153	-7	456107.8980	-5
4	1	7/2	3	3	0	7/2	4	456339.1110	-16				
4	1	5/2	3	3	0	7/2	2	456340.9775	8				
4	1	5/2	2	3	0	3/2	2	456342.8655	25	456573.5263	26	456111.3411	18
4	1	5/2	1	3	0	3/2	1	456342.8655	-40	456573.7593	-9	456111.5494	-6
4	1	5/2	3	3	0	9/2	4	456345.0690	-10				
4	1	11/2	5	3	0	5/2	4	456346.3180	-4				
4	1	11/2	5	3	0	9/2	5	456346.9840	-13				
4	1	9/2	6	3	0	7/2	5	456347.4478	6	456578.8324	38	456115.7840	39
4	1	11/2	7	3	0	9/2	6	456347.4478	-4	456578.8324	-11	456115.7840	-9
4	1	7/2	2	3	0	7/2	2	456349.5723	35				
4	1	11/2	6	3	0	9/2	5	456349.5723	0				
4	1	11/2	4	3	0	9/2	3					456117.0690	1
4	1	5/2	4	3	0	3/2	3					456117.2310	-2
4	1	7/2	5	3	0	5/2	4	456349.9400	2				
4	1	7/2	3	3	0	5/2	2			456582.0590	6	456118.4780	8
4	1	9/2	4	3	0	7/2	3			456582.0590	-9	456118.4780	-1
4	1	11/2	5	3	0	9/2	4			456582.4040	-13	456118.7700	-10
4	1	9/2	3	3	0	7/2	2	456350.0370	16				
4	1	7/2	5	3	0	9/2	5	456350.6230	10				
4	1	9/2	5	3	0	7/2	4	456350.8074	-11	456582.5420	-8	456118.8760	-7
4	1	7/2	4	3	0	7/2	5	456351.2310	12				
4	1	5/2	1	3	0	3/2	0	456352.0260	-29			456119.9540	-27
4	1	7/2	5	3	0	9/2	4	456354.0420	4				
4	1	7/2	4	3	0	5/2	3	456355.0160	11	456587.1273	23	456122.7070	15
4	1	7/2	3	3	0	5/2	3	456355.4249	6	456587.4700	10	456122.9930	8
4	1	5/2	3	3	0	3/2	2	456355.5129	15	456588.0240	27	456123.4595	18
4	1	5/2	2	3	0	3/2	1	456356.5829	-6	456588.8670	-3	456124.1762	0

								$H^{79}Br$-$H^{81}Br$		$H^{79}Br$-$H^{79}Br$		$H^{81}Br$-$H^{81}Br$	
J'	V'	F_1'	F'	J"	V"	F_1"	F"	Observed (MHz)	O-C (kHz)	Observed (MHz)	O-C (kHz)	Observed (MHz)	O-C (kHz)
4	1	9/2	5	3	0	7/2	5	456363.3294	4	456596.4422	9	456130.4848	6
4	1	5/2	3	3	0	9/2	3	456364.4860	0				
4	1	9/2	3	3	0	3/2	2	456364.5810	32				
4	1	5/2	3	3	0	3/2	3	456366.4788	-4	456599.5078	-4	456133.0579	-5
4	1	7/2	4	3	0	9/2	4	456370.6158	-5	456603.7212	-4		
4	1	9/2	3	3	0	9/2	3	456373.5419	4	456607.3514	12	456139.6111	4
4	1	9/2	4	3	0	5/2	4	456374.0680	-2	456608.1871	-2	456140.3075	-3
4	1	9/2	4	3	0	9/2	5	456374.7360	-9				
4	1	9/2	3	3	0	3/2	3	456375.5420	7				
4	1	9/2	4	3	0	9/2	4	456378.1641	-5				
4	1	9/2	6	3	0	9/2	6	456378.6675	-2	456612.5294	-1		
4	1	9/2	5	3	0	9/2	5	456379.2870	-15				
4	1	7/2	3	3	0	9/2	3	456390.4310	-11				
4	1	7/2	3	3	0	3/2	3	456392.4300	-9				
4	1	9/2	5	3	0	9/2	6	456394.5460	-7				
3	1	3/2	3	4	0	7/2	3			444678.4786	-12	444512.0960	-2
3	1	9/2	6	4	0	9/2	6	444608.4477	5	444693.0374	8	444524.2490	8
3	1	9/2	5	4	0	9/2	5	444609.2600	6				
3	1	9/2	4	4	0	9/2	4	444610.0360	-7				
3	1	3/2	3	4	0	9/2	3	444610.6120	6				
3	1	9/2	3	4	0	9/2	3	444612.5934	-5			444527.7028	2
3	1	9/2	3	4	0	7/2	2	444613.1020	-16				
3	1	5/2	4	4	0	9/2	4	444614.2736	10	444698.7269	7	444528.9968	8
3	1	9/2	4	4	0	7/2	4	444617.2734	-3	444702.6625	-3	444532.2815	-3
3	1	3/2	3	4	0	5/2	3	444619.4123	10	444704.6442	16	444533.9523	15
3	1	9/2	3	4	0	5/2	3	444621.4060	11				
3	1	5/2	4	4	0	7/2	4	444621.5120	16				
3	1	9/2	6	4	0	11/2	6	444621.7320	-12				
3	1	3/2	2	4	0	9/2	3	444622.0910	4				
3	1	7/2	5	4	0	9/2	5	444625.8990	-13	444711.4503	-16	444539.6374	-8

								$H^{79}Br$-$H^{81}Br$		$H^{79}Br$-$H^{79}Br$		$H^{81}Br$-$H^{81}Br$	
J'	V'	F_1'	F'	J"	V"	F_1"	F"	Observed (MHz)	O-C (kHz)	Observed (MHz)	O-C (kHz)	Observed (MHz)	O-C (kHz)
3	1	3/2	1	4	0	5/2	2	444628.5290	-1	444714.4633	2	444542.1507	2
3	1	3/2	2	4	0	5/2	3	444630.8935	11	444716.6923	15	444544.0110	10
3	1	3/2	0	4	0	5/2	1	444632.0010	-25			444545.3810	-25
3	1	9/2	4	4	0	7/2	5	444633.0660	-12				
3	1	5/2	3	4	0	7/2	3	444633.1659	-6	444719.7122	-3	444546.5350	0
3	1	5/2	3	4	0	7/2	4	444633.5815	6	444720.0550	1	444546.8174	3
3	1	3/2	3	4	0	5/2	4	444635.8670	-12	444722.7290	-10	444549.0580	-13
3	1	9/2	3	4	0	5/2	4					444549.2890	-36
3	1	9/2	4	4	0	11/2	5			444723.0100	-23	444549.2890	-17
3	1	9/2	5	4	0	11/2	6					444550.5380	11
3	1	9/2	6	4	0	11/2	7	444638.3200	-7			444551.1430	-10
3	1	5/2	2	4	0	7/2	3	444638.4760	-4			444551.2590	-1
3	1	7/2	4	4	0	9/2	5	444639.0080	-6			444551.7700	-7
3	1	7/2	3	4	0	9/2	4	444639.0540	2			444551.7700	-54
3	1	9/2	5	4	0	11/2	5	444640.2100	3				
3	1	7/2	5	4	0	9/2	6	444641.0716	-1	444728.3265	2	444553.7302	-1
3	1	3/2	1	4	0	5/2	1	444641.5790	-21	444728.8720	-25	444554.1977	-19
3	1	9/2	4	4	0	5/2	3	444641.7770	8				
3	1	3/2	2	4	0	5/2	2	444642.9420	6	444730.5465	10	444555.5943	5
3	1	7/2	2	4	0	5/2	3	444646.0200	24				
3	1	7/2	4	4	0	7/2	3					444561.9910	-9
3	1	5/2	3	4	0	9/2	3	444649.2800	8				
3	1	7/2	4	4	0	7/2	4	444650.6031	2	444738.5492	2	444562.2810	2
3	1	7/2	5	4	0	7/2	5	444653.2960	-5				
3	1	5/2	2	4	0	9/2	3	444654.5890	8				
3	1	3/2	2	4	0	5/2	1	444655.9884	-17	444744.9560	-16	444567.6430	-14
3	1	9/2	4	4	0	11/2	4	444656.7580	-10				
3	1	7/2	5	4	0	11/2	5	444656.8580	-6	444744.3767	-10	444567.1616	-7
3	1	5/2	3	4	0	5/2	3	444658.0844	16	444745.8746	21	444568.3895	15
3	1	9/2	4	4	0	5/2	4	444658.2348	-12	444746.5586	-18	444568.9639	-15

								$H^{79}Br$-$H^{81}Br$		$H^{79}Br$-$H^{79}Br$		$H^{81}Br$-$H^{81}Br$	
J'	V'	F_1'	F'	J"	V"	F_1"	F"	Observed (MHz)	O-C (kHz)	Observed (MHz)	O-C (kHz)	Observed (MHz)	O-C (kHz)
3	1	5/2	4	4	0	11/2	4	444660.9920	4	444750.2946	9		
3	1	7/2	3	4	0	9/2	3	444661.9864	5	444751.8326	3	444573.3762	3
3	1	5/2	4	4	0	5/2	4	444662.4717	5				
3	1	5/2	2	4	0	5/2	3	444663.3830	6	444751.5239	11	444573.1073	8
3	1	7/2	4	4	0	11/2	5	444669.9600	-7				
3	1	5/2	3	4	0	5/2	2	444670.1327	12	444759.7275	14		
3	1	5/2	3	4	0	5/2	4					444583.5150	7
3	1	7/2	4	4	0	5/2	3	444675.1040	9	444764.3637	16	444583.8531	14
3	1	5/2	2	4	0	5/2	2	444675.4300	0	444765.3765	4	444584.6876	0
5	1	7/2	4	4	0	9/2	5	457687.5590	-9			457443.0240	-15
5	1	7/2	3	4	0	7/2	3	457687.9787	-6	457933.6941	-7	457442.5850	-8
5	1	7/2	3	4	0	7/2	4	457688.3908	2			457442.8720	0
5	1	7/2	5	4	0	7/2	5	457695.3619	-4				
5	1	13/2	5	4	0	7/2	5	457696.5430	-4			457450.2442	-5
5	1	7/2	2	4	0	5/2	3	457696.9480	2				
5	1	11/2	4	4	0	9/2	4	457698.7148	8			457451.0990	4
5	1	7/2	4	4	0	7/2	3	457698.7148	-37			457453.2564	-5
5	1	7/2	5	4	0	11/2	5	457698.9232	-7			457452.1597	-8
5	1	7/2	4	4	0	7/2	4	457699.1616	6			457453.5402	-1
5	1	13/2	5	4	0	11/2	5	457700.1014	-9				
5	1	7/2	3	4	0	9/2	3	457704.0970	11				
5	1	11/2	4	4	0	7/2	3	457705.5430	7				
5	1	13/2	6	4	0	9/2	6	457705.8147	7	457954.2103	1	457459.7160	0
5	1	11/2	4	4	0	7/2	4	457705.9540	14				
5	1	7/2	2	4	0	5/2	2	457708.9984	0	457956.0655	-1	457461.2812	-5
5	1	9/2	6	4	0	9/2	6	457709.3080	12				
5	1	9/2	4	4	0	9/2	5					457463.6240	-21
5	1	9/2	5	4	0	9/2	5	457712.8045	-8			457464.9794	-12
5	1	7/2	3	4	0	5/2	3	457712.8942	12			457464.4405	8
5	1	7/2	4	4	0	9/2	3	457714.8590	7				

								$H^{79}Br$-$H^{81}Br$		$H^{79}Br$-$H^{79}Br$		$H^{81}Br$-$H^{81}Br$	
J'	V'	F_1'	F'	J"	V"	F_1"	F"	Observed (MHz)	O-C (kHz)	Observed (MHz)	O-C (kHz)	Observed (MHz)	O-C (kHz)
5	1	13/2	6	4	0	7/2	5	457718.0330	-4				
5	1	13/2	8	4	0	11/2	7	457719.4972	2			457471.0080	-5
5	1	11/2	7	4	0	9/2	6					457471.3260	6
5	1	7/2	4	4	0	5/2	3					457475.1050	4
5	1	9/2	5	4	0	7/2	4					457475.4960	3
5	1	7/2	3	4	0	5/2	2	457724.9396	5			457476.0210	0
5	1	9/2	5	4	0	9/2	6					457479.0788	1
5	1	11/2	6	4	0	9/2	6	457737.3260	6			457487.5436	2
5	1	7/2	4	4	0	11/2	4					457490.2220	62
5	1	7/2	5	4	0	5/2	4					457471.8260	-15
5	1	7/2	4	4	0	5/2	4	457740.1187	-8	457990.6987	-13		
5	1	9/2	5	4	0	7/2	5	457740.1960	-6				
5	1	9/2	5	4	0	11/2	5	457743.7540	-11			457492.5060	-9
5	1	11/2	5	4	0	7/2	5	457745.2350	3			457495.0339	-4
5	1	11/2	4	4	0	11/2	4	457745.4300	-2			457494.1970	4
5	1	11/2	4	4	0	5/2	4	457746.9120	2				
5	1	11/2	5	4	0	11/2	5	457748.7911	-5				
5	1	11/2	7	4	0	11/2	7	457749.7501	-4				
4	1	11/2	7	5	0	11/2	7	443052.9504	5	443118.2527	3	442988.1530	5
4	1	11/2	5	5	0	11/2	5	443055.2016	-8				
4	1	11/2	4	5	0	11/2	4	443056.4550	1	443122.2204	-1	442991.4661	0
4	1	7/2	5	5	0	11/2	5	443058.8287	3	443123.5844	9	442992.5990	7
4	1	11/2	5	5	0	9/2	5	443060.0320	-3	443126.2470	-10	442994.8270	-6
4	1	5/2	4	5	0	7/2	4	443061.6640	7	443126.7487	9	442995.2514	6
4	1	11/2	4	5	0	7/2	4	443063.1220	-9				
4	1	7/2	5	5	0	9/2	5	443063.6600	9				
4	1	9/2	6	5	0	11/2	6	443067.4961	-13	443133.3620	-15	443000.7770	-9
4	1	5/2	2	5	0	7/2	3	443076.4990	4	443143.4000	8	443009.1600	2
4	1	11/2	5	5	0	9/2	6	443077.8150	-10				
4	1	5/2	1	5	0	7/2	2	443078.0040	-26				

								$H^{79}Br$-$H^{81}Br$		$H^{79}Br$-$H^{79}Br$		$H^{81}Br$-$H^{81}Br$	
J'	V'	F_1'	F'	J"	V"	F_1"	F"	Observed (MHz)	O-C (kHz)	Observed (MHz)	O-C (kHz)	Observed (MHz)	O-C (kHz)
4	1	5/2	3	5	0	7/2	4	443078.9330	8				
4	1	11/2	4	5	0	13/2	5	443080.6170	3				
4	1	11/2	6	5	0	13/2	7	443081.7950	-5				
4	1	11/2	7	5	0	13/2	8	443081.9100	-9				
4	1	7/2	3	5	0	9/2	4	443081.9760	-8				
4	1	9/2	3	5	0	9/2	3	443082.1770	2				
4	1	9/2	4	5	0	11/2	5	443082.9490	-9				
4	1	9/2	5	5	0	11/2	6	443083.3750	-17			443015.5030	-17
4	1	11/2	6	5	0	13/2	6	443083.8710	2				
4	1	9/2	6	5	0	11/2	7	443084.1660	3	443151.9340	-3	443016.2920	-3
4	1	9/2	3	5	0	7/2	4	443087.9900	13				
4	1	5/2	3	5	0	7/2	3	443089.1594	7	443157.8974	8	443021.2846	8
4	1	5/2	2	5	0	7/2	2	443091.6970	-16	443160.2256	-22	443023.2350	-13
4	1	9/2	5	5	0	9/2	5	443092.3372	-3	443160.6865	-7	443023.6150	-1
4	1	9/2	5	5	0	9/2	4	443093.6660	-9				
4	1	9/2	6	5	0	9/2	6	443094.2417	-6				
4	1	9/2	6	5	0	13/2	6	443097.7072	-9	443165.1914	-13	443027.3870	-7
4	1	7/2	4	5	0	11/2	4	443097.7983	9				
4	1	9/2	3	5	0	7/2	3	443098.2170	13				
4	1	11/2	5	5	0	13/2	5	443101.7386	-13	443172.3970	17	443033.3959	17
4	1	5/2	3	5	0	7/2	2	443104.3530	-18				
4	1	7/2	4	5	0	7/2	4	443104.4714	5	443172.6910	10	443033.6363	11
4	1	7/2	3	5	0	7/2	4	443104.8770	-4				
4	1	9/2	4	5	0	11/2	4	443105.3457	8	443176.1649	-2	443036.5455	3
4	1	7/2	5	5	0	7/2	5	443106.5542	1	443174.8150	-36	443035.4220	-27
4	1	7/2	3	5	0	7/2	3	443115.1116	3				
6	1	9/2	4	5	0	9/2	5	459040.0810	-4				
6	1	9/2	4	5	0	9/2	4			459303.8810	-6	458779.3470	-8
6	1	9/2	5	5	0	11/2	5	459044.3940	-5				
6	1	9/2	6	5	0	9/2	6	459046.3690	-4	459310.5266	11	458784.9054	9

								$H^{79}Br$-$H^{81}Br$		$H^{79}Br$-$H^{79}Br$		$H^{81}Br$-$H^{81}Br$	
J'	V'	F_1'	F'	J"	V"	F_1"	F"	Observed (MHz)	O-C (kHz)	Observed (MHz)	O-C (kHz)	Observed (MHz)	O-C (kHz)
6	1	15/2	6	5	0	9/2	6			459310.5266	-7		
6	1	9/2	5	5	0	9/2	5	459049.2234	0	459313.5820	-5	458787.4545	-5
6	1	9/2	6	5	0	13/2	6	459049.8380	-4	459312.1520	-9	458786.2660	-9
6	1	13/2	5	5	0	11/2	5	459050.2405	0	459311.6284	8	458785.8149	2
6	1	9/2	5	5	0	9/2	4	459050.5600	1				
6	1	13/2	5	5	0	9/2	5	459055.0740	9				
6	1	9/2	3	5	0	7/2	3	459057.1990	3	459320.4266	2	458793.1776	-2
6	1	15/2	6	5	0	13/2	6			459312.1520	-28		
6	1	9/2	4	5	0	11/2	4	459057.6440	4				
6	1	15/2	7	5	0	11/2	7	459058.9670	7	459324.3285	0		
6	1	11/2	7	5	0	11/2	7	459062.4680	14				
6	1	9/2	4	5	0	7/2	4	459064.3204	3	459327.4764	11	458799.0612	5
6	1	11/2	6	5	0	11/2	6	459065.5950	-10	459329.9500	-14	458801.1208	-11
6	1	9/2	5	5	0	11/2	4	459066.7890	10				
6	1	15/2	9	5	0	13/2	8			459335.5240	-5		
6	1	15/2	7	5	0	13/2	6	459072.5230	10				
6	1	11/2	7	5	0	9/2	6	459072.5230	-16				
6	1	13/2	5	5	0	11/2	4	459072.6373	17				
6	1	13/2	7	5	0	11/2	6	459073.1913	-5				
6	1	13/2	6	5	0	11/2	5	459073.3379	-3				
6	1	9/2	5	5	0	7/2	4	459073.4747	19				
6	1	11/2	5	5	0	9/2	4	459073.7851	-8				
6	1	9/2	4	5	0	7/2	3	459074.5544	10			458809.2360	-22
6	1	11/2	6	5	0	9/2	5	459074.5544	1			458809.2360	8
6	1	13/2	7	5	0	11/2	7	459089.8548	5	459356.7329	6	458823.5055	1
6	1	9/2	5	5	0	7/2	5	459092.1167	-10				
6	1	9/2	5	5	0	13/2	5					458826.0200	14
6	1	11/2	6	5	0	9/2	6	459092.3400	-3				
6	1	11/2	6	5	0	13/2	6	459095.8040	-8	459361.7830	-8	458827.7310	-9
6	1	13/2	5	5	0	7/2	5			459362.8647	-31	458828.6387	-31

								$H^{79}Br$-$H^{81}Br$		$H^{79}Br$-$H^{79}Br$		$H^{81}Br$-$H^{81}Br$	
J'	V'	F_1'	F'	J"	V"	F_1"	F"	Observed (MHz)	O-C (kHz)	Observed (MHz)	O-C (kHz)	Observed (MHz)	O-C (kHz)
6	1	13/2	6	5	0	9/2	6	459095.9550	0	459363.9397	-5	458829.5310	-9
6	1	13/2	5	5	0	13/2	5	459096.7830	1			458828.6387	0
6	1	13/2	6	5	0	13/2	6	459099.4150	-9				
6	1	13/2	8	5	0	13/2	8	459100.3680	-2	459367.2836	-7	458832.3311	-9
5	1	13/2	8	6	0	13/2	8			441522.8131	8	441431.9770	4
5	1	7/2	5	6	0	9/2	5			441529.4358	-35	441437.5524	7
5	1	13/2	6	6	0	11/2	6			441529.6730	-12	441437.7130	-3
5	1	11/2	7	6	0	13/2	7			441535.7014	-12	441442.7469	-8
5	1	7/2	3	6	0	9/2	4			441549.4792	11	441454.2617	7
5	1	7/2	2	6	0	9/2	3			441550.2100	-20		
5	1	11/2	7	6	0	13/2	8			441555.3780	-3		
5	1	7/2	4	6	0	9/2	4			441562.2405	10	441464.9251	2
5	1	11/2	6	6	0	11/2	6			441562.9734	-3	441465.5380	-3
5	1	11/2	7	6	0	15/2	7			441566.6793	-8	441468.6404	-9
5	1	7/2	3	6	0	9/2	3			441567.8491	-14	441469.6138	-16
5	1	9/2	4	6	0	9/2	4					441485.5330	4
5	1	13/2	6	6	0	15/2	6			441577.1078	1		
5	1	9/2	5	6	0	9/2	5			441577.7729	10		
6	1	15/2	9	7	0	15/2	9	439880.9210	32			439855.7693	5
6	1	9/2	6	7	0	11/2	6	439887.6860	-4				
6	1	15/2	6	7	0	15/2	6					439858.6126	-3
6	1	11/2	7	7	0	15/2	7					439859.6448	7
6	1	13/2	8	7	0	15/2	8	439892.1834	-9			439865.2064	-5
6	1	13/2	6	7	0	15/2	7	439910.1440	-5				
6	1	13/2	8	7	0	15/2	9	439910.4650	7				
6	1	13/2	7	7	0	15/2	8	439910.6340	-11				
6	1	11/2	6	7	0	13/2	6	439911.3931	0				
6	1	9/2	5	7	0	11/2	5	439915.7472	10	439945.3667	13		
6	1	13/2	7	7	0	13/2	7	439916.7535	-2	439945.2158	-1		
6	1	13/2	8	7	0	13/2	8	439917.8040	7				

								$H^{79}Br$-$H^{81}Br$		$H^{79}Br$-$H^{79}Br$		$H^{81}Br$-$H^{81}Br$	
J'	V'	F_1'	F'	J"	V"	F_1"	F"	Observed (MHz)	O-C (kHz)	Observed (MHz)	O-C (kHz)	Observed (MHz)	O-C (kHz)
6	1	13/2	8	7	0	17/2	8	439921.3340	-13	439948.3590	-2		
6	1	13/2	5	7	0	11/2	5	439921.6010	23				
6	1	9/2	4	7	0	11/2	4	439924.0646	-10	439953.5675	-9	439894.8858	-17
6	1	11/2	6	7	0	11/2	6			439961.8880	12	439901.8300	3
6	1	11/2	7	7	0	17/2	7					439902.2210	-2
6	1	11/2	7	7	0	11/2	7			439962.3433	-4		
6	1	13/2	6	7	0	15/2	6	439931.8940	17	439963.5680	-1	439903.2416	-3
7	1	11/2	5	6	0	11/2	5			460652.1174	-6	460094.9226	-4
7	1	17/2	7	6	0	11/2	7					460099.2430	-4
7	1	11/2	7	6	0	11/2	7			460657.2810	2		
7	1	11/2	7	6	0	15/2	7			460658.5010	-12	460100.2582	-13
7	1	17/2	7	6	0	15/2	7			460658.5010	-22		
7	1	11/2	6	6	0	11/2	6			460659.8318	-7	460101.3688	-5
7	1	11/2	4	6	0	9/2	4			460665.1678	5	460105.8296	0
7	1	17/2	8	6	0	13/2	8			460672.8587	1	460112.2460	1
7	1	11/2	5	6	0	9/2	5			460674.7842	8	460113.8596	4
7	1	13/2	7	6	0	13/2	7			460677.9861	-16	460116.5286	-11
7	1	17/2	10	6	0	15/2	9			460682.3780	-3		
7	1	11/2	7	6	0	15/2	6			460682.8150	7		
7	1	17/2	7	6	0	15/2	6			460682.8150	-3		
7	1	11/2	7	6	0	9/2	6			460682.8150	-11		
7	1	17/2	7	6	0	9/2	6			460682.8150	-21		
7	1	15/2	9	6	0	13/2	8			460683.1750	16		
7	1	15/2	8	6	0	13/2	8			460704.5595	7	460138.7363	2
7	1	11/2	6	6	0	15/2	6			460707.2598	-2	460141.0038	-4
7	1	13/2	7	6	0	15/2	7			460708.9687	-8	460142.4260	-8
7	1	15/2	6	6	0	9/2	6			460709.4700	-13	460142.8510	-14
7	1	15/2	7	6	0	11/2	7			460710.5780	-5		
7	1	15/2	6	6	0	15/2	6					460142.8510	1
7	1	15/2	9	6	0	15/2	9			460713.5130	-8	460146.2248	-12

								$H^{79}Br$-$H^{81}Br$		$H^{79}Br$-$H^{79}Br$		$H^{81}Br$-$H^{81}Br$	
J'	V'	F_1'	F'	J"	V"	F_1"	F"	Observed (MHz)	O-C (kHz)	Observed (MHz)	O-C (kHz)	Observed (MHz)	O-C (kHz)
8	1	13/2	6	7	0	13/2	6	461684.0450	-6	461978.9434	-2	461389.7470	-7
8	1	13/2	8	7	0	13/2	8	461686.6270	-3	461983.1380	4	461393.2581	-1
8	1	13/2	7	7	0	13/2	7	461688.6050	-2	461985.3640	-6	461395.1160	-6
8	1	19/2	8	7	0	17/2	8	461690.9120	-14	461984.0878	-15	461394.0590	-11
8	1	19/2	8	7	0	13/2	8			461983.1380	-2		
8	1	13/2	8	7	0	17/2	8			461984.0878	-8		
8	1	17/2	7	7	0	15/2	7	461691.1330	3	461984.2852	9	461394.2120	7
8	1	17/2	7	7	0	13/2	7	461693.7550	-3				
8	1	13/2	5	7	0	11/2	5	461694.7230	1	461989.6748	9	461398.7214	2
8	1	19/2	9	7	0	15/2	9			462000.0550	3	461407.4030	17
8	1	15/2	9	7	0	15/2	9	461705.5230	14				
8	1	13/2	6	7	0	11/2	6	461706.3080	-9	462001.3143	7	461408.4444	3
8	1	15/2	8	7	0	15/2	8	461708.1410	-9	462004.8015	-13	461411.3529	-7
8	1	19/2	8	7	0	17/2	7	461711.6750	1				
8	1	13/2	8	7	0	11/2	7	461711.7810	-3				
8	1	17/2	10	7	0	15/2	9	461712.2680	13				
8	1	15/2	6	7	0	13/2	5	461712.7930	3				
8	1	19/2	9	7	0	17/2	8	461712.7930	-14				
8	1	13/2	7	7	0	11/2	6	461713.0990	-3				
8	1	17/2	9	7	0	15/2	8	461713.6380	-7				
8	1	13/2	6	7	0	11/2	5	461713.7460	22				
8	1	17/2	8	7	0	15/2	7	461713.7810	-1				
8	1	15/2	7	7	0	13/2	6	461714.1050	-2				
8	1	15/2	8	7	0	13/2	7	461714.2630	3				
8	1	17/2	9	7	0	15/2	9	461731.9200	9	462031.1910	8	461433.4105	7
8	1	15/2	8	7	0	17/2	8			462035.1080	-8		
8	1	17/2	7	7	0	11/2	7			462035.2320	-1	461436.7890	-9
8	1	17/2	8	7	0	13/2	8			462036.3562	-2	461437.7284	-3
8	1	13/2	7	7	0	11/2	7	461733.2470	-9				
8	1	17/2	7	7	0	17/2	7	461737.5530	3				

								$H^{79}Br$-$H^{81}Br$		$H^{79}Br$-$H^{79}Br$		$H^{81}Br$-$H^{81}Br$	
J'	V'	F_1'	F'	J"	V"	F_1"	F"	Observed (MHz)	O-C (kHz)	Observed (MHz)	O-C (kHz)	Observed (MHz)	O-C (kHz)
8	1	17/2	10	7	0	17/2	10	461740.0860	-6	462038.9422	-5	461439.8900	-11
7	1	17/2	10	8	0	17/2	10	438264.4560	13				
7	1	11/2	7	8	0	13/2	7	438270.7610	-10				
7	1	15/2	9	8	0	17/2	9	438274.7470	-5				
7	1	11/2	4	8	0	13/2	5	438290.3320	-16				
7	1	11/2	5	8	0	13/2	6	438290.5300	3				
7	1	11/2	6	8	0	13/2	7	438291.8930	-50				
7	1	15/2	7	8	0	17/2	8	438293.4380	-10				
7	1	15/2	9	8	0	17/2	10	438293.5070	9				
7	1	15/2	8	8	0	17/2	9	438293.8870	-13				
7	1	13/2	7	8	0	15/2	7	438295.0570	-1				
7	1	11/2	6	8	0	13/2	6	438298.3560	2				
7	1	11/2	5	8	0	13/2	5	438308.6510	-8				
7	1	17/2	8	8	0	19/2	8	438313.1010	-2				
7	1	15/2	7	8	0	17/2	7	438315.0210	24				
7	1	13/2	8	8	0	13/2	8	438317.4150	20				
7	1	13/2	7	8	0	13/2	7	438317.4150	-23				
7	1	13/2	6	8	0	13/2	6	438321.5220	9				
9	1	15/2	7	8	0	15/2	7	462973.9620	-2	463284.5888	2	462664.0360	2
9	1	15/2	9	8	0	15/2	9	462975.8930	6				
9	1	21/2	9	8	0	19/2	9	462980.1520	-13				
9	1	19/2	8	8	0	17/2	8	462980.5760	3				
9	1	15/2	6	8	0	13/2	6	462983.2380	4			462671.6269	5
9	1	15/2	9	8	0	19/2	9			463288.8607	-1	462667.6095	-4
9	1	15/2	8	8	0	15/2	8			463290.1018	-1	462668.6465	4
9	1	21/2	10	8	0	17/2	10			463306.0670	9		
9	1	15/2	7	8	0	13/2	7	462996.3390	-5	463306.9345	14	462682.7037	5
9	1	17/2	9	8	0	17/2	9	462998.1570	-7	463310.5021	-6		
9	1	21/2	9	8	0	19/2	8	463000.9840	-1				
9	1	15/2	9	8	0	13/2	8	463001.0720	0				

								$H^{79}Br$-$H^{81}Br$		$H^{79}Br$-$H^{79}Br$		$H^{81}Br$-$H^{81}Br$	
J'	V'	F_1'	F'	J"	V"	F_1"	F"	Observed (MHz)	O-C (kHz)	Observed (MHz)	O-C (kHz)	Observed (MHz)	O-C (kHz)
9	1	15/2	6	8	0	13/2	5	463001.3610	-5				
9	1	21/2	10	8	0	19/2	9	463002.1130	10				
9	1	17/2	7	8	0	15/2	6	463002.1130	18				
9	1	19/2	8	8	0	17/2	7	463002.1130	-10				
9	1	17/2	10	8	0	15/2	9	463002.1130	-18				
9	1	15/2	8	8	0	13/2	7	463002.3020	7				
9	1	15/2	7	8	0	13/2	6	463002.7660	11				
9	1	19/2	10	8	0	17/2	9	463002.9860	0				
9	1	19/2	9	8	0	17/2	8	463003.1020	1				
9	1	17/2	8	8	0	15/2	7	463003.3610	1				
9	1	17/2	9	8	0	15/2	8	463003.4340	6				
9	1	19/2	10	8	0	17/2	10	463021.7490	16	463336.7463	12	462707.6170	12
9	1	15/2	8	8	0	13/2	8	463022.7180	-11				
9	1	19/2	8	8	0	19/2	8	463026.9690	-7				
9	1	15/2	8	8	0	19/2	8			463338.8678	-9		
9	1	17/2	9	8	0	19/2	9			463340.2700	-6		
9	1	19/2	11	8	0	19/2	11			463343.5530	-29	462713.3089	-6
8	1	19/2	8	9	0	19/2	8	436629.5330	29				
8	1	19/2	9	9	0	19/2	9	436629.9860	29				
8	1	13/2	8	9	0	15/2	8	436633.7900	-6				
8	1	17/2	10	9	0	19/2	10	436637.3530	-1				
8	1	15/2	8	9	0	17/2	8	436658.3720	2				
8	1	13/2	7	9	0	15/2	7	436660.8960	12				
8	1	17/2	9	9	0	17/2	9	436661.6350	4				
8	1	17/2	10	9	0	17/2	10	436662.1670	17				
8	1	13/2	6	9	0	15/2	6	436672.7210	0				
8	1	19/2	9	9	0	21/2	9	436676.3560	1				
8	1	15/2	9	9	0	15/2	9	436680.6230	4				
8	1	15/2	8	9	0	15/2	8	436680.9130	-9				
8	1	15/2	7	9	0	15/2	7	436684.1750	20				

								$H^{79}Br$-$H^{81}Br$		$H^{79}Br$-$H^{79}Br$		$H^{81}Br$-$H^{81}Br$	
J'	V'	F_1'	F'	J"	V"	F_1"	F"	Observed (MHz)	O-C (kHz)	Observed (MHz)	O-C (kHz)	Observed (MHz)	O-C (kHz)
10	1	17/2	8	9	0	17/2	8	464243.1350	10				
10	1	17/2	10	9	0	17/2	10	464244.5780	14				
10	1	23/2	10	9	0	21/2	10	464248.8240	-13				
10	1	19/2	8	9	0	17/2	9	464249.6290	-9				
10	1	17/2	7	9	0	15/2	7	464251.3760	5				
10	1	17/2	8	9	0	15/2	8	464265.6720	-4				
10	1	17/2	9	9	0	15/2	9	464291.5550	-3				
9	1	15/2	8	10	0	17/2	8	435003.4310	20				
9	1	15/2	7	10	0	17/2	7	435016.4700	12				
9	1	21/2	10	10	0	23/2	10	435019.5040	12				
9	1	17/2	8	10	0	17/2	8	435026.8770	21				
11	1	19/2	9	10	0	19/2	9	465491.6070	11				
11	1	19/2	10	10	0	19/2	10	465494.1750	15				
11	1	19/2	8	10	0	17/2	8	465499.0720	6				
11	1	19/2	9	10	0	17/2	9	465514.3040	-28				

Table A 9. $(HI)_2$ observed frequencies (MHz) and residuals (kHz) from fit to a linear molecule.

J'	V'	I_{tot}'	F'	J"	V"	I_{tot}"	F"	Observed (MHz)	O-C (kHz)
1	1	1	0	0	0	1	1	512557.1724	47
1	1	2	1	0	0	2	2	512565.439	-51
1	1	2	1	0	0	0	0	512569.9796	139
1	1	5	5	0	0	5	5	512579.0021	22
1	1	1	2	0	0	3	3	512584.5271	-125
1	1	1	2	0	0	1	1	512589.9444	103
1	1	2	3	0	0	4	4	512615.1986	-106
1	1	2	3	0	0	2	2	512618.2403	22
1	1	4	4	0	0	4	4	512633.214	-83
1	1	3	4	0	0	3	3	512653.2445	-67
1	1	3	4	0	0	5	5	512657.1485	98
1	1	3	3	0	0	3	3	512679.0404	-52
1	1	4	5	0	0	4	4	512688.9916	-84
1	1	5	6	0	0	5	5	512714.5617	67
1	1	2	2	0	0	2	2	512714.816	39
1	1	1	1	0	0	1	1	512739.182	-8
1	1	3	2	0	0	3	3	512748.182	-97
1	1	0	1	0	0	2	2	512748.382	2
1	1	4	3	0	0	4	4	512751.8212	-106
1	1	0	1	0	0	0	0	512752.92	189
1	1	3	2	0	0	1	1	512753.5983	130
1	1	4	3	0	0	2	2	512754.862	21
1	1	5	4	0	0	3	3	512759.741	-105
1	1	5	4	0	0	5	5	512763.6443	59
2	1	5	5	1	0	5	4	513240.8662	56
2	1	1	3	1	0	3	2	513253.3503	15
2	1	0	2	1	0	0	1	513256.711	97
2	1	1	1	1	0	1	1	513276.787	84
2	1	2	0	1	0	0	1	513281.3123	123
2	1	5	4	1	0	5	4	513285.6935	69
2	1	0	2	1	0	2	2	513291.2957	-32
2	1	5	5	1	0	5	6	513291.634	71
2	1	4	3	1	0	4	3	513293.479	-23
2	1	3	2	1	0	3	2	513297.3035	19
2	1	2	1	1	0	0	1	513299.3	90
2	1	5	6	1	0	5	6	513302.4349	24
2	1	3	2	1	0	1	1	513312.172	124
2	1	4	4	1	0	4	5	513317.2872	-96
2	1	3	5	1	0	5	4	513323.8235	62
2	1	1	3	1	0	3	3	513324.7028	-119
2	1	3	1	1	0	3	2	513328.1095	12
2	1	2	1	1	0	2	2	513333.8853	-38
2	1	4	3	1	0	2	2	513334.9376	28
2	1	3	4	1	0	5	4	513341.704	40

J'	V'	I_{tot}'	F'	J"	V"	I_{tot}"	F"	Observed (MHz)	O-C (kHz)
2	1	2	4	1	0	4	3	513348.6793	-44
2	1	5	5	1	0	3	4	513350.8284	-80
2	1	1	3	1	0	3	4	513351.387	-89
2	1	4	5	1	0	4	5	513358.0029	-80
2	1	4	2	1	0	4	3	513359.238	-42
2	1	4	2	1	0	0	1	513366.1134	139
2	1	3	2	1	0	3	3	513368.6592	-112
2	1	5	4	1	0	3	3	513368.9758	-93
2	1	4	4	1	0	4	4	513374.9145	-104
2	1	3	3	1	0	3	2	513375.5493	31
2	1	2	3	1	0	4	3	513381.9205	-30
2	1	0	2	1	0	2	3	513391.0471	-72
2	1	4	4	1	0	2	3	513393.6019	-21
2	1	5	4	1	0	3	4	513395.6604	-62
2	1	4	2	1	0	2	2	513400.699	11
2	1	4	6	1	0	4	5	513406.0227	-79
2	1	2	2	1	0	4	3	513408.5846	-29
2	1	1	2	1	0	3	2	513410.1606	27
2	1	5	3	1	0	5	4	513412.047	81
2	1	2	4	1	0	4	5	513413.575	-108
2	1	2	2	1	0	0	1	513415.4625	155
2	1	4	5	1	0	4	4	513415.6308	-87
2	1	5	7	1	0	5	6	513415.956	75
2	1	4	3	1	0	4	4	513416.006	-90
2	1	1	3	1	0	1	2	513422.4619	18
2	1	2	3	1	0	2	2	513423.3801	22
2	1	1	2	1	0	1	1	513424.988	90
2	1	3	4	1	0	3	3	513425.042	-65
2	1	1	1	1	0	1	2	513431.028	-19
2	1	5	5	1	0	5	5	513431.6789	70
2	1	3	5	1	0	3	4	513433.6896	-169
2	1	4	3	1	0	2	3	513434.6883	-13
2	1	5	6	1	0	5	5	513442.4909	34
2	1	0	2	1	0	2	1	513445.6963	66
2	1	3	3	1	0	3	3	513446.9046	-101
2	1	2	2	1	0	2	2	513450.0442	23
2	1	3	4	1	0	3	4	513451.6703	-91
2	1	1	1	1	0	1	0	513464.9776	105
2	1	3	2	1	0	1	2	513466.4182	25
2	1	2	0	1	0	2	1	513470.3002	95
2	1	2	4	1	0	4	4	513471.2032	-115
2	1	3	3	1	0	3	4	513473.5923	-67
2	1	5	4	1	0	5	5	513476.5113	89
2	1	2	1	1	0	2	1	513488.2867	60
2	1	2	4	1	0	2	3	513489.89	-33

J'	V'	I_{tot}'	F'	J"	V"	I_{tot}"	F"	Observed (MHz)	O-C (kHz)
2	1	5	3	1	0	3	3	513495.322	-87
2	1	3	1	1	0	1	2	513497.222	16
2	1	4	2	1	0	2	3	513500.448	-32
2	1	2	3	1	0	4	4	513504.4431	-102
2	1	3	5	1	0	5	5	513514.6386	80
2	1	5	3	1	0	3	4	513522.0055	-58
2	1	3	4	1	0	5	5	513532.5205	59
4	1	1	3	3	0	3	3	514779.758	5
4	1	2	3	3	0	4	3	514781.1661	71
4	1	5	5	3	0	5	4	514781.8786	169
4	1	4	4	3	0	2	5	514782.073	-49
4	1	0	4	3	0	4	4	514782.3252	-63
4	1	4	3	3	0	2	4	514782.6226	-44
4	1	4	2	3	0	4	1	514788.3318	-177
4	1	2	2	3	0	2	2	514787.9392	52
4	1	4	4	3	0	4	3	514797.2358	71
4	1	1	5	3	0	5	5	514797.831	19
4	1	4	3	3	0	4	2	514799.1413	6
4	1	5	6	3	0	5	5	514799.7047	15
4	1	3	5	3	0	3	4	514801.386	-66
4	1	4	1	3	0	4	1	514801.4375	-125
4	1	2	5	3	0	2	4	514802.526	-26
4	1	4	2	3	0	4	2	514802.576	23
4	1	2	6	3	0	2	5	514803.5255	-39
4	1	3	4	3	0	3	3	514803.465	40
4	1	4	5	3	0	4	4	514804.2766	-15
4	1	3	6	3	0	3	5	514804.739	-35
4	1	5	3	3	0	3	4	514804.9275	-64
4	1	5	3	3	0	5	3	514805.69	171
4	1	1	4	3	0	1	3	514805.803	20
4	1	2	4	3	0	2	3	514806.3306	20
4	1	3	7	3	0	3	6	514806.4578	-68
4	1	3	1	3	0	3	1	514806.958	-107
4	1	1	5	3	0	1	4	514808.138	-29
4	1	0	4	3	0	0	3	514809.044	10
4	1	4	8	3	0	4	7	514809.5168	-88
4	1	4	0	3	0	4	1	514809.6914	-172
4	1	2	2	3	0	2	1	514811.19	-75
4	1	5	9	3	0	5	8	514811.9832	53
4	1	4	6	3	0	4	5	514812.9557	-111
4	1	5	1	3	0	5	2	514813.4993	-46
4	1	4	7	3	0	4	6	514813.81	-34
4	1	5	6	3	0	5	6	514814.975	-70
4	1	5	7	3	0	5	6	514815.824	-79
4	1	5	8	3	0	5	7	514823.4899	143

J'	V'	I_{tot}'	F'	J"	V"	I_{tot}"	F"	Observed (MHz)	O-C (kHz)
4	1	5	4	3	0	5	4	514825.4938	177
4	1	4	5	3	0	4	5	514826.4632	-100
4	1	2	3	3	0	4	4	514830.9165	-44
4	1	4	3	3	0	4	3	514834.0741	80
4	1	4	2	3	0	4	3	514837.5024	91
4	1	2	5	3	0	2	5	514838.808	-28
4	1	5	5	3	0	5	5	514838.997	-18
4	1	5	2	3	0	5	3	514841.56	193
4	1	1	4	3	0	3	4	514842.9574	-52
4	1	2	6	3	0	4	6	514843.013	-6
4	1	3	5	3	0	3	5	514843.232	-46
4	1	3	4	3	0	1	4	514843.625	-28
4	1	4	4	3	0	4	4	514846.9866	-44
4	1	4	3	3	0	2	2	514857.8363	85
4	1	2	3	3	0	0	3	514857.6334	27
5	1	5	3	4	0	5	2	515455.5056	24
5	1	5	2	4	0	5	1	515455.9732	-137
5	1	1	4	4	0	3	4	515466.6867	-3
5	1	3	3	4	0	3	3	515472.6402	104
5	1	5	5	4	0	5	4	515473.134	171
5	1	5	6	4	0	5	5	515480.9233	94
5	1	5	8	4	0	5	7	515497.8212	-43
5	1	5	9	4	0	5	8	515500.3602	155
5	1	4	8	4	0	4	8	515451.3814	-95
5	1	5	8	4	0	5	8	515451.9509	164
7	1	5	10	6	0	5	10	516762.2791	129
7	1	5	4	6	0	5	3	516793.4151	56
7	1	5	3	6	0	5	2	516795.0404	-53
7	1	5	5	6	0	5	4	516795.9853	120
7	1	5	6	6	0	5	5	516799.1618	105
7	1	5	9	6	0	5	9	516796.4416	-25
7	1	5	2	6	0	5	1	516799.7684	-155
7	1	4	10	6	0	4	9	516810.2042	-52
7	1	5	10	6	0	5	9	516814.2033	-26
7	1	4	8	6	0	4	8	516816.4946	-111
7	1	4	3	6	0	4	3	516820.6644	-101
7	1	5	3	6	0	5	3	516824.0894	80
7	1	5	4	6	0	5	4	516825.1123	132
7	1	5	7	6	0	1	7	516831.6492	-78
7	1	5	8	6	0	5	8	516836.3534	-97
0	1	5	5	1	0	5	4	511081.8432	32
0	1	3	3	1	0	5	4	511085.456	75
0	1	2	2	1	0	4	3	511090.688	-57
0	1	1	1	1	0	3	2	511092.3686	-15
0	1	0	0	1	0	0	1	511093.358	73

J'	V'	I_{tot}'	F'	J"	V"	I_{tot}"	F"	Observed (MHz)	O-C (kHz)
0	1	4	4	1	0	4	3	511093.5028	-24
0	1	3	3	1	0	3	2	511097.3826	44
0	1	2	2	1	0	0	1	511097.562	122
0	1	1	1	1	0	1	1	511107.2336	86
0	1	2	2	1	0	2	2	511132.147	-6
0	1	5	5	1	0	5	6	511132.6049	42
0	1	4	4	1	0	4	5	511158.3993	-88
0	1	3	3	1	0	3	3	511168.7351	-90
0	1	5	5	1	0	3	4	511191.8096	-99
0	1	3	3	1	0	3	4	511195.4241	-55
0	1	4	4	1	0	4	4	511216.0261	-96
0	1	2	2	1	0	2	3	511231.8977	-47
0	1	4	4	1	0	2	3	511234.714	-13
0	1	1	1	1	0	1	2	511261.4816	-10
0	1	3	3	1	0	1	2	511266.4948	48
0	1	5	5	1	0	5	5	511272.66	51
0	1	0	0	1	0	2	1	511282.344	43
0	1	2	2	1	0	2	1	511286.5475	92
0	1	1	1	1	0	1	0	511295.4247	107
1	1	1	2	2	0	3	3	510259.687	-39
1	1	5	5	2	0	3	4	510272.9687	18
1	1	3	4	2	0	5	3	510278.3447	-2
1	1	5	5	2	0	3	5	510291.2896	-135
1	1	4	4	2	0	2	3	510297.789	-4
1	1	2	3	2	0	4	2	510303.1438	-65
1	1	3	3	2	0	5	3	510304.1402	12
1	1	1	2	2	0	3	1	510308.6287	-76
1	1	2	3	2	0	2	4	510314.0551	-62
1	1	3	3	2	0	1	2	510318.472	73
1	1	2	1	2	0	2	1	510319.63	123
1	1	3	4	2	0	3	3	510328.4041	20
1	1	5	5	2	0	5	4	510330.915	57
1	1	4	4	2	0	2	4	510332.073	-35
1	1	1	2	2	0	3	2	510340.6474	67
1	1	1	0	2	0	1	1	510344.2856	-53
1	1	2	2	2	0	2	2	510348.8211	20
1	1	3	4	2	0	3	4	510351.116	95
1	1	3	3	2	0	3	3	510354.2002	34
1	1	2	1	2	0	0	2	510363.4707	-21
1	1	5	5	2	0	5	6	510366.0726	90
1	1	3	4	2	0	3	5	510369.4358	-59
1	1	2	3	2	0	4	3	510371.255	51
1	1	1	1	2	0	1	2	510373.274	-33
1	1	3	2	2	0	5	3	510373.324	10
1	1	2	2	2	0	2	3	510376.3467	-13

J'	V'	I_{tot}'	F'	J"	V"	I_{tot}"	F"	Observed (MHz)	O-C (kHz)
1	1	3	3	2	0	3	4	510376.9123	110
1	1	5	5	2	0	5	5	510376.9698	-166
1	1	0	1	2	0	2	2	510382.386	-18
1	1	5	6	2	0	5	7	510384.261	35
1	1	5	4	2	0	5	3	510384.8398	-42
1	1	1	2	2	0	1	3	510385.9332	-60
1	1	3	2	2	0	1	2	510387.611	26
1	1	4	5	2	0	2	4	510387.849	-38
1	1	4	3	2	0	2	2	510388.8692	4
1	1	4	4	2	0	4	3	510389.2718	76
1	1	4	4	2	0	4	5	510389.531	-61
1	1	4	5	2	0	4	6	510395.6537	-98
1	1	3	4	2	0	5	4	510409.0612	133
1	1	2	3	2	0	4	4	510413.5375	-129
1	1	2	3	2	0	0	2	510416.27	49
1	1	4	3	2	0	2	3	510416.394	-30
1	1	3	2	2	0	3	3	510423.3403	-12
1	1	5	6	2	0	3	5	510426.8494	-91
1	1	4	4	2	0	4	4	510431.5538	-104
1	1	0	1	2	0	4	2	510433.277	-93
1	1	5	4	2	0	3	3	510434.8586	-61
1	1	3	3	2	0	3	2	510435.1626	142
1	1	4	3	2	0	4	2	510439.7649	-66
1	1	4	5	2	0	4	5	510445.308	-63
1	1	4	3	2	0	2	4	510450.6765	-62
1	1	3	4	2	0	1	3	510454.6503	-2
1	1	3	4	2	0	5	5	510455.1163	-90
1	1	5	4	2	0	3	4	510457.6099	54
1	1	2	2	2	0	4	3	510467.8285	66
1	1	2	2	2	0	2	1	510469.001	207
1	1	3	2	2	0	3	1	510472.2838	-47
1	1	5	4	2	0	3	5	510475.932	-98
1	1	3	3	2	0	1	3	510480.4476	14
1	1	1	1	2	0	3	2	510490.0193	90
1	1	5	6	2	0	5	6	510501.6327	135
1	1	0	1	2	0	2	1	510502.567	170
1	1	3	2	2	0	3	2	510504.3019	95
1	1	4	3	2	0	4	3	510507.878	52
1	1	5	6	2	0	5	5	510512.5325	-119
1	1	2	2	2	0	0	2	510512.8439	65
1	1	5	4	2	0	5	4	510515.5584	95
1	1	1	1	2	0	1	1	510526.431	28
1	1	0	1	2	0	0	2	510546.41	28
1	1	3	2	2	0	1	3	510549.5873	-33
1	1	5	4	2	0	5	5	510561.6137	-128

J'	V'	I_{tot}'	F'	J"	V"	I_{tot}"	F"	Observed (MHz)	O-C (kHz)
2	1	0	2	3	0	2	2	509565.4153	31
2	1	4	5	3	0	2	5	509569.7613	-26
2	1	2	3	3	0	2	3	509584.1584	-1
2	1	4	3	3	0	4	3	509585.2945	86
2	1	3	4	3	0	3	4	509588.2146	-57
2	1	3	4	3	0	5	3	509588.96	160
2	1	2	4	3	0	2	4	509589.0484	-54
2	1	4	4	3	0	4	4	509593.959	-37
2	1	5	4	3	0	5	4	509594.7249	213
2	1	5	6	3	0	5	7	509596.172	118
2	1	5	3	3	0	5	2	509601.8828	-75
2	1	5	7	3	0	5	8	509605.2196	23
2	1	5	5	3	0	5	5	509607.0095	7
2	1	1	2	3	0	1	3	509607.5571	-2
2	1	2	1	3	0	2	2	509608.004	24
2	1	3	1	3	0	3	2	509608.454	73
2	1	4	3	3	0	2	2	509609.057	91
2	1	4	5	3	0	4	6	509609.1923	-50
2	1	3	3	3	0	3	4	509610.132	-38
2	1	2	2	3	0	2	3	509610.8213	-1
2	1	4	6	3	0	4	7	509612.0282	-110
2	1	3	5	3	0	3	5	509612.136	-58
2	1	2	0	3	0	2	1	509613.2662	-71
2	1	4	4	3	0	4	5	509616.1407	-127
2	1	1	1	3	0	1	2	509616.467	-27
2	1	4	6	3	0	2	5	509617.822	16
2	1	1	3	3	0	1	4	509617.8746	-52
2	1	0	2	3	0	0	3	509618.1209	-17
2	1	3	5	3	0	3	6	509620.8956	-88
2	1	5	3	3	0	1	3	509621.3511	4
2	1	3	2	3	0	3	3	509621.6676	20
2	1	5	5	3	0	5	6	509622.2841	-74
2	1	2	4	3	0	2	5	509625.3321	-55
5	1	5	4	6	0	5	3	507128.575	43
5	1	3	5	6	0	5	5	507129.019	136
5	1	3	7	6	0	3	7	507130.4615	-56
5	1	3	4	6	0	5	4	507131.085	115
5	1	5	5	6	0	3	5	507130.9973	14
5	1	5	6	6	0	5	5	507132.153	93
5	1	2	7	6	0	2	7	507132.522	-75
5	1	5	6	6	0	3	6	507137.2364	20
5	1	1	6	6	0	5	7	507138.991	36
5	1	3	4	6	0	3	5	507140.9197	27
5	1	5	7	6	0	5	7	507141.1222	29
5	1	1	6	6	0	5	6	507145.0647	-7

J'	V'	I_{tot}'	F'	J"	V"	I_{tot}"	F"	Observed (MHz)	O-C (kHz)
5	1	5	7	6	0	5	6	507147.19	-20
5	1	5	9	6	0	3	9	507147.3	-144
5	1	5	3	6	0	5	3	507152.412	46
5	1	5	2	6	0	5	2	507154.3205	-64
5	1	5	1	6	0	5	1	507156.5465	-173
5	1	4	7	6	0	4	7	507160.537	-117
5	1	5	9	6	0	5	10	507160.8584	115
5	1	3	8	6	0	3	8	507161.3756	-82
5	1	5	10	6	0	5	11	507162.0253	-26
5	1	2	5	6	0	2	6	507164.0046	-51
5	1	5	8	6	0	5	9	507164.3679	-37
5	1	0	5	6	0	0	6	507170.7507	-59
5	1	4	3	6	0	4	4	507171.4921	-30
5	1	1	6	6	0	1	7	507172.3256	-79
5	1	5	6	6	0	5	7	507173.1531	-3
5	1	5	5	6	0	3	6	507174.4456	32
5	1	3	5	6	0	5	6	507176.0922	-3
5	1	5	1	6	0	5	2	507177.9672	-41
5	1	3	4	6	0	3	4	507178.8274	-82
5	1	5	2	6	0	5	3	507183.3688	69
5	1	5	3	6	0	5	4	507184.1085	122
5	1	3	5	6	0	1	5	507187.1737	-16
5	1	4	9	6	0	4	9	507204.0829	-59
5	1	5	9	6	0	5	9	507212.7842	-39
5	1	3	7	6	0	5	7	507225.4484	63
5	1	3	6	6	0	3	6	507226.6686	78
5	1	1	5	6	0	3	5	507227.9408	77
5	1	5	10	6	0	5	10	507248.2484	173

Table A 10. FTMW spectroscopic data of the observed isotopomers of OC:HI.

J'	F'	J'	F'	OC–HI	$O^{13}C$–HI	$^{18}O^{13}C$–HI	OC–IH	$O^{13}C$–IH	OC–DI	$O^{13}C$–DI	OC–ID	CO–DI
4	9/2	3	7/2					9077.5117				
4	11/2	3	9/2				9289.0869	9112.1641			9300.6766	
4	13/2	3	11/2				9280.1494	9103.2129			9291.1696	
5	5/2	4	3/2	8992.3974	8808.8951		11566.829	11345.606			11578.5478	
5	5/2	4	5/2	9135.2934								
5	7/2	4	5/2	8979.4323	8795.8947		11552.472	11331.217				
5	7/2	4	7/2		8941.8429		11714.2715					
5	9/2	4	7/2	8985.8376	8802.3025		11559.6885	11338.4365				
5	9/2	4	9/2				11665.4014					
5	11/2	4	9/2	9003.9910	8820.4919		11579.8994	11358.6807			11592.3912	
5	11/2	4	11/2	8979.6569			11552.1904					
5	13/2	4	11/2	9021.3350	8837.9108		11598.9424	11377.7891			11612.7608	
5	13/2	4	13/2									
5	15/2	4	13/2	9015.7294	8832.2904		11592.6953	11371.5322			11606.1117	
6	7/2	5	5/2	10799.1012	10578.9465		13888.8916	13623.4893			13903.7358	
6	9/2	5	7/2	10790.7658	10570.5844		13879.6836	13614.2559			13893.9136	
6	11/2	5	9/2	10795.5905	10575.4181		13885.1035	13619.6807			13899.6631	
6	11/2	5	11/2				13970.6084					
6	13/2	5	11/2	10807.8740	10587.7299		13898.749	13633.3545			13914.1926	
6	15/2	5	13/2	10818.8442	10598.7459		13910.8008	13645.4463			13927.0787	
6	17/2	5	15/2	10814.7113	10594.6024		13906.1904	13640.8271			13922.1728	11607.0234
7	9/2	6	7/2	12602.8214	12346.0281	11551.0996			12581.8965			13525.7871
7	11/2	6	9/2	12597.0178	12340.2075	11545.2676	16200.9873		12575.5645			13519.249
7	13/2	6	11/2	12600.7724	12343.9685	11549.0156			12579.6396			13523.4834
7	13/2	6	13/2	12665.7020								
7	15/2	6	13/2	12609.6526	12352.8685	11557.9297	16215.0518		12589.3203			13533.5029
7	17/2	6	15/2	12617.2131	12360.4621	11565.5325	16223.3584		12597.6045			13542.0518
7	19/2	6	17/2	12614.0453	12357.2841	11562.3789	16219.8193		12594.1441	12340.4131		13538.4609
8	11/2	7	9/2			13203.1465			14381.3672	14091.4102		
8	13/2	7	11/2			13198.8496			14376.707			
8	15/2	7	13/2	14403.6192		13201.8516			14379.9678	14090.0039		
8	17/2	7	15/2	14410.3432		13208.6045	18529.875		14387.3037	14097.3525		
8	19/2	7	17/2	14415.8710		13214.1807			14393.3564	14103.4238		15472.9424
8	21/2	7	19/2			13211.6670	18533.1387		14390.6201	14100.6807		15470.1006
9	13/2	8	11/2							15853.5576		17394.2285
9	15/2	8	13/2							15849.9766		17390.5439
9	17/2	8	15/2							15852.6455		17393.3135
9	19/2	8	17/2			14858.5938				15858.4111		17399.2666
9	21/2	8	19/2			14862.8418				15863.0391		17404.0303
9	23/2	8	21/2			14860.8084				15860.8193		17401.7246

VITA

Name: Blake Anthony McElmurry

Address: Texas A&M University
Department of Chemistry
MS3255
College Station, TX 77843

Email Address: blakeam@tamu.edu

Education: Ph.D., Chemistry, Texas A&M University, College Station, TX, 2008.
B.S., Chemistry, Texas A&M University, College Station, TX, 2001.